Title

ELECTROCHEMICAL AND SPECTROELECTROCHEMICAL STUDIES OF SOME COORDINATION COMPOUNDS IN HIGH OXIDATION STATES

Author

Balfe, C.A.

Publication Date

1984

Lawrence Berkeley Laboratory

UNIVERSITY OF CALIFORNIA

Materials & Molecular Research Division

ELECTROCHEMICAL AND SPECTROELECTROCHEMICAL STUDIES OF SOME COORDINATION COMPOUNDS IN HIGH OXIDATION STATES

C.A. Balfe
(Ph.D. Thesis)

January 1984

Prepared for the U.S. Department of Energy under Contract DE-AC03-76SF00098

DISCLAIMER

LBL-17269

ELECTROCHEMICAL AND SPECTROELECTROCHEMICAL STUDIES OF SOME COORDINATION COMPOUNDS IN HIGH OXIDATION STATES

Carol Ann Balfe
(Ph.D. Thesis)

Lawrence Berkeley Laboratory
University of California
Berkeley, California 94720

January 1984

This work was supported by the Director, Office of Energy Research, Office of Basic Energy Sciences, Chemical Sciences Division of the U.S. Department of Energy under Contract Number DE-AC03-76SF00098.

Electrochemical and Spectroelectrochemical Studies of Some Coordination Compounds in High Oxidation States

by

Carol Ann Balfe

Electrochemical and Spectroelectrochemical Studies of Some Coordination Compounds in High Oxidation States

By Carol Ann Balfe

ABSTRACT

The composition and reactivity of several transition metal coordination complexes in high oxidation states have been explored using electrochemical methods. The effect of various axial anions on the reactivity and solution structure of manganese(III)tetraphenylporphyrins has been studied using voltammetric and spectroelectrochemical methods. Several rhodotorulic acid complexes of vanadium in the +4 and +5 oxidation state have been identified and their solution chemistry explored using these same methods. The ligand, N,N'-di(2-aminomethylpyridyl)malondiamide and its Ni(II), Cu(II), and Co(III) complexes have been prepared and characterized, and preliminary electrochemical studies have been conducted.

Semiderivative linear sweep voltammetry (SDLSV), a method which involves a transformation of the current-potential curve obtained in cyclic voltammetry, has been used to explore each of the chemical systems and was implemented with simple analog circuitry. Spectroelectrochemistry in optically transparent thin-layer cells (OTTLE) has been used to characterize the electron transfer processes observed in the voltammetric studies.

In the studies of manganese(III) porphyrins ($XMn^{III}TPP$) a set of previously unreported electron trans-

fer processes has been shown to be due to axial ligand oxidation for X = Cl^-, Br^-, I^-, CH_3COO^-, N_3^-, NO_2^-, and OCN^-. The potentials for two successive one-electron oxidations of the porphyrin ring have been determined to be 0.96 and 1.26 V *vs* the $Ag/AgNO_3$(0.01M), TEAP(0.1M), CH_3CN reference electrode; spectra of these species have been determined. In four cases it has been established that a six-coordinate species, $[X_2Mn^{III}TPP]^-$, forms in solution in the presence of excess axial anion for several anions. The $Mn^{IV/III}$ couple has been observed, its identity confirmed spectrally, and its stability been shown to be profoundly affected by the nature and concentration of the axial ligand.

Electrochemical studies of vanadium and rhodotorulic acid solutions as a function of pH, ligand:metal ratio, and prior exposure to air have demonstrated complex behavior for this system. Under anaerobic conditions oxovanadium(IV) rhodotorulate (VORA) has been isolated from (1:1) solutions of H_2RA and vanadium; a species in which the vanadyl oxygen has been displaced by a hydroxamate has been isolated from solutions of vanadium and rhodotorulic acid (~2:1). Under aerobic conditions oxovanadium(V) species, $V^{V}ORA(OH)$ or $V^{V}ORA(OCH_3)$, are formed.

The copper(II) complex of the malondiamide ligand crystallizes as the trihydrate in the space group $P2_1/c$, with lattice constants a = 9.932(4)Å, b = 22.049(9)Å, c = 22.049(9)Å and β = 104.54(3)° The complex is square

pyramidal with a carbonyl oxygen of an adjacent molecule weakly bonding in the axial position. The nickel complex, which is diamagnetic, has been characterized by ^1H NMR and is proposed to be square planar. The cobalt complex is six-coordinate and is formulated as $[Co^{III}(L)(NH_3)_2][Cl]$. Preliminary electrochemical studies show that the coppper complex is oxidized irreversibly, and the nickel complex is reduced reversibly to a nickel(I) complex in DMF at 2.06 V *vs* a Ag/Ag^+(0.01 M) reference electrode.

ACKNOWLEDGMENTS

There comes a time when all good things must end - even graduate school at Berkeley. Before the final curtain falls, however, I must stop to thank some very special people, without whose help this work would not have been possible.

Ken Raymond has been supportive and understanding above and beyond the call of duty. For his careful reading of this dissertation, helpful discussions along the way, and for always being there in time of need, the deepest gratitude is offered. Professor Ken Sauer deserves a merit award for his patience and wisdom during times of crisis. My special thanks to him. My deep appreciation goes to Marcin Majda for the time and careful thought he gave to the reading of this dissertation and for his helpful comments. Without Dick Anderson's diversionary dicussions about the Giants and his lively love of chemistry, life on the fifth floor of Latimer would have been measurably duller. Thank you, Dick. To June Smith I offer my thanks for all of little things which only she can offer.

Without the early help of Professors Arthur Hubbard of UC Santa Barbara and Fred Hawkridge of Virginia Commonwealth University, the projects undertaken for this dissertation would never have materialized. I thank each of them for their hospitality and helpful suggestions.

Likewise, I extend my gratitude to Professor Ann Walker of San Francisco State University, who has been a model, a friend, and a mentor.

Many of my fellow graduate students have enriched my experience at Berkeley. Special thanks are extended to Rob Scarrow for his patience, programming, and friendsip. Mark Camenzind was a special friend during these past few months. His keen eye for typos, and his thoughtful comments will be well remembered. Karrie Hansen has been a true friend in science. Our many good times together both socially and scientifically have been among the truly pleasurable experiences of these last years. Bruce Schardt, John Smegal, and Mark Bowers, my companions of 401 Latimer, are thanked for their help and commiseration. All of the members of the Raymond group will be fondly remembered for their friendship and willingness to help.

Finally, there are my family and friends who were always there when the going got rough. My dearest friend Mary Ann was always there to listen. For that alone I cannot thank her enough. To my brother, Kevin, for his helping hand and sympathetic ear goes a giant hug of gratitude. And so too, to Mom and Dad, who were always interested and helped in so many ways, go a loving thank you. And finally, to my dear friend Norman, whose patience, love, and faithful kindness have made it all wothwhile in the end, go my unending gratitude and love.

DEDICATION

To Emily, Joelle, Matthew, Michaela, Andrew,

Brendan, Felix, and Amanda,

who are the future.

TABLE OF CONTENTS

List of Tables

List of Figures

List of Abbreviations

Symbol	Meaning
A	Electrode surface area
C*	Concentration of electroactive species in bulk
D	Diffusion coeeficient of electroactive species
E	Potential (Volts)
E_{APP}	Applied potential
$E_{1/2}$	Half-wave potential
$E^{o\prime}$	Formal potential
E_{λ}	Switching potential in a linear potential sweep experiment
E_P	Peak potential in a linear potential sweep experiment
E_{PA}	Anodic peak potential
E_{PC}	Cathodic peak potential
ΔE_P	Difference between E_{PC} and E_{PA}
E_{PW}	Peak width at half peak height in a semiderivative LSV experiment
$e(t)$	Semiderivative current ($\mu A \cdot s^{-1/2}$)
e_p	Semiderivative peak current
e_{PA}	Semiderivative anodic peak height
e_{PC}	Semiderivative cathodic peak height
$\mathcal{F}$	Faraday (96,480 Coul/eq)
H_2RA	Rhodotorulic acid
l	Path length of OTTLE
n	Number of electrons transferred in an electrochemical reaction

OTTLE	Optically transparent thin layer electrochemical cell
q	Electrical charge (coulombs)
R	Universal gas constant (8.314 J/coul)
T	Temperature (°K)
t	Time (seconds)
TBAP	Tetrabutylammonmium perchlorate
TBAX	Tetrabutylammonium X
TEAP	Tetraethylammonium perchlorate
$XMn^{III}TPP$	Manganese(III) tetraphenylporphyrin X, where X = some axial anion

CHAPTER 1

Electrochemical Methods

I. Introduction

Since electron transfer processes are often involved in the reactions of transition metal coordination complexes, electrochemical methods are ideally suited for investigating these systems. Typical questions which an inorganic chemist may wish to explore include: What are the reduction potentials of electron transfer processes? What is the product of a given oxidation or reduction? Do oxidation/reduction reactions occur at the metal or on the ligand(s)? Are there other chemical steps which precede or follow the electron transfer reaction(s)? What is the rate of the electron transfer reaction? What are the stability constants of given metal complexes?

Manganese porphyrin complexes, vanadium rhodotorulic acid complexes, and copper(II), nickel(II), and cobalt(III) malondiamide complexes are the subjects of the investigations reported in this dissertation. Each of these systems is well-suited to studies using electrochemical and spectroelectrochemical methods. In Chapters 2 and 3 an understanding of the oxidation chemistry of manganese(III) porphyrins is sought. In Chapter 4 the chemistry of oxovanadium(IV), $[VO^{2+}]$, oxovanadium(V), $[VO^{3+}]$, and vanadium(IV), $[V^{4+}]$ and the naturally occurring dihydroxamic acid, rhodotorulic acid, is presented. The focus of this chapter is the characterization of the

oxidation state and coordination environment of several vanadium hydroxamate complexes. In Appendix 1 preliminary electrochemical studies of Cu^{2+}, Ni^{2+}, and Co^{3+} complexes of the ligand N,N'-di(2-aminoethylpyridyl)malondiamide are reported.

The electrochemical methods chosen for probing these systems are: 1) semiderivative cyclic voltammetry,[1] 2) spectroelectrochemistry using optically transparent thin-layer electrochemical cells (OTTLE)[2-4], and 3) coulometry using thin-layer techniques.[5] In this chapter I will briefly describe these methods and some of the experimental limitations imposed by the chemical properties of the systems being investigated. In addition a description of materials and instrumentation will be presented.

II. Semiderivative Linear Sweep Voltammetry

A. Background

Linear sweep voltammetry was employed by electrochemists as early as 1938.[6] The technique consists of varying the potential between an ideally polarizable (working) electrode and an idealy non-polarizable (reference) electrode as a linear function of time. The current between the working electrode and a second ideally polarizable (counter) electrode is then monitored. A convenient variation of the technique is to record the current-potential curve in one direction, and then to reverse the

direction of the potential sweep at some switching potential, E_λ, and record the *i*-E curve in the reverse direction. This is accomplished by applying a triangular wave form and is known as triangular wave or cyclic voltammetry.[7] A typical triangular wave form and a resulting current-potential (i-E) curve (cyclic voltammogram) for a diffusion controlled, reversible electron transfer is shown in Figure 1-1.

Early theoretical studies on this technique were reported independently by Randles[8] and Sevcik[7] in 1948. Still later the theory of irreversible and quasi-reversible charge transfer systems without complicating homogeneous kinetics was developed by Matsuda and Ayabe.[9] The theory for systems in which homogeneous solution reactions either precede or follow the charge transfer reaction was developed by Saveant, and coworkers,[10-12] and by Nicholson and Shain.[13] The technique of cyclic voltammetery has been described in numerous texts and reviews,[14-16] and so a detailed description will not be presented here. Instead the related technique of semiderivative voltammetry will be described in terms of its relationship to the more commonly used cyclic voltammetry.

FIGURE 1-1

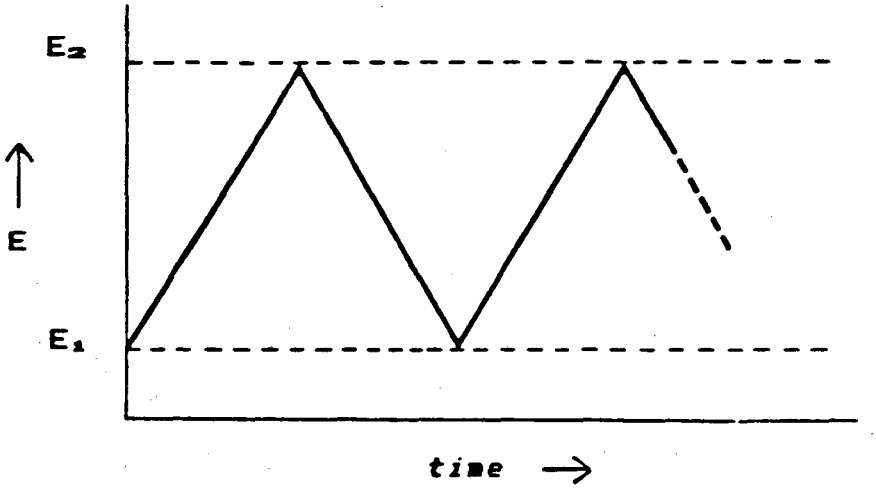

A. TRIANGULAR WAVE FORM

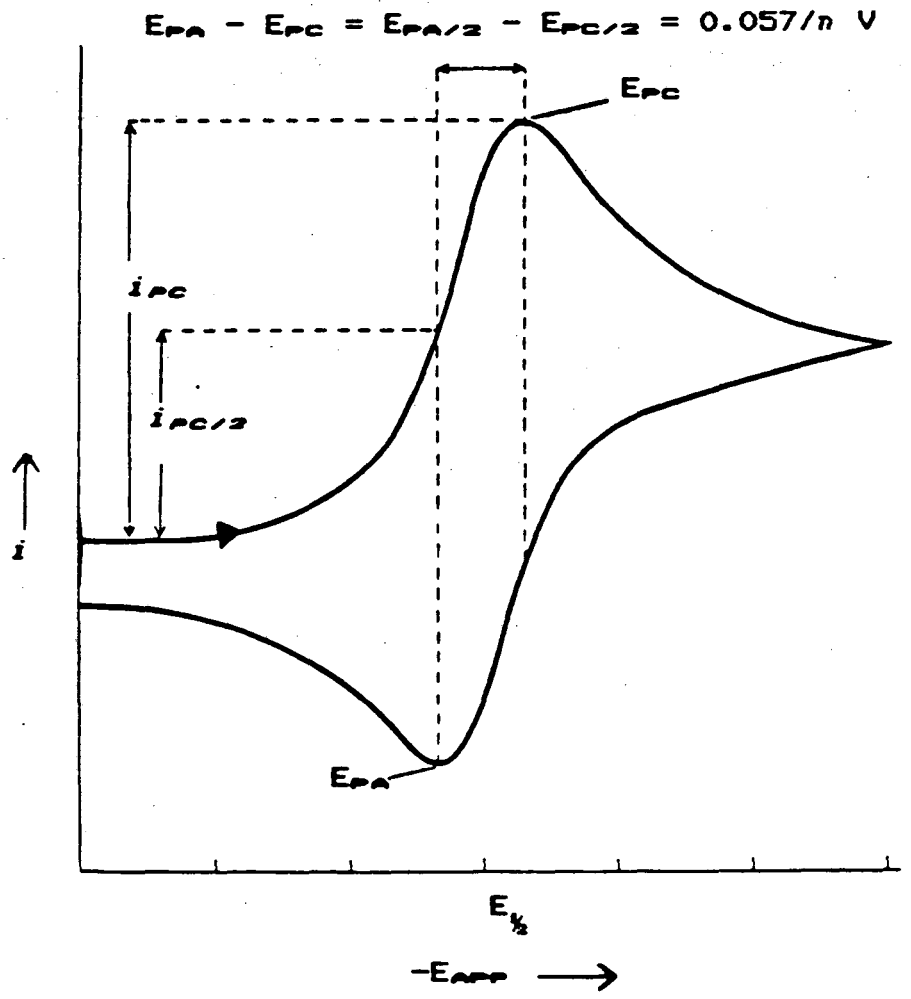

B. CYCLIC VOLTAMMOGRAM

In 1970 Oldham and Spanier[17] introduced the use of a semidifferentiation operator to relate the concentration of an electroactive species at the surface of an electrode to the faradaic current density. This method was presented as an improvement over the classical Fick's law approach for the prediction of voltammetric relationships. Shortly thereafter Oldham introduced a new method based on this approach, which he called semi-integral electroanalysis.[18,19] In later papers the related technique of semiderivative electroanalysis was introduced, and a theoretical treatment for diffusion controlled reversible and irreversibe charge transfer processes was presented.[20-24] Analog circuitry for implementing both semi-integral and semiderivative electroanalysis was described,[20,23] and recently an algorithm by which the value of the semiderivative may be calculated was reported.[25]

At about the same time Saveant and coworkers[26,27] proposed a similar transformation of the current-time curve using convolution integrals. This method is more general and is applicable to some systems with complicating homogeneous kinetics for which the semiderivative approach is not suitable. However, the simplicity of implementation of the semiderivative method rendered it the method of choice for the work presented in this dissertation.

In the method of semi-integral electroanalysis the

current, $i(t)$, is operated on by the semi-integral operator $d^{-\frac{1}{2}}/dt^{-\frac{1}{2}}$ to generate the function:[20,21]

$$\pi(t) \equiv \frac{d^{-\frac{1}{2}}}{dt^{-\frac{1}{2}}} i(t)$$

Oldham described this function, $\pi(t)$, as intermediate between $i(t)$ and the electric charge, $q(t)$:

$$q(t) \equiv \frac{d^{-1}}{dt^{-1}} i(t) \equiv \int_0^t i(t)dt$$

He also pointed out that this function could be regarded as the semiderivative of the charge, where the semidifferentiation operator is intermediate between the identity operator and differentiation:

$$i(t) \equiv \frac{d}{dt} q(t)$$

$$\pi(t) \equiv \frac{d^{\frac{1}{2}}}{dt^{\frac{1}{2}}} q(t)$$

Analysis of the $\pi(t)$ *vs* E_{app} curve for a reversible, diffusion controlled charge transfer at a planar stationary electrode has shown that the equation for the potential is given by:[21]

$$E = E_{\frac{1}{2}} + \frac{RT}{n\mathcal{F}} \ln\left[\frac{\pi_d - \pi}{\pi}\right]$$

It can be seen that this relationship is of the same form

as that obtained for classical d.c. polarography.[28] Hence, by analogy to d.c. polarography, differentiation of the $\psi(t)$-E curve yields a curve with a shape similar to that of a differential pulse polarogram. Thus, differentiation of the semi-integral yields the semiderivative of the current which is defined as:[23]

$$e \equiv \frac{d^{\frac{1}{2}} i}{dt^{\frac{1}{2}}} \equiv \frac{d\psi}{dt}$$

The wave shape for a diffusion controlled, reversible charge transfer is obtained by semdifferentiating the current with respect to the potential[22]:

$$e \equiv \frac{d^{\frac{1}{2}} i}{dE^{\frac{1}{2}}} = \frac{d\psi}{dE} = - \frac{n\mathcal{F}\psi_d}{4RT} \operatorname{sech}^2 \left[\frac{n\mathcal{F}}{} (E - E_{\frac{1}{2}}) \right]$$

This wave has a peak, E_p, equal to $E_{\frac{1}{2}}$, and a peak height, e_p, which is given by:

$$e_p = - \frac{n^2 \nu \& A D_o^{\frac{1}{2}} C_o^*}{4RT}$$

In Figure 1-2 an example of a typical cyclic voltammogram and the corresponding semi-integral and semiderivative voltammograms for a reversible, diffusion controlled one electron transfer are shown. The relationships for the peak height, peak width, and peak potential for reversible diffusion controlled charge transfers[23,24] are shown in Table 1-1. Shown for comparison are the

analogous relationships for cyclic voltammetr[9,13]

Inspection of Table 1-1 and Figure 1-2 reveals that the semiderivative technique offers a great improvement in resolution over cyclic voltammetry. In systems where successive charge transfer steps are involved this enhanced resolution becomes very important. In the semiderivative voltammogram the base line is essentially flat within the potential limits of the solvent. Thus, peak heights are much easier to measure than in cyclic voltammetry, where semi-empirical methods[29] are often used. The dependence of peak height on n^2 also makes the differentiation between a one-electron and a two-electron transfer less ambiguous than in cyclic voltammetry (However, the value of *n* is best determined by an independent method, such as coulometry.)

The manganese(III) tetraphenylporphyrin system described in Chapters 2 and 3 of this dissertation is a system for which the advantages offered by the enhanced resolution of the semiderivative method were especially important. Figure 1-3 shows a cyclic voltammogram and a semiderivative voltammogram of a typical manganese(III)-porphyrin. As will be shown in Chapter 2, it would have been difficult to interpret this system fully without the enhanced resolution offered by use of the semiderivative technique.

TABLE 1-1

CHARACTERISTICS OF SEMIDERIVATIVE CYCLIC VOLTAMMOGRAMS

COMPARED TO STANDARD CYCLIC VOLTAMMOGRAMS [a]

FEATURE	CYCLIC VOLTAMMETRY [13]	SEMIDERIVATIVE VOLTAMMETRY [24]
PEAK HEIGHT	$i_p(t)$, (μA)	$e_p(t)$, $\mu A \cdot s^{-\frac{1}{2}}$
EXPRESSION	$i_p(t) = kn^{3/2}\nu A D_o^{1/2} C_o^*$ [b]	$e_p(t) = \frac{n^2 \nu \vartheta A D_o^{1/2} C_o^*}{4RT}$
PEAK POTENTIAL	E_p, (Volts)	E_p, (Volts)
EXPRESSION	$E_{pc} = E_{\frac{1}{2}} + 1.1 \frac{RT}{n\vartheta}$	$E_p = E_{\frac{1}{2}}$
PEAK SEPARATION	ΔE_p, (Volts)	ΔE_p, (Volts)
EXPRESSION	$\Delta Ep = \lvert(E_{pa} - E_{pc})\rvert$	$\Delta E_p = (E_{pa} - E_{pc})$
	$= 2.2 \frac{RT}{n\vartheta}$	$= 0$
PEAK WIDTH PARAMETER	$\lvert(E_{p/2} - E_{\frac{1}{2}})\rvert$ (Volt)	E_{pw} [c] (Volts)
EXPRESSION	$\lvert(E_{p/2} - E_{\frac{1}{2}})\rvert = 1.09 \frac{RT}{n\vartheta}$	$E_{pw} = 3.53 \frac{RT}{n\vartheta}$

a For diffiusion controlled, reversible charge transfer.

b $k = 2.69 \times 10^5$

c E_{pw} = the peak width at half height of a peak e_p.

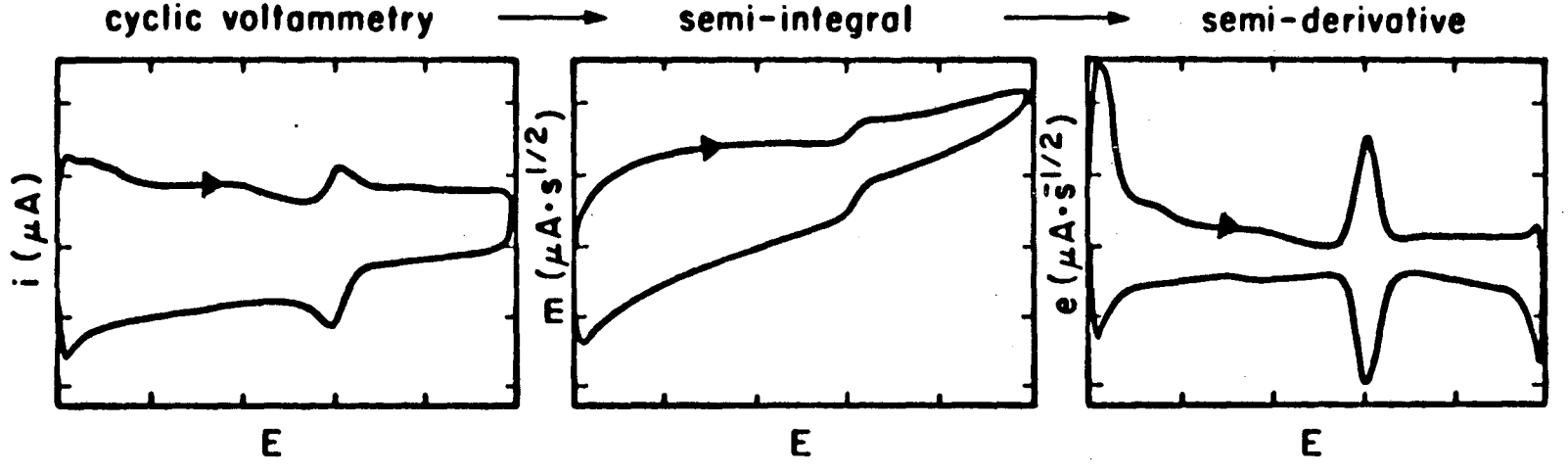

$i(t)$ $\quad m \equiv \dfrac{d^{-1/2}}{dt^{-1/2}}\, i(t) \equiv \dfrac{d^{1/2}}{dt^{1/2}}\, q(t) \quad e \equiv \dfrac{dm}{dt} = \dfrac{d^{1/2}\, i(t)}{dt^{1/2}}$

FIGURE 1-2

EFFECT OF SEMIINTEGRATION AND SEMIDIFFERENTIATION

FIGURE 1-3

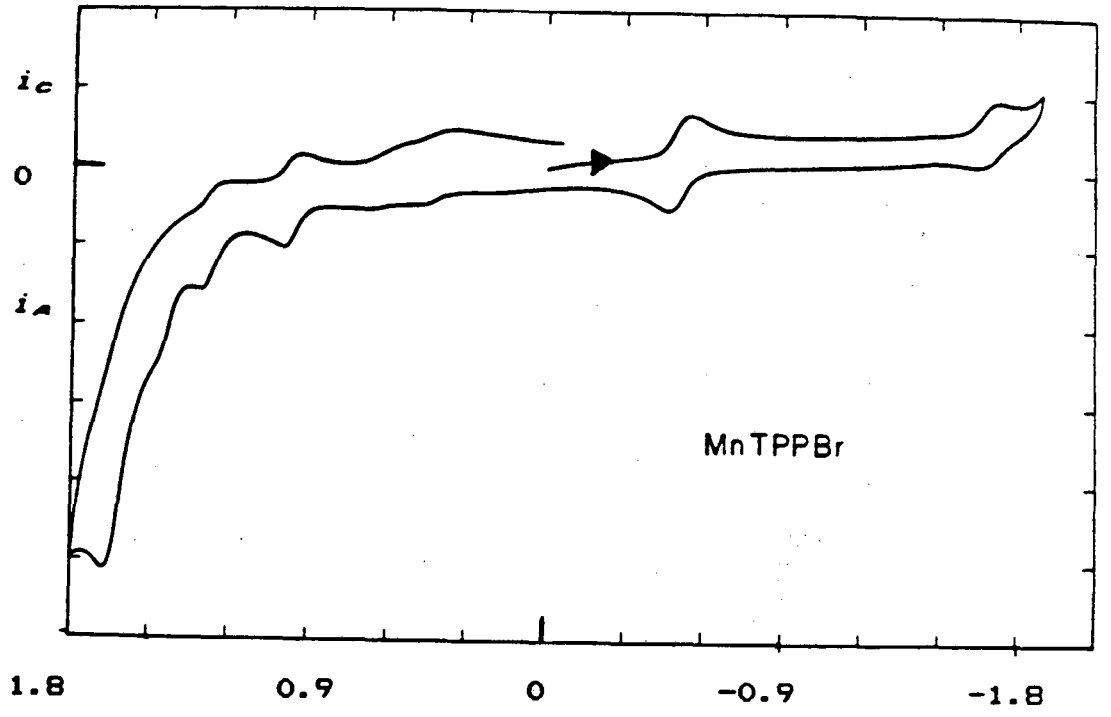

CYCLIC VOLTAMMOGRAM

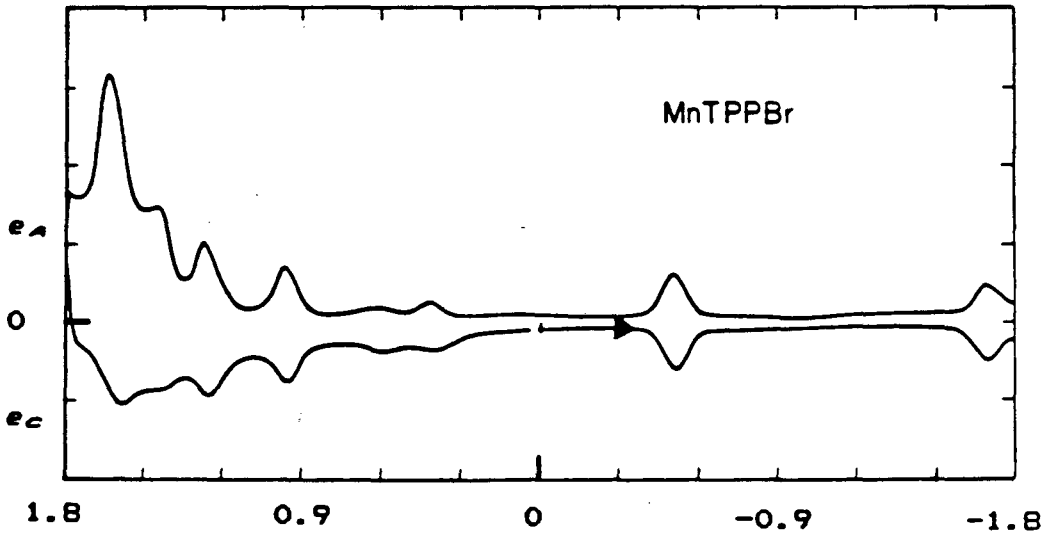

SEMIDERIVATIVE VOLTAMMOGRAM

B. Implementation

Experiments were performed using the Princeton Applied Research Model 173 Potentiostat/galvanostat interfaced with either a Model 176 current-follwer or a Model 179 digital coulometer. The Model 178 Electrometer Probe was used to monitor the potential between the working and reference electrodes, and the Model 175 Universal Programmer was used to generate the waveform. The semiderivative circuit (described below) was inserted in series between the voltage output of the current-follower and the Y-axis of the recording device The semiderivative circuit was fitted with a toggle switch to allow alternate recording of a standard i-E curve. For scan rates, $\nu \leq 200$ mV/s, a Hewlett-Packard Model 7040A XY recorder was used. A Tektronix Type 549 Storage Oscilloscope with a Type 1A1 Dual Plug-In Unit was fitted with an Oscillotron MII camera and was used to record scans at rates, $\nu \geq 500$ mV·s^{-1}.

The analog circuit used for transforming the i-E curve of cyclic voltammetry to the e-E curve of semiderivative voltammetry was based on those described by Oldham.[20,23] The semi-integrating circuit used was that Shown in Figure 10 of reference 20. (There is a resistor which is incorrectly labelled as 830 kΩ; the correct value is 8300 kΩ.[23]) The semidifferentiator was built using the circuit shown in Circuit B of Figure 4 in refence 23. A CA3140T operational amplifier and a 15 volt power supply

were used.

A comment on the output obtained using this particular circuit is in order here. The output of the semidifferentiating cicuit is given by:[23]

$$V_{out} = -(2.00\ s^{\frac{1}{2}})\ \frac{d^{\frac{1}{2}}}{dt^{\frac{1}{2}}}$$

Thus, the effect of the circuit is to multiply the sensitivity setting of the PAR 13 Potentiostat by a factor of 0.5 $s^{-\frac{1}{2}}$ and to change the sign of the current axis. Thus, a current range set to 10 μA full scale will actually give 5 μA full scale signal. The conventions used for the cathodic and anodic current directions for semiderivative voltammograms and cyclic voltammograms are opposite one another in all the results presented in this dissertation. Figure 1-4 illustrates the conventions used for *i*-E and *e*-E curves throughout tis work. All semiderivative voltammograms are scaled to the correct current output.

The accuracy of the semiderivative circuit was verified using a solution that was 1mM in Cu^{2+}, Pb^{2+}, Cd^{2+}, and Zn^{2+} with 0.1 M KNO_3 as electrolyte. Using a hanging mercury drop electrode of known surface area, semiderivative voltammograms at 200, 100, 50 and 20 $mV \cdot s^{-1}$ were recorded. The peak heights, peak widths, and relative peak potentials were measured and were found to agree, within experimental error, with the values predicted by theory. Likewise, a plot of e_p *vs* ν, the scan rate, was found to be linear as predicted. Similar results were obtained for

the ferrocene/ferrocenium couple in acetonitrile using the cell:

Pt	Ferrocene (1.0 mM) TEAP (0.1 M) CH_3CN	TEAP (0.1 M) CH_3CN	$AgNO_3$ (0.01 M) TEAP (0.1 M) CH_3CN	Ag

It is this system which is illustrated in Figure 1-4.

A schematic of the cell used for voltammetric studies is Shown in Figure 1-5. The working electrode was a platinum, planar electrode purchased from Bioanalytical Systems, Lafayette, Indiana. The tip of the Luggin capillary was placed close to the working electrode to minimize *i*R drop across the cell.[30] The Luggin capillary itself served as a salt bridge, and solutions were chosen to minimize liquid junction potentials.[41] A reference electrode appropriate to the solvent used in the body of the cell was used (See below). The counter electrode was a platinum wire sealed into the bottom of the cell. Solutions were typically degassed by bubbling for at least 10 minutes with argon gas prior to potential sweep experimentsand were kept under a blanket of argon during experiments.

FIGURE 1-4

CV and SD LSV CONVENTIONS

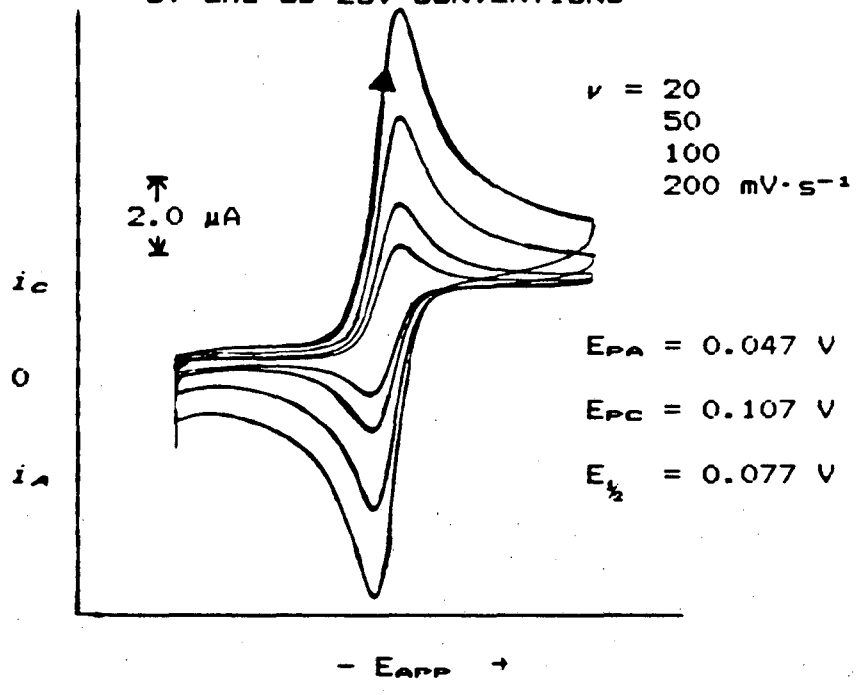

CYCLIC VOLTAMMOGRAM

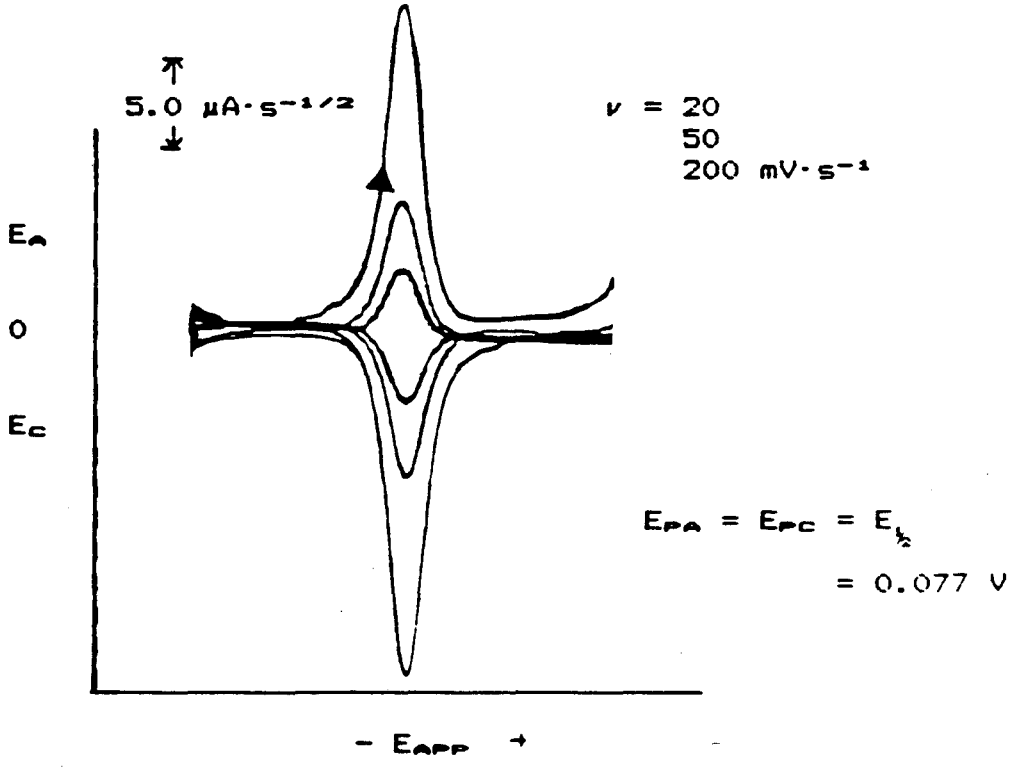

SEMIDERIVATIVE VOLTAMMOGRAM

FIGURE 1-5

CELL USED FOR SEMIDERIVATIVE VOLTAMMETRY

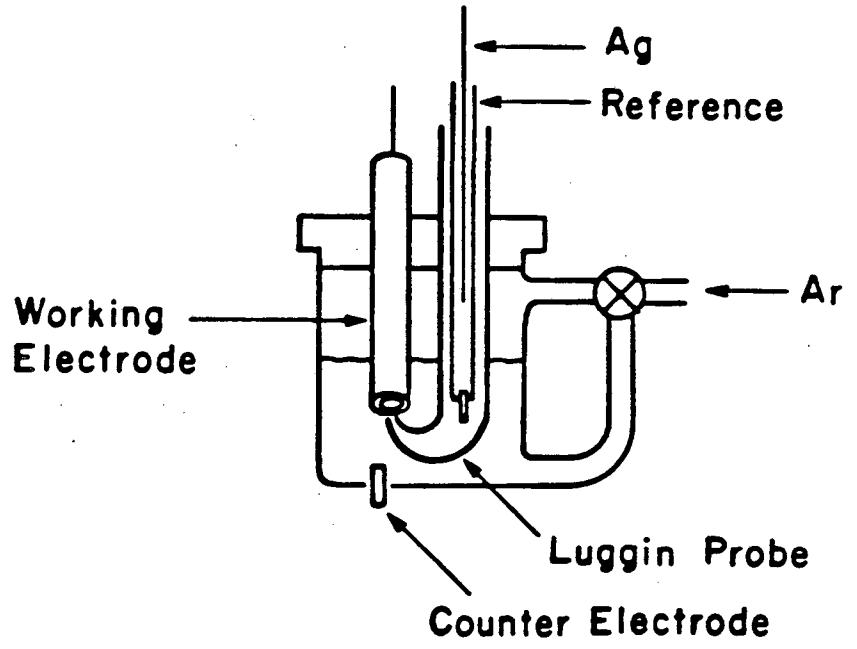

Working Electrode	Electro-active Species (~1 mM) Electrolyte (~1.0 M) Solvent	Electrolyte (~0.1 M) Solvent (Luggin Capillary)	Reference Solution	Ag Wire (Reference Electrode)

III. Spectroelectrochemistry

A. Background

Insight into the structure and oxidation state of a coordination compound can often be obtained from its UV/visible spectrum. Consequently, the ability to monitor changes in the UV/visible spectrum during an electrochemical experiment would be a valuable asset to the researcher. Spectroelectrochemical techniques provide just this ability.

The first optically transparent electrode (OTE) was a glass coated with a thin transparent film of antimony-doped tin oxide (Nesa Glass), introduced by Kuwana and coworkers.[31] Since that time a variety of other optically transparent electrodes have been reported.[32] The first optically transparent thin-layer electrode (OTTLE) was an electroformed gold mesh (500 to 2000 lines/in).[2] Since the spectroelectrochemical studies reported in this work employed OTTLE's, a brief description of the characteristics of electrochemical behavior in thin-layers of solution follows.

B. Thin-layer Electrochemistry

Thin-layer electrochemistry is performed in cells in which the reactant is confined in a thin layer, l, at the surface of the electrode.[5] If this layer is kept smaller than the diffusion layer which would exist under conditions of semi-infinite diffusion, the equations describing

results for a current-potential curve are greatly simplified. In Table 1-2 some of the important characteristics of thin-layer electrochemistry are listed. It is important to note that these equations apply for cells in which the total reactant present within the thin-layer cavity is constant:

$$C_O^\circ = C_O + C_R$$

In addition, the scan rate must be slow enough that the reactant is exhaustively electrolyzed on the time-scale of the experiment. This latter limiting condition is expressed by the relationship:[5]

$$| \nu | \leq \frac{RT}{nF} \frac{\pi^2 D}{3l^2} \log \left(\frac{2}{\epsilon + 1} - 1 \right)$$

where ν is the scan rate and ϵ is the relative error which can be tolerated in i_p (Table 1-2). For example, if l = 1×10^{-3} cm, $D = 10^{-5}$ cm$^2 \cdot$s^{-1}, $E^\circ - E(0) = -0.2$ V, and T = 298 K, then to achieve 1% accuracy:

$$| \nu | = 1.0 \log \frac{1 + \epsilon}{1 - \epsilon}$$

$$| \nu | \leq 10 \text{ mV} \cdot \text{1s}^{-}$$

TABLE 1-2

CHARACTERISTICS OF THIN-LAYER ELECTROCHEMICAL CELLS [5]

FEATURE	RELATIONSHIP
POTENTIAL SWEEP EXPERIMENTS	
PEAK HEIGHT	$i_p = \frac{n^2 \mathcal{F}^2 V C_o \nu}{4RT}$
PEAK POTENTIAL	$E_{pa} = E_{pc} = E^{o'}$
COULOMETRY	
TOTAL CHARGE [a]	$Q = n\mathcal{F}VC_o$ $= n\mathcal{F}N_o$
TIME OF ELECTROLYSIS [b]	$t = \frac{l^2}{\pi^2 D_o}$

a The charge, Q, may also be obtained from the time-integral of the current-potential curve.

b This represents a lower limit for an ideally reversible sytem and ignores any ohmic resistance in the cell.

A useful advantage of thin-layer electrochemistry is that, *n*, the number of electrons transferred in a reaction, can be determined simultaneously with a linear sweep experiment by determining the time-integral of the current-potential curve. Alternatively, a potential-step experiment may be performed and the value of *n* may be determined from the charge *vs* time curve. Since the time of electrolysis is very short for a thin-cell (see Table 1-2), coulometric experiments can be done more quickly than in conventional cells. A further advantage of the thin-layer cells is that interferences from surface-active impurities in the solution are minimized unless they are present in very high concentration. This is a result of the fact that the solution is confined within the thin-layer and impurities cannot continue to diffuse to the surface during the course of an experiment.

C. IMPLEMENTATION

1. Instrumentation and Determination of $E_{½}$

The same electrochemical isntrumentation described for SDLSV experiemnts was used. However, since thin-layer electrochemical cells were being used, the semi-derivative circuit was omitted. A Hewlett Packard Model HP 8450 UV/vis spectrometer interfaced with an X-Y plotter Model HP 7225B and a Model HP 82901M Flexible Disc Drive was used to measure, record, and store spectra. A Data Precision Model 3500 digital volt-ohm meter was used to monitor

the potential between the reference and working electrodes and was connected at the electrometer.

Spectroelectrochemical data were obtained from linear sweep voltammetric (LSV) experiments In a typical LSV experiment cyclic scans were done at 1 $mV \cdot s^{-1}$ between two potential limits which were chosen on the basis of the results of previously performed semi-derivative LSV experiments. A spectrum was recorded before any potential was applied, and the open circuit potential was noted. This "rest" potential was usually used as the initial potential for the first scan for a given cell. The spectrometer was programmed to measure and store on disk a spectrum at selected intervals, typically every 30 s (*i.e.* every 30 mV). Since the spectrometer program and the potential scan were started simultaneously, a record of absorbance as a function of applied potential was obtained.

To determine the potentials at which spectral changes occurred, plots of absorbance, A, *vs* E_{app} and dA/DE *vs* E_{app} from the linear sweep experiments were made at wavelengths chosen from the observed spectra. Whenever possible, these plots were made for two or more wavelengths.

Verification of this method for thin cells was obtained by determining the potentials $E_{1/2}$ for the $Mn^{III/II}$ couple for several manganese(III) porphyrins (See Chapter 2) from plots of dA/dE *vs* E_{app}. Excellent agreement was obtained with values of $E_{1/2}$ determined from *i*-E curves

recorded for the same cell. The values of $E_{\frac{1}{2}}$ were also in agreement with values determined from SDLSV experiments in conventional cells. Peak separations, E_{pw}, for both i-E and dA/dE *vs* E_{app} curves were larger than predicted by theory. This was due to large internal cell resistances typically observed in spectroelectrochemical thin-cells of similar design.[36]

2. Cell design

In Figure 1-6 is shown the design of the OTTLE cell, which is a sandwich cell based on the design reported by Bowden and Hawkridge.[3] . The only modifications of the design reported in the literature are that the ports for the Hamilton valves were machined as an integral part of the cell body, rather than being cemented on, and the port for the filling valve was placed on the side rather than in front.

Since the manganese porphyrin complexes were soluble only in nonaqueous solvents, different materials from those used by Bowden and Hawkridge[3] were required.[34] The cell body was constructed of ERTALYTE, a strong, machinable thermoplastic (manufactured by ERTA PlAstics of Tielt, Belgium)[44] which replaced the Lucite used for studies in aqueous media. Instead of Viton O-rings, RTV 112 Silicone Rubber (manufactured by General Electric) was used to make molded gaskets. (See Appendix 2 for method for making gaskets). The same RTV Silicone Rubber replaced Epoxy glue to seal both the quartz windows and the

threaded Luer fittings of the Hamilton valves.

2. Cell Preparation

Inert atmosphere techniques[35] were used to fill the cells. A typical arrangement of the spectroelectrochemical cell, degassing bulb, and Schlenk tube attached to a dual-manifold Schlenk line is shown in Figure 1-7.

Solutions are degassed using several freeze-pump-thaw cycles in the Schlenk tube, A. At the same time the OTTLE cell is prepared. Initially the reference compartment, K, is omitted from the cell. It is filled with reference solution and added later, as described below. The rest of the cell is assembled, fitted to the degassing bulb, and the unit attached to the Schlenk line. Valves E, F and G are opened, the whole unit is evacuated, and then it is filled with Argon. While under positive pressure of Argon, the reference electrode cap, J, is briefly removed and the filled reference compartment, K, is inserted. The cap, J is replaced and valve G is closed. The cell body is once again evacuated, and then valve F is closed. The degassing bulb, D, is then filled with Argon. Using a steel, hollow canula, C, the degassed solution in tube A is transferred to the degassing bulb using a pressure differential, achieved by inserting a venting tube into the serum stopper of the degassing bulb. Once the solution transfer is complete, valve E is opened to the Argon line of the Schlenk line, and the canula and vent

are removed. Valve E is then reclosed, and valve F is opened to permit filling of the cell body. Care must be taken at this point to avoid bubbles. Once the liquid has risen (as observed in the cell window), valve G is opened to allow partial filling of the compartment, L. The reference electrode cap, J, is cracked open momentarily to allow any bubbles to escape and the liquid to rise about halfway up into compartment L to insure adequate solution contact with the reference electrode. The reference cap is replaced and valve F is closed to separate the cell from the degassing bulb. Before removing the cell from the degassing bulb, it is advisable to verify that electrical contact has been made throughout the cell. This is done by measuring the resistance between each of the electrodes. The cell is then removed and placed in the cell compartment of the UV/visible spectrometer. (See Appendix 2 for the design of the cell holder made to fit the cell compartment of the Hewlett-Packard Model 8450 UV/visible spectrophotometer)

3. Calibration of Cell Volume (V) and Cell Thickness (l)

For interpretation of the results of spectroelectrochemical experiments, the cell volume, V, and the cell thickness, l, must be calibrated.

To determine the cell volume, V, a coulometric experiment is performed using an electroactive species of known value of n, the number of electrons transferred, in a solution of known concentration. Using the relation-

ship:[5]

$$Q = n\mathcal{F}VC_o$$

the value of V may be calculated. Since the thickness, *l*, corresponds to the optical path length, this value is easily determined by measuring the UV/visible spectrum of a solution of known concentration of a species for which extinction coefficients are known. The electrochemical electrode area , A_{ec}, may then be calculated. ($A_{ec} = V/l$). If the ratio of the electrochemical electrode area to the geometrical area (A_{ec}/A_{geom}) is constant for a given electrode material, this ratio may be used to calculate the cell volume, thus simplifying calibration of the cell for repeated experiments. The ratio of the electrochemical electrode area to the geoemtrical area may be calculated for a given electrode material. If this process is repeated several times with similar results, this calculated factor may be used to calculate the cell volume, thus simplifying calibration of the cell for repeated experiments.

For the work described in this dissertation, manganese(III) tetraphenylporphyrin acetate (See Chapter 3) was used to calibrate the cell thickness, *l*. Coulometric determination of the cell volume was accomplished using the $Fe(CN)_6^{3-}/Fe(CN)_6^{2-}$ couple, as suggested by DeAngelis and Heineman.[36] When the OTTLE material was gold mesh, a ratio $A_{ec}/A_{geom} \sim 1.65(\pm 0.05)$ was obtained. When reticu-

lated vitreous carbon (RVC) was used for the OTTLE, however, too much variation was observed in this ratio; thus, the cell volume had to be calibrated electrochemically.

For the gold minigrid electrodes the path length, l, varied from 0.10 to 0.14 mm, and the cell volume, V, varied from 20 to 40 µl. These values are typical of those reported in the literature for OTTLE's.[2,3,36] The RVC electrodes were typically 0.5 mm thick. Since this thickness exceeds the normal thickness required for a thin-layer electrode at the lowest attainable scan rate (1 $mV \cdot s^{-1}$), these cells were not used for determination of n. However, they were useful in monitoring spectral changes accompanying electrochemical processes.

FIGURE 1-6

DESIGN OF OPTICALLY TRANSPARENT THIN LAYER

ELECTROCHEMICAL CELL (OTTLE)

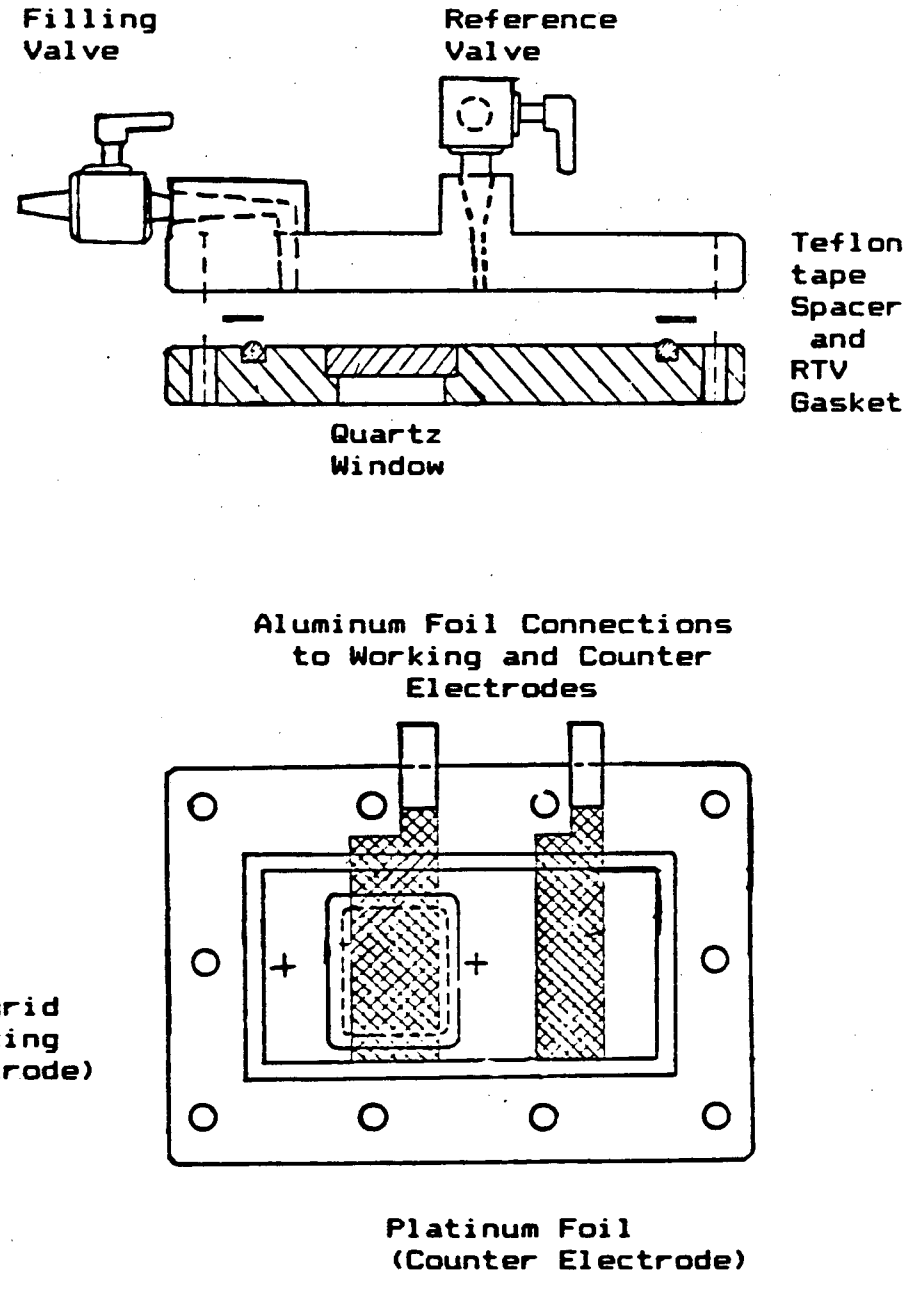

FIGURE 1-7

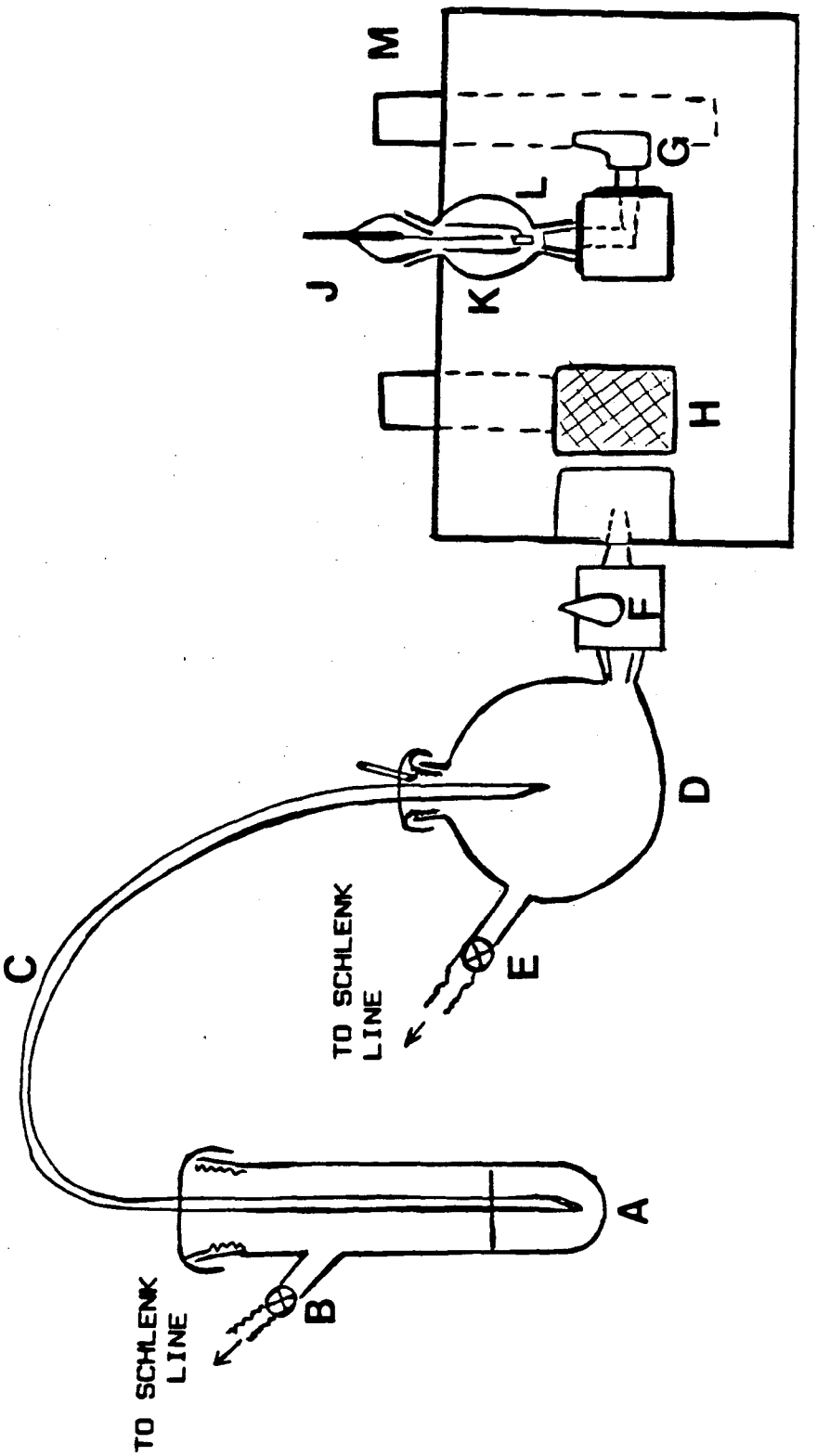

FILLING OF OTTLE

III. Materials

A. Solvents

The solvents acetonitrile, methylene chloride, dimethyl formamide (DMF), and dimethylsulfoxide (DMSO) were purchased from Burdick and Jackson. Before any new solvent container was opened, a round-bottomed 1- or 2-liter Schlenk flask[35] fitted with Kontes HyVac stopcocks was flame-dried, evacuated, and then filled with Argon. The solvent was then transferred from its container immediately after opening, into the prepared flask using inert atmosphere techniques.[35]

The solvents DMF, DMSO, and CH_2Cl_2 were stored over molecular sieves (Linde, 4Å). Background voltammograms (+2.3 to -2.3 V) for acetonitrile which had been stored in flame-dried flasks in an Argon atmosphere over either molecular sieves or alumina were compared with voltammograms obtained with solvent which had been stored in similar flasks without dessicant. No detectable difference was observed for either of these solvents. The UV/visible spectrum of the acetonitrile stored without desiccant remined unchanged (Absorbance < .01 from 200 to 800 nm using a 1.0 cm cell); solvent stored over dessicant, however, showed an increase in absorbance between 200 and 250 nm. Hence, acetonitrile was stored without desiccant to avoid any chemical decomposition. All solvents were stored in a dark place to minimize photo-initiated decomposition.

Water was triply distilled using a "pyrodistillation" apparatus similar to that described by Conway *et.al.*[37] The Pt-Rh gauze used by Conway as a catalyst for oxidation of organic contaminants was found to be unnecessary (See below), and so was omitted from the still. A schematic of the simplified design is shown in Appendix 2. The criterion for purity of the water was the ability to produce the current-potential profile for a clean Pt electrode in aqueous 1N H_2SO_4 between potential limits of 0.0 and 1.23 V *vs.* NHE.[37] (See Figure 1-8 and description below for cleaning Pt electrodes.)

B. Reference Electrodes

1. In Water

In aqueous solution a Ag/AgCl(s),KCl(1.0 M) reference electrode was used. To make the electrode a freshly cut piece of silver wire (Alfa, 0.25mm, 99.99% purity) was anodized in a solution of HCl (6.0 M) for ~ 30 s using a 1.5 V battery and a Pt wire as the cathode. The electrode compartment for both semiderivative and spectroelectrochemical experiments was a three mm (o.d.) glass tube into which a porous ceramic frit had been sealed. To avoid clogging the frit with electrolyte, the reference electrode compartments were stored in water when not in use. The electrode was calibrated against a Quinhydrone electrode[39,40] at pH 6.16 and 4.01. Its potential determined at 25° is +0.230(±.005 V) *vs* NHE.

2. In nonaqueous solvents

In nonaqueous solution reference electrodes appropriate to each solvent were used to minimize liquid junction potentials.[41] In acetonitrile, DMF and DMSO the reference electrode used was the half cell:[42]

$$Ag(s) \;|\; \begin{array}{l} AgNO_3 \ (0.01\ M) \\ TEAP \ (0.1\ M) \\ Solvent \end{array} \;||$$

The solvent in the reference compartment was the same as in the cell body and in the Luggin probe. For CH_2Cl_2 a silver wire in a solution of TBAP(0.1 M) in CH_2Cl_2 was used.[43] Each of these reference electrodes was calibrated *vs* the ferrocene/ferrocenium couple.[42] Again, in order to avoid clogging the ceramic frit, reference electrode compartments were rinsed with solvent after use and stored in acetonitrile when not in use.

C. Working Electrodes

1. Platinum

The working electrode for semiderivative voltammetric studies in nonaqueous solvents was a planar Pt (0.25 cm diameter) purchased from Bioanalytical Systems, Lafayette, Indiana; in aqueous studies a Pt electrode modified by adsortion of iodine on the clean Pt surface was used.

In both cases the Pt electrode was cleaned before each experiment by the procedure described below. The electrode was first polished by hand on a polishing cloth (Buehler) using an aqueous suspension of alumina (Buehler, 0.3 microns). The electrode was then rinsed with pyrolytically disttilled water (See above) and treated electrochemicaly. The cell used for this treatment was:

$$\text{Pt(s)} \;|\; H_2SO_4 \text{ (1 M)} \;\|\; H_2SO_4 \text{ (1 M)} \;\|\; \begin{matrix}\text{AgCl(s)} \\ \text{KCl (1.0 M)}\end{matrix} \;|\; \text{Ag(s)}$$

Initially a potential of 1.4 V was applied for ~10 minutes or until the cuurent had decayed to $\lesssim$ 40 μA. The potential was then stepped to 0.0 V for ~5 min or until the current had again decayed to $\lesssim$ 40 μA. The potential was then swept between potential limits of +1.2 and −0.23 V *vs* the Ag/AgCl, KCl (1.0 M) reference electrode, at a scan rate of 200 $mV \cdot s^{-1}$ for 20 to 30 successive cycles or until the pattern ascribed to a clean Pt electrode[36] was observed and remained unchanged. A typical voltammogram recorded for a clean Pt electrode is shown in Figure 1-8A.

2. Modified Platinum Electrode

For voltammetric studies of the vanadium/rhodotorulic acid system (Chapter 4) aqueous solutions at positive potentials (to ~ $\gtrsim$ 0.8 V at low pH) were required. For this purpose the Pt electrode described above was modified by adsorbing iodine on the surface, a method

which had been previously demonstrated using thin-layer electrochemical cells.[38] After cleaning the Pt electrode and treating it electrochemically as described above, the electrode was immersed in a solution of concentrated NaI for ~2 minutes. It was then removed, rinsed with pyrolitically distilled water, and placed in the same cell used for the electrochemicl cleaning. The potential was swept between limits of +1.0 V and -0.23 V (the initial potential was 0.3 V) for 5 to 10 cycles or until a flat voltammogram was observed as shown in bigure 1-8B. The electrode was once again rinsed with distilled water and was used immediately. The stability of the electrode was verified by repeating background potential sweeps at the end of each experiment.

SUMMARY

In this chapter I have presented a brief background and description of the electrochemical methods used in this research with particular emphasis on semiderivative voltammetry and spectroelectrochemistry in thin-layer cells (OTTLE). A description of solvent treatment, reference electrodes and working electrodes has also been presented. Further experimental details related to the specific systems being discussed will be presented in chapters 2, 3 and 4.

FIGURE 1-8

A. PLATINUM ELECTRODE IN 1N H_2SO_4

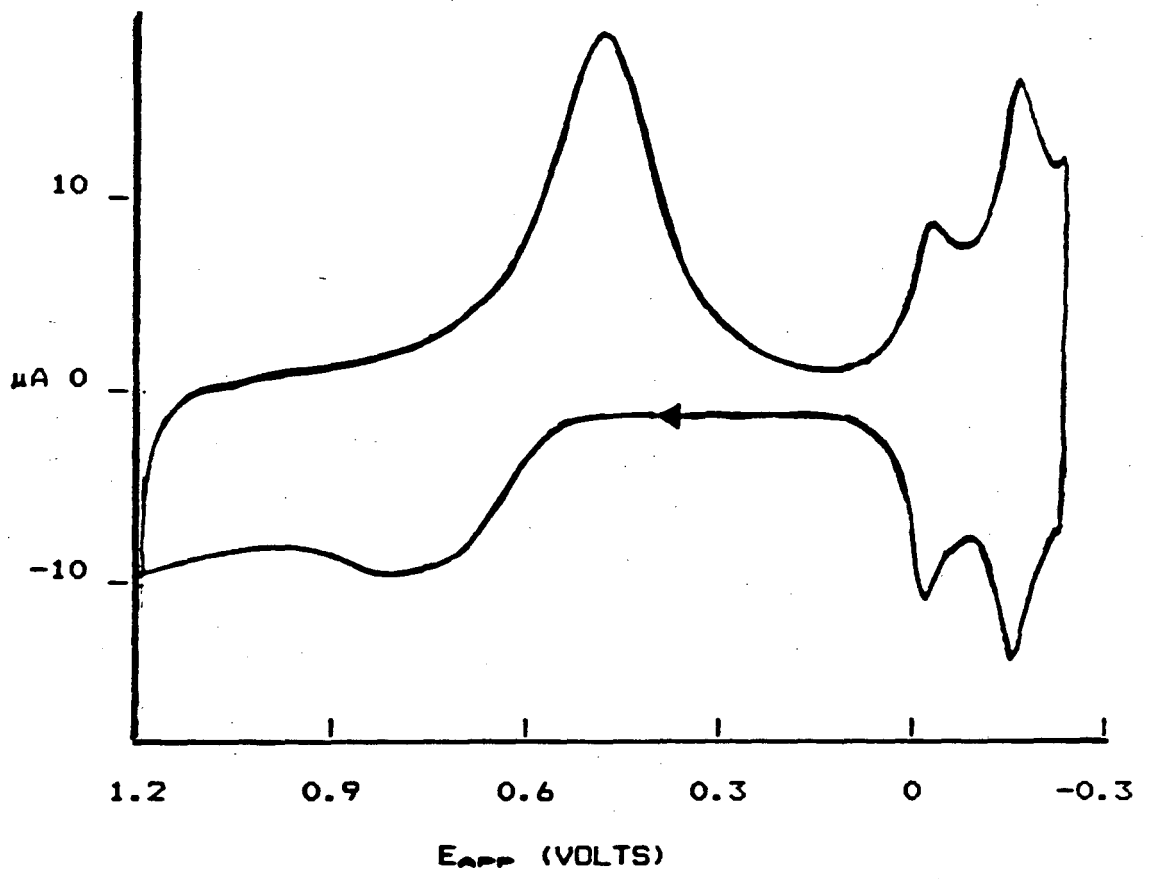

B. PLATINUM ELECTRODE MODIFIED BY ADSORBTION OF IODINE

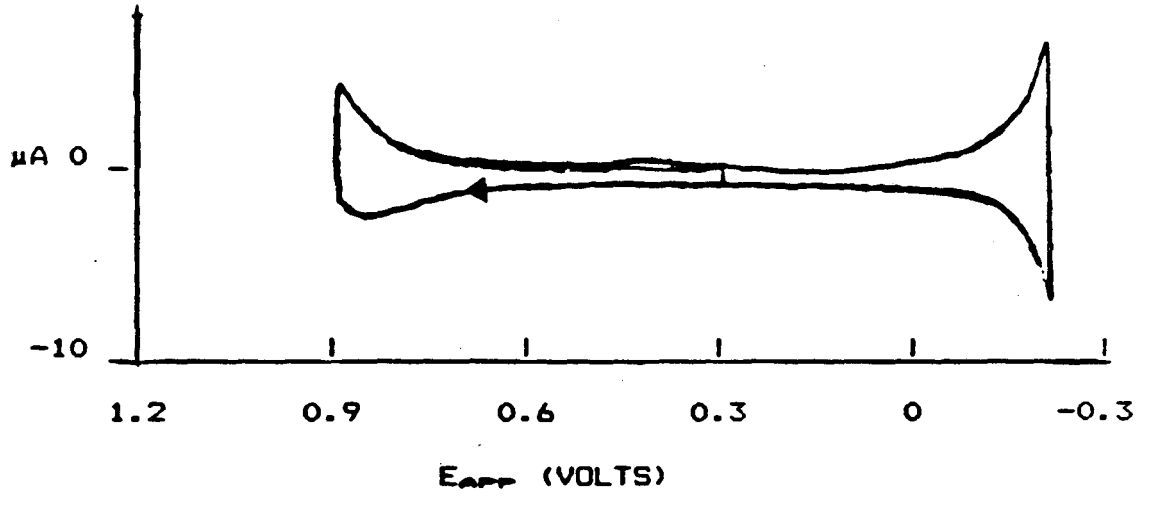

REFERENCES

(1) Goto, M.; Ishii, D. *Electroanal. Chem.*, 1975, *61*, 361-365.

(2) Murray, R.W.; Heineman, W.R.; O'Dom, G.W. *Anal. Chem.*, 1967, *13*, 1666-1668.

(3) Hawkridge, F.M.; Bowden E.F. *J. Electroanal. Chem.*, 1981, *125*, 367-386.

(4) Hawkridge, F.M., personal communication.

(5) a) Hubbard, A.T. *CRC Critical Rev. Anal. Chem.*, 1973, 3, 201-241.

b) Hubbard, A.T.; Anson, F.C. *Electroanal. Chem.* 1971, *4*, 129- 214.

(6) Matheson, L.A.; Nicholson, N. *Trans. Electrochem. Soc.*, 1938, *73*, 193-210.

(7) Sevcik, A. *Coll. Czech. Chem. Comm.*, 1948, *13*, 349-377.

(8) Randles, J.E.B. *Trans. Faraday Soc.*, 1948, *44*, 327-338..

(9) Matsuda, H.; Ayabe, Y. *Z. Electrochem.*, 1955, *59*, 494-503.

(10) Saveant, J.M.; Vianello, E. *Electrochim. Acta*, 1963, *8*, 905-923.

(11) *Ibid.*, 1967, *12*, 629-646.

(12) Nadjo, L.; Saveant, J.M. *J. Electroanal. Chem.*, 1973, *48*, 113-145.

(13) Nicholson, R.S.; Shain, I. *Anal. Chem.*, 1964, 36, 707-723.

(14) Z. Galus, "Fundamentals of Electrochemical Analysis," Wiley, London, 1976.

(15) W.J. Albery, "Electrode Kinetics," Academic Press, New York, 1975.

(16) A.J. Bard and L.R. Faulkner, "Electrochemical Methods: Fundamentals and Applications," Wiley, New York, 1980.

(17) Oldham, K.B.; Spanier, J. *J. Electroanal. Chem.*, 1970, *26*, 331-341.

(18) Oldham, K.B. *Anal. Chem.*, 1972, *44*, 196-198.

(19) Grenness, M.; Oldham, K.B. *Anal. Chem.*, 1972, *44*, 1121-1129.

(20) Oldham, K.B. *Anal. Chem.*, 1973, *45*, 39-47.

(21) Goto, M.; Oldham, K.B. *Anal. Chem.*, 1976, *48*,1671-1676.

(22) Goto, M.; Ishii, D. *Electroanal. Chem. and Interfac. Electrochem.*, 1975, *61*, 361-365.

(23) Dalrymple-Alford, P.; Goto, M.; Oldham, K.B. *Anal. Chem.*, 1977, *49*, 1390-1394.

(24) Dalrymple-Alford, P.; Goto, M.; Oldham, K.B. *J. Electroanal. Chem.*, 1977, *85*, 1-15.

(25) Oldham, K *J. Electroanal. Chem.*, 1981, *121*, 341-342.

(26) Andrieux, C.P.; Nadjo, L.; Savéant, J.M. *J. Electroanal. Chem.*, 1970, *26*, 147-188.

(27) Imbeaux, J.C.; Savéant, J.M. *J. Electroanal. Chem.*, 1973, *44*, 169-187.

(28) L. Meites. "Polarographic Techniques," 2nd ed.,

Wiley-Interscience, 1958, Chapter 2 and references therein.

(29) Nicholson, R.S. *Anal. Chem.*, 1968, *38*, 1406.

(30) Barnatt, S. *J. Electrochem. Soc.*, 1952, *99*, 549-553.

(31) Kuwana, T.; Darlington, R.K.; Leedy, D. W. *Anal. Chem.*, 1964, *36*, 2023-2025.

(32) Kuwana, Heineman, T.; Heineman, W.R. *Acct. Chem. Res.*, 1976, *9*, 241-248.

(33) Reilly, C.N. *Rev. Pure Appl. Chem.*, 1968, *18*, 137-151.

(34) The alternate materials used for construction of cells for spectroelectrochemical studies in non-aqueous solvents were all suggested to the author by Professor Fred Hawkridge of Virginia Commonwealth University, Richmond, VA. The ERTALYTE used for construction of the cell bodies was a generous gift from Professor Hawkridge.

(35) Shriver, D.F. "The Manipulation of Air-Sensitive Compounds". New York, N.Y., McGraw-Hill, 1969.

(36) DeAngelis, T.P.; Heineman, W.R. *J. Chem. Educ.*, 1976, *53*, 594-595.

(37) Conway, B.E.; Angerstein-Kozlowska, Sharp, W.B.A.; Criddle, E.E. *Anal. Chem.*, 1973, *45*, 1331-1336.

(38) Hubbard, A.T. *Acct. Chem. Res.*, 1980, *13*, 177-184.

(39) Ives, D.J.C. and Janz, G.J. "Reference Electrodes: Theory and Practice", Academic Press, New York, 1961, Chapter 6.

(40) Bates, R.G. "Determination of pH: Theory and Practice", New York, Wiley, 1973, Chapter 9.

(41) Cox, B.G.; Parker, A.J.; Waghorne, W.E. *J. Amer. Chem. Soc.*, 1973, 95, 1010-1014.

(42) Diggle, J.W.; Parker, A.J. *Electrochim. Acta*, 1973, *18*, 975-979.

(43) Bard, A.J., Personal Communication.

(44) ERTALYTE may be purchased from Chemplast, Inc., 150 Dey Road, Wayne, New Jersey, 07407.

CHAPTER 2

Voltammetric Studies of Manganese Porphyrin Oxidations Using Semi-Derivative Linear Sweep Voltammetry

INTRODUCTION

Porphyrins, metalloporphyrins, and their partially reduced relatives, the chlorins, serve as the prosthetic group for numerous proteins and play an important role in such diverse functions as oxygen binding in hemoglobin,[1] electron transfer in the cytochromes,[2] oxygen transfer in oxygenases,[3] and light harvesting in photosynthetic plants.[4] Iron is typically found as the metal in the porphyrin, or heme, unit of hemoglobin and the cytochromes, while magnesium is found in chlorophylls. A variety of synthetic porphyrin ligands has been made, however,[5] and almost every metal on the Periodic Table has been substituted into the porphyrin ring.[6]

In recent years a number of studies have appeared in which synthetic manganese(III)porphyrins have been demonstrated to be catalysts for transfer of substituents to alkanes.[7-13] Since oxidized manganese porphyrins have been proposed as intermediates in these catalytic reactions, much work has been done to isolate oxidized manganese porphyrin intermediates.[14-22] In another set of studies, manganese porphyrins have been shown to participate in the photon initiated oxidation of water.[24-22] Again, oxidized manganese porphyrins have been proposed as inter-

mediates, and studies have been done to try to characterize and identify these species.[26]

Although, in the studies mentioned above, the chemical oxidation of a number of manganese porphyrins was examined, little had been done to explore the electrochemistry of manganese porphyrin oxidations. Hence, an electrochemical study of the oxidation of the synthetic porphyrin, manganese(III) 5, 10, 15, 20- tetraphenylporphyrin, $XMn^{III}TPP$, where X = F^-, Cl^-, Br^-, I^-, CH_3COO^-, N_3^-, OCN^-, NO_2^-, ClO_4^-, OH^-, and BF_4^-, and PF_6^- was under taken. The goals in this research were:

1) To learn how many oxidation states are accessible using semi-derivative linear sweep voltammetry (SDLSV) and the conditions described in the experimental section.

2) To determine the reduction potentials and n, the number of electrons transferred, for the various oxidation processes which are observed.

3) To gain some insight into the conditions that control which products are formed by chemical oxidation.

4) To observe the electronic spectra of any of the oxidized products observed in (1). *i.e.* to characterize chemically, the oxidation products observed in (1)

5) To use the information obtained from these electrochemical studies to predict possible conditions for obtaining other oxidation products.

This study consisted of two principal phases: the first used SDLSV to identify and characterize the oxida-

tion processes which can be observed for $XMn^{III}(TPP)$ as a function of the axial ligand, X^-; the second involved a series of spectroelectrochemical studies of the processes observed in the LSV studies using the thin-layer techniques described in Chapter 1. In this chapter I will summarize the known manganese porphyrin chemical and electrochemical oxidation chemistry , describe the SDLSV experiments, and discuss those results. In Chapter 3 I will describe and discuss the spectroelectrochemical studies in light of the known chemical oxidation chemistry of manganese porphyrins.

MANGANESE PORPHYRIN OXIDATION CHEMISTRY

1. Chemical Oxidants

In Figure 2-1 the reader will find structural formulae for some naturally occurring and synthetic porphyrins. The synthetic porphyrin, 5, 10, 15, 20 - tetraphenylporphyrin (H_2TPP) and some of its phenyl-substituted derivatives was chosen for these studies because: 1) it is easy to synthesize; 2) its manganese(III) complexes are soluble in acetonitrile, the solvent of choice for our electrochemical studies; 3) the ligand itself and its manganese(III) complexes are stable to air and light; 4) chemical oxidations had been carried out on this porphyrin.

FIGURE 2-1

PORPHYRIN STRUCTURES

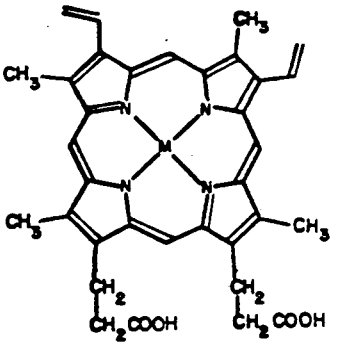

PROTOPORPHYRIN IX

(M = Fe for naturally occurring hemes)

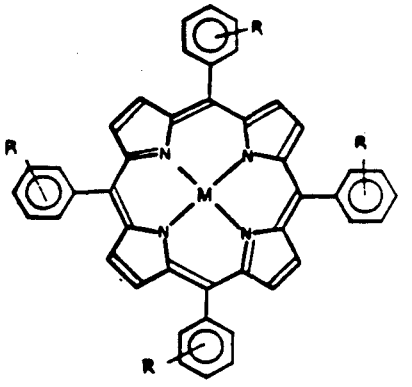

TETRAPHENYLPORPHYRINS

R = H (H_2TPP)

= *p*-OCH_3 (H_2T*p*-OMePP)

= *m*-CH_3 (H_2T*m*-TPP)

= *m*-CF_3 (H_2T*m*CF_3PP)

(X)MANGANESE(III)TETRAPHENYLPORPHYRIN

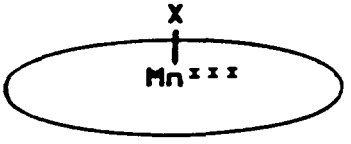

X = F^-, Cl^-, Br^-, I^-, AcO^-, OCN^-, NO_2^-, CN^-, ClO_4^-, BF_4^-, PF_4^-

A brief description of some of the pertinent chemistry of manganese porphyrins follows. As one can see from Figure 2-1, the porphyrin ligand is a planar, macrocyclic, aromatic, dibasic molecule, which, when deprotonated, forms a tetraaza dianion. Thus, porphyrin complexes with divalent metal ions are neutral. When manganese(II) is complexed by a porphyrin in air, the manganese is autooxidized to Mn(III) to yield porphinatomanganese(III)$^+$, ([Mn^{III}Porphyrin]$^+$).[27,28] Thus, whenever we refer to "oxidized manganese porphyrins", we will mean *oxidized relative to the air-stable [Mn^{III}Porphyrin]$^+$.* The positive charge may be neutralized by a complexing anion, X^-, such as a halide or pseudohalide, which binds axially to the Mn(III) central metal ion perpendicular to the plane of the porphyrin. In a weakly coordinating solvent, the resulting complex is five-coordinate, having approximately C_{4v} symmetry and may be formulated as d^4, *h.s.* XMn^{III}Porphyrin. In a strongly coordinating solvent such as CH_3OH, pyridine, or DMSO, a d^4, *h.s.*, six-coordinate complex, (X)(S)Mn^{III}Porphyrin, probably forms.[29] In the presence of an axial ligand of sufficiently high ligand-field strength, such as imidazolate, a *l.s.* Mn^{III}porphyrin has been observed.[30] If the axial ligand is a weakly coordinating anion, such as ClO_4^-, or BF_4^-, a salt, [Mn^{III}Porphyrin$^+$][X^-], results.

When a metalloporphyrin undergoes oxidation or reduction, whether by chemical or electrochemical means, the

electron transfer reaction may take place at either the metal center or on the porphyrin ring itself. In the case of manganese porphyrins, examples of both kinds of reaction have been observed. (See below).

Several research groups have reported isolating oxidized manganese porphyrins. Among the products characterized and reported, several clearly involve oxidation at the metal center. Indeed, both manganese(IV)[14-17] and manganese(V)[19-21] complexes have been isolated and fully characterized. In other studies the one-electron oxidation product was Xmanganese(III)tetraphenylporphyrin$^{+\cdot}$, the porphyrin π radical cation.[21,22] Other workers have observed the manganese(III)porphyrin π-radical cation in solution and have characterized it by its electronic spectrum.[24] In our laboratories spectra of oxidized $Mn^{III}TPP$ have been observed which could not be clearly identified as any known oxidation product.[31] It is possible that these spectra are those of a 2-electron oxidation product, such as $XMn^{III}TPP^{++}$, the manganese(III)porphyrin dication.

In Table 2-1 the reader will find a summary of the oxidation products observed to date as well as information on the reaction conditions used and the method(s) of characterization.

TABLE 2-1

MANGANESE(III)PORPHYRIN OXIDATION PRODUCTS

OXIDIZED PORPHYRIN	STARTING MATERIAL	SOLVENT	OXIDANT	REFERENCE
Mn(IV)PORPHYRINS				
$[N_3Mn^{IV}TPP]_2O$ [a]	$N_3Mn^{III}TPP$	PhCl Hexane	PhIO	14
$[(OCN)Mn^{IV}TPP]_2O$ [b]	$(OCN)Mn^{III}TPP$	PhCl Hexane	PhIO	14
$(MeO)_2Mn^{IV}TPP$ [a]	$(OAc)Mn^{III}TPP$ NaOMe	MeOH	PhIO	15
$(OCN)_2Mn^{IV}TPP$ [a]	$(MeO)_2Mn^{IV}TPP$ HNCO	$MeCl_2$ Hexane	--	16
$(N_3)_2Mn^{IV}TPP$ [b]	$(MeO)_2Mn^{IV}TPP$	$MeCl_2$ MeOH	--	16
$Cl_2Mn^{IV}TPP$ [c]	$(MeO)_2Mn^{IV}TPP$ HCl or Me_3SiCl	$MeCl_2$ Hexane	--	31
$(OAc)_2Mn^{IV}TPP$ [c]	$(MeO)_2Mn^{IV}TPP$ HOAc (2-4 eq)	CCl_4 hexane	--	31
$(NC)_2Mn^{IV}TPP$ [c]	HCN	CCl_4	--	21
$[(PhI(X)O)Mn^{IV}TPP]_2O$ X = Cl^-, Br^- [c]	$XMn^{III}TPP$ X = Cl^-, Br^-	PhCl Heptane	PhIO	18
$[PhI(OAc)O]_2Mn^{IV}TPP$ [c]	$(OAc)Mn^{III}TPP$	PhCl	PhIO	17

TABLE 2-1 (cont'd)

OXIDIZED PORPHYRIN	STARTING MATERIAL	SOLVENT	OXIDANT	REFERENCES
Mn(V)PORPHYRINS				
$NMn^{V}TPP$[b]	(MeO)Mn^{III}TPP NH_3/H_2O	$MeCl_2$	NaOCl	19
$NMn^{V}OEP$[b]	(MeO)Mn^{III}OEP NH_3/H_2O	$MeCl_2$	NaOCl	19
$NMn^{V}OEPMe_2$[b]	$NMn^{V}OEP$	THF	--	21
$NMn^{V}TPP$[a]	$XMn^{III}TPP$ (X = Cl^-, Br^-) excess OAc^-,NH_3	$MeCl_2$	PhIO	20
Mn^{III}PORPHYRIN$^{+\cdot}$ (PORPHYRIN π-RADICAL CATION)				
$[XMn^{III}TPP]^{+\cdot}$ [b]	$XMn^{III}TPP$	$MeCl_2$ Benzene	Phenoxathiin hexachloro-antimonate	22 23 26 50

a Isolated and characterized by X-ray Crystallography.

b Isolated and characterized by elemental analysis and spectroscopic methods.

c Characterized in solution by spectroscopic methods, but not isolated in pure form.

2. Electrochemistry of Manganese Porphyrins

The electrochemistry of porphyrins and metalloporphyrins has been extensively studied in the past 20 years.[27,28,32,35-50] In the early voltammetric studies, polarography (*i.e.* voltammety at a dropping mercury electrode) was used to investigate the successive one-electron reductions of a variety of porphyrins and their complexes with metal ions[32,33]. Later investigators used cyclic voltammetry (CV or CLSV) at solid electrodes to observe both oxidations and reductions and to investigate the kinetics of heterogeneous electron transfer[35-50]

These early studies reveal that the porphyrin ligand itself can be reduced by four successive one-electron transfers to yield mono-, di-, tri-, and tetra- anions.[32,33] Likewise, the ligand can be oxidized in at least two steps to yield mono- and di- cations. Redox reactions have also been observed at the central metal-ion in metalloporphyrins.[32,33,35,38,39] Thus, a fundamental problem in electrochemical studies of metalloporphyrins is to distinguish between porphyrin-based and metal-based electron transfer reactions. For this purpose spectroscopic methods and magnetic studies of the reduced or oxidized species are useful.

The earliest report of reduction potentials for manganese porphyrins was based on potentiometric, spectral titrations of Xmanganese(III)hematoporphyrinIX dimethyl ester, $XMn^{III}Hm$, (X = Cl, OAc^-).[27,28] A pH-dependent,

one-electron reduction which was identified by the electronic spectrum of the product as the Mn(III) → Mn(II) couple was observed. Likewise, a pH-dependent, one-electron oxidation was observed. The oxidative titration was followed by visible spectroscopy, the spectrum of the oxidation product reported, and the observed oxidation assigned as the Mn(III) → (IV) couple with no further characterization.

Boucher and Garber[38] were the first to report a systematic voltammetric study of manganese(III) porphyrins in nonaqueous solvents. Using polarography they examined the reductions of several Mn(III)porphyrins in DMF or CH_3CN as a function of axial ligand, X^-, and observed reductions at potentials near those observed by others [32,33] for ring reductions of other metalloporphyrins. They also observed a wave for each complex at potentials much less negative than those of typical ring reductions. These they characterized by visible spectroscopy and assigned to the Mn(III) → Mn(II) reduction. The half-wave potentials for the ring reductions were independent of the anion, X^-, while those for the manganese reduction were not. The order of the half-wave potential, $-E_{\frac{1}{2}}$, for the $Mn^{III/II}$ couple for several porphyrins is:

$$F^- > OAc^- \gtrsim N_3^- > OCN^- > OH_- > Cl^- > SCN^- \gtrsim Br^- > I^-$$

The authors noted that this order corresponds to the stability of the then known manganese(III) porphyrins.

They also noted an ordering of $-E_{1/2}$ for different porphyrins which corresponds to the ordering of the pKa's of the ligand.

Kadish and coworkers have subsequently investigated the effects of solvent, counterion and various nitrogenous bases on the electrochemistry of the Mn(III) → Mn(II) reduction potential. They confirmed the assignment of the reported couple to metal reduction, measured stability constants for axial ligation by a number of nitrogenous bases, and investigated the kinetics of electron transfer for the reaction as a function of solvent, counterion, porphyrin ligand substituent, and basicity of various nitrogenous bases.[42-44]

The electrochemistry of manganese(III)porphyrin oxidations has been much less extensively investigated than has the reduction chemistry. This is at least partly due to the relatively high potentials at which these reactions take place (see Table 2-2). Fuhrhop and coworkers[39] reported observing an oxidation at 1.12 V *vs. SCE* for (OH)Mn(III)OEP in butyronitrile; they reported a second process at > 1.4 V. For each of these observations no further characterization was reported, nor was an assignment of the reaction to ligand or metal oxidation offered. After we had begun the studies reported in this dissertation, Kadish and Kelly[49] reported one-electron oxidations for $XMn^{(III)}TPP$ in $MeCl_2$, $EtCl_2$, PhCN, CH_3CN and PrCN for X = ClO_4^-, Cl^-, Br^-, I^-, SCN^- and N_3^-. They assigned this

reaction to the formation of the porphyrin π radical cation, based on the constancy of the observed reduction potential with X. Consistent with this assignment is the report of an electrochemical synthesis of [ClMn^{III}Por][ClO$_4$], where Por = TPP, (*p*-OCH$_3$)TPP, or OEP. The product was characterized by EPR, UV/vis and infrared spectrosopy and identified as the π radical cation.

As pointed out earlier, a number of Mn(IV) and Mn(V) porphyrins have been synthesized using chemical oxidants such as C$_6$H$_5$IO and NaOCl. However, no definitive evidence for a metal-centered electrochemical oxidation of a Mn(III)porphyrin had been reported. Furthermore, the reduction potential(s) of the most commonly used oxidant, C$_6$H$_5$IO, had not been investigated. Indeed, such studies would be difficult because of the insolublity of the parent compound, C$_6$H$_5$IO, and the reactivity of its derivatives.[51]

The purpose of this research was to extend the knowledge of the potentials at which Mn(III)porphyrins are oxidized. It was postulated that at least two oxidations should be observable if the appropriate experimental conditions were chosen. In this chapter I will describe the SDLSV studies in which oxidations as a function of the anion, X$^-$ were investigated. In Chapter 3 I will describe the spectroelectrochemical studies which were done in order to characterize and confirm the assignments of the observed oxidations

EXPERIMENTAL

MATERIALS

Solvents used for electrochemical studies were treated as described in Chapter 1. All other solvents were reagent grade and used as received.

The supporting electrolytes, TEAP, $TEABF_4$, $TEAPF_6$, and TBAP (tetraethyl and tetra-*n*-butyl -perchlorate, -tetrafluoroborate, and -hexafluorophosphate) were synthesized by literature methods.[61] The alkyl ammonium salts TBAX, X = OAc^-, N_3^-, F^-, OCN^-, NO_2^- were purchased from Fluka and stored in an inert atmospheres dry box until used. The salts, TBAX, X = Cl^-, Br^- and I^- were purchased from Eastman Kodak Company and used as received. All porphyrin ligands and manganese porphyrins were prepared by literature methods[62,63] and purified by column chromatography, followed by recrystallization from toluene/heptane. Since $FMn^{III}TPP$ is insoluble in CH_3CN, it was generated *in situ* by addition of TBAF to a solution of $(PF_6)Mn^{III}TPP$ in CH_3CN. To slow the precipitation of the product, Al_2O_3 was added to absorb water of hydration from TBAX. Even with these precautions, it was difficult to prevent precipitation, and so fewer experiments were performed with X = F^- than with the other axial anions, and no spectroelectrochemical experiments were done.

INSTRUMENTATION

Instrumentation and cells used for semiderivative voltammetric experiments were the same as described in Chapter 1. No *i*R compensation was used for experiments carried out in acetonitrile. In dichloromethane, however, the *i*R compensation device on the Princeton Applied Research Model 179 Digital Coulometer was used.

METHODS

Semi-derivative cyclic voltammetric scans were performed on solutions of $XMn^{III}TPP$ in acetonitrile using the cell:

W.E. (Pt or Au)	XMnTPP (0.1 to TEAP (0.1 M) CH_3CN	TEAP (0.1M) CH_3CN	$AgNO_3$ (0.01M) TEAP (0.1 M) CH_3CN	Ag

The potential was swept between potential limits of +2.0 to -2.0 V for each $XMn^{III}TPP$ to determine the regions where oxidations and reductions take place. For these initial experiments, scans were begun at the rest (open circuit) potential of the cell (usually near 0.0 V) and scanned toward negative potentials first. Once the appropriate potential ranges had been identified, voltammograms with narrower ranges were recorded to determine reversibility and the half-wave potentials, $E_{1/2}$. Although the region of positive potential was the subject of this

study, the negative region was scanned in order to: 1) verify the purity of the porphyrin by comparing the observed reduction processes with literature values, and 2) observe the effects of oxidations on the position and shape of reduction processes after repeated scans. For each $XMn^{III}TPP$ the effects of changing each of the following was examined:

1) scan rate (from 20 mV/s to 10 V/s)

2) concentration of $XMn^{III}TPP$ (from 0.10 to 1.0 mM)

3) concentration of electrolyte (0.05 to 1.0M)

4) switching potential, E_λ

In addition, the voltammetric responses of $(OAc)Mn^{III}TPPP$, in the non-coordinating solvent, dichloromethane, were examined.

The studies reported in this chapter were all done using a platimun working electrode. However, voltammograms using the planar Au working electrode were also recorded in order to determine its suitability as an electrode material for spectroelectrochemical studies,

Half-wave potentials, $E_{\frac{1}{2}}$, were measured as the average of the cathodic and anodic peaks, $(E_{pa} + E_{pc})/2$. Peak heights, e_{pa} and e_{pc}, were corrected for background, e_c, obtained from voltammograms of solvent and electrolyte solutions.

RESULTS

Figure 2-2 is an idealized semiderivative cyclic voltammogram for the potential region +2.0 to -2.4 volts for $XMn^{III}TPP$. It illustrates regions where almost identical behavior was observed for each $XMn^{III}TPP$, as well as, the regions where significant differences were observed.

In this section, I will describe the processes and patterns which were observed in each region shown in Figure 2-2 for each XMn^{III}Porphyrin we studied. Since region D, from 0.0 to -2.0 V, had been previouly well-studied, that region will be described first. Of the oxidizing regions, B exhibited the simplest behavior and the least variation with axial anion, X^-. The most complex (and unexpected) patterns were observed in region C, where no redox processes had been previously reported. Finally, the patterns observed at very anodic potentials (Region A) will be described. Because these processes occurred at potentials where background current was high, these are the most poorly understood.

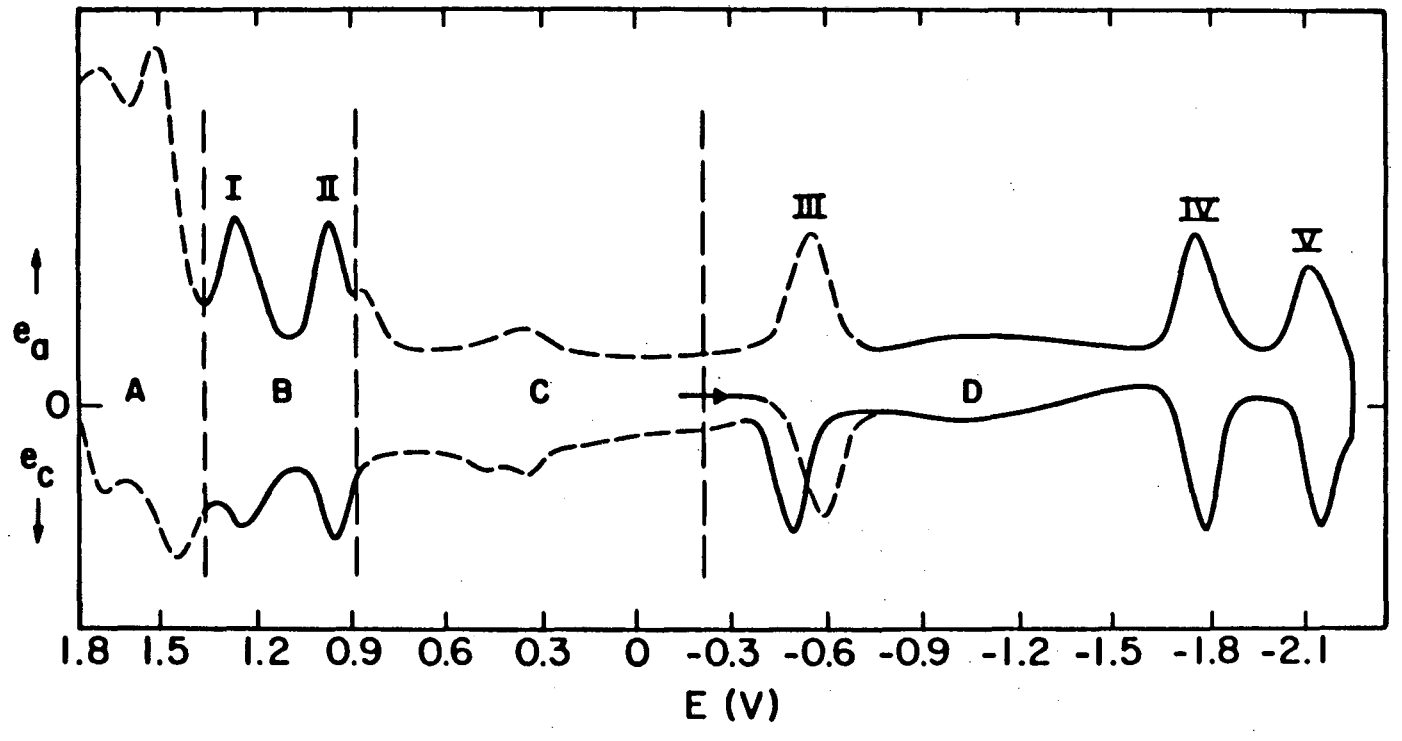

FIGURE 2-2

IDEALIZED SEMIDERIVATIVE VOLTAMMOGRAM

REDUCTIONS:

1. $Mn^{III/II}$ Couple

The first reduction encountered is represented in Figure 2-2 by Peak III and is assigned to the $Mn^{III/II}$ couple. This process has been previously reported for X = Cl^-, Br^-, I^-, N_3^-, and ClO_4^-.[38,49] In Table 2-2 the reader will find a summary of the potentials observed and a comparison with previously reported values. As expected for a metal-centered reduction, the peak potential varies with the axial ligand over a range of ~240 mV. The peak height ratios, e_{pa}/e_{pc}, and peak widths, E_{pw}, were typical of diffusion-controlled, quasi-reversible, one-electron transfers.[64-66] In addition, the observed potentials were independent of concentration of the porphyrin, and the peak height, e_p was proportional to ν, the scan rate.

Although well-behaved reductions were observed for single scans from 0.0 to -2.0 V, an unexpected pattern emerged when the potential range was +2.0 to -2.0 V. The first scan was well-behaved if the initial potential was ~0.0 V and the initial scan direction was negative. However, repeated scans resulted in an anodic shift of the $Mn^{III/II}$) couple for X = N_3^-, NCO^-, OAc^-, NO_2^-, and OH^-. No such shift was observed for ClO_4^-, BF_4^-, PF_6^-, I^- or Br^-, however. A possible explanation for this unexpected behavior will be discussed in conjuction with the patterns observed in regions B and C and in the presence of excess axial anion.

TABLE 2-2

Mn(III) → Mn(II) REDUCTION POTENTIALS

PORPHYRIN		E_{pa}	E_{pc}	$E_{1/2}$	LITERATURE [a]
$XMn^{III}TPP$					
Cl^-		-0.513(9)	-0.517(4)	-0.52(1)	-0.52 [38,49]
Br^-		-0.504(9)	-0.510(5)	-0.51(1)	-0.49 [49]
I^-		-0.468(3)	-0.480(3)	-0.474(6)	-0.48 [49]
OH^-		-0.572(2)	-0.588(2)	-0.580(4)	--
	Shifted [b]	-0.47(1)	-0.49(1)	-0.48(2)	--
OAc^-		-0.550(9)	-0.570(3)	-0.56(1)	--
	Shifted [a]	---	-0.484(3)	---	--
N_3^-		-0.576(9)	-0589(10)	-0.58(2)	-0.58 [49]
	Shifted [b]	-0.488(6)	-0.48(1)	-0.48(2)	--
NCO^-		-0.516(2)	-0.54(1)	-0.53(1)	--
	Shifted [b]	-0.485(2)	-0.500(5)	-0.495(7)	--
NO_2^-		-0.518(8)	-0.532(6)	-0.52(1)	--
	Shifted [b]	-0.49(1)	-0.484(6)	-0.49(2)	--
ClO_4^-		-0.466(3)	-0.481(6)	-0.474(9)	-0.48 [49]
PF_6^-		-0.486(2)	-0.487(8)	-0.49(1)	--
BF_4^-		-0.476(2)	-0.480(3)	-0.478(5)	--
"F^-"		-0.69(1)	-0.75(1)	-0.72(1)	--

TABLE 2-2 (cont'd)

Mn(III) → Mn(II) REDUCTION POTENTIALS

PORPHYRIN	E_{pa}	E_{pc}	$E_{1/2}$	LITERATURE [a]
Substituted Porphyrins				
(OAc)MnT(*p*-CF_3)PP	-0.42(1)	-0.53(2)	-0.48(3)	--
(OAc)MnT(*p*-OMe)PP	-0.54(1)	-0.66(1)	-0.60(1)	--

a Literature values were reported *vs* SCE. The values shown have had 0.29 V subtracted to give the potential *vs* the $Ag/AgNO_3$(0.01M), TEAP(0.1M),CH_3CN reference electrode used for this work.

b Shifted potentials are the new potentials which resulted after a second scans to anodic potentials of ~+2.0 V. Unshifted potentials were those which resulted on first scans in a cathodic direction, with an initial potential of ~0.0 V.

2. Porphyrin Ring Reductions

A summary of the porphyrin ring reductions observed is presented in Table 2-3. A smaller and less systematic variation in the peak potentials of the two ring reductions than for the those of the metal-centered reduction is apparent. At the same time, the shifts for the substituted porphyrin ligands are in the direction predicted for electron-releasing and electron-withdrawing substituents, respectively. The second ring reduction was observed cleanly for only some of the axial anions. This may be, in part, a result of the difficulty in keeping the solution free of traces of water. Only those reductions which were cleanly observable for every porphyrin sample for a given X are reported. Again, the observed reductions exhibit the features characteristic of diffusion-controlled, quasi-reversible, one-electron transfers.[64-66]

TABLE 2-3

FIRST AND SECOND RING REDUCTIONS

PORPHYRIN	First Ring Reduction		Second Ring Reduction	
XMnTPP	$E_{1/2}$ (This work)	$E_{1/2}$ (Lit)[a]	$E_{1/2}$ (This work)	$E_{1/2}$ (Lit)
Cl⁻	-1.770(4)	-1.76 [49]	-2.11(1)	-1.99 [38]
		-1.67 [38]		
Br⁻	-1.692(7)	-1.76 [49]	-2.12(1)	--
I⁻	-1.662(5)	--	--	--
OH⁻	-1.78(1)	--	--	--
OAc⁻	-1.77(1)	--	-2.13(1)	--
N_3^-	-1.77(1)	-1.76 [49]	-2.14(1)	--
NCO⁻	-1.77(1)	--	--	--
NO_2^-	-1.82(2)	--	--	--
ClO_4^-	-1.652(2)	--	-2.11(1)	--
BF_4^-	-1.78(1)	--	--	--
PF_6^-	-1.78(2)	--	--	--
Substituted Porphyrins				
OAcMnT(*m*-CF_3)TPP	-1.619(3)	--	-1.98(1)	--
OAcMnT(*p*)-OmePP		--		--

a Literature values are reported *vs* SCE. The potentials listed have had 0.29 V subtracted to give the potential *vs* the Ag/$AgNO_3$(0.01M), TEAP(0.1M), CH_3CN reference electrode.

OXIDATIONS

Three distinct regions were observed in the potential range from 0.0 to +2.0 V. In regions A and C the characteristics of the observed redox processes varied greatly with X, the axial ligand, and with E_λ, the switching potential. In region B, however, the peak heights, peak shapes, and potentials of the observed oxidations varied very little with axial ligand.

1. Ring Oxidations.

In Table 2-4 and 2-5, the peak potentials for the two peaks observed in Region B are listed. Peak II (See Figure 2-2) corresponds to the ring oxidation reported for X = Br^- I^-, and N_3^-.[49] Peak I, on the other hand, has not been previously reported, although an oxidation at ">1.4V *vs* SCE" has been reported for Mn^{III}OEP.[39] This process is probably due to the second porphyrin ring oxidation. As was the case for the ring reductions, the shifts observed for the substituted porphyrins were in the directions expected for their respective substituents. Further evidence for ring oxidations at the potentials represented by peaks I and II will be presented in Chapter 3.

The electron transfer processes represented by peaks I and II can be characterized as one-electron, quasi-reversible, diffusion-controlled processes, based on the following observations:[64-66]

1) The peak potentials, E_{pa} and E_{pc} were invariant with concentration of $XMn^{III}TPP$ over a range of 0.1 to 1.0 M.

2) The half-wave potentials, $E_{1/2}$ varied only slightly with scan rate ($\lesssim$ 20mV) over at least a 10-fold change in scan rate.

3) E_{pw}, the peak width at half-height, was about 90 to 120 mV for scan rates of 20-200 $mV \cdot s^{-1}$.

4) The quantity $(E_{pa} - E_{pc}) \lesssim$ 20mV for all axial anions (except F^- which was irreversible for peak I).

5) The peak heights, e_p, were about the same ($\pm$ 10%) as those observed for peaks III and IV, the well characterized one-electron reductions.

6) The ratio e_{pa}/e_{pc} varied from ~0.8 to ~1.0 for peak II and from ~1.5 to ~1.0 for peak I when scans were done over a sufficiently narrow potential range (0.6 to 1.0 V for peak II; 0.75 to 1.35 V for peak I).

TABLE 2-4

FIRST RING OXIDATION

PORPHYRIN	E^{pa}	E^{pc}	$E_{1/2}$	LITERATURE[a]
XMn^{III}TPP				
Cl^-	0.94(2)	0.94(1)	0.94(3)	0.94 [38]
Br^-	0.961(2)	0.957(3)	0.959(5)	0.96 [49]
I^-	0.960(2)	0.957(2)	0.959(5)	0.96 [49]
OH^-	0.958(3)	0.954(5)	0.956(5)	--
OAc^-	0.961(2)	0.958(3)	0.959(5)	--
N_3^-	0.957(4)	0.955(4)	0.956(8)	0.96 [49]
OCN^-	0.959(2)	0.953(3)	0.956(5)	--
NO_2^-	0.960(1)	0.959(2)	0.960(2)	--
ClO_4^-	0.960(1)	0.954(5)	0.956(8)	--
BF_4^-	0.953(2)	0.948(4)	0.950(6)	--
PF_6^-	0.960(3)	0.98(1)	0.97(1)	--
"F-"	0.98(2)	0.96(1)	0.97(2)	--
Substituted Porphyrins				
(OAC)MnT(p-CF_3)PP	0.857(1)	1.068(4)	1.079(10)	--
(OAC)MnT(p-OMe)PP	1.089(2)	0.823(8)	0.840(10)	--

a Literature values were reported *vs* SCE. The potentials shown have had 2.91 V subtracted to give the potential *vs* the Ag/$AgNO_3$ reference electrode used for the studies reported in this work.

b Cl^- was difficult to determine accurately because of the broad shoulder from the prewave. See Figure 2-9.

TABLE 2-5

SECOND RING OXIDATION

PORPHYRIN	E_{pa}	E_{pc}	$E_{1/2}$
$XMn^{III}TPP$			
Cl^-	1.25(2)	1.238(7)	1.24(2)
Br^-	1.259(2)	1.254(5)	1.257(9)
I^-	1.260(3)	1.244(8)	1.25(1)
OH^-	1.267(8)	1.259(2)	1.26(1)
OAc^-	1.263(7)	1.250(6)	1.26(1)
N_3^-	1.25(2)	1.245(4)	1.25(2)
OCN^-	1.260(1)	1.252(2)	1.254(3)
NO_2^-	1.260(1)	1.255(3)	1.258(4)
ClO_4^-	1.260(3)	1.252(3)	1.256(6)
BF_4^-	1.260(1)	1.243(6)	1.252(7)
PF_6^-	1.278(1)	1.275(1)	1.277(3)
"F-"	1.260(1)	--	1.26 [a]
Substituted Porphyrins			
MnT(p-CF_3)PPOAC	1.368(8)	1.34(1)	1.35(2)
MnT(p-OMe)PPOAc	1.112(3)	1.080(1)	1.110(4)

a Irreversible. No reduction observed.

2. Prewaves

In region C some unexpectedly complex behavior was observed. For $XMn^{III}TPP$ where X = Cl^-, Br^-, I^-, OAc^-, OCN^-, N_3^-, and NO_2^-, small waves were observed between the potentials of the Mn(III) reduction and the first ring oxidation (peaks II and III). None were observed for X = ClO_4^-, BF_4^-, PF_6^-, OH^- or F^-. To our knowledge, no electron transfer processes have been reported in this region, and one author has specifically stated that no redox processes occurred between +1.2 and -1.4V *vs* SCE (~0.9 and -1.1V *vs* the $Ag/Ag^+(10^{-2}M)$ reference electrode), for $ClMn^{III}TPP$ in $MeCl_2$.[39] Since impurities in the manganese porphyrin itself were a possible source for these unexpected waves, care was taken to minimize this possibility. The potentials of these waves (I shall call them *prewaves* since they appear *before* the oxidations being studied) varied with the axial ligand and were quite reproducible from one sample to another. This suggested that the prewaves may be due to oxidations of free axial ligand which were present either as an impurity or as a result of dissociation of the axial ligand to form a solvated porphyrin and a free axial ligand.

It seems unlikely that the prewaves were due to impurities alone because of the following observations:

1) The peak heights of the prewaves were significant fractions ($\geq$ 25% in all cases except for NCO^- which was $\leq$ 10%) of the well-behaved one-electron processes repre-

sented by peaks I-V.

2) Prewaves were observed even for samples which were pure by criteria of elemental analysis and electronic spectra.

3) Crystallization from toluene/heptane would almost certainly have eliminated any excess ionic impurities due to excess axial anion.

4) We observed no prewaves in $MeCl_2$, confirming the observation reported by Kadish and Kelly.[39]

In order to gain more insight into the electron transfer processes in the prewave region, C, (and in region A) the electrochemistry of the free axial ligands, added as the tetra(*n*-butyl)ammonium salts, TBAX was investigated. In like manner voltammetry of solutions containing ~1 to 20 mM TBAX and ~1mM $XMn^{III}TPP$ was done. Typical results for these experiments are shown in Figures 2-3 through 2-6, in which representative SD voltammagrams for selected $XMn^{III}TPP$, TBAX, and their mixture are presented. Examples of typical valtammograms for all $XMn^{III}TPP$ can be found in Appendix 3. The potentials observed in the prewave region for $XMn^{III}TPP$ and TBAX are summarized in Tables 2-6 and 2-7, respectively. In Table 2-8, the effects of adding TBAX to solutions of ~1mM $XMn^{III}TPP$ are summarized.

The results of the experiments just described fall into several groups:

1) Those for which no prewaves are observed (ClO_4^-,

PF_6^-, BF_4^-, Figure 2-3).

2) Those for which the processes observed in the prewave region for TBAX, $XMn^{III}TPP$, and TBAX + $XMn^{III}TPP$ are very similar to each other (Br^- and I^-)$^-$, Figure 2-4).

3) Those for which electrochemical processes observed in the prewave region for TBAX are different from those observed for $XMn^{III}TPP$ (Cl^-, N_3^-, OCN^-, NO_2^-, OAc^-, OCN^-, F^-, and OH^-, Figures 2-5 and 2-6).

A. ClO_4^-, BF_4^-, PF_6^-

The results of this control group were expected and exclude the possibility that traces of water or other impurities were the source of the prewaves.

B. Br^-, I^-

In Group 2 (Figures 2-4), the similarity of both the potentials and relative peak heights of the free axial ligand and of $XMn^{III}TPP$ is consistent with the dissociation of the axial ligands, X = Br^- and I^-. However, the behavior of (I^- + $IMn^{III}TPP$) differed from that of (Br^- + $BrMn^{III}TPP$) with repeated scanning. When scans were done from 0.0 to +2.0 V for I^-, peaks I and II (the first and second ring oxidations) gradually disappeared, until only the pattern due to free I^- was observable. When E_λ was changed back to -2.0 V the pattern for $IMn^{III}TPP$ reappeared. Repeated scanning of the analogous solution containing bromide resulted in no observable loss of the characteristic $BrMn^{III}TPP$ *e*-E curve.

FIGURE 2-3

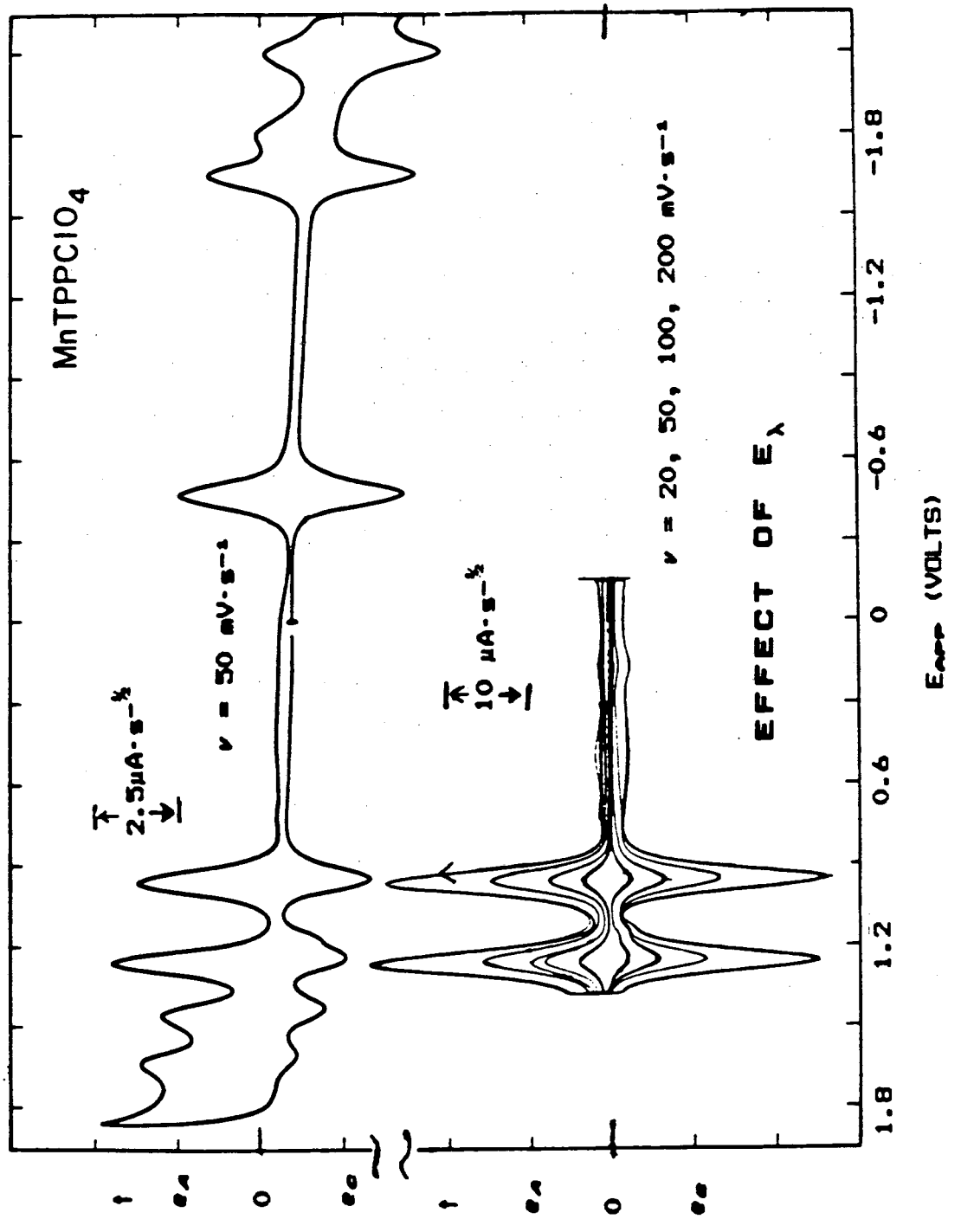
MnTPPClO4
2.5μA·s^-½
ν = 50 mV·s^-1
10 μA·s^-½
ν = 20, 50, 100, 200 mV·s^-1
EFFECT OF E_λ
1.8
1.2
0.6
0
-0.6
-1.2
-1.8
E_app (VOLTS)

C. NO_2^-, Cl^-

In Group 3 (FIgure 2-5) more complex patterns were observed. For X = NO_2^-, the *potentials* of the prewave for $TBANO_2$ and $(NO_2)Mn^{III}TPP$ are near each other, but their *peak shapes* are quite different from one another. Furthermore, addition of $TBANO_2$ to a solution of the porphyrin does not result in a growth in the peak height of the prewave, although broadening does occur.

In a similar manner, TBACl, has a single peak at ~0.63 V, while the prewave observed for $ClMn^{III}TPP$ occurs at ~0.75 V and is very dependent on scan-rate. The addition of TBACl to $ClMn^{III}TPP$ results in a broad, intense wave near 0.63 V, which grows in intensity with increased concentration of TBACl. At the same time the peak at 0.94 V increases in intensity, broadens, and shifts in a cathodic direction to ~0.90 V. The shoulder at ~0.75 V is no longer distinguishable. For both of these cases (Cl^- and NO_2^-) no new peaks are observed on addition of free X^- to solutions of $XMn^{III}TPP$.

FIGURE 2-4

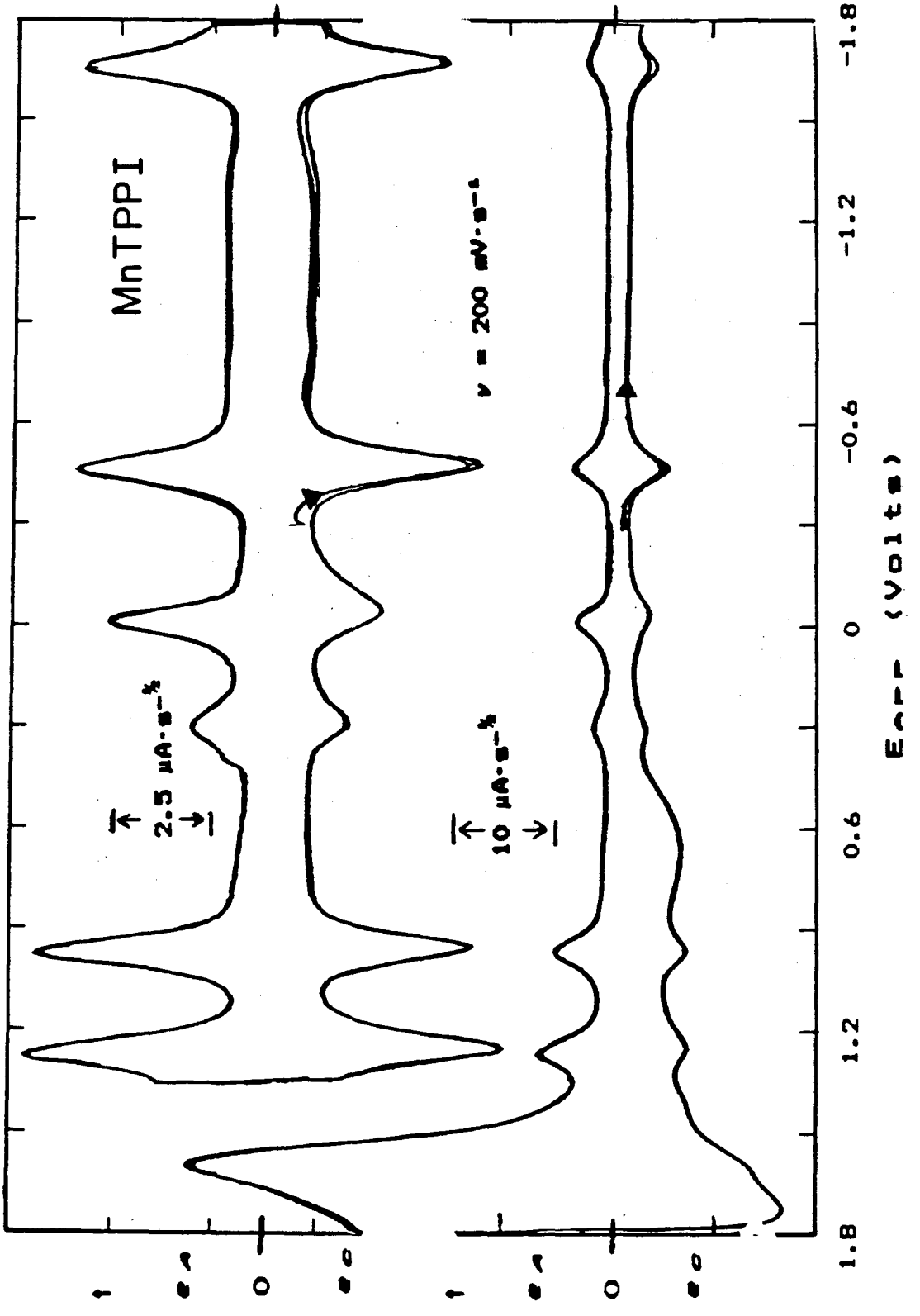

FIGURE 2-4B

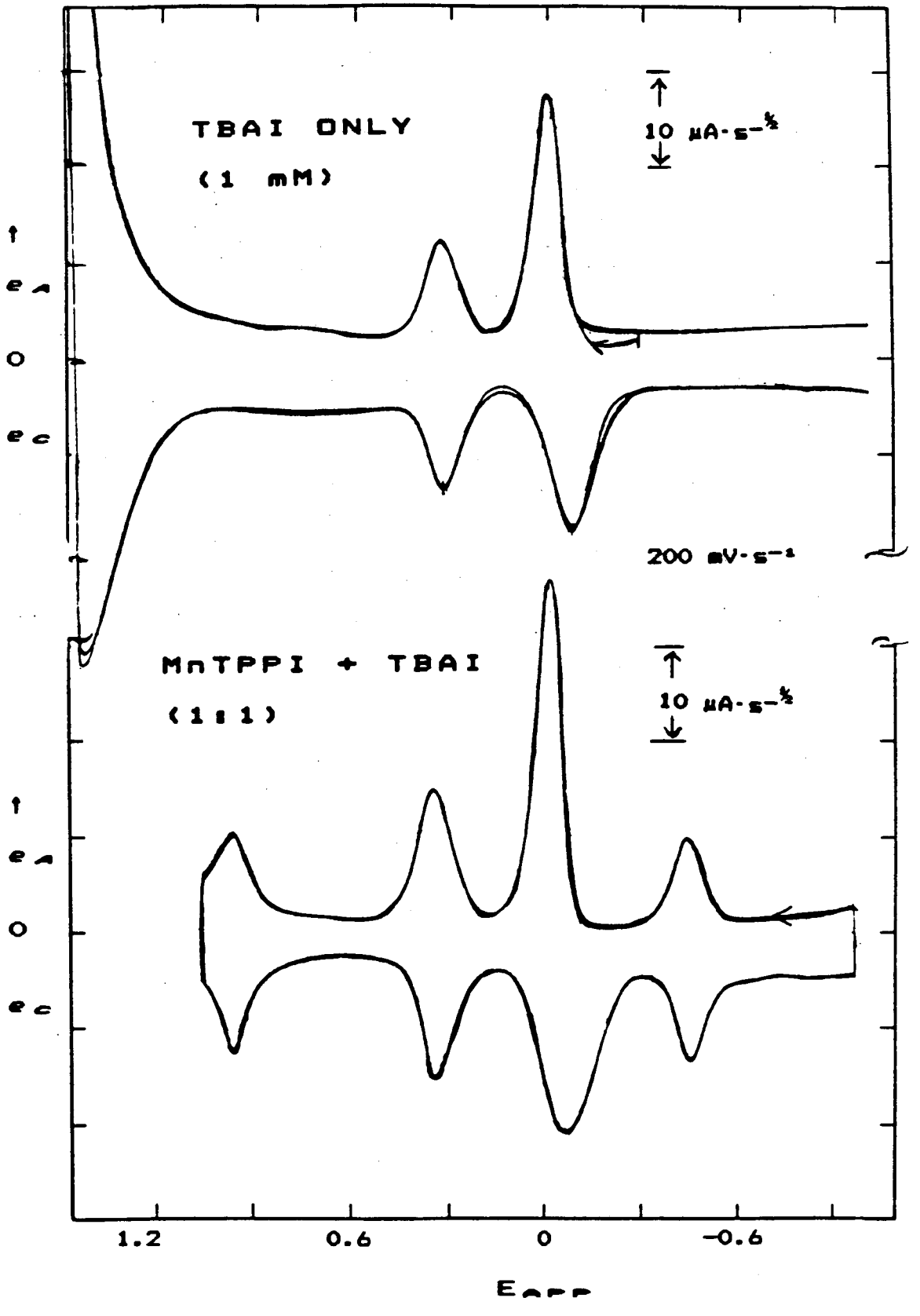
TBAI ONLY
(1 mM)
10 μA·s^-½
200 mV·s^-1
MnTPPI + TBAI
(1:1)
10 μA·s^-½
1.2
0.6
0
-0.6
E appl

FIGURE 2-5

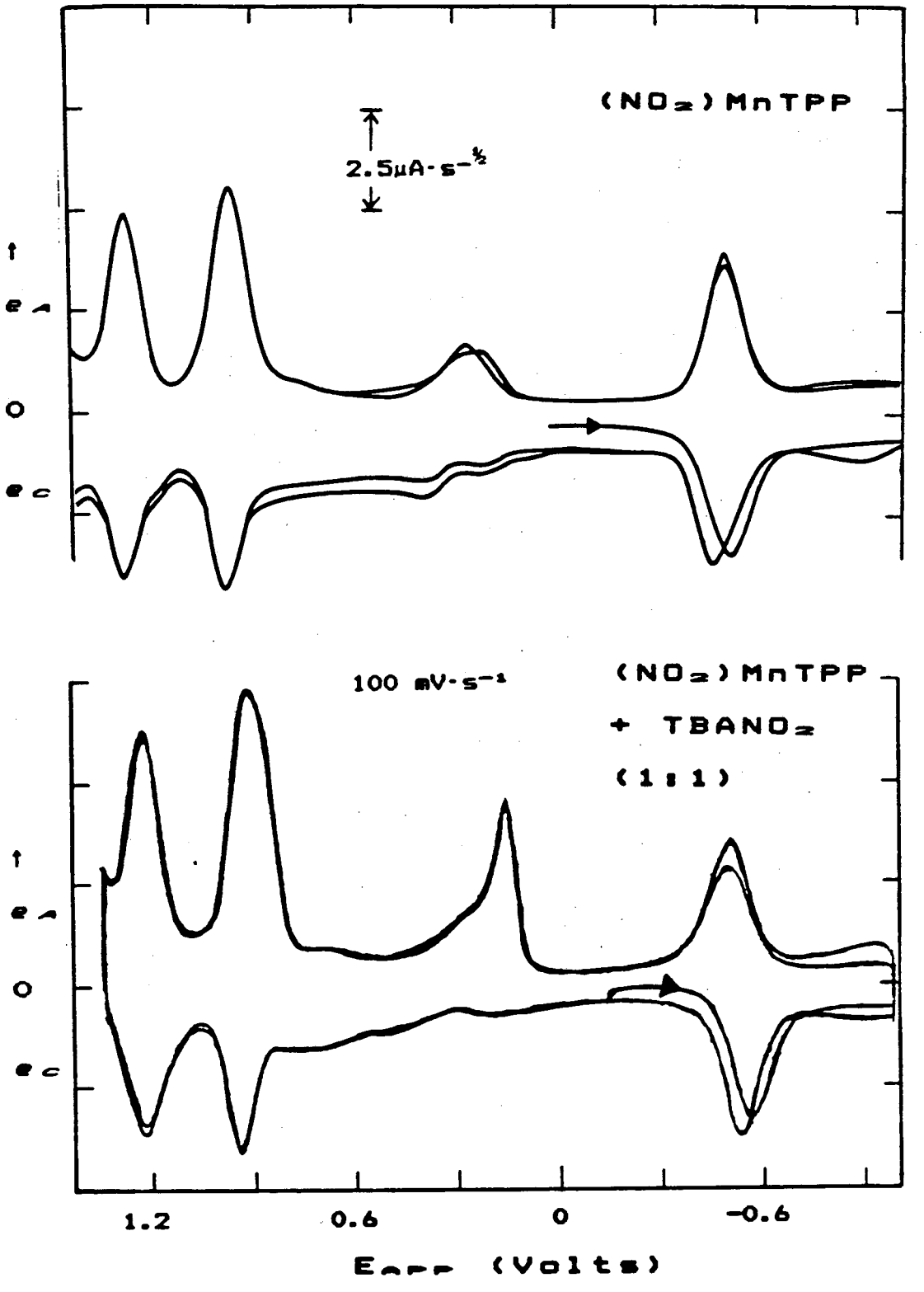
(NO2)MnTPP
2.5μA·s^-½
100 mV·s^-1
(NO2)MnTPP
+ TBANO2
(1:1)
1.2
0.6
0
-0.6
E app (Volts)

D. N_3^-, NCO^-, OAc^-

Each of the $XMn^{III}TPP$ in the group (Figure 2-6) exhibited a new wave in the presence of excess axial ligand, which has been assigned to the $Mn^{IV/III}$ couple.

The anion, N_3^-, (Figure 2-6) exhibits quite different behavior from that observed for Cl^- or NO_2^-. The free ligand shows a sharp, irreversible wave at ~0.41V, while the prewave for $N_3Mn^{III}TPP$ occurs at ~0.85 V. In the absence of excess N_3^- (added as $TBAN_3$), the prewave peak height decreases with repeated full scans. When $E_\lambda \lesssim 0.90$ V, however, the prewave persists. (See Figure 2-6). Addition of 1-2 mM $TBAN_3$ results in the growth of the prewave at ~0.84 V and the appearance of a new, irreversible, anodic wave at 0.12 V. When $E_\lambda \lesssim 0.60$ V, the new wave becomes quasi-reversible. (See Figure 2-6). With a 3- to 5- fold excess of N_3^-, the prewave grows, becomes very sharp, and the first ring oxidation at 0.96 V disappears. The wave due to free N_3^- appears at ~0.45 V, while the new wave grows slightly in intensity. At these higher concentrations of $TBAN_3$, this new wave also starts to exhibit quasi-reversible behavior at switching potentials as anodic as 1.2 V . Addition of successive aliquots of $TBAN_3$ up to ~10-fold excess, results in continued growth of the prewave and free ligand waves. The new wave becomes more nearly reversible ($e_{pa}/e_{pc} \rightarrow 1.0$ and $re_{pa} \rightarrow 90$ mV). However, its peak height does not continue to increase indefinitely, but rather it remains fairly

constant at a peak height approximately that of the ring oxidations and of the $Mn^{III/II}$ couple. The half-wave potential of this new wave shifts to more cathodic potentials with continued addition of $TBAN_3$ to the $N_3Mn^{III}TPP$ solutions. (See Table 2-8). These patterns suggest a electron transfer process involving $N_3Mn^{III}TPP$, possibly oxidation at the metal center.

Solutions of TBA(NCO) alone, show little evidence of undergoing oxidations or reductions at concentrations $\lesssim$ 10mM. At higher concentrations, a broad, irreversible wave at ~1.0 V appears. (See Appendix 3, Figure A3-6.) The porphyrin, $OCNMn^{III}TPP$, exhibits a small prewave at ~0.71 V, which grows in intensity and shifts to slightly more positive potentials with the addition of 1- to 2-fold excess of TBA(NCO). Two other waves also grow in at ~0.38 and 0.87 V. At the same time the $Mn^{III/II}$) couple becomes very broad and E_{pc} shifts to much more cathodic potentials (-0.68 V). Further addition of TBA(NCO) results in loss of the porphyrin waves almost entirely, suggesting adsorption of NCO^-.

The porphyrin, $(OAc)Mn^{III}TPP$, exhibits two prewaves of approximately equal intensity at ~0.77 V and ~0.63 V at 200 $mV \cdot s^{-1}$. (See Table 2-12 and Appendix 3, Figure A3-6). The wave at 0.63 V shifts dramatically to more cathodic potentials at slower scan rates (~0.45 V at 20 $mV \cdot s^{-1}$). At 200 $mV \cdot s^{-1}$ both peaks decrease ~20% in intensity; at slower scan rates no such decrease is observable. No

electrochemical activity is observed for TBA(OAc) alone for concentrations up to ~20 mM . At higher concentrations the presence of water of hydration interferes with further investigation of free OAc^-. As was the case for N_3^- and NCO^-, addition of TBA(OAc) to solutions of (OAc)Mn^{III}TPP results in growth of both prewaves, as well as the appearance of a new wave at ~0.38 V. On first scan some indication of a reversible process was apparent for this new wave. It did not remain reversible, however, with repeated scans or with addition of further aliquots of TBA(OAc). Again, complex processes (possibly adsorption) occur with large excesses of OAc^- (See Appendix 3, Figure A3-7). Hence, further investigation of this process was limited to spectroelectrochemical studies.

Since a sample of (CN)Mn^{III}TPP was not available, its electochemical behavior was observed by adding TBACN to solutions of (BF_4)Mn^{III}TPP. (See Chapter 3 for more detail on this system.) The observed behavior was essentially the same as that observed for NMnTPP.

FIGURE 2-6A

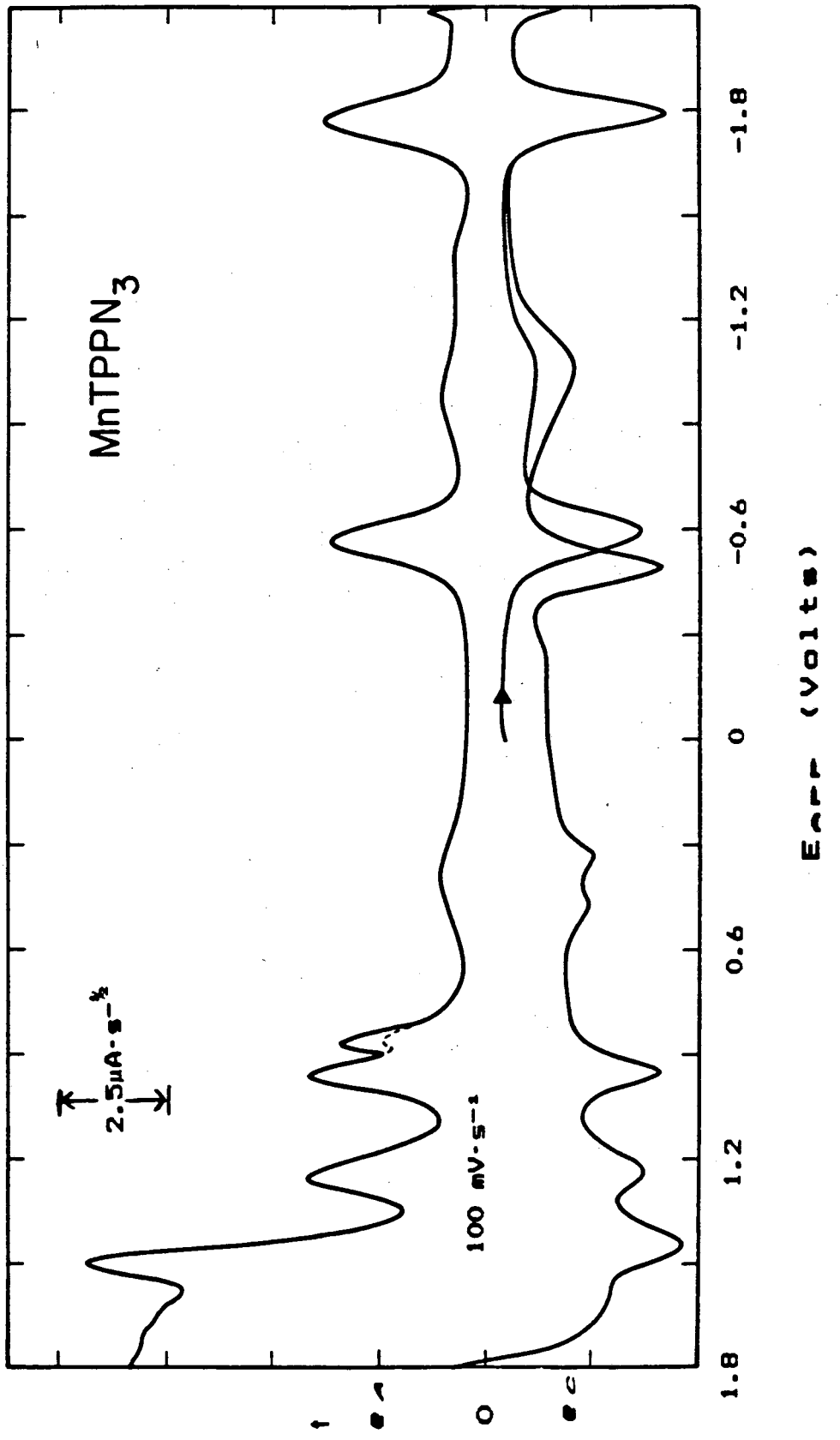

FIGURE 2-6B

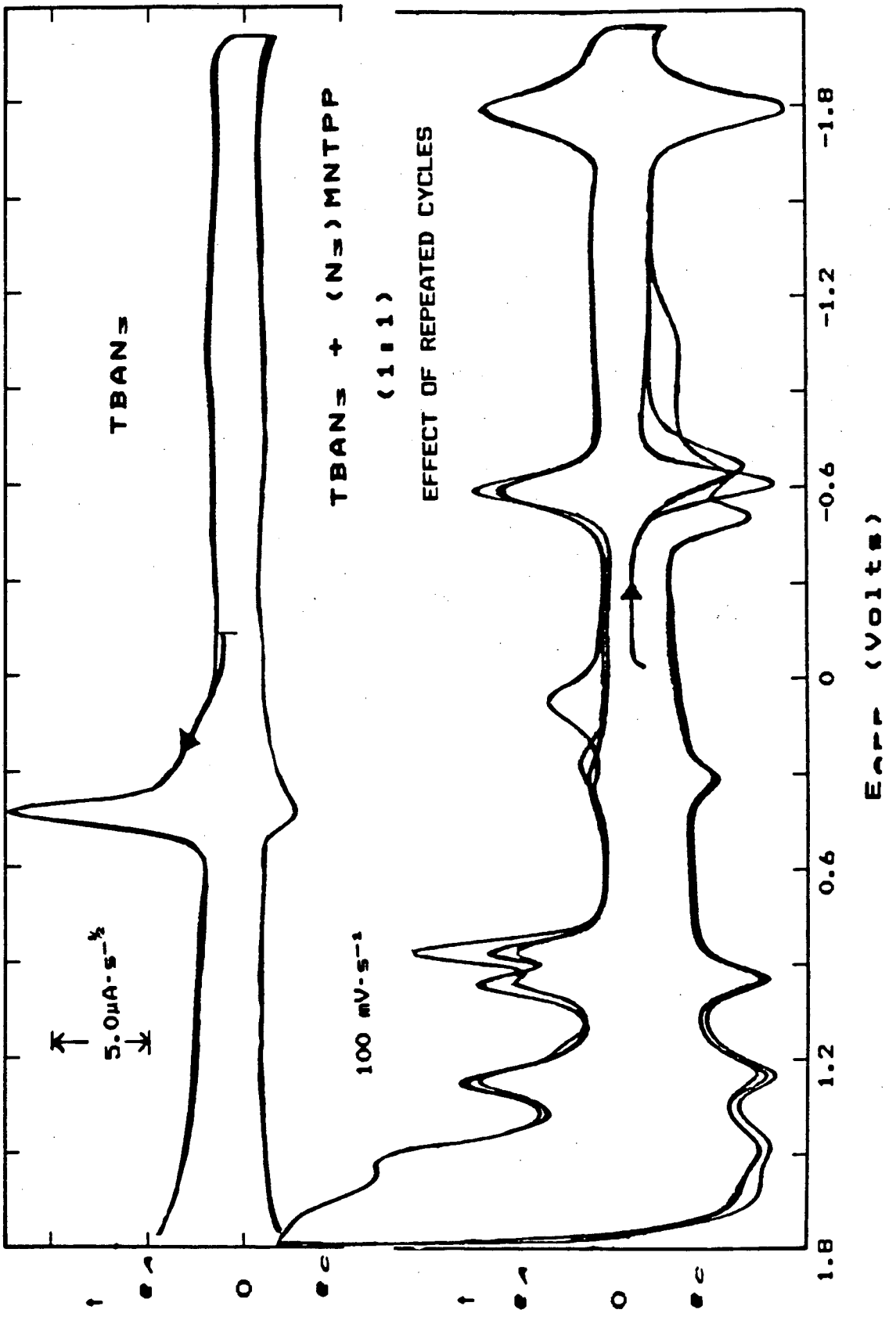
TBAN=
TBAN= + (N=)MNTPP
(1:1)
EFFECT OF REPEATED CYCLES
5.0μA·s⁻½
100 mV·s⁻¹
1.8
1.2
0.6
0
-0.6
-1.2
-1.8
Eapp (Volts)

FIGURE 2-6C

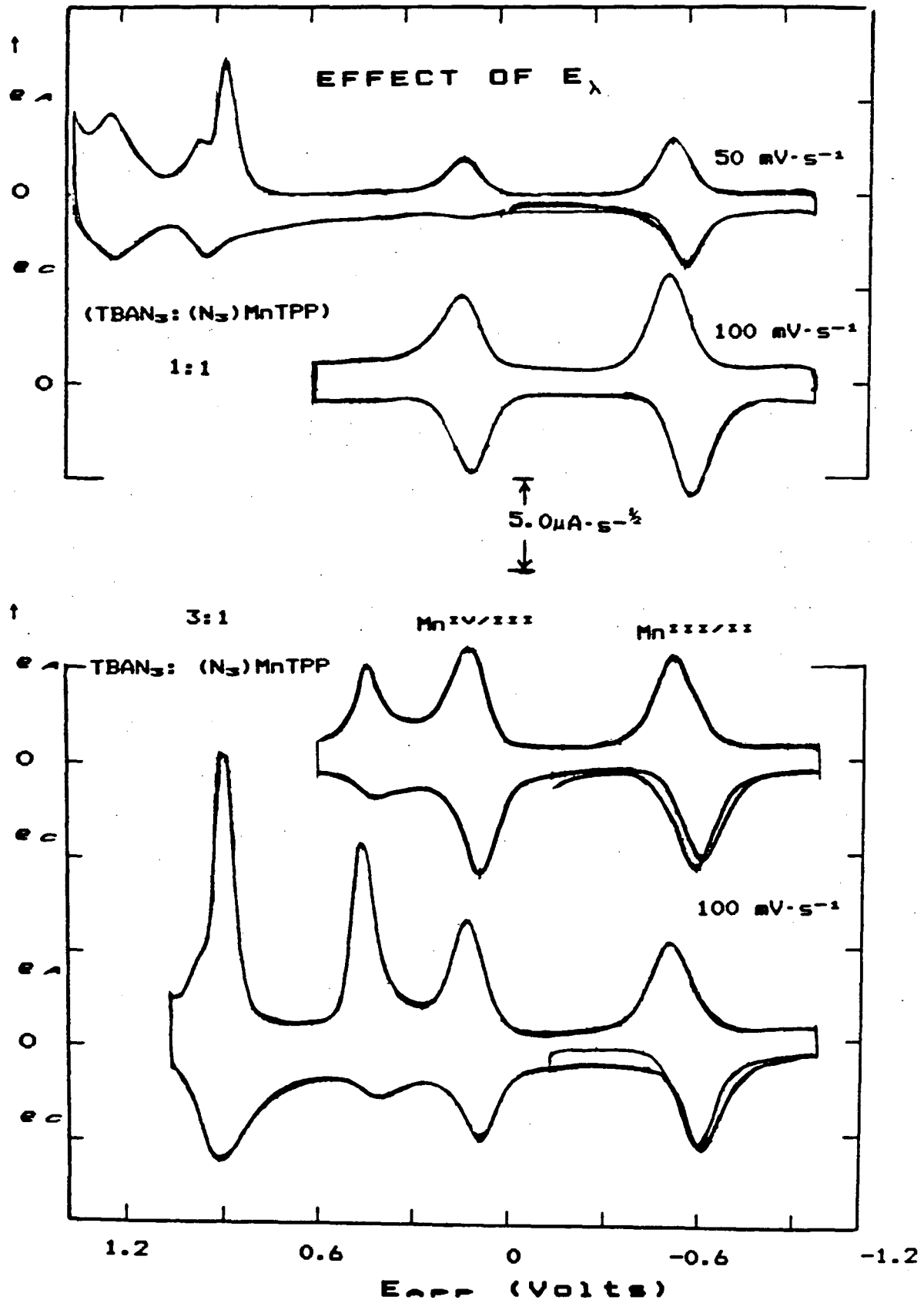
EFFECT OF E_λ
50 mV·s⁻¹
100 mV·s⁻¹
(TBAN₃: (N₃)MnTPP)
1:1
5.0μA·s^-½
3:1
TBAN₃: (N₃)MnTPP
Mn^IV/III
Mn^III/II
100 mV·s⁻¹
1.2
0.6
0
-0.6
-1.2
E_appl (Volts)

TABLE 2-6

PREWAVES

PORPHYRIN		E_{pa}	E_{pc}	$E_{1/2}$
$XMn^{III}PP$				
Cl^-		0.75(5) [a]	--	0.75(5)
Br^-	(1)	0.63(1)	0.58(1)	0.60(2)
	(2)	0.41(3)	0.37(1)	0.39(4)
I^-	(1)	0.313(2)	0.307(2)	0.310(4)
	(2)	-0.049(2)	-0.068(2)	-0.059(4)
OH^-		--	--	--
OAc^-	(1)	0.77(2)	--	0.77(2)
	(2)	0.63(2) [a]	--	--
N_3^-		0.84(2) [a]	--	0.84(2)
OCN^-		0.71(2)	--	0.71(2)
NO_2^-		0.24(1)	0.21(1)	0.22(2)
ClO_4^-		--	--	--
BF_4^-		--	--	--
PF_6^-		--	--	--
"F-"				
Substituted Porphyrins				
(OAc)MnT(o-CF_3)PP		0.72(4)	--	--
(OAc)MnT(p-OMe)PP		0.45(2)	--	--

a Potential reported is at 200 mV/s. The potential shifted to more negative potentials at slower scan rates.

TABLE 2-7

TBAX ONLY

$XMn^{III}TPP$		E_{pa}	E_{pc}	$E_{1/2}$	LITERATURE [a]
Cl^-		0.63(1)	0.59(1)	0.61(1)	0.81 [72]
Br^-	(1)	0.65(1)	0.62(1)	0.64(1)	0.71 [72]
	(2)	0.35(1)	0.27(1)	0.31(2)	0.41 [72]
I^-	(1)	0.311(2)	0.306(6)	0.311(6)	0.26 [72]
	(2)	-0.054(7)	-0.083(7)	-0.069(14)	-0.04 [72]
OH^-		--	--	--	
OAc^-		--	--	--	
N_3^-		0.41(1) [b]	0.41(1)	0.41(1)	0.38 [79,80]
OCN^-		~1.0 [c]	--	--	--
NO_2^-		0.15(1) [b]	0.15(1)	0.15(1)	--
ClO_4^-		--	--	--	--
PF_6^-		--	--	--	--
BF_4^-		--	--	--	--
"F-"		--	--	--	--

a Literature values were obtained *vs* SCE. The potentials shown have had 0.29 V subtracted to give the potential *vs* the $Ag/AgNO_3(10^{-2}\ M)$ reference electrode used for the stuies reported in this work.

b Irreversible, very scan dependent waves.

c Very broad wave, only appeared at concentrations > 10 mM.

TABLE 2-8

PREWAVE REGION (MnTPPX + TBAX)

PORPHYRIN		E_{pa}	E_{pc}	$E_{1/2}$
$XMn^{III}TPP$				
Cl^-	1)	0.616(6)	0.450(15)	0.533(21)
	2)	0.920(16)	0.935(7)	0.928(23) [a]
Br^-	1)	0.38(4)	0.38(2)	0.38(6)
	2)	0.65(1)	0.61(1)	0.63(2)
I^-	1)	0.322(6)	0.29(3)	0.31(4)
	2)	-0.04(2)	-0.084(6)	-0.06(3)
OH^-		-	-	-
OAc^-	1)	0.79(1)	-	-
	2)	0.64(1)	-	-
	3)	0.38(1)	-	-
N_3^-	1)	0.86(2)	-	-
	2)	0.41(1)	-	-
	3)	0.105(1) [b]	0.063	0.084
NCO^-	1)	0.870(2)	-	-
	2)	0.73(3)	-	-
	3)	0.39(2) [b]	-	-

TABLE 2-8, cont'd

PREWAVE REGION (MnTPPX + TBAX)

PORPHYRIN		E_{pa}	E_{pc}	$E_{1/2}$
$XMn^{III}TPP$				
NO_2^-	1)	0.248(2)	-	-
	2)	0.150(2)	-	-
ClO_4^-		-	-	-
BF_4^-		-	-	-
PF_6^-		-	-	-
"F-"	1)	0.325	-	-
	2)	0.813	-	-

a This wave appears to be that of the shifted ring oxidation.

b This is a new wave which is not present for either TBAX alone or for $XMn^{III}TPP$ alone.

Third and Fourth Oxidations

A summary of the potentials and relative peak heights for the third and fourth oxidations observed for $XMn^{III}TPP$ are summarized in Table 2-9 and 2-10. While these processes vary considerably in relative intensity, their half-wave potentials are remarkably near to one another. The two anions which exhibited the most atypical behavior were X = ClO_4^- and I^-. In the case of ClO_4^-, the third and fourth waves were much less intense than the first two oxidations (Peaks I and II), and became more well-defined at slower scan rates (See Figure 2-3). For X = I^- only one, very intense wave was observed. Its peak height was ~4 times the height of the first two oxidations and increased in intensity for repeated scans until the height reached a maximum. For the other anions, the peak heights (corrected for the large background currents at these extreme potentials) were ~1.5 to 2 times the height of Peaks I and II, varying somewhat from one anion to another. In each case, the particular pattern observed was reproducible from one sample to another, suggesting some dependence on the nature of the anion.

TABLE 2-9

THIRD RING OXIDATION

	E_{pa}	E_{pc}	$E_{1/2}$	e_{pa}/e_{pc}	e_{pa}(Rel) [a]
$XMn^{III}TPP$					
Cl^-	1.46(1)	1.49(1)	1.48(2)	~1.5	~2
Br^-	1.42(1)	1.44(2)	1.43(3)	~2	~1
I^-	1.56(2)	1.61(2)	1.58(4)	~4	~5
OH^-	1.39(8)	-- [a]	--		
OAc^-	1.46(2)	1.42(1)	1.44(3)	~1.6	~1
N_3^-	1.44(1)	1.48(1)	1.46(2)	~2.2	~2
NCO^-	1.42(1)	1.43(1)	1.42(2)	~1	~2
NO_2^-	1.40(7)	1.44(4)	1.4(1)	~1	?
ClO_4^-	1.44(1)	1.46(1)	1.45(1)	0.9 [b]	~0.3
PF_6^-	1.47(2)	--	--	--	~1
BF_4^-	1.42(2)	1.39(1)	1.40(3)	~2	~1
"F-"	--	--	--	--	--
Substituted Porphyrins					
(OAc)MnT(p-CF_3)PP	--	--	--	--	--
(OAc)MnT(p-OMe)PP	1.40(3)	--	--	--	--

a The peak height ratio of the observed peak to that of the first ring oxidation or the $Mn^{III/II}$ couple (one- electron transfers).

b The peak heights for ClO_4^- were less than those for the one-electron. Enhanced reversibility was observed at slower scan rates.

TABLE 2-10

FOURTH RING OXIDATION

		E_{pa}	E_{pc}	$E_{1/2}$	e_{pa}/e_{pc}	e_{pa}(rel) [a]
$XMn^{III}TPP$						
Cl^-		1.61(1)	1.64(1)	1.62(2)	~2	~2
Br^-		1.59(1)	1.63(1)	1.61(2)	~2.5	~2
I^-		--	--	--	--	
OH^-		1.65(2)	1.52(2)	????		~2
OAc^-		1.65(4)	1.60(2)	1.64(6)	~4	~2
N_3^-		1.59(1)	1.62(1)	1.60(2)	~2	~1
NCO^-		1.60(1)	1.63(1)	1.62(2)	~2.7	~2
NO_2^-	(1)	1.62(2)	1.61(1)	1.62(2)	~2	~1.5
	(2)	1.76(1)	1.74(2)	~3	~2	
ClO_4^-		1.61(1)	1.64(1)	1.62(2)	~0.7	~0.3
PF_6^-		1.68	--	--	--	~2
BF_4^-		1.62(3)	1.57(1)	1.60(4)	~2.5	~2
"F-"		--	--	--	--	
OAcMnT(*o*-CF_3)PP		1.68(2)	1.76(3)	1.72(5)	~3	~1
OAcMnT(*p*-OMe)PP		1.61(2)	--	--	--	??

a The peak height ratio of the observed peak to that of one of the one-electron transfer processes, such as the ring oxidations, or the $Mn^{III/II}$ couple.

DISCUSSION

In the Results section several different regions and patterns of electrochemical behavior were described. The simplest patterns were observed in region B (Peaks I and II in Figure 2-2) where the first two porphyrin ring oxidations were observed. More complex behavior was observed in region C, where no electrochemical activity had been expected. In region D, some unexpected shifts in the $Mn^{III/II}$ couple were also observed. From these two unexpected sets of behavior, some important insights into the solution equilibria and the oxidation chemistry of manganese(III)porphyrins has been gained. Finally, some electron transfer processes at very anodic potentials (Region A, Figure 2-1) were observed which are poorly understood as of this writing. In this section I will discuss some of the insights gained from these voltammetric studies.

Ring Oxidations

Peaks I and II at 0.96 and 1.26 V can be unambiguously assigned as the successive, one-electron oxidations of the porphyrin ring to form the π-radical cation and dication, respectively. Although verification of this assignment by spectral or magnetic studies is desirable (spectral studies will be presented in Chapter 3), electrochemical criteria alone are sufficient in this case. The constancy of the observed potentials (See Tables 2-3 and 2-4) is strong evidence by itself that the porphyrin

ring, rather than the manganese ion, is being oxidized. Molecular orbital calculations, empirical correlations with electronic spectra, and the observation of very long axial bond distances in X-ray crystal structures imply that the HOMO for h.s. $XMn^{III}TPP$ is the dz^2 orbital.[34,67,68] Hence, the redox potential of a metal-centered oxidation is expected to vary with axial ligand. Porphyrin ring oxidations, on the other hand, are unlikely to be affected greatly by the nature of the axial ligand. In addition to the constancy of the observed potentials, a difference of 0.29(±.05) V between the first and second ring oxidations has been accepted as diagnostic of successive, one-electron porphyrin ring oxidations.[39,68] The difference of 0.30 V that we observe between the potentials for peaks I and II, then, is further evidence of successive, one-electron ring oxidations.

Prewave Region

The prewave region and the unexpected shifts in the heretofore, well-characterized $Mn^{III/II}$ reduction, are more complex to interpret. As pointed out in the Results section, the absence of prewaves for $XMn^{III}TPP$ for the control experiments (X = ClO_4^-, BF_4^-, and PF_6^-) verify that the prewave behavior is, indeed, a result of an oxidation involving the axial anions themselves, rather than the porphyrin ring or the metal ion.

1. Br^-, I^-

It is clear that in the case of Br^- and I^-, the axial anion is dissociated from the porphyrin to a large extent in the acetonitrile/electrolyte solution and that the electrochemistry observed in the prewave region is due to free axial ligands. This equilibrium can probably best be described by the following :

$$XMn^{III}TPP + nCH_3CN = [(CH_3CN)_nMn^{III}TPP]^+ + X^- \quad (1)$$

where n = 1 or 2.

Not only are the patterns observed for TBAX and $XMn^{III}TPP$ very similar to one another, but no other change is observed in the positions of the other porphyrin redox processes on addition of TBAX to the porphyrin solutions. The two successive oxidations observed for free X^- have been previously observed in a number of nonaqueous solvents and have been identified as being due to the following reactions:

$$(1) \quad 3X^- \rightarrow X_3^- + 2e^-$$

$$(2) \quad 2X_3^- \rightarrow 3X_2 + 1e^-$$

where X = Cl^-, Br^-, and I^-.[69-73] In Table 2-7 are listed the previously reported potentials in CH_3CN solution for Cl^-, Br^- and I^- for comparison with the potentials observed in this study.

The observation of large prewaves for Br^- and I^- is also consistent with data published during the course of

the experimental work for this dissertation. In that study, Kadish[49] reports the equivalent conductances for $XMn^{III}TPP$ ($X = ClO_4^-$, Cl^-, I^-, and N_3^-). The magnitudes of the observed conductances strongly suggest that the ClO_4^- and I^- are almost completely dissociated in CH_3CN, while the Cl^- and N_3^- are only slightly dissociated. Kadish also looked at the effect of ionic strength and concluded from spectral data, that high ionic strength favors dissociation of the axial anions in polar solvents such as CH_3CN or pyridine. Based on the voltammetric results reported here, it seems likely that Br^- is also dissociated in CH_3CN to a large degree. This point will be addressed further in Chapter 3.

One complication arises in the case of iodide, in that the waves for the porphyrin ring oxidations disappear with repeated scans from 0.0 V to +2.0 V. Possible destruction of the porphyrin ring is ruled out by the observation that the porphyrin ring oxidation pattern reemerges, even at fast scan rates, when the negative switching potential is changed to -2.0 V. A possible explanation is that adsorption of iodine on the surface of the electrode becomes so extensive that further electrochemical processes are inhibited. Certainly adsorption of iodine on Pt electrodes has been well documented in aqueous solution.[73-75] Unfortunately, similar studies in nonaqueous solvents have not been reported, to the best of our knowledge. A problem with this explanation lies in

trying to explain why the electron transfers of the ring would be blocked, since in aqueous solution adsorption of iodine enhances electron transfer (See Chapters 1 and 4 for discussion and examples).

2. N_3^-, NCO^- and OAc^-

The anions N_3^-, NCO^-, and OAc^- present a quite different picture. Of these, N_3^- was the most "well-behaved" and so will be discussed first.

In this case (and for Cl^- and NO_2^- discussed in the next section) the potentials of the prewaves and of the free anion, as $TBAN_3$, differ substantially from one another. Both the prewave for $N_3Mn^{III}TPP$ at ~0.86 V and the irreversible wave at 0.41 V for $TBAN_3$ increase in intensity with addition of successive aliquots of $TBAN_3$ to porphyrin solutions. In addition, the first porphyrin ring oxidation shifts from 0.96 V to 0.90 V. This set of observations is similar to those observed for Cl^- and NO_2^- and will be discussed in detail in the next section.

The new wave, which appears first at ~0.38 V and shifts to ~0.09 V with successive additions of $TBAN_3$, cannot be explained by an oxidation of axial ligand, since a negative shift in the potential of the axial ligand would be difficult to explain. This new wave is certainly due to a one-electron oxidation of the species $N_3Mn^{III}TPP$, since e_{pa} and e_{pc}, the peak heights, remain constant and are about equal to those of the ring oxidations, the

metal-centered reduction, and the ring reductions. It is most likely that this new wave is a metal-centered oxidation to a $Mn^{IV}TPP^{+\cdot}$ species, possibly $(N_3)_2Mn^{IV}TPP$. The following observations lend support to this assignment:

1) The new wave becomes quasi-reversible for $E_\lambda \leq 0.60$ V.

2) Appearance of the wave for free N_3^- appears only after greater than a two-fold molar excess of N_3^- is added.

A significant contribution to the decreased reversibility of the $Mn^{(IV)/(III)}$ couple when $E_\lambda \geq 0.60$ V is the fact that the free ligand, N_3^- is apparently oxidized to form $N_3\cdot$, according to the following reactions[79,80]:

$$1)\quad N_3^- \rightleftharpoons N_3\cdot + e^-$$

$$2)\quad 2N_3\cdot \xrightarrow{\text{fast}} N_6 + 3N_2$$

Thus, any free N_3^- in solution would be oxidized irreversibly for scans to very anodic potentials. If a strongly coordinated axial ligand is required to achieve a metal-centered oxidation for Mn(III)Porphyrins, then removal of the excess ligand would render the process irreversible. In addition, enhanced reversibility, as evidenced by narrower peak widths, E_{pw}, and peak height ratios, i_{pa}/i_{pc} which approach unity, is observed for a) narrow scan ranges (0.0 to +0.60 V) and b) higher concentrations of excess $TBAN_3$. Again, this is consistent with a metal-centered oxidation which is favored by the presence of a

strongly coordinating axial ligand which can occupy the sixth coordination site. Further support for the assignment of this process to that of the $Mn^{IV/III}$ couple was obtained from spectroelectrochemical studies which will be presented in Chapter 3.

The cases of X = NCO^- and OAc^- are more difficult to interpret than N_3^-. Since each of these anions alone is stable to oxidation in the prewave region for TBA(NCO) or TBA(OAc), explanations invoking oxidation of dissociated ligand are inadequate. Oxidation of the coordinated ligand is also unlikely, unless the Mn^{III}TPP acts as a catalyst. Nevertheless, one cannot dismiss involvement of the axial ligand in these redox processes, since for both X = NCO^- and OAc^-, the prewaves grow in intensity with addition of TBAX to the porphyrin solution.

Unfortunately, the electrochemistry of neither of these anions has been extensively studied by voltammetry in nonaqueous solution. For the case of NCO^-, only reductions using polarography at a DME have been reported.[81] Thus, no literature values for potentials in the prewave region are available, nor are anodic potential limits. Surface studies of HNCO on Pt surfaces indicate that it adsorbs strongly on a clean Pt surfaces in ultra-high vacuum[87,88]. However, its behavior on electrodes has not been reported to our knowledge. Thus, while the blocking of the porphyrin ring oxidations in the presence of excess NCO^- may to be due to adsorption of free axial ligand,

verification of this would require extensive investigation.

Studies of acetate or of systems in HOAc as a solvent have been more extensive, although none specifically reports the potential limits.[82-84] Studies of the Kolbe reaction[86], however, suggest that no electrochemical processes occur in the prewave region that was observed for OACMn^{III}TPP. Furthermore, when glacial HOAc is used as the solvent, no oxidation appears until ~2.0 V *vs* SCE[85]. It is clear that HOAc adsorbs on Pt electrodes in water.[81-84] Again, no studies of adsorption in nonaqueous have been reported. We have seen evidence of strong adsorption waves for (OAc)Mn^{III}TPP, even in the absence of excess OAc^-, which are enhanced by addition of TBAOAc. (See Appendix 3, Figure A3-7).

It is reasonable to assign as a metal-centered oxidation, the new wave which appears at ~0.38 V on addition of TBA(OAc) or TBA(NCO) to solutions of the respective porphyrins. Although the new waves are irreversible, even for narrow scan ranges for these anions, the fact that they appear in the same general potential region as for X = N_3^- suggests a similar process. Since these waves appear before the prewaves for both NCO^- and OAc^- and do not grow in intensity with additions of more than a 2-fold excess of added TBAX, it is likely that they are one-electron transfers. Because of the irreversibility of the waves, and the inability to study the system at high concentrations of TBAX, confirmation of this assignment

had to come from the spectroelectrochemical studies which are described in Chapter 3.

3. Cl^- and NO_2^-

Interpretation of the results obtained for these anions is more ambiguous than for Br^- and I^-. In both of the present cases, the large difference between the potentials of the prewave and of the free anion ($\geq$ 100 mV) argue against a simple dissociation of the porphyrin species and subsequent oxidation of the free anion. On the other hand, the changes which take place on addition of TBAX to Mn(III)porphyrin solutions argue for anelectron transfer process involving the axial ligand. Since there were some differences in the patterns observed for Cl^- and NO_2^-, I will discuss each of them separately.

Any explanation of the prewaves observed for $ClMn^{III}TPP$, must take into account both the small, but significant, shift in the potential of the first ring oxidation, the scan rate dependence of the prewave itself, and the disappearance of this wave on addition of excess Cl^- to the porphyrin solution. Some possible explanations include:

1) The small dissociation constant for $XMn^{III}TPP$ in CH_3CN/TEAP solution results in a CE mechanism[64] (Chemical reaction, followed by an Electron transfer), as in the example below.

(1) $ClMn^{III}TTPP + CH_3CN \underset{k_b}{\overset{k_f}{\rightleftharpoons}} (CH_3CN)_nMn^{III}TPP + Cl^-$

(2) $3Cl^- \rightleftharpoons Cl_3^- + 2e^-$

In this case, a shift in the potential toward more positive potential for the Cl_3^-/Cl^- couple would be expected.

2) The prewave is due to the oxidation of the axial ligand still bonded to the Mn(III). As such, its potential might be expected to be shifted to more positive potentials relative to the free ligand. It is reasonable that such a process would also alter the positions of the ring oxidations, although it is not clear that a negative shift would be expected.

3) The prewave for $ClMn^{III}TPP$ is not due to oxidation of the axial ligand at all, but is due to oxidation at the metal center. This seems unlikely, however, since the waves continue to grow with increasing concentration of free Cl^- in contrast to the cases of N_3^-, NCO^-, and OAc^- where a metal-centered oxidation is almost certainly observed.

NO_2^- presents a similarly puzzling case. The fact that the prewave remains nearly constant in intensity with increasing concentration of excess TBA(NO_2) would tend to argue against oxidation of dissociated NO_2^- (Explanation 1 above, for X = Cl^-). Oxidation of bonded axial ligand or oxidation of the manganese remain possible ex-

planations.

In the cases of each of these axial anions, further studies are required to explain the puzzling prewave region. Some insight has been gained by spectroelectrochemical studies, as will be shown in Chapter 3.

4. OH^- and F^-

The last anions to be examined were F^- and OH^-. Unfortunately, these results were very inconclusive. In the case of OH^-, it was impossible to obtain any results in the presence of excess anion, because addition of even very small quantities of TBA(OH) resulted in immediate precipitation of the porphyrin. Since no prewaves were observed for $(OH)Mn^{III}TPP$, we can assume that the anion was tightly bound, and therefore, was not oxidized either as the free ligand or while bound to the metal. The shift in potential of the ring reduction with repeated anodic scans (See below) does, however, suggest that at sufficiently high potentials the axial ligand is oxidized, leaving only the species $(CH_3CN)_nMn^{III}TPP^+$ at the surface of the electrode. The fact that we observed a new process on addition of TBAF to $(PF_6)Mn^{III}TPP$ similar to that observed for N_3^-, NCO^-, and OAc^-, suggests that a metal-centered oxidation may occur for $X = F^-$, as well. However, since we were only able to perform this experiment successfully once (*i.e.* without precipitation) this assignment is very tentative.

Shift in $Mn^{III/II}$ Couple

A final insight into the nature of the processes occurring in the prewave region, is found in the observation of unexpected anodic shifts of the $Mn^{III/II}$ reduction with repeated scanning to very anodic potentials for X = N_3^-, NCO^-, OAc^-, NO_2^- and OH^- and a smaller, shift for X = Cl^-. This result would be expected for a mechanism in which the axial ligands themselves are irreversibly oxidized at switching potentials, E_λ, more anodic than the respective prewaves. In either of these cases, only the species, $(CH_3CN)_nMn^{III}TPP^+$ would be left at the surface of the electrode for the cathodic portion of the scan. At very slow scan rates, $XMn^{III}TPP$ would have time to diffuse to the electrode surface, resulting in smaller shifts or none at all. This is, indeed, what is observed. In the presence of excess axial ligand, on the other hand, this shift would be expected to be suppressed, even for very anodic E_λ. This is verified by the observation that the potentials of the metal-centered reductions shift to even more negative potentials for the anions OAc^-, N_3^- NCO^-, NO_2^-, and Cl^- in the presence of excess axial anion. Unfortunatly, these potentials are less reliable, because the waves are also broadened considerably, probably due to the everpresent problem of water of hydration in the tetraalkylammonium salts.

The observation that the anions X = ClO_4^-, BF_4^-,

PF_6^-, Br^- and I^- exhibit no shift in the $Mn^{III/II}$ couple with repeated scanning is consistent with the explanation offered above. For ClO_4^-, BF_4^- and PF_6^-, the potential observed is almost certainly that of the solvated porphyrin. Likewise, since $IMn^{III}TPP$ and $BrMn^{III}TPP$ are highly dissociated initially, their potentials are also that of the solvated species. Hence, the observed potentials show no further shift, even with anodic scans.

If the above explanation holds true, it is possible that the potential of the $Mn^{III/II}$ couple is a good indicator of the degree of association of the given axial ligand in the solvent/electrolyte solution. It also lends support to the arguments which invoke oxidation of the axial ligand to explain the prewaves described previously.

Third and Fourth Oxidations

One of the most surprising results of these studies was the observation of two well-resolved oxidations at potentials > 1.4 V. *vs* the $Ag/Ag^+(10^{-2}$ M) reference electrode. With the exceptions of X = ClO_4^-, NO_2^-, and I^-, most of the patterns observed were similar to one another, in that the third oxidation was the less intense of the two very anodic processes. Given the similarity in half-wave potentials for each of these processes for all of the anions except I^-, it is quite likely that these represent third and fourth ring oxidations. The appearance of a fifth oxidation for X = NO_2^- is possibly due to an oxida-

tion involving the axial ligand itself.

It is probable that the exceptional behavior observed for I^- is the result of adsorption of I^- on the electrode surface to form Pt-I. Certainly the very intense wave at ~1.58 V is due to the presence of free I^-, rather than any manganese porphyrin species. This is based on the similarity of the patterns for free TBAI, $IMn^{III}TPP$, and that observed for repetitive scans to +2.0 V for TBAI added to porphyrin. (See Figure 2-4 and Results).

The anion ClO_4^- represents another anomaly. The third and fourth oxidations are the most well-resolved and most nearly reversible of all of those we observed. It is difficult to explain the relative peak heights observed in terms of one-electron ring oxidations. Chemical follow-up reactions would seem to be ruled out, however, by the observation of increased reversibility at slower scan rates. Differences between ClO_4^- and the anions Cl^-, Br^-, OAc^-, NO_2^-, OCN^-, and N_3^- might be explained by the differences in a) the stability to oxidation of the anions, and b) the tendency to adsorb on the electrode surface. (Such differences seem unlikely for X = BF_4^- and PF_4^-, however.) Nevertheless, the most likely explanation for these oxidations appears to be the successive third and fourth ring oxidations of the porphyrin with possible interference from adsorption processes on the electrode surface. As we shall see in Chapter 3, further investiga-

tion of these processes was less rewarding than for the previously described electron transfers.

SUMMARY

In summary, evidence for several previously unobserved processes has been presented in this Chapter. Two oxidations have been observed which can be assigned to porphyrin ring oxidations. For $XMn^{III}TPP$, where X = N_3^-, NCO^- and OAc^-, a new wave which appears on addition of TBAX to porphyrin solutions has been tentatively assigned as the previously unreported $Mn^{IV/III}$ couple. Axial ligand dissociation and subsequent oxidation has been shown to be responsible for the prewaves observed for Br^- and I^-. The assignment of the prewaves for Cl^-, NO_2^-, N_3^-, OAc^-, and NCO^- is uncertain, although a mechanism involving axial ligand oxidation seems likely. The unexpected shift in the $Mn^{III/II}$ reduction for X = N_3^-, OH^-, NO_2^-, OAc^-, and NCO^- has been shown to be related to the prewave processes providing further evidence for axial ligand oxidations in the prewave regions. Finally, oxidations at very anodic potentials have been observed and tentatively assigned as ring oxidations with possible contributions from adsorption processes. In the case of I^-, oxidation of the adsorbed axial ligand is clearly involved, rather than porphyrin ring oxidations.

Further evidence for a number of the assignments presented above will be presented in Chapter 3.

REFERENCES

(1) Gibson, Q.H. in "The Porphyrins", Vol V, D. Dolphin, Ed.; Academic Press, New York, N.Y., 1979, Chapter 5.

(2) Mauzerall, D. in "The Porphyrins", Vol. V, D. Dolphin, Ed.; Academic Press, New York, N.Y., 1979, Chapter 2.

(3) Groves, J.T. *Advances in Inorg. Biochem.* , 1979, 119-145.

(4) Mauzerall, D.; Hong, F.T. in "Porphyrins and Metalloporphyrins" K.M. Smith, Ed., Elsevier, Amsterdam, 1975, Chapter 17.

(5) Smith, K.M. in "Porphyrins and Metalloporphyrins", K.M. Smith, Ed., Elsevier, Amsterdam, 1975, Chapter 2.

(6) J.W. Buchler in "The Porphyrins" D. Dolphin, Ed., Vol I, Academic Press, New York, N.Y., 1979, Chapter 10.

(7) Tabushi, I; Koga, N. *Tetrahedron Lett.*,1979, 3681-3684.

(8) Groves, J.T.Jr.; Kruper, W.J.; Haushalter, R.C. *J. Am. Chem. Soc.* 1976, *102*, 6375-6377.

(9) Hill, C.L.; Schardt,B.C. *J. Am. Chem. Soc.*, 1980, *102*, 374-6375.

(10) Chang, C.K.; Ebina, F. *J. Chem. Soc., Chem. Comm.*, 1981, 778-779.

(11) Mansuy , D.; Bartoli, J-F.; Chottard, J-C;

Lange, M. *Angew. Chem. Int. Ed. Engl.*, 1980, *19*, 909-910.

(12) Hill, C.L.; Smegal, J.A. *Nouv. J. Chimie*, 1982, *6*, 287-289.

(13) Mansuy, D.; Bartoli, J-F.; Momenteau, M. *Tetrahedron Lett.* 1982, *23*, 2781-2784.

(14) Schardt, B.C.; Hollander, F.J.; Hill, C.L. *J. Am. Chem. Soc.*, 1982, *104*, 964-3971.

(15) Camenzind, M.J.; Hollander, F.J.; Hill, C.L. *Inorg. Chem.*, 1982, *21*, 4301-4308.

(16) Camenzind, M.J.; Hollander, F.J.; Hill, C.L. submitted for publication.

(17) Smegal, J.A.; Schardt, B.C.; Hill, C.L. *J. Am. Chem. Soc.* 1983, *105*, 3510-3515.

(18) Smegal, J.A.; Hill, C.L. *J. Am. Chem. Soc.*, 1983, *105*, 2920-2922.

(19) Buchler, J.W.; Dreher, C.; Kiong, L.L. *Z. Naturforsch.* 1982, *37b*, 1155-1162.

(20) Hill, C.L.; Hollander, F.J. *J. Am. Chem. Soc.*, 1982, *104*, 7318-7319.

(21) Buchler, J.W; Dreher, C.; Lay, K-L.; Lee, Y.J.A.; Scheidt, W.R. *Inorg. Chem.*, 1983, *22*, 888-891.

(22) Goff, H.M.; Phillippi, M.A.; Boersma, A.D.; Hansen, A.P. *Adv. in Chem. Series.* 1982, *210*, 357-375.

(23) Scholz, W.; Reed, C.A. *unpublished results* personal communication.

(24) Porter, G. *Proc. Roy. Soc. London A.* 1978, *362*,

281-303.

(25) Harriman, A.; Porter, G. *J. Chem. Soc. Faraday Tans. II*, 1979, *75*, 1543-1552.

(26) Carnieri, N.; Harriman, A. *Inorg. Chim. Acta*, 1982, *62*, 103-107.

(27) Loach, P.A.; Calvin, M. *Biochem.*, 1963, *2*, 361-371.

(28) Calvin, M. *Pure and Appl. Chem.*, 1965, *15*, 1-10.

(29) Day, V.W.; Stults, B.R.; Tassett, E.L.; Day, R.O.; Marianelli, R.S. *J. Am. Chem. Soc.*, 1974, *96*, 2650-2652.

(30) Landrum, J.T.; Scheidt, W.R.; Reed, C.A. *J. Am. Chem. Soc.*, 1980, *102*, 6729-6735.

(31) Mark Camenzind, *This laboratory, unpublished results.*

(32) Clack, D.W.; Hush, N.S. *J. Am. Chem. Soc.*, 1965, *87*, 4238-4243.

(33) Felton, R.H.; Linschitz, H. *J. Am. Chem. Soc.*, 1966, *88*, 1113-1116.

(34) Boucher, L.J. *Coord. Chem. Rev.*, 1972, *7*, 289-329.

(35) Stanienda, A.; Biehl, G. *Z.Phys. Chem. (Frankfurt am Main)*, 1967, *52*, 254-275.

(36) Manasson, J.; Wolberg, A.; *J. Am. Chem. Soc.*, 1970, *92*, 2982- 2291.

(37) Fajer, J.; Borg, D.C.; Forman, A.;Dolphin, D.; Felton, R.H. *J. Am. Chem. Soc.*, 1970,, *92*, 3451- 3459.

(38) Boucher, L.J.; Garber, H.K. *Inorg. Chem.* 1970, *9*, 2644-2649.

(39) Fuhrhop, J. H.; Kadish, K.M.; Davis, D.G.; *J. Am. Chem. Soc.*, 1973, *95*, 5140-5147.

(40) Fuhrhop, J.H. *Structure and Bonding*, 1974, *18*, 1-67.

(41) Wolberg, A. *Israel. J. Chem.*, 1974, *12*, 1031-1035.

(42) Kadish, K.M.; Morrison, M.M.; *J. Am. Chem. Soc.*, 1976, *98*, 3326-3328.

(43) Fuhrhop, J.J. in "Porphyrins and Metalloporphyrins", Kevin Smith, Ed., Elsevier, New York, 1978, Chapter 14.

(44) Kadish, K. M.; Morrison, M.M. *Bioinorg. Chem.*, 1977, *7*, 107-115.

(45) Williams, R.F.X.; Hambright, P. *Bioinorg. Chem.*, 1978, *9*, 537-544.

(46) Kadish, K.M.; Bottomley, L.A.; Kelly, S.; Schaepper, D.; Shiue, L.R. *Bioelectrochem. and Bioenergetics*, 1981, *8*, 213-222.

(47) Kadish, K.M.; Sweetland, M.; Cheng, J. *Inorg. Chem.*, 1978, *17*, 2795-2797.

(48) Kadish, K.M.; Kelly, S. *Inorg. Chem.*, 1979, *18*, 2968-2971.

(49) Kelly, S.L.; Kadish, K.M. *Inorg. Chem.*, 1982, *21*, 3631-3639.

(50) Shimomura, E.T.; Phillippi, M.A.; Goff, H.M.; Schatz, W.F.; Reed, C.A. *J. Am. Chem. Soc.*, 1981, *103*, 6778-6780.

(51) Schardt, B.C.; Hill, C.L. *Inorg. Chem.*, 1983, *22*, 1563-1565.

(52) Armstrong, N.R.; Lin, A.W.C.; Fujihara, M.; Kuwana, T. *Anal. Chem.*, 1976, 741-750.

(53) Oldham, K.B. *Anal. Chem.*, 1973, *45*, 39-47.

(54) Dalrymple-Alford, P.; Goto, M.; Oldham, K.B. *Anal. Chem.*, 1977, *49*, 1390-1394.

(55) Hubbard, A.T. *CRC Critical Rev. Anal. Chem.*, 1973, *3*, 201-241.

(56) Hubbard, A.T.; Anson, F.C. *Electroanal. Chem.* 1971, *4*, 129- 214.

(57) Murray, R.W.; Heineman, W.R.; O'Dom, G.W. *Anal. Chem.*, 1967, *13*, 1666-1668.

(58) Bowden E.F.; Hawkridge, F.M. *J. Electroanal. Chem.*, 1981, *125*, 367-386.

(59) Diggle, J.W.; Parker, A.J. *Electrochim. Acta*, 1973, *18*, 975-979.

(60) Shriver, D.F. "The Manipulation of Air-Sensitive Compounds". New York, N.Y., McGraw-Hill, 1969.

(61) House, H.O.; Feng, E.; Peet, N.P. *J. Org. Chem.*, 1971, 36, 2371-2375.

(62) Adler, A.D.; Longo, F.R.; Yoshida, Z.; Kim, J. *J. Inorg. Nucl. Chem.*, 1970, 32, 2443-2445.

(63) Ogoshi, Watanabe, E.; Yoshida, Z.; Kincaid, J.; Nakamoto, K. *J. Am. Chem. Soc.*, 1973, 95, 2845-2849.

(64) Nicholson, R.S.; Shain,I.; *Anal. Chem.*, 1964, 36, 706-723.

(65) Dalrymple-Alford, P.; Goto, M.; Oldham, K. B. *J. Electroanal. Chem.*, 1977, *85*, 1-15.

(66) Toman, J.T. Ph.D. Thesis, University of California, Berkely, Ca, 1982.

(67) Zerner, M.; Gouterman, M. *Theoret. Chim. Acta (Berl)*, 1966, *4*, 44-63.

(68) Kadish, K.; Davis, D.G.; Fuhrhop, J.H. *Angew, Chem. Internat. Ed.*, 1972, *11*, 1014-1016.

(69) Kolthoff, I.M.; Coetzee, J.F.*J. Am. Chem. Soc.*, 1957, *79*, 1852-1858.

(70) Iwamoto, R.T. *Anal. Chem.*, 1959, *31*, 955.

(71) Desbarres, J. *Bull. Soc. Chim. France*, 1961, 502-506.

(72) Nelson, I.V.; Iwamoto, R.T. *J. Electroanal. Chem.*, 1964, *7*, 218-221.

(73) Hubbard, A.T. *Acc. Chem. Res.*, 1980, *13*, 177-184.

(74) Felton, T.E.; Hubbard, T.E. *J. Electroanal. Chem.*, 1979, *100*, 473-491.

(75) Garwood, G.A.; Hubbard, A.T. *Surf. Sci.*, 1980, *92*, 617-635.

(76) Boucher, L.J. *Ann. N.Y. Acad. Sci.*, 1973, *206*, 409-418.

(77) Dickinson, L.C.; Chien, J.W.C. *J. Biol. Chem.* 1977, *10*, 6156-6152.

(78) Day, V.W.; Stults, B.R.; Tasset, E.L.; Day, R. O.; Marianelli, R. S. *J. Am. Chem. Soc.*, 1974, *96*, 2650-2652.

(79) Plzak, V.; Wendt, H. *Ber. Bunsenges Phys. Chem.*, 1979, *83*, 481-486.

(80) Cauquis, G.; Serve, D. *Bull. Soc. Chim. France*,

1979, 145-152.

(81) O. Hammerich and V.D. Parker in 'The Chemistry of Cyanates and Their Thio Derivatives," Vol.I, S. Patai, Ed., Wiley, Chichester, England, 1977, Chapter 9.

(82) Mastagastino, M.; Casalbore, G.; Valcher, S.; *Electroanal. Chem.*, 1973, 44, 37-45.

(83) Parker, V.D.; Eberson, L. *J. Chem. Soc. Chem. Com.*, 1969, 340.

(84) Nelson, I.V.; Iwamotot, R.T.; *Anal. Chem.*, 1963, 35, 867-871.

(85) Wieckowski, A.; Sobkowski, J.; Zebenay, P.; Krzysztof, F. *Electrochimica Acta*, 1981, 25, 1111-1119.

(86) Sekine, I.; Ohkawa, H.; *Electrochimica Acta*, 1980, 25, 1647-1653.

(87) Solymosi, F.; Bańsagi, *J. Phys. Chem.*, 1979, 83, 532-553.

(88) Solymosi, F.; Kiss, J. *Surf. Sci.*, 1981, 108, 641-659.

CHAPTER 3

Spectroelectrochemical Studies of Manganese Porphyrin Oxidations

Optical spectra of porphyrins and metalloporphyrins have been widely used for characterization of electronic structure and for identification of porphyrin species. In theoretical studies[1] the characteristic absorption spectra of porphyrins have been used to construct molecular orbital diagrams of porphyrins and metalloporphyrins, and a review of the optical spectra and electronic structure of these species has recently appeared.[2]

In early studies the spectroscopy and electronic structure[3,4] of manganese(III)porphyrin complexes were explored. A review of manganese porphyrins[5] included a summary of UV/vis spectral data for Mn(III) and Mn(II) porphyrin complexes. An optical spectrum was reported for the one-electron oxidation observed for an oxidative titration of Mn^{III}hematoporphyin(IX) dimethyl ester.[6] This spectrum was assigned to that of a Mn(IV) species, although its assignment was not confirmed by other characterization.

A typical metalloporphyrin spectrum (See Figure 3-1) is characterized by two Q bands between 500 and 600 nm and a B band between 380 and 400 nm. The Q bands, which are quasi-allowed, (ϵ = 1.2 to 2 x 10^4 $M^{-1}\cdot cm^{-1}$) are classified as an α and β band; the α band is at-

tributed to the lowest energy excited singlet, while the β band has been shown to have vibrational modes mixed in. The B band, often known as the Soret band, is strongly allowed (ϵ = 2 to 4 x 10^5 $M^{-1}\cdot cm^{-1}$) and is attributed to the second excited singlet. Both the B band and the Q bands have been assigned as $\pi \rightarrow \pi^*$ transitions of the porphyrin ligand.

Manganese(III)porphyrin spectra differ from the "normal" metalloporphyrin spectrum described above, in that they have prominent ($\epsilon > 10^3$ $M^{-1}\cdot cm^{-1}$) "extra" bands in the region $\lambda > 320$ nm. Figure 3-2 illustrates a typical manganese(III)porphyrin spectrum and shows a qualitative MO diagram with the transitions which are commonly assigned to each band.[1,2,5] The "extra bands" are attributed to LMCT($a_{1u}(\pi)$,$a_{2u}(\pi) \rightarrow e_g(d\pi)$), an assignment which predicts a dependence of bands V and VI on the nature of the axial ligand. Indeed, Boucher[3-5] has shown that the energy order for band V for XMn(III)Etioporphyrin(H_2O) is:

$$F^- > OAc^- > NCO^- > OH^- \sim Cl^- > N_3^- \sim NCS^- \sim Br^- > I^-$$

This is the same order observed for the reduction potentials of the $Mn^{III/II}$ couple.[8] (See Introduction, Chapter 2) In these same studies Boucher also noted moderate solvent shifts for the absortion maxima for Mn(III)porphyrins, and again, bands V and VI were the most affected. For non-coordinating to moderately coordinating solvents such as acetone, CH_3CN, $CHCl_3$, and CH_2Cl_2, the most polar-

izable (as measured by the refractive index of the solvent) exhibited the lowest energy absorption. In strongly coordinating solvents, the absorption maxima were independent of the axial anion and exhibited energy shifts in the order:

H_2O > EtOH ~ MeOH > $C_4H_{11}OH$ ~ DMSO ~ DMF ~ n-$BuNH_2$ > Py

The spectra of manganese(II)porphyrins (See Figure 3-3) have been designated by Gouterman[2] as "pseudonormal", since they have a large B (Soret) band at ~440 to 444 nm and are missing the "extra" bands of the manganese(III)porphyrin spectra. Although Mn(II)porphyrins are d^5, *h.s.* in which the d orbitals are half-filled, Gouterman[2] argues that the LMCT transitions ($a_{1u}(\pi)$,$a_{2u}(\pi)$ → $e_g(d\pi)$) are too high in energy to be observed.

In more recent work spectra of one-electron oxidized manganese porphyrins have been reported.[9-16] An example of a typical manganese(IV)porphyrin spectrum is shown in Figure 3-4.[9-12] These spectra are characterized by loss of bands III and IV between 500 and 600 nm (See Figure 3-4) and the appearance of a band in the region of 520 to 540 nm. Similarly, an intense band in the region of 410 to 420 nm replaces bands V, Va, and VI of the Mn(III)porphyrin spectrum.

The spectra of porphyrin π radical cations have also been reported[13-16] (See Figure 3-5) and are characterized by the presence of bands III and IV between 500 to 600 nm

and bands V and VI near 390 and 490 nm. This spectrum resembles that of $(ClO_4)Mn^{III}TPP$ although the relative intensities of bands V and VI have been reversed, and band V has shifted to lower energy. No theoretical studies have yet appeared on the spectra of the oxidized manganese porphyrins.

The only published spectra for two-electron oxidized manganese porphyrins are those of the (nitrido)manganese(V)porphyrins.[17,18] (See Figure 3-5.) These spectra resemble those of Mn^{V}porphyrins in that they are characterized by loss of bands III and IV and the appearance of a band at ~530 to 540 nm ($NMn^{V}OEP$ has a second band at 560 nm[17]). A band in the region of 400 to 420 nm replaces bands V, Va and VI of the Mn^{III}porphyrin spectrum and appears sharper and more intense than the comparable band observed for Mn^{V}porphyrins.

In this Chapter I will describe the results of both spectral and spectroelectrochemical studies. It will be shown from spectral studies that adding excess axial anion to a solution of $XMn^{III}TPP$ in acetonitrile leads to formation in solution of several previously unreported six-coordinate manganeses(III)porphyrins. Spectroelectrochemical results will be presented which confirm the prewave assignments proposed in Chapter 2. Likewise, confirmation of the assignment of the $Mn^{III/IV}$ couple for $X = OAc^-$, N_3^-, OCN^-, and CN^- and determination of $E_{1/2}$ for this couple will be given. Spectral evidence will also be

also be presented which confirms the assignment of the first ring oxidation. Finally, the first report of the spectrum of the manganese(III)porphyrin dication ($[Mn^{III}TPP^{\cdot\cdot}]^{+3}$) will also be presented.

FIGURE 3-1

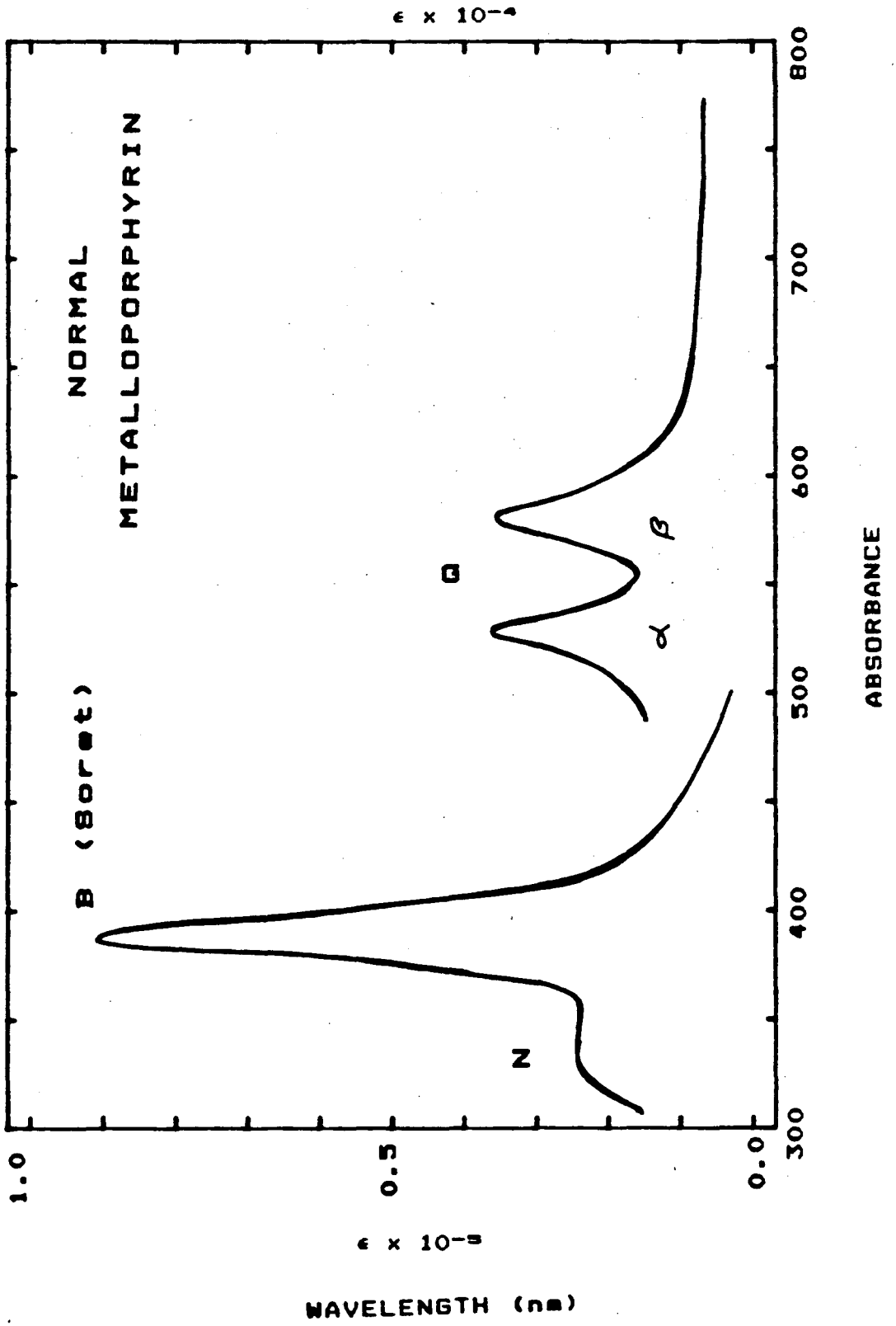
ε x 10⁻⁴
NORMAL
METALLOPORPHYRIN
B (Soret)
Q
α
β
N
800
700
600
500
400
300
1.0
0.5
0.0
ε x 10⁻⁵
ABSORBANCE
WAVELENGTH (nm)

FIGURE 3-2

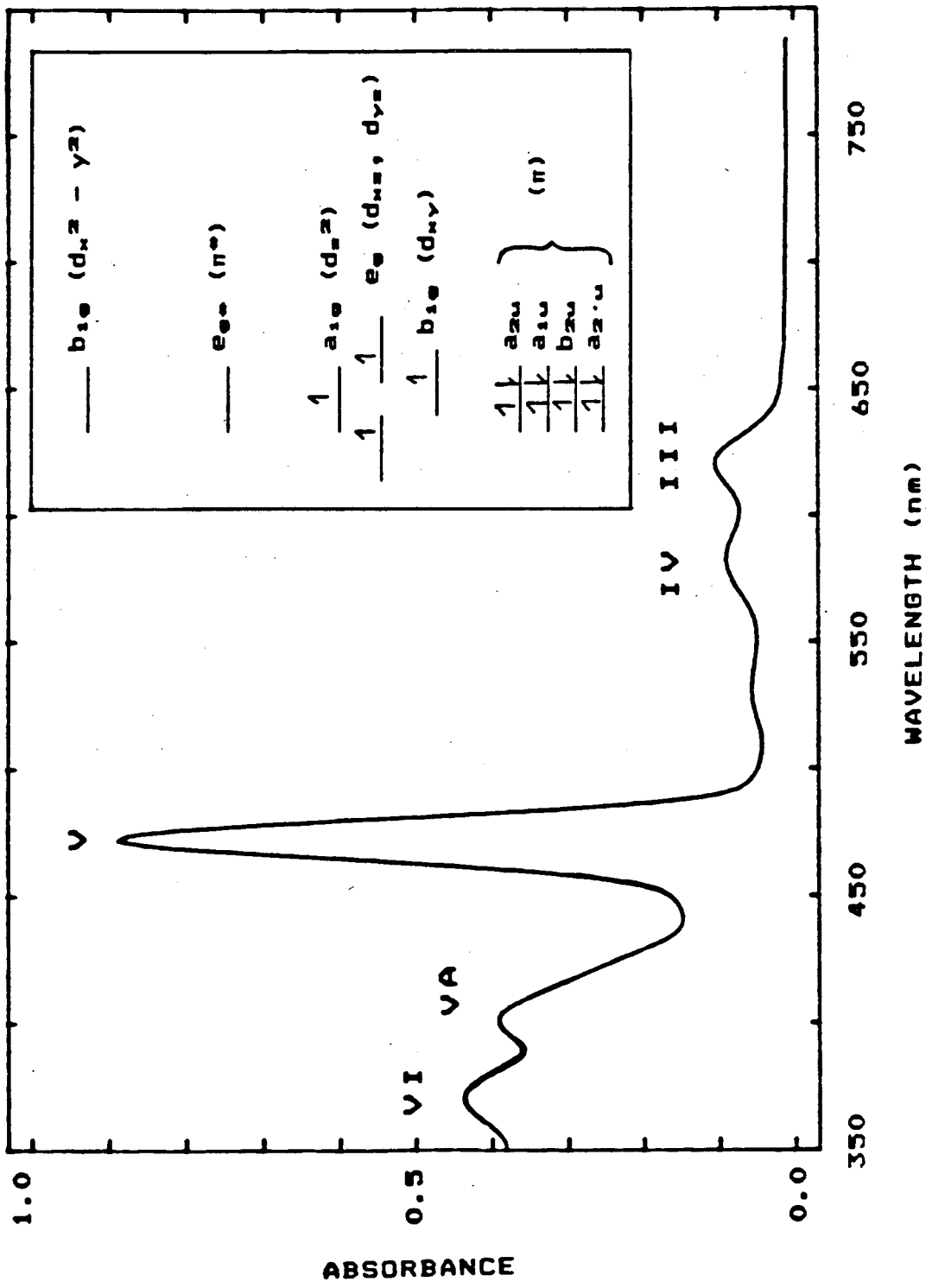
ABSORBANCE
1.0
0.5
0.0
350
450
550
650
750
WAVELENGTH (nm)
V
VI
VA
IV
III
II
I

FIGURES 3-3 THROUGH 3-6

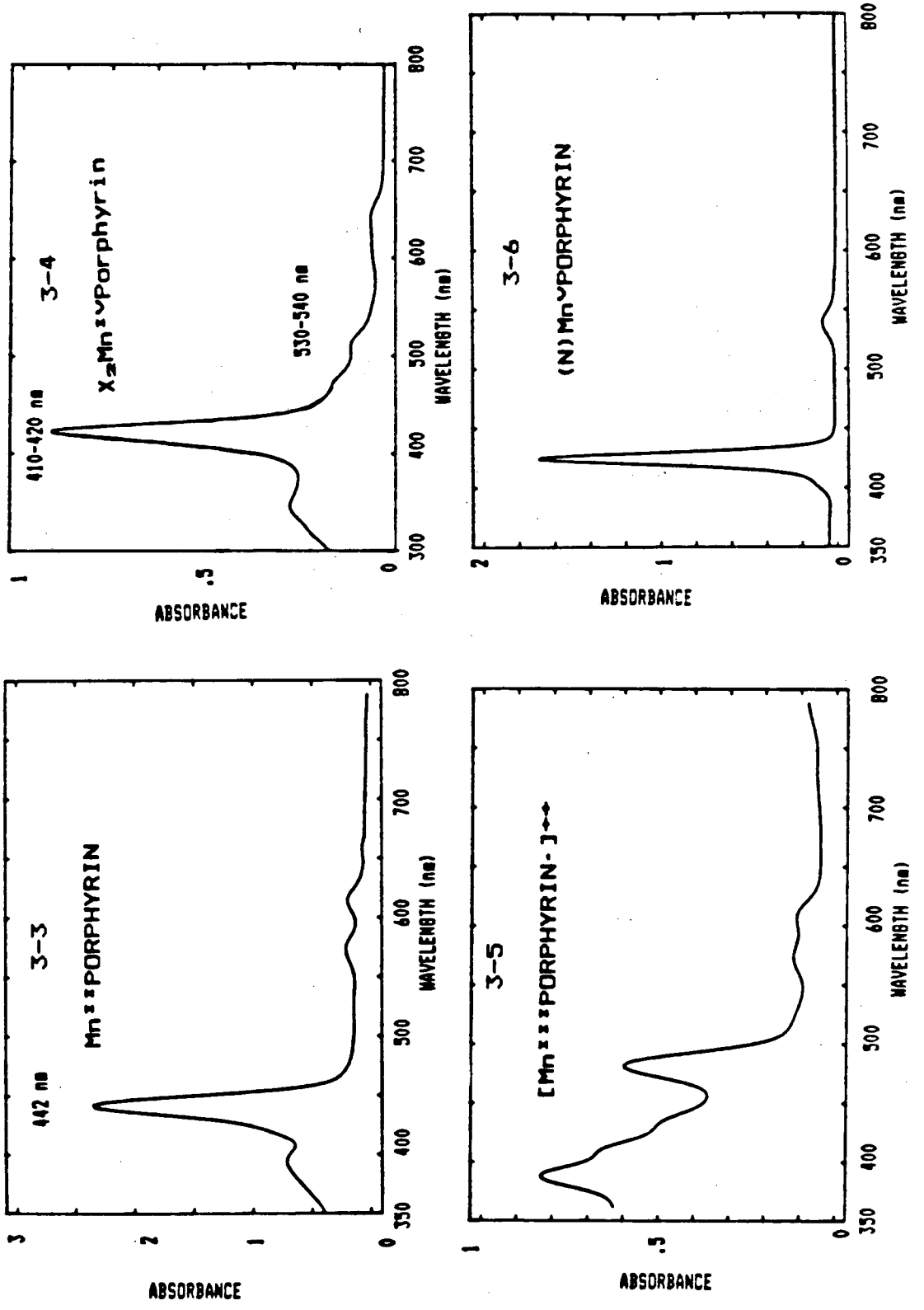

EXPERIMENTAL

MATERIALS

All chemicals and solvents were as described in Chapter 1. The working electrode for the optically transparent thin-layer electrochemical cells (OTTLE) were electroformed gold mesh (200 lines per inch) obtained from Buckbee-Mears. The electrode material was handled with forceps to avoid contamination of the surface. Each thin-layer gold mesh electrode was used for only one experiment and then discarded. The OTTLE cells were disassembled after each experiment, and the Ertalyte cell body was soaked in 6M HNO_3 or, if necessary, *aqua regia* to remove porphyrin stains from the surface. They were rinsed with triply distilled water and allowed to dry before being reassembled. RTV 112 silicone rubber purchased from General Electric was used to make the gaskets and to seal the quartz windows in the OTTLE cells.

INSTRUMENTATION

Instrumentation for spectroelectrochemical experiments was the Model 173 Potentiostat/Galvanostat from Princeton Applied Research interfaced with a Hewlett Packard Model 8450 UV/Vis Spectrometer as described in Chapter 1. The voltage between the reference electrode and the working electrode was monitored at the electrometer using a Data Precision Model 3500 digital volt-ohm meter.

METHODS

All solutions were degassed by repeated freeze-pump-thaw cycles on a dual manifold Schlenk line[18] before being transferred to the OTTLE cells. Filling of the cells was as described in Chapter 1. The reference electrode was the $Ag/AgNO_3$ (10^{-2} M), TEAP (0.1 M), CH_3CN and was calibrated as described in Chapter 1.

Spectroelectrochemical data were obtained from linear sweep voltammetric (LSV) experiments done at a scan rate, ν, of 1 $mV \cdot s^{-1}$ between two potential limits which were chosen on the basis of the results of the semi-derivative LSV experiments described in Chapter 2. A spectrum was recorded before any potential was applied, and the open circuit potential was noted. This "rest" potential was usually used as the initial potential for the first scan for a given cell. The spectrometer was programmed to record spectra every 30 seconds as described in Chapter 1. In all cases the same cell was cycled several times through each potential region to insure that no decomposition of the porphyrin had occurred during the course of the experiment. To determine the potentials at which spectral changes occurred, plots were made of absorbance, A, at selected wavelengths *vs* E_{app} and dA/DE *vs* E_{app} as described in Chapter 1.

RESULTS

I. Spectra of $XMn^{III}TPP$

In order to interpret the results of spectroelectrochemical studies, the spectrum was measured of each $XMn^{III}TPP$ in CH_3CN alone, in CH_3CN with 0.1 M TEAP, and in CH_3CN with both TEAP and TBAX in varying ratios. Since some unexpected results were obtained in these control experiments, a more careful examination of these spectra was required.

Spectra of most $XMn^{III}TPP$ in CH_3CN only and in CH_3CN with up to 1.0M TEAP differed only slightly from one another or from spectra of the same $XMn^{III}TPP$ in solvents such as CH_2Cl_2 or C_6H_6. As expected, each $XMn^{III}TPP$ was characterized by a spectrum unique to the given axial anion. Typically, the observed differences were most pronounced in the wavelengths and relative intensities of bands V, Va, and VI.

Addition of .002 to 0.1 M TBAX to ~1 mM solutions of $XMn^{III}TPP$ in CH_3CN produced new spectra for X = I^-, OAc^-, N_3^-, NCO^-, NO_2^-, and CN^-. For all other X^- addition of TBAX produced minor changes, usually in relative intensities of absorption bands. Figures 3-7 through A4-10 in Appendix 4 show spectra for $XMn^{III}TPP$ in CH_3CN, CH_3CN with 0.1 M TEAP, and CH_3CN with various concentrations of TBAX.

A description of the kinds of spectral changes observed for each group of anions follows:

1) ClO_4^- (Figure 3-7) Addition of TEAP resulted in

negligible spectral changes.

2) BF_4^- (Figure 3-8) The spectra of $(BF_4)Mn^{III}TPP$ in CH_3CN only or in the presence of 0.1 M TEA(BF_4) differed significantly from each other in the relative intensities, but not in the energies, of the observed absorption bands. The addition of 0.1 M TEAP to ~1 mM $BF_4Mn^{III}TPP$, however, resulted in a shift of band V from 476 to 484 nm to yield a spectrum virtually indistinguishable from that of $(ClO_4)Mn^{III}TPP$.

3) Cl^- and Br^- (Figures 3-9 and 3-10): Addition of 0.1 M TEAP or 0.1 M TBAX to ~ 1mM solutions of $XMn^{III}TPP$ each yielded small spectral changes. In each case addition of TEAP resulted in spectra more nearly resembling those of $(ClO_4)Mn^{III}TPP$, while addition of TBAX resulted in spectra with more of the characterisics oF $XMn^{III}TPP$ in CH_2Cl_2.

4) I^- (Figure 3-11): In CH_3CN with no electrolyte, a spectrum very similar to that of $(ClO_4)Mn^{III}TPP$ was observed. Addition of 0.1 M TBAI yielded a shift in band V from 484 nm to 496 nm and large shifts in the positions and relative intensities of all other bands, resulting in a spectrum closely resembling that of $IMn^{III}TPP$ in CH_2Cl_2. In CH_3CN with 0.1 M TEAP a shift of band V in the opposite direction, to 480 nm, with a concomitant decrease in the relative intensities of bands VI to band V occurred.

5) NO_2^-, OAc^-, N_3^-, and NCO^- (Figures 3-12 through 3-15): Addition of 0.1 M TEAP to solutions of each of

these $XMn^{III}TPP$ yielded only small spectral changes. Addition of 0.1 M TBAX, however, yielded 12 to 16 nm shifts of band V to higher energy and significant changes in the wavelength and relative intensities of all other bands.

6) CN^- (Figure 3-16): This spectrum was obtained by addition of aliquots of solutions of 0.1 M TBA(CN) to ~1 mM solutions of $(BF_4)Mn^{III}TPP$. The spectrum produced when the ratio of $TBACN/BF_4Mn^{III}TPP$ was ~1.0 appeared to be that of a mixture of species. For ratios of $TBACN/BF_4Mn^{III}TPP \geq 2$ the band at 492 nm disappeared, but all other bands remained unchanged. This spectrum was indistinguishable from one observed in CH_2Cl_2 which was attributed to the formation of the six-coordinate $[NC)_2Mn^{III}TPP]^-$ species.[19]

A summary of the wavelengths and estimated extinction coefficients for the observed absorption maxima for each $XMn^{III}TPP$ in CH_3CN only, in CH_3CN + 0.1M TEAP, and in CH_3CN + 0.1 M TBAX is presented in Table 3-1.

TABLE 3-1

SPECTRA OF MANGANESE(III)PORPHYRINS IN CH_3CN

	ABSORPTION BAND[a]				
XMn^{III}TPP	VI	VA	V	IV	I
Cl^-	373(3.2)	399(2.7)	476(6.6)	582(.55)	620(.66)
+ TBACl	370(3.0)	400(2.8)	474(6.6)	582(.63)	620(.74)
+ TEAP	386(3.6)	—	474(6.6)	582(.63)	620(.74)
Br^-	379(3.4)	—	486(6.7)	586(.72)	624(.87)
+ TBABr	378(6.0)	402(4.4)	484(8.3)	588(.83)	626(1.08)
+ TEAP	381(5.5)	—	482(6.3)	582(.76)	620(.80)
I^-	389(7.8)	408(5.3)	484(3.9)	576(.89)	608(.89)
+ TBAI	386(8.8)	—	496(5.1)	—	638(1.2)
+ TEAP	387(5.2)	406(4.2)	480(4.2)	574(.90)	620(.80)
OAc^-	372(3.6)	396(3.5)	468(8.7)	576(.76)	612(.76)
+ TBA(OAC)	385(2.9)	--	452(13.9)	570(.94)	610(.80)
+ TEAP	373(4.0)	396(3.9)	468(9.8)	576(.86)	612(.86)
N_3^-	383(7.3)	399(6.5)	482(7.0)	590(.86)	628(1.22)
+ $TBAN_3$	372(4.1)	412(4.7)	470(6.1)	586(.86)	624(.96)
+ TEAP	381(4.7)	—	482(4.7)	592(.55)	628(.79)
NCO^-	373(3.9)	399(3.5)	472(8.7)	582(.73)	618(.84)
+ TBA(NCO)	360(2.5)	396(2.9)	458(10.0)	578(.74)	618(.79)
+ TEAP	373(3.9)	399(3.6)	472(8.7)	582(.76)	618(.86)

TABLE 3-1 (cont'd)

XMn^{III}TPP	ABSORPTION BAND[a] VI	VA	V	IV	III
NO_2^-	388(5.1)	400(4.8)	474(8.1)	578(.92)	614(.95)
+ TBA(NO_2)	369(2.5)	396(2.9)	462(5.9)	574(.51)	612(.49)
+ TEAP	380(5.9)	400(5.5)	474(9.8)	578(1.1)	614(1.1)
CN^- [b]	—	—	—	—	—
$CN^-/BF_4^- \leq 1$	--	—	492	—	—
$CN^-/BF_4^- \geq 2$	410(4.0)	430(4.8)	456(2.7)	544(.72)	578(.72)
ClO_4^-	389(6.0)	408(4.4) 432(2.8)	484(3.7)	574(.85)	610(.81)
+ TEAP	389(6.0)	410(4.5) 432(2.9)	484(3.8)	574(.88)	608(.83)
BF_4^-	389(6.4)	410(4.7) 434(3.0	484(3.8)	574(.92)	610(.87)
+ TEA(BF_4)	383(4.9)	—	472(6.3)	574(.89)	612(.84)
+ TEAP	383(4.9)	—	472(6.3)	574(.89)	612(.84)

a Wavelength (nm). Extinction coefficient ($\epsilon \times 10^{-4}$) is in parentheses.

b No spectrum for (CN)Mn^{III}TPP was obtained, since the CN^- spectrum was generated from addition of aliquots of 0.1M TBA(CN) to 1 mM solutions of (BF_4)MN^{III}TPP in CH_3CN 0.1M TEAP.

FIGURE 3-7

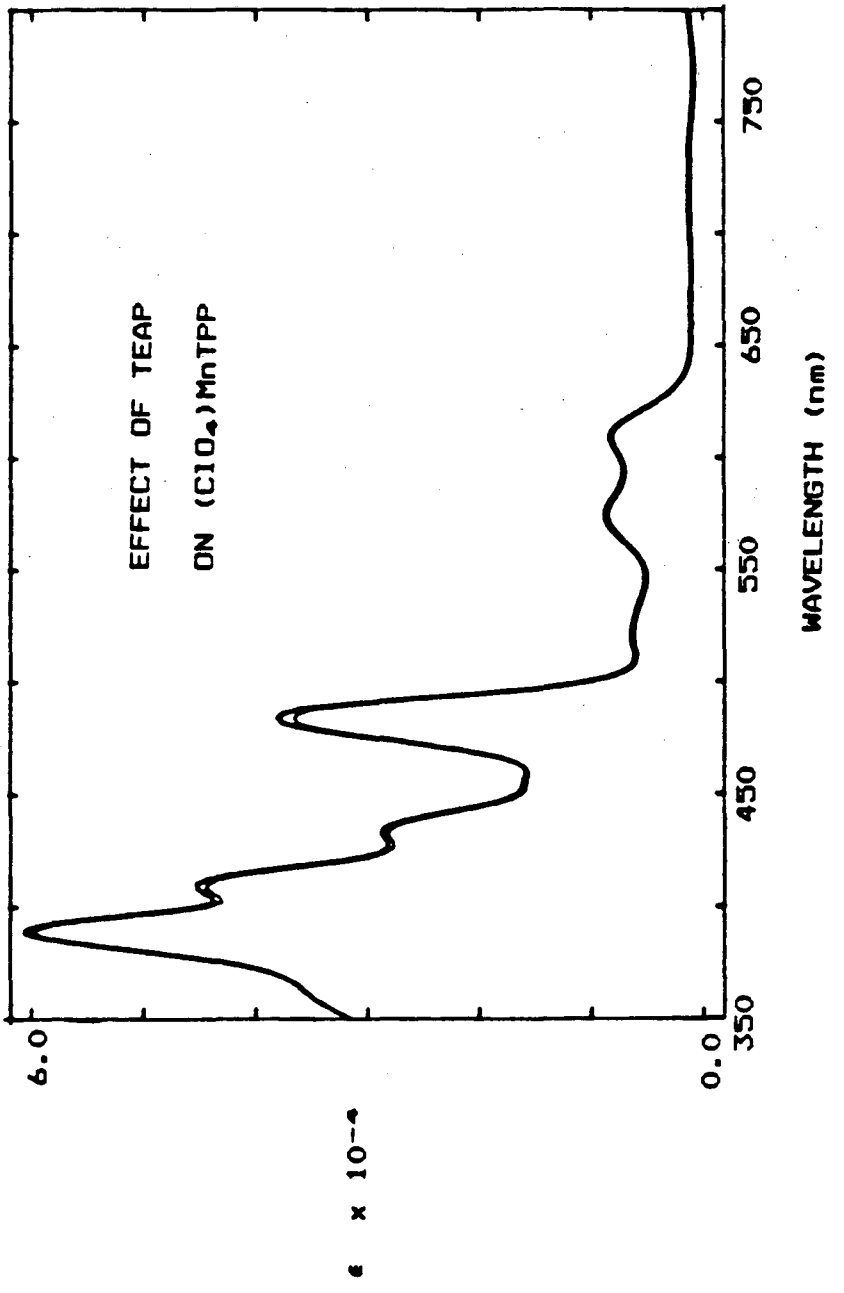
EFFECT OF TEAP
ON (ClO4)MnTPP
6.0
0.0
350
450
550
650
750
WAVELENGTH (nm)
ε x 10⁻⁴

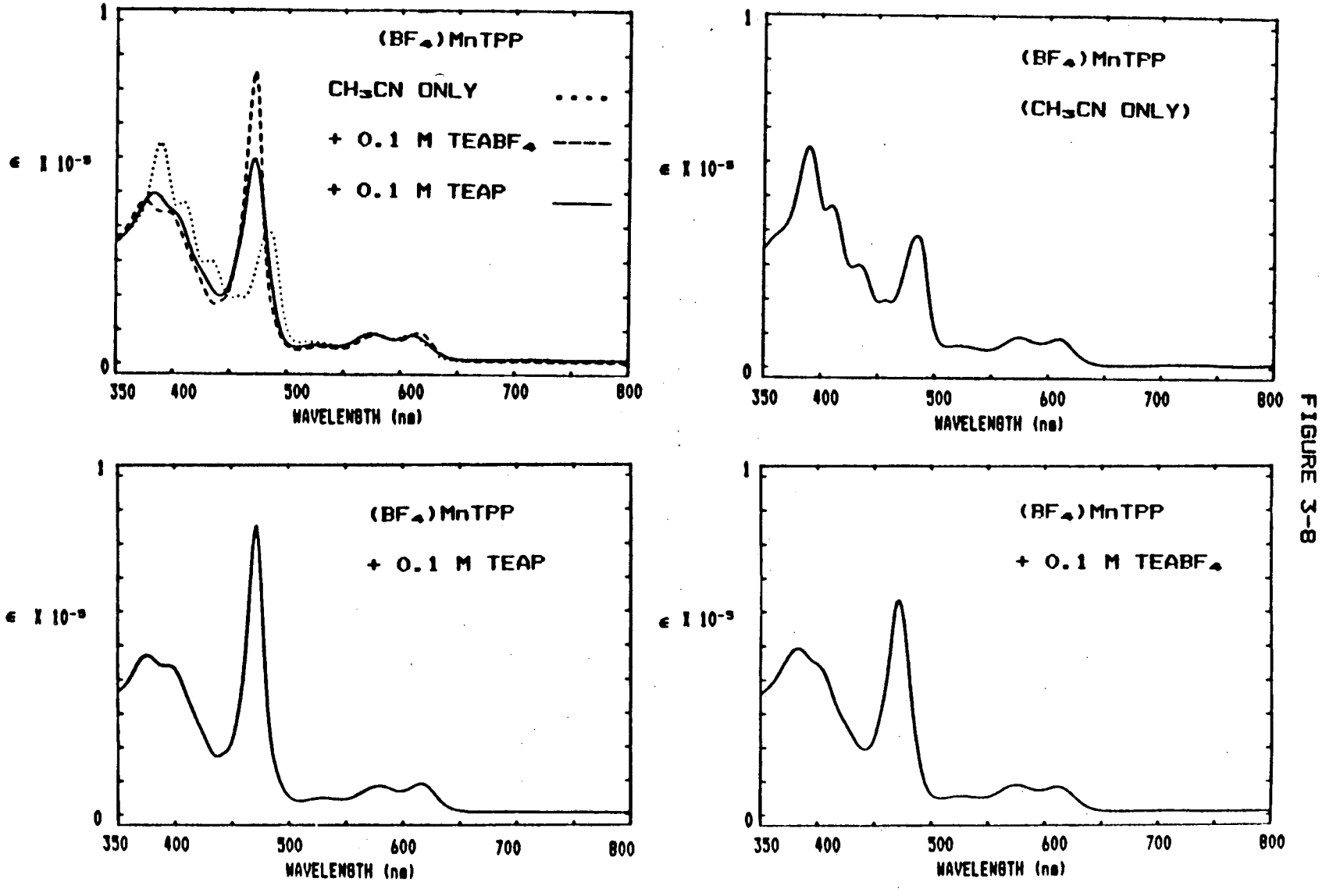
(BF4)MnTPP
CH3CN ONLY
+ 0.1 M TEABF4
+ 0.1 M TEAP
ε X 10⁻⁵
WAVELENGTH (nm)
(BF4)MnTPP
(CH3CN ONLY)
(BF4)MnTPP
+ 0.1 M TEAP
(BF4)MnTPP
+ 0.1 M TEABF4

FIGURE 3-8

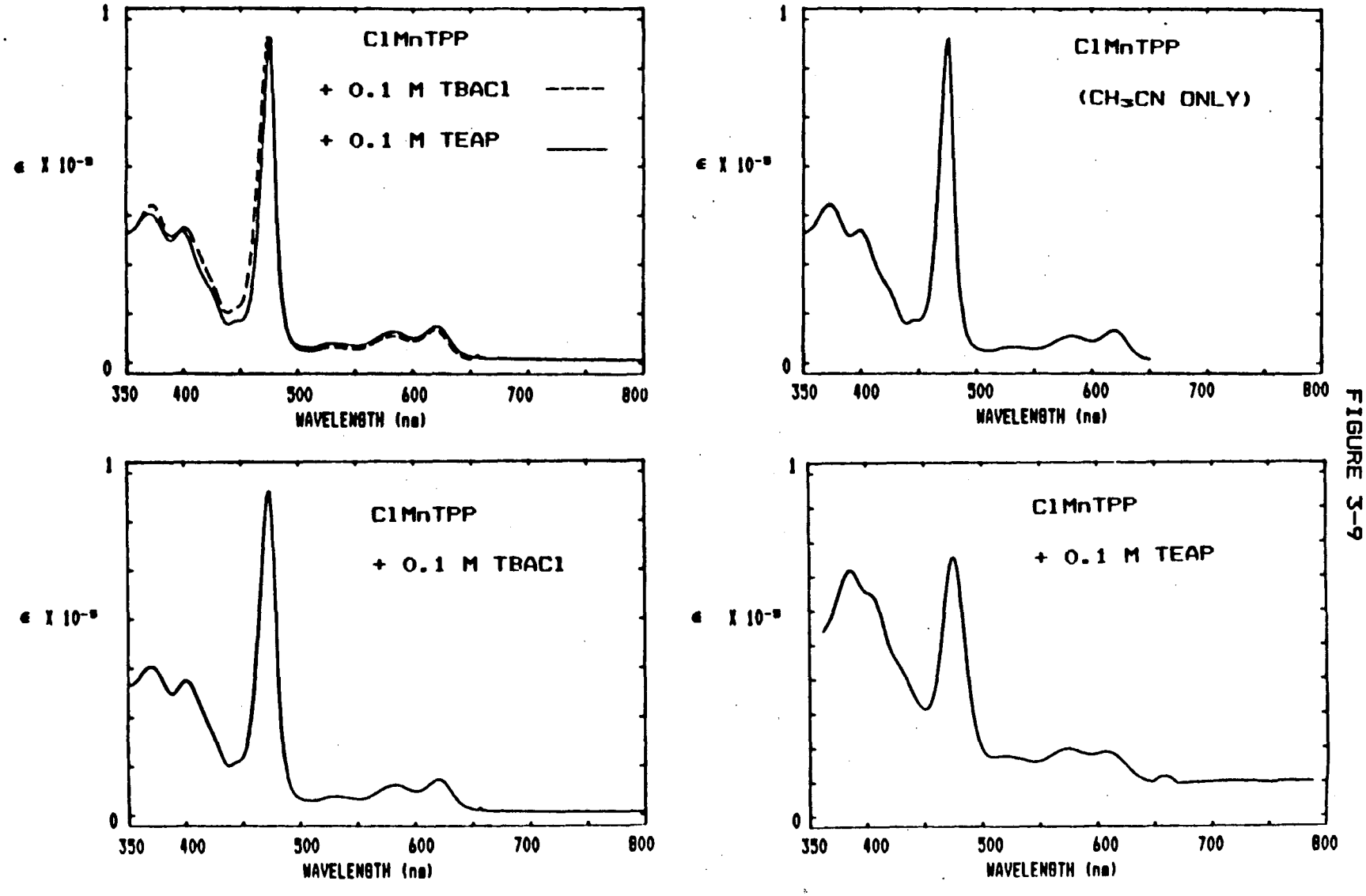
ClMnTPP
+ 0.1 M TBACl
+ 0.1 M TEAP
ε X 10⁻⁴
WAVELENGTH (nm)
ClMnTPP
(CH₃CN ONLY)
ε X 10⁻⁴
WAVELENGTH (nm)
ClMnTPP
+ 0.1 M TBACl
ε X 10⁻⁴
WAVELENGTH (nm)
ClMnTPP
+ 0.1 M TEAP
ε X 10⁻⁴
WAVELENGTH (nm)

FIGURE 3-9

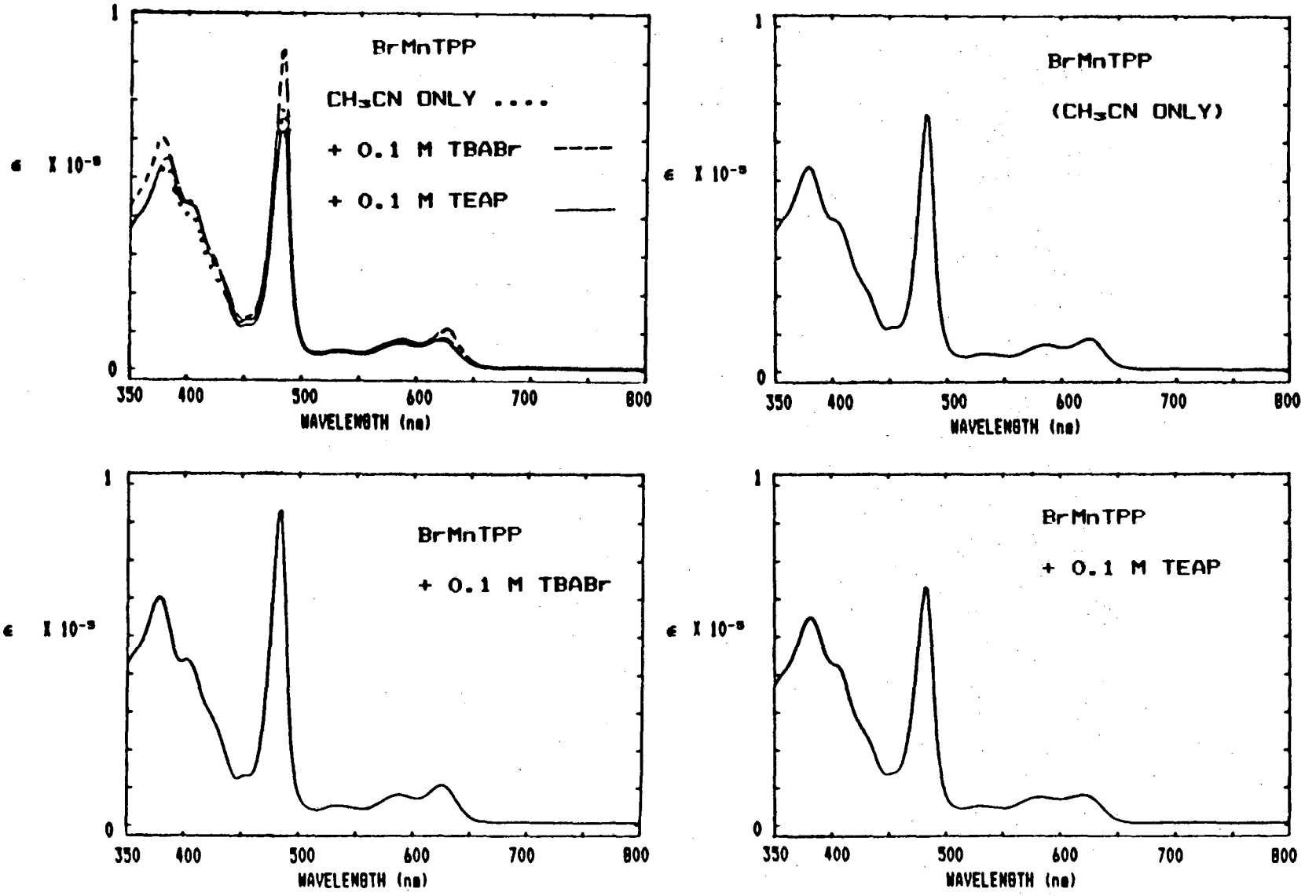
BrMnTPP
CH3CN ONLY ....
+ 0.1 M TBABr ----
+ 0.1 M TEAP ——
ε X 10⁻⁵
1
0
350 400 500 600 700 800
WAVELENGTH (nm)
BrMnTPP
(CH3CN ONLY)
BrMnTPP
+ 0.1 M TBABr
BrMnTPP
+ 0.1 M TEAP

FIGURE 3-10

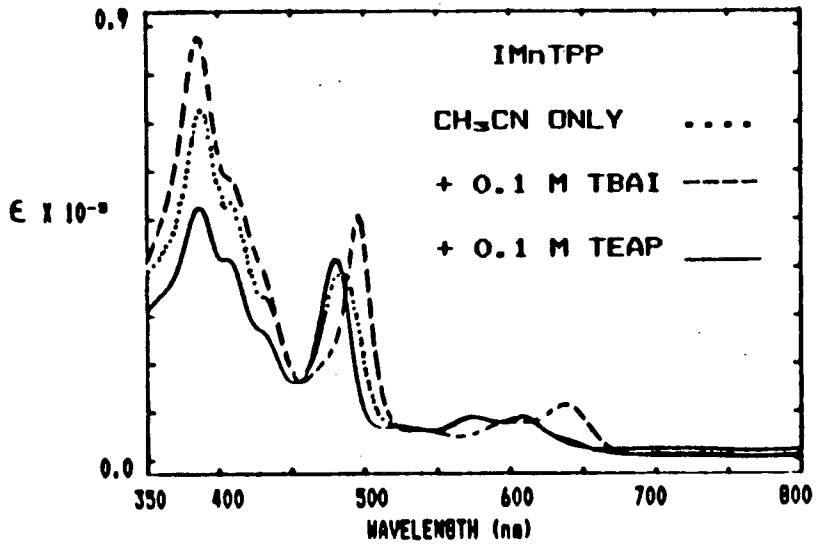
IMnTPP
CH3CN ONLY
+ 0.1 M TBAI
+ 0.1 M TEAP
ε X 10⁻⁴
0.9
0.0
350
400
500
600
700
800
WAVELENGTH (nm)

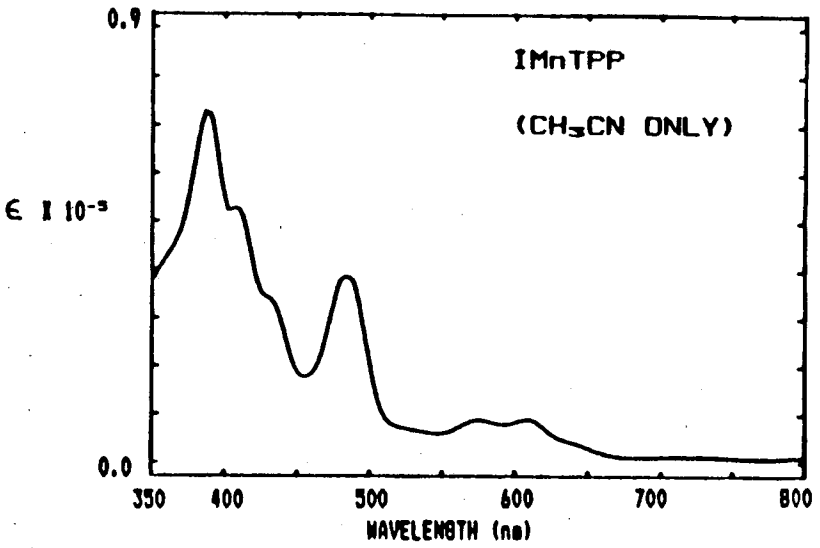
IMnTPP
(CH3CN ONLY)
ε X 10⁻⁴
0.9
0.0
350
400
500
600
700
800
WAVELENGTH (nm)

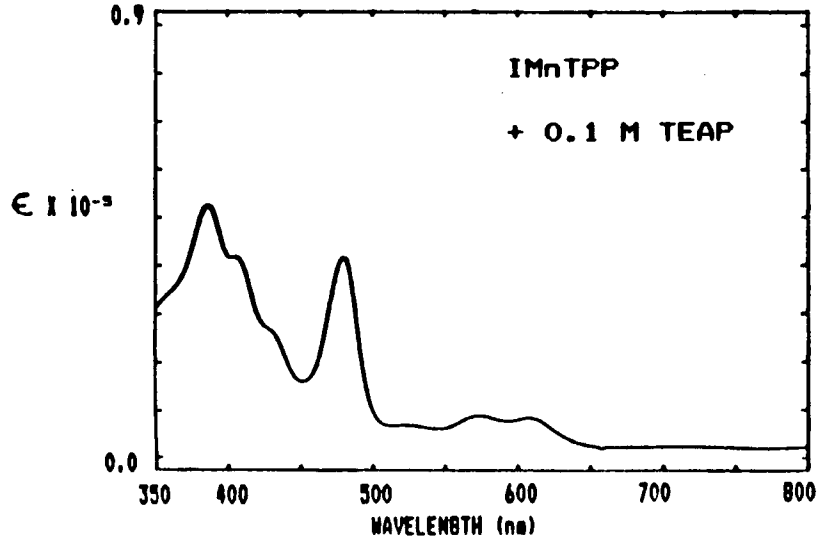
IMnTPP
+ 0.1 M TEAP
ε X 10⁻⁴
0.9
0.0
350
400
500
600
700
800
WAVELENGTH (nm)

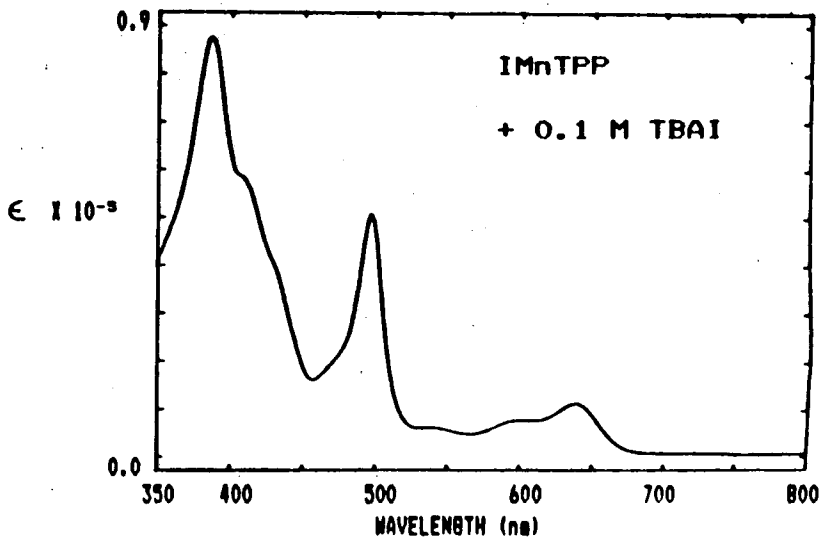
IMnTPP
+ 0.1 M TBAI
ε X 10⁻⁴
0.9
0.0
350
400
500
600
700
800
WAVELENGTH (nm)

FIGURE 3-11

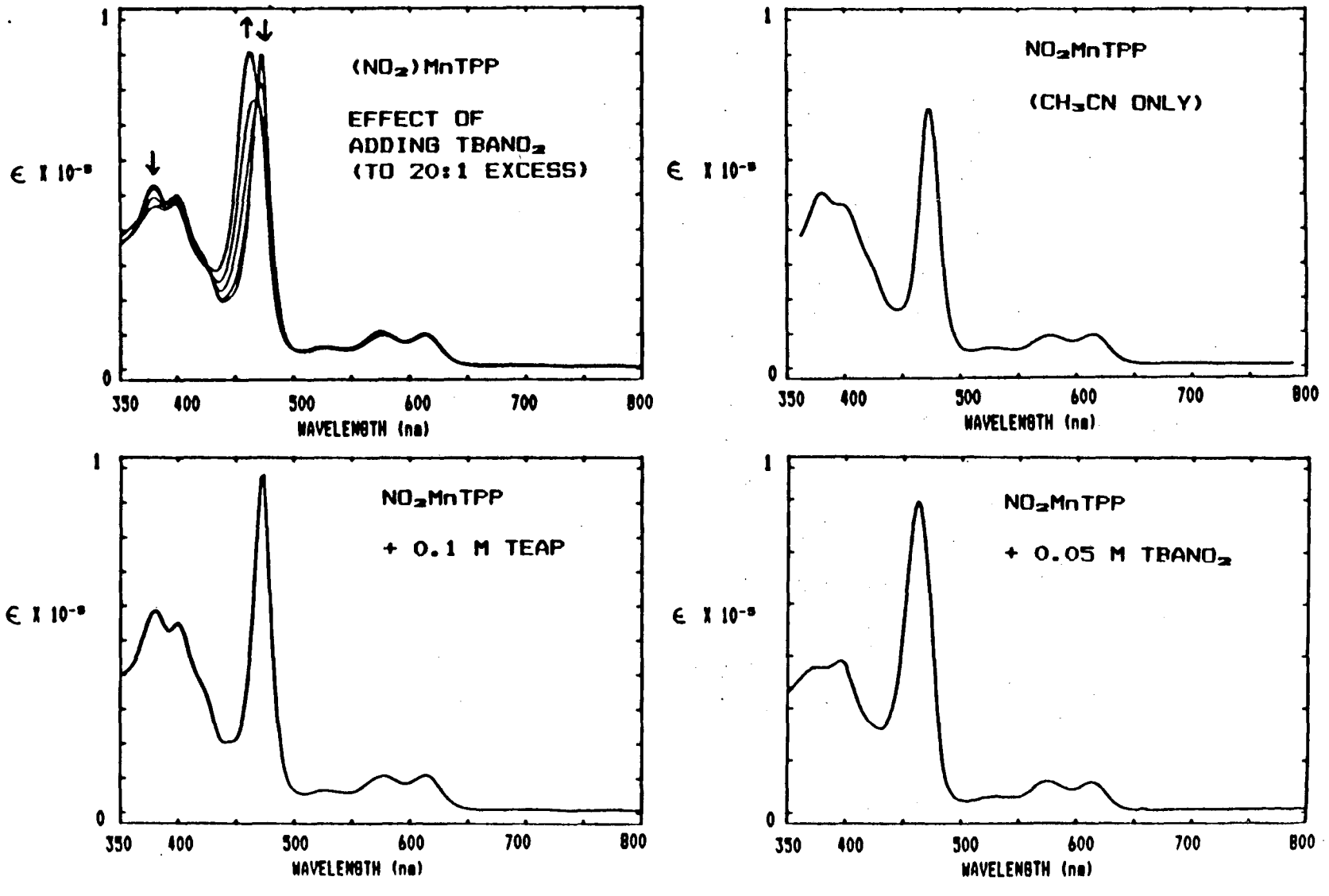
(NO2)MnTPP
EFFECT OF
ADDING TBANO2
(TO 20:1 EXCESS)
NO2MnTPP
(CH3CN ONLY)
NO2MnTPP
+ 0.1 M TEAP
NO2MnTPP
+ 0.05 M TBANO2
ε X 10-5
WAVELENGTH (nm)
350
400
500
600
700
800
1
0

FIGURE 3-12

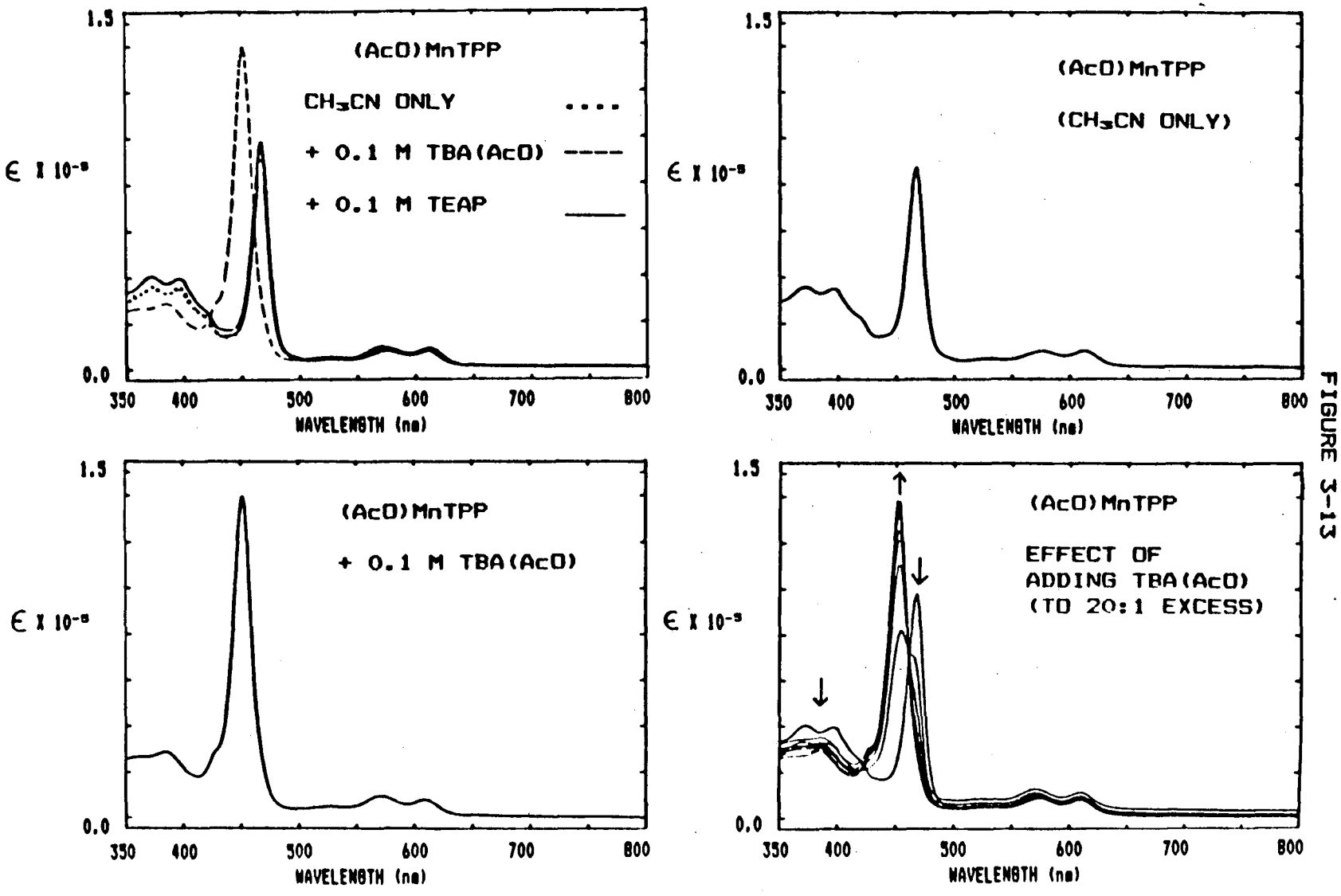
(AcO)MnTPP
CH3CN ONLY
+ 0.1 M TBA(AcO)
+ 0.1 M TEAP
ε X 10⁻⁵
1.5
0.0
350
400
500
600
700
800
WAVELENGTH (nm)
(AcO)MnTPP
(CH3CN ONLY)
(AcO)MnTPP
+ 0.1 M TBA(AcO)
(AcO)MnTPP
EFFECT OF
ADDING TBA(AcO)
(TO 20:1 EXCESS)

FIGURE 3-13

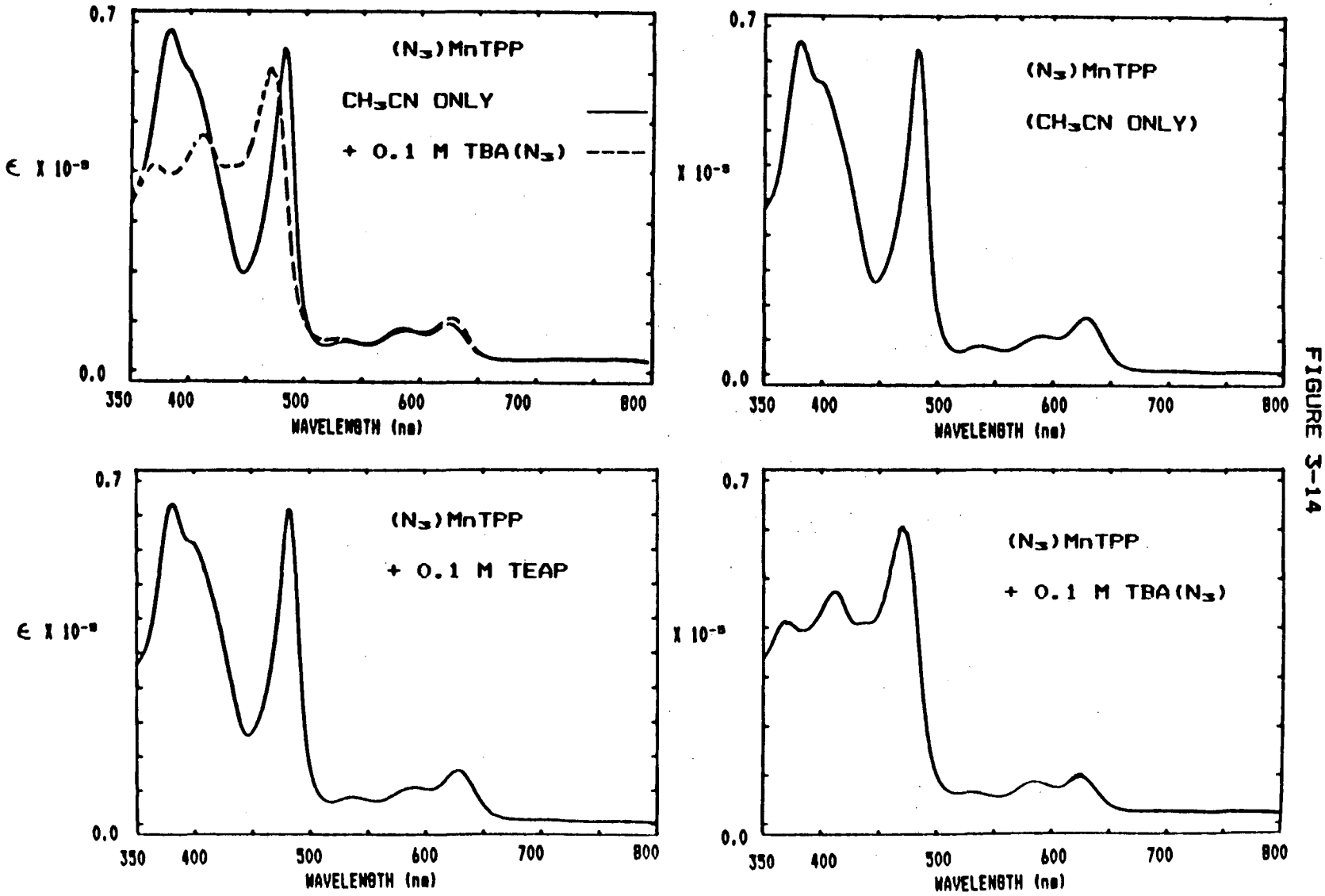
0.7
0.0
ε X 10⁻⁵
(N₃)MnTPP
CH₃CN ONLY
+ 0.1 M TBA(N₃)
350 400 500 600 700 800
WAVELENGTH (nm)
(N₃)MnTPP
(CH₃CN ONLY)
X 10⁻⁵
(N₃)MnTPP
+ 0.1 M TEAP
(N₃)MnTPP
+ 0.1 M TBA(N₃)

FIGURE 3-14

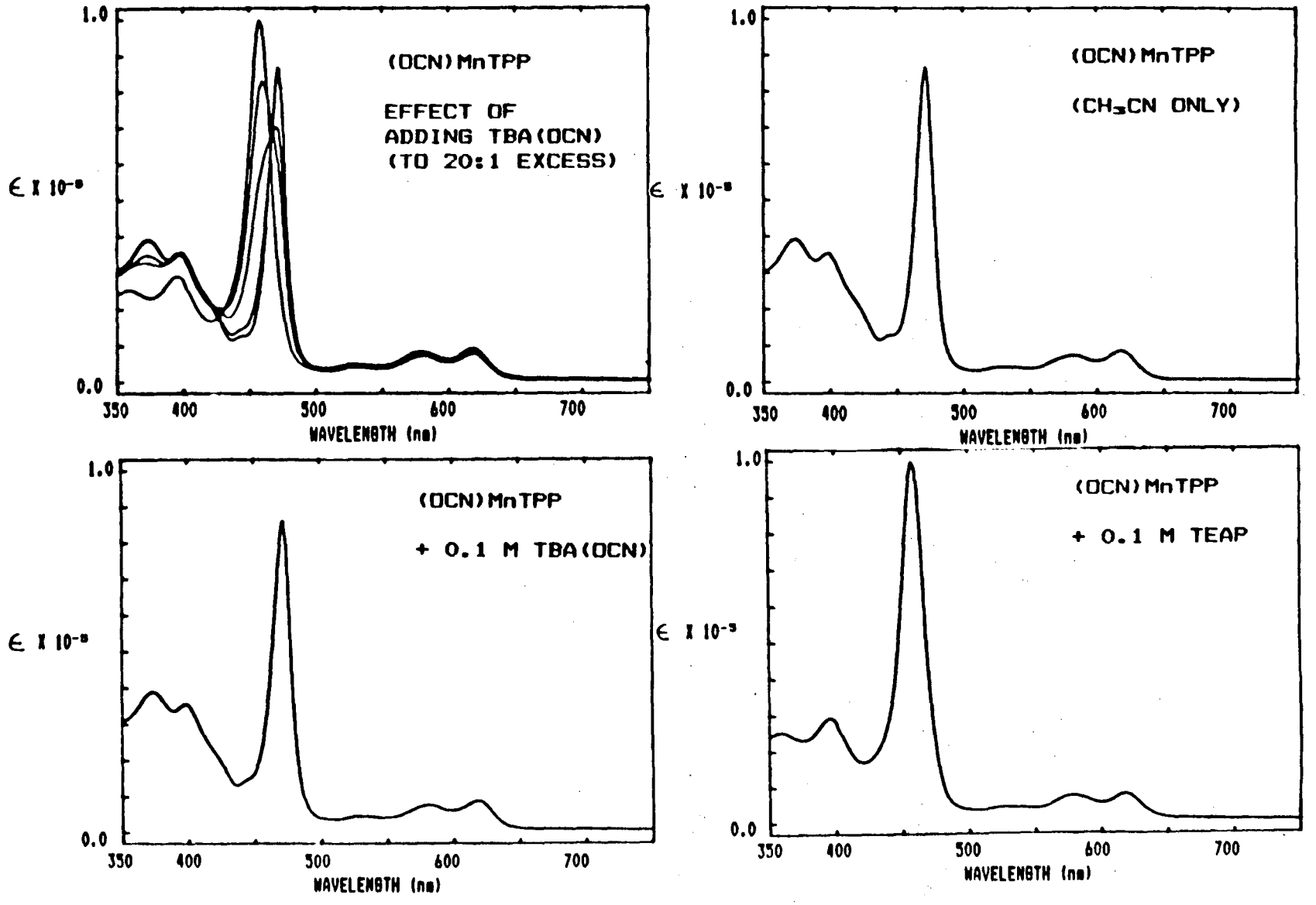
(OCN)MnTPP
EFFECT OF
ADDING TBA(OCN)
(TO 20:1 EXCESS)
(OCN)MnTPP
(CH3CN ONLY)
(OCN)MnTPP
+ 0.1 M TBA(OCN)
(OCN)MnTPP
+ 0.1 M TEAP
ε X 10⁻⁴
WAVELENGTH (nm)
1.0
0.0
350
400
500
600
700

FIGURE 3-15

FIGURE 3-16

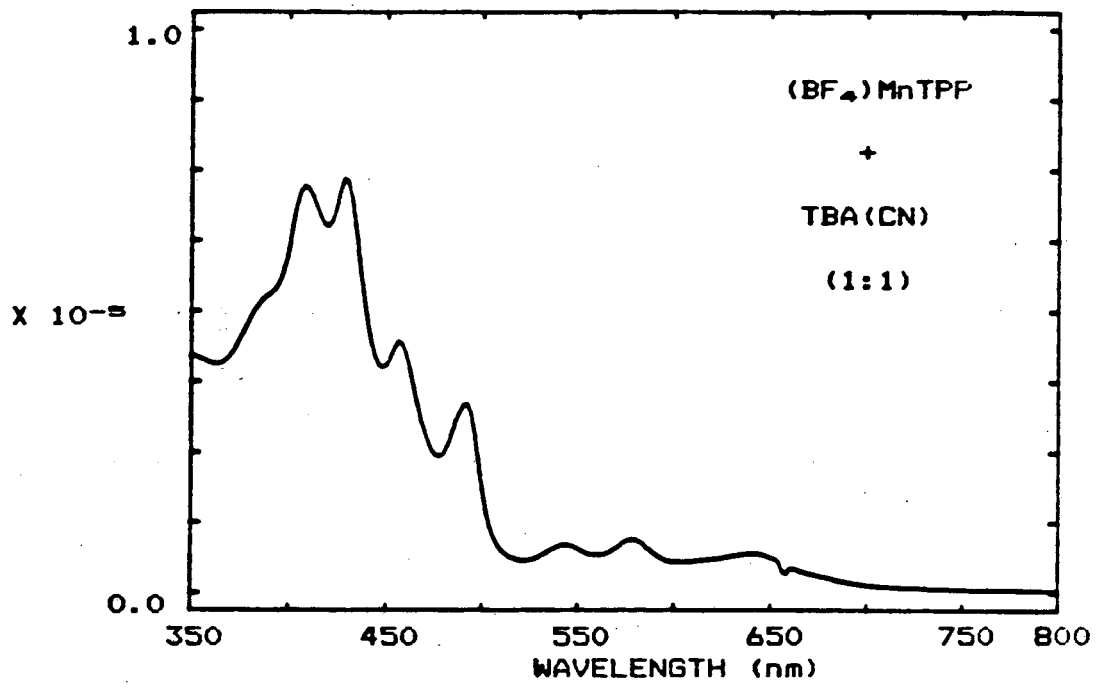
1.0
0.0
X 10-5
(BF4)MnTPP
+
TBA(CN)
(1:1)
350
450
550
650
750
800
WAVELENGTH (nm)

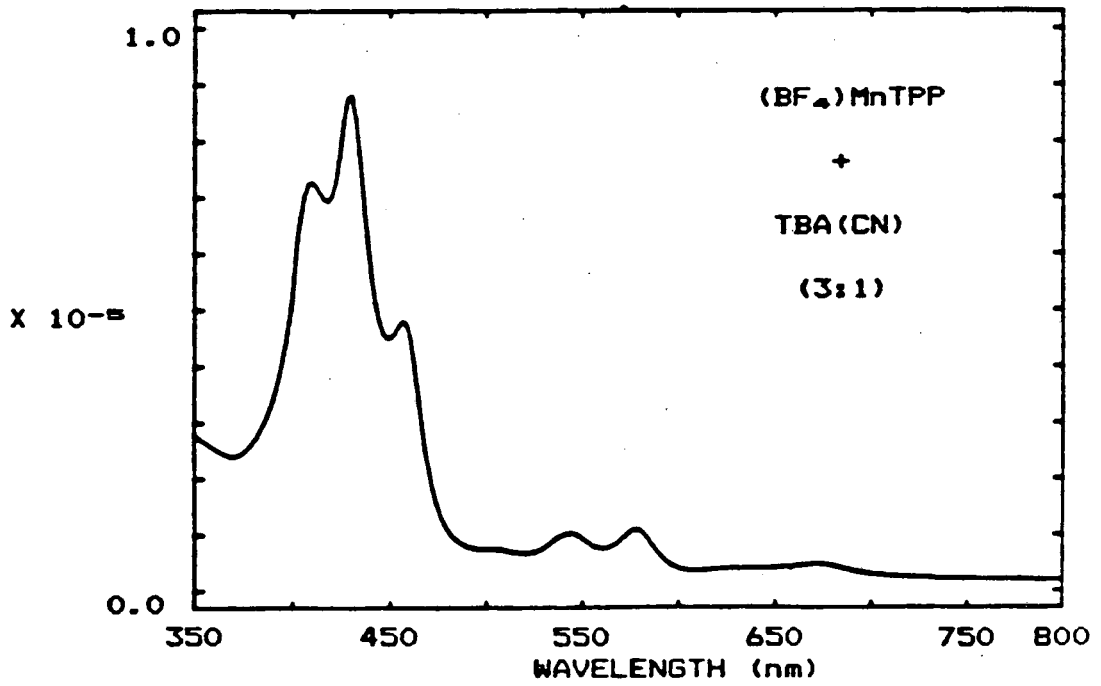
1.0
0.0
X 10-5
(BF4)MnTPP
+
TBA(CN)
(3:1)
350
450
550
650
750
800
WAVELENGTH (nm)

II. SPECTROELECTROCHEMICAL STUDIES

Spectroelectrochemical studies were carried out for $XMn^{III}TPP$ for X = ClO_4^-, Cl^-, Br^-, NO_2^-, OAc^-, N_3^-, NCO^- and CN^-. Spectral studies in the presence of 0.1M TEAP as the supporting electrolyte with no excess axial anion were carried out for X = ClO_4^-, Cl^-, Br^-, NO_2^-, N_3^-, and OAc^-. Studies in the presence of .002M to 0.1M TBAX were carried out for X = Cl^-, NO_2^-, OAc^-, N_3^-, NCO^- and CN^-.

A. No excess axial anion

In the absence of excess axial anions the results of spectroelectrochemical studies falls into two categories:

1) No spectral changes were observed in the prewave region. (X = ClO_4^-)

2) Significant spectral changes were observed in the prewave region. (X = Cl^-, Br^-, OAc^-, NO_2^-, N_3^-)

In the region from 0.90 V to 1.5 V all of the $XMn^{III}TPP$ exhibited virtually identical behavior. At potentials which were close to those observed for the first and second ring oxidations in the LSV studies of Chapter 2 two successive spectral changes were observed for each X^-. Similarly, control experinents of cycles in a negative potential region from -0.30 V to -0.90 V yielded a virtually identical $Mn^{II}TPP$ spectrum for each X^-.

1. ClO_4^-

Both LSV and potential step experiments gave the same results. Repeated cyclic scans or potential steps in the region between 0.0 V and 0.75 V resulted in negligible spectral changes. The first spectral change for scans in an anodic direction was observed between 0.8 and 1.0 V. The resultant spectrum was the same as that of $[Mn^{III}TPP\cdot]^{+2}$, the porphyin π radical cation. The second change, which began near 1.0 V, manifested itself as a decrease in absorption of the whole spectrum between 350 and 600 nm. Reversing the scan direction resulted in restoration of the original spectrum with a slight decrease in total intensity. Typical spectral changes as a function of applied potential are shown in Appendix 4.

Since the spectroelectrochemistry was carried out in thin-cells, linear potential sweeps from 0.0 V to -0.90 V were done after completion of cyclic LSV experiments to insure that no loss in the integrity of the porphyrin had occurred. Spectra recorded with an open circuit after completion of an experiment showed a reduction of $\lesssim$ 10% of the initial intensity, suggesting little degradation of the porphyrin during the course of 3-4 hours of electrochemical experiments.

2. Cl^-, Br^-, OAc^-, NO_2^- and N_3^-

In the absence of excess axial anion each of these $XMn^{III}TPP$ showed patterns which were similar to one an-

other. Spectral changes were observed in the prewave region (0.00 V to 0.80 V). Although the potentials at which these changes occurred varied with axial ligand, the final spectrum observed near 0.80 V was the same for each X^- and was indistinguishable from that observed for $(ClO_4)Mn^{III}TPP$. In the region from ~0.8 V to ~1.5 V the behavior of each of these $XMn^{III}TPP$ was the same as that described for $(ClO_4)Mn^{III}TPP$. The reverse scan from ~1.5 V to ~0.0 V also resulted in spectral changes identical to those observed for the perchlorate. The final spectrum observed for each case was indistinguishable from that of $(ClO_4)Mn^{III}TPP$ rather than that of the original $XMn^{III}TPP$.

Figure 3-17 shows typical examples of the absorbance changes observed in the prewave region, while Figures 3-18 and 3-19 illustrate the spectral changes corresponding to the two successive ring oxidations. Typical spectral changes and plots of absorbance as a function of applied potential for each $XMn^{III}TPP$ described above may be found in Appendix 4 (Figures A4-2 through A4-8)

FIGURE 3-17

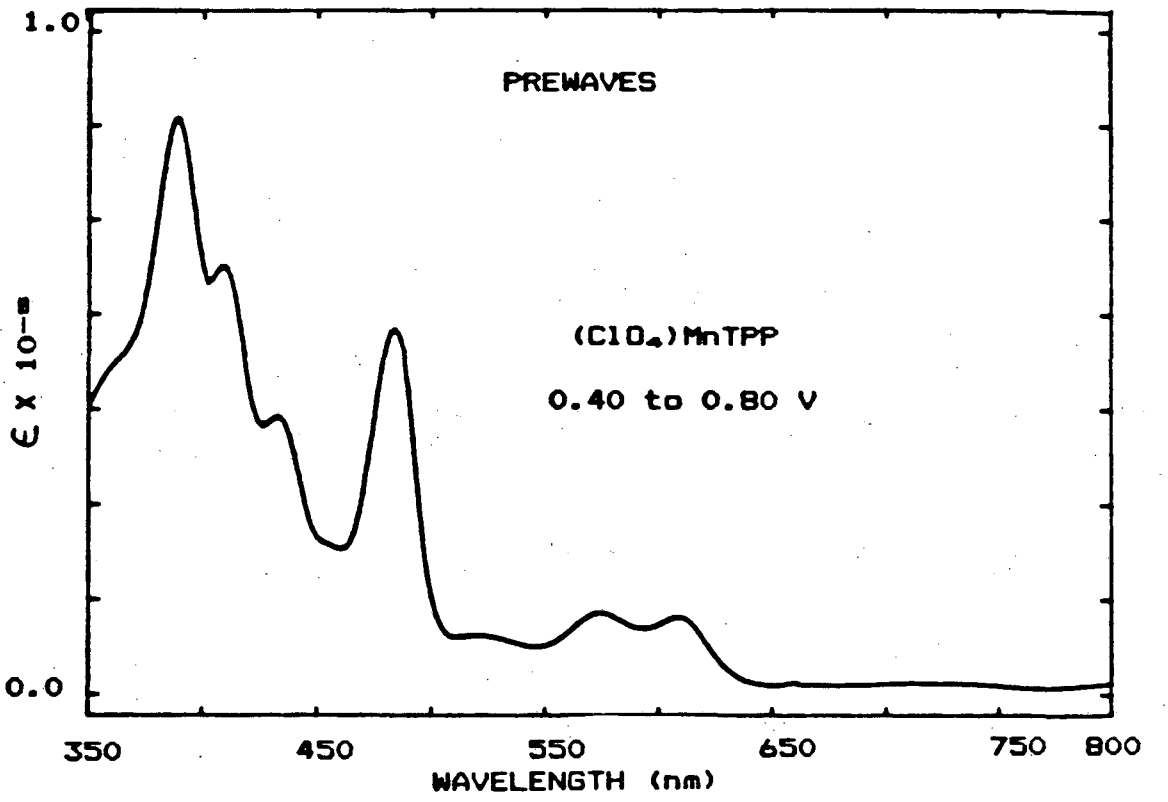
1.0
PREWAVES
(ClO4)MnTPP
0.40 to 0.80 V
ε x 10-3
0.0
350
450
550
650
750
800
WAVELENGTH (nm)

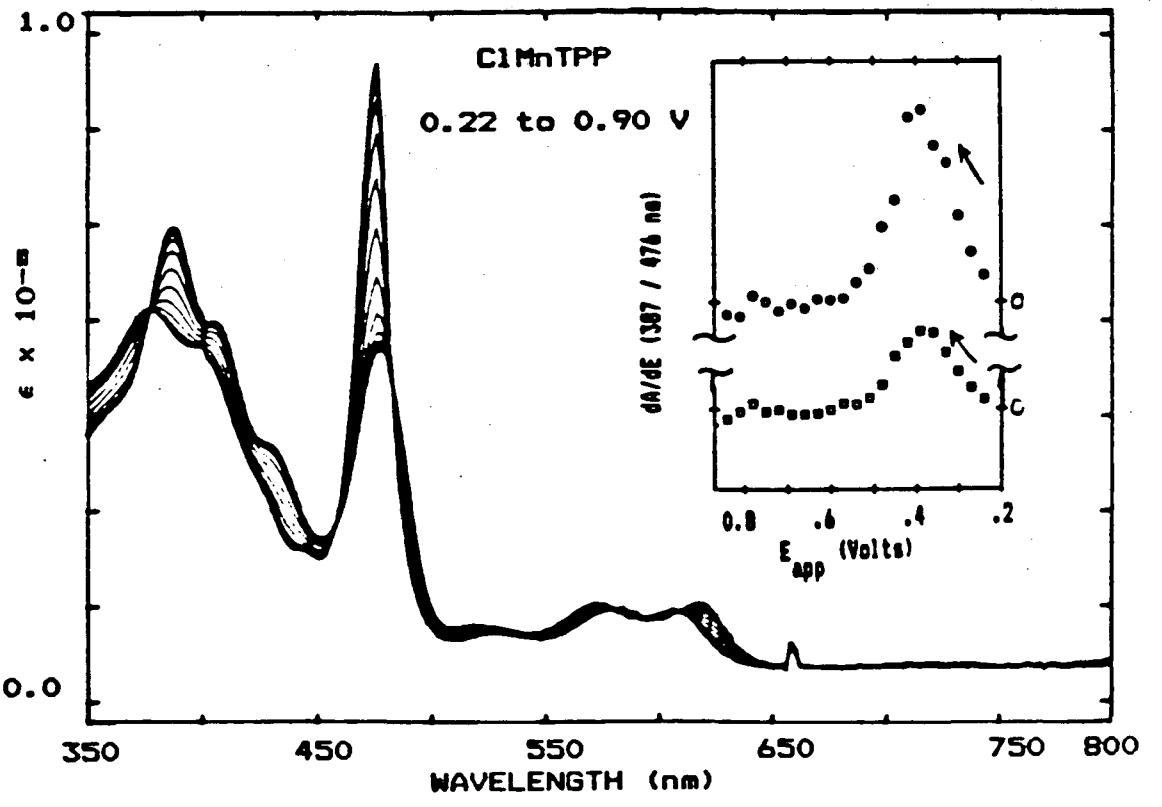
1.0
ClMnTPP
0.22 to 0.90 V
ε x 10-3
dA/dE (387 / 476 nm)
0.8
.6
.4
.2
E app (Volts)
0.0
350
450
550
650
750
800
WAVELENGTH (nm)

FIGURE 3-18

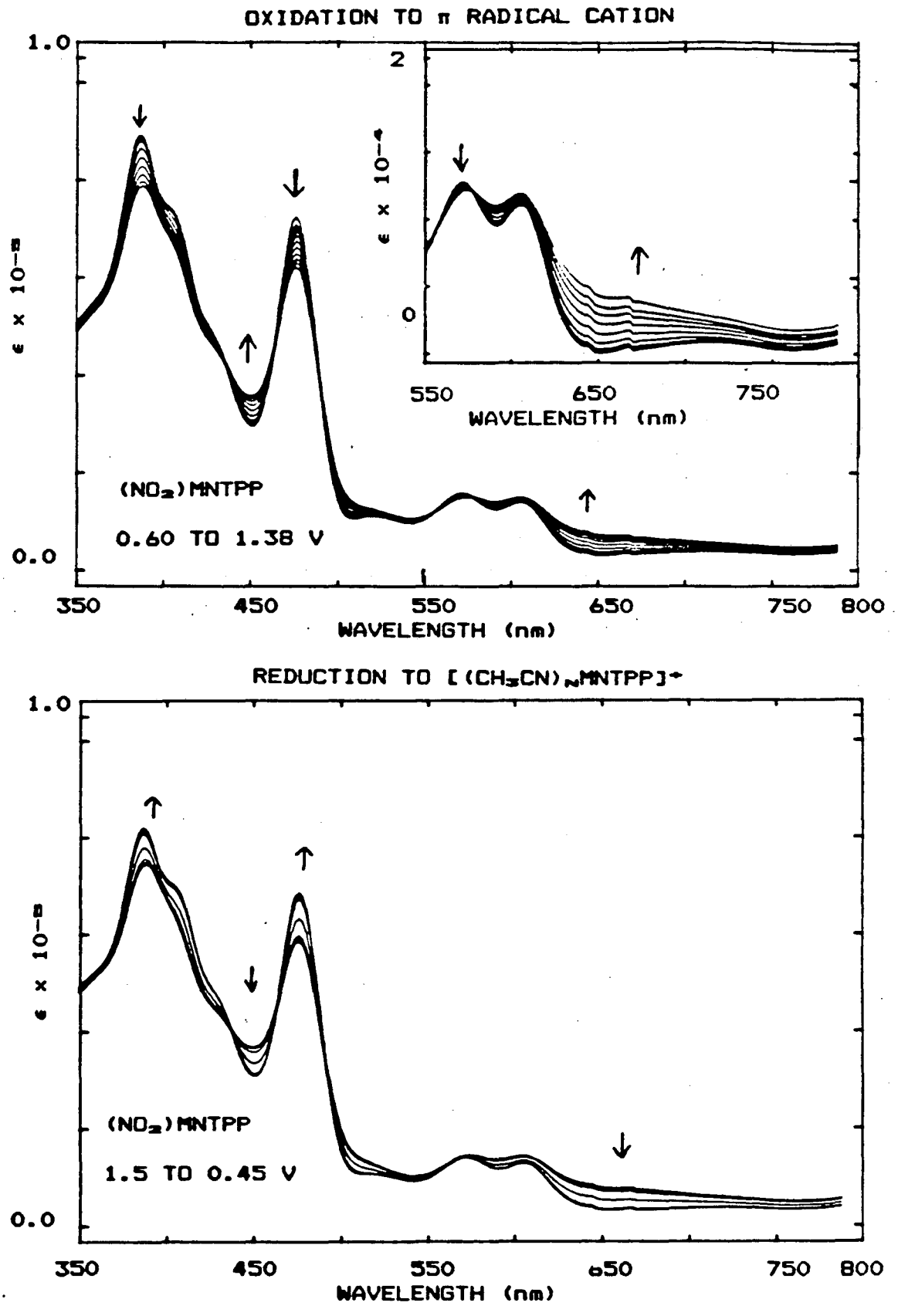
OXIDATION TO π RADICAL CATION
1.0
0.0
ε x 10⁻⁵
2
0
ε x 10⁻⁴
550
650
750
WAVELENGTH (nm)
(NO₂)MNTPP
0.60 TO 1.38 V
350
450
550
650
750
800
WAVELENGTH (nm)
REDUCTION TO [(CH₃CN)₂MNTPP]⁻
1.0
0.0
ε x 10⁻⁵
(NO₂)MNTPP
1.5 TO 0.45 V
350
450
550
650
750
800
WAVELENGTH (nm)

FIGURE 3-19

OXIDATION TO PORPHYRIN DICATION

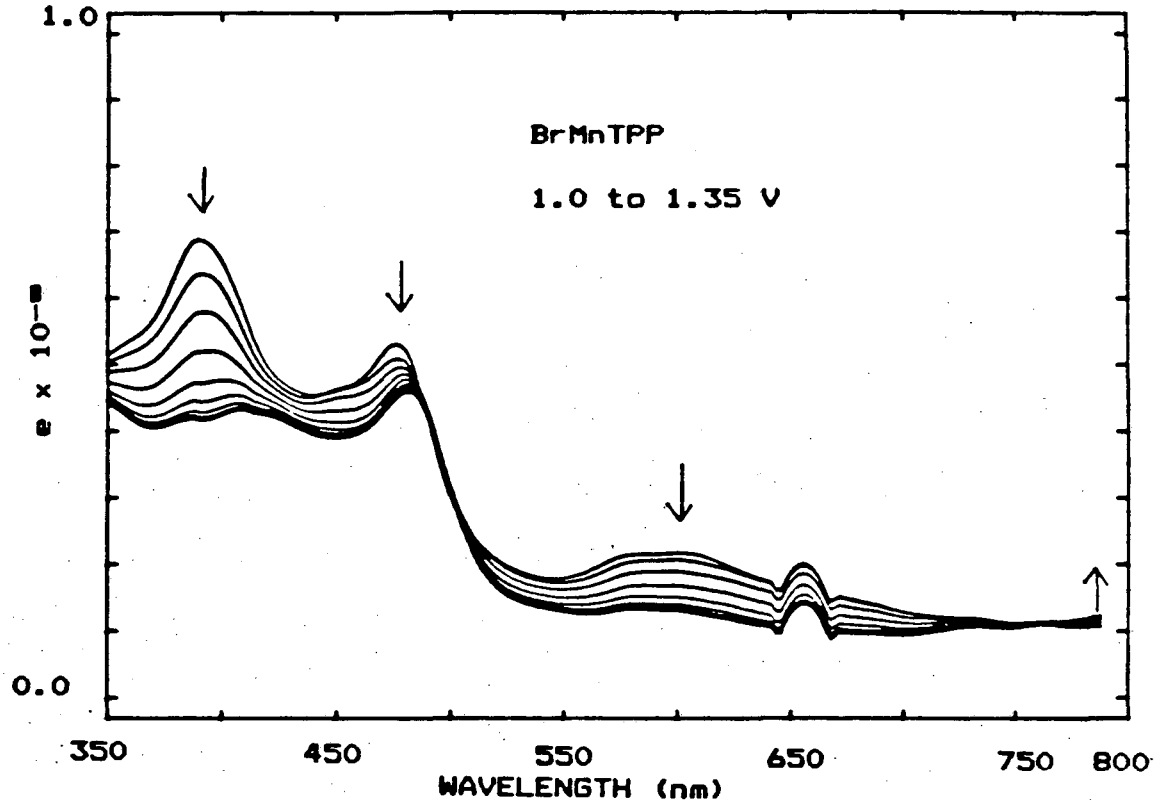

REDUCTION BACK TO π RADICAL CATION

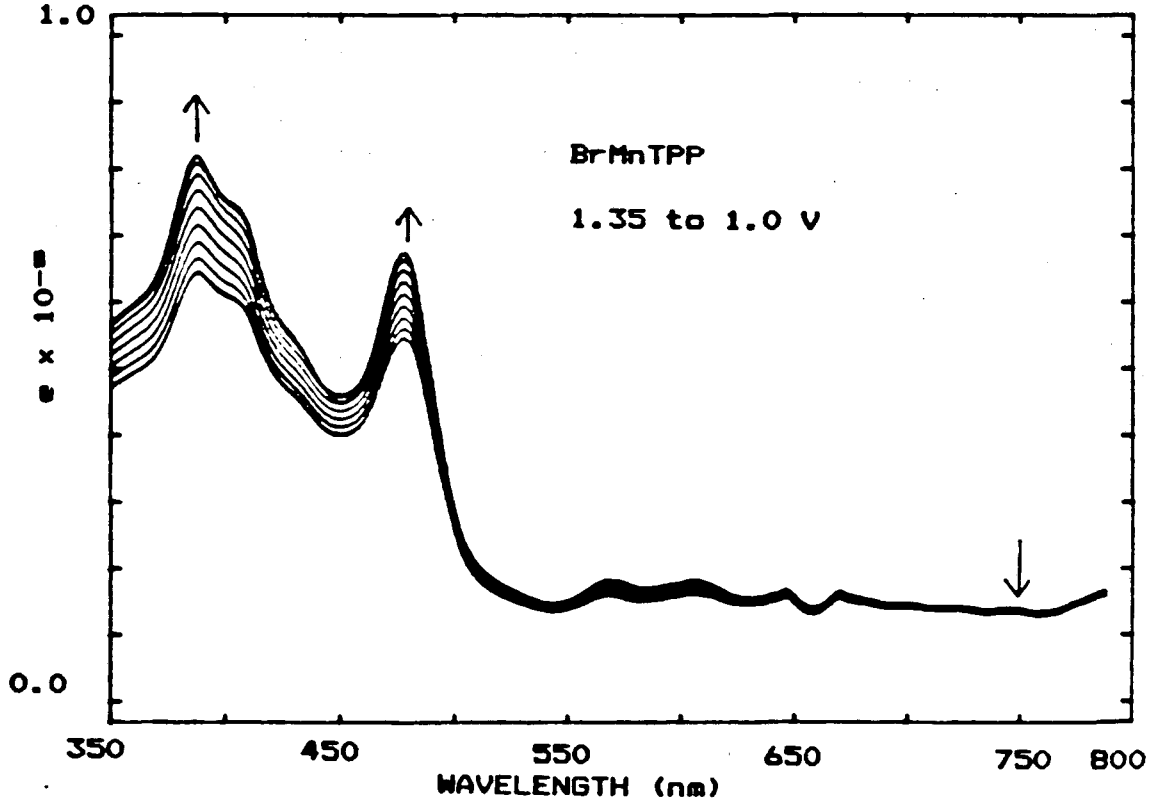

B. Effect of added TBAX

Electrochemical oxidations of solutions of ~1 mM $XMn^{III}TPP$ in the presence of 0.002 to 0.1 M TBAX produced new spectra in the potential region from 0.0 V to 0.6 V for $X = OAc^-$, N_3^- and NCO^-. Each of these new spectra is characterized by the presence of an intense absorbance maximum ($\epsilon \sim 5 \times 10_4$) between 410 and 420 nm, a second maximum ($\epsilon \sim 10^3$) between 530 and 540 nm, and the absence of any bands between 550 and 650 nm. As such, they are typical of $[Mn^{IV}TPP]^{+\cdot}$ species . Neither $ClMn^{III}TPP$ nor $(NO_2)Mn^{III}TPP$ in the presence of .01 M to 0.1 M TBAX exhibited this new spectrum. Instead, each of these $XMn^{III}TPP$ exhibited spectral changes essentially the same as those observed with 0.1 M TEAP only in solution. In the prewave region conversion to the perchlorate spectrum was observed; this was followed by the appearance of the porphyrin π radical cation and dication spectra. In the presence of excess Cl^- or NO_2^- the final "rest" spectrum was essentially the same as the starting spectrum, whereas with no excess anion the rest spectrum was that of the perchlorate. Typical spectral changes and plots of absorbance or dA/dE *vs* the applied potential are presented in Appendix 4.

The results for those anions for which $[Mn^{IV}TPP]^{+\cdot}$ spectra were observed will be described in detail. Figure 3-20 and 3-21 show a representative example of the formation of the Mn(IV) complex and a resultant Mn(IV)porphyrin

spectrum respectively.

1. Acetate

Spectroelectrochemical experiments were performed on cells containing three different concentrations of TBA(OAc). Although $[Mn^{IV}TPP]^{+\cdot}$ type spectra were observed for each, the overall behavior varied with the concentration of added TBA(OAc), and so each will be described separately.

a. 0.002M TBA(OAc)

The initial spectrum was typical of that of (OAc)-$Mn^{III}TPP$ in the absence of a large excess of TBA(OAc) For the anodic scan from -0.3 V to 1.1 V, the first maximum absorbance change occurred at 0.38 V to give a typical $[Mn^{IV}TPP]^{+\cdot}$ spectrum; the second occurred at 0.6 V to yield a spectrum strongly resembling that of (ClO_4)-$Mn^{III}TPP$; the final change, which occurred at 1.1 V, yielded a spectrum like that of the π-radical cation.

For the sweep in the reverse direction from 1.10 to -0.3 V the observed spectral changes corresponds to the formation of the solvate, $[(CH_3CN)_nMn^{III}TPP]^{+}$, near 0.2 V and then to the initial $(AcO)Mn^{III}TPP$ species at ~0.14 V. This final spectrum was reduced ~25% in intensity relative to the initial spectrum. No spectrum characteristic of a $[Mn^{IV}TPP]^{+\cdot}$ species was observed during this scan.

b. 0.01M TBA(OAc)

The initial spectrum showed evidence of a mixture of (OAc)Mn^{III}TPP species as suggested by the presence of absorption maxima at both 454 and 464 nm.

During the anodic portion of the cycle the potential at which the first maximum absorbance change occurred was 0.17(±.04) V. Once again, the initial change resulted in a typical $[Mn^{IV}TPP]^{++}$ spectrum. From ~0.3 to 1.2 V the $[Mn^{IV}TPP]^{++}$ spectrum decreased in intensity, but no evidence for either the $(ClO_4)Mn^{III}$TPP or the π-radical cation was observed. Instead, the final spectrum observed at ~1.1 V more nearly resembled that of the porphyrin dication. (See Figure A4-6E in Appendix 4).

When the scan direction was reversed the spectrum again increased in intensity, and the $[Mn^{IV}TPP]^{++}$ spectrum reappeared, although the maximum absorbance at 414 nm was less than that observed during the anodic portion of the cycle. At potentials < 0.3 V a gradual change in the spectrum occurred until, at -0.2 V, the final spectrum was observed. This spectrum was that of (OAc)Mn^{III}TPP in the absence of excess OAc^-, although decreased to about half the intensity of the starting spectrum.

c. 0.1M TBA(OAc)

The initial spectrum was the same as that described for (OAc)Mn^{III}TPP in the presence of a large excess of OAc^-, *i.e.* only a single absorbance was observed for band

V at 452 nm. During the first anodic scan evidence for the formation of a $[Mn^{IV}TPP]^{++}$ species was again observed. Near 0.6 V the whole spectrum began to decrease in intensity until, at ~1.0 V, it had been completely bleached. Neither scanning back to -0.3 V, nor stepping the potential to -0.9 V restored the original spectrum .

2. Azide (0.01 M TBA(N_3)

During the course of a series of cyclic LSV experiments, the switching potential, E_λ, was varied. The potential ranges examined were from -0.3 to 0.6 V and from -0.3 to 1.2 V, respectively.

The initial spectrum for each fresh cell was the same as for $(N_3)Mn^{III}TPP$ in the presence of a large excess of N_3^-. For all anodic scans a $[Mn^{IV}TPP]^{++}$ spectrum with absorbance maxima at 414 and 534 nm was observed to appear between -0.3 and 0.3 V. A second process characterized by the appearance of a spectrum with an intense absorbance below 400 nm and a weaker band at ~482 nm occurred between 0.3 and 0.6 V. Continuing the LSV experiment from 0.6 to 1.2 V resulted in loss of the $[Mn^{IV}TPP]^{++}$ spectrum and appearance of a spectrum similar to that of $[Mn^{III}TPP]^{+\cdot}$, the π-radical cation.

During the cathodic scan from 1.2 to -0.3 V three processes were observed: 1) Between 1.2 and 0.6 V a new spectrum with an absorbance maximum at 460 nm emerged; 2) between 0.6 and 0.1 V a small increase in the absorbances ar 414 and 534 nm occurred; and 3) between 0.1 and -0.3 V

these absorbance disappeared, and the final $[Mn^{III}TPP]^+$ spectrum was observed.

If the switching potential for the sweep in the positive potential direction was set to 0.6 V, a similar pattern was observed. During the reduction, however, disappearance of the $[Mn^{IV}TPP]^{++}$ to yield the final $[Mn^{III}TPP]^+$ spectrum exhibited nearly isosbestic behavior. (See Figure A4-7C, Appendix 4).

For both sets of experiments, *i.e.* E_λ = 1.2 or 0.6 V, the final $[Mn^{III}TPP]^+$ spectrum differed from any of the $(N_3)Mn^{III}TPP$ spectra described earlier in this chapter and from the $(ClO_4)Mn^{III}TPP$ spectrum observed as the final spectrum in the absence of excess N_3^-. The most notable difference was the shift of band V to 466 nm, a wavelength shorter than that observed in the presence of 0.1 M $TBAN_3$.

3. Cyanate (TBA(NCO))

a. 0.01 M TBA(NCO)

Spectroelectrochemical experiments were done for $(OCN)Mn^{III}TPP$ in the presence of .01 M and 0.1 M TBA(NCO) respectively. No $[Mn^{IV}TPP]^{++}$ type spectrum was observed for 0.01 M TBA(NCO). Indeed, the changes observed were essentially the same as for other $XMn^{III}TPP$ in the absence of TBAX. In the prewave region two sets of changes occurred. The first, at ~ 0.3 V corresponded to the

formation of a "normal" (OCN)Mn^{III}TPP spectrum; the second yielded the $[(CH_3CN)_nMn^{III}TPP]^+$ solvated porphyin spectrum in a two-step process with maximum absorbance changes occurring at 0.64 and 0.77 V. Finally, betwen 0.9 and 1.4 V the formation of the porphyrin π radical cation and dication were observed. The cathodic scan resulted in a retracing of these steps with the exception that the final spectrum was that of the "normal" (OCN)Mn^{III}TPP.

b. 0.1 M TBA(NCO)

In the presence of 0.1 M TBA(NCO), however, anodic scans yielded the now familiar $[Mn^{IV}TPP]^{++}$ spectrum with absorbance maxima at 418 and 534 nm. Isosbestic behavior was observed between 0.0 and 0.69 V with the maximum absorbance change occurring at 0.44(±.02). When the anodic portion of the cycle was extended to 1.2 V, the $[Mn^{IV}TPP]^+$ spectrum gradually decreased, yielding a final spectrum at 1.2 V that resembled that of the porphyrin π dication. The reverse scan from 1.2 to 0.0 V did not show any evidence for a $[Mn^{IV}TPP]^{++}$ species. The final spectrum at 0.0 V for all experiments, regardless of switching potential, was that of the original (OCN)Mn^{III}TPP in the presence of large excess of TBA(NCO).

4. Cyanide ($MnTPPBF_4$ + TBACN)

Spectroelectrochemical experiments were conducted on

cells containing *ca.* 1 mM $(BF_4)Mn^{III}TPP$, 0.1 M TEAP, and 0.01 M TBA(CN). After filling the OTTLE cell a change in color to bright green was observed in the cell window. The electronic spectrum confirmed that the complex had been reduced to $Mn^{II}TPP$. Consistent with this observation, the open circuit potential was -1.10 V. A spectral change characterized by isosbestic behavior was observed between -0.9 and -0.3 V which corresponded to the Mn(II) → Mn(III) oxidation. Between -0.3 and 0.3 V a second spectral change occurred which resulted in the appearance of a $[Mn^{IV}TPP]^{+2}$ spectrum. However, irreversible bleaching of the entire spectrum occurred before the conversion was complete. Stepping the potential to -1.0 V did not result in reversal of this bleaching. Repetition of the experiment with fresh solutions yielded the same results.

FIGURE 3-20

OXIDATION TO $[Mn^{V}TPP]^{2+}$

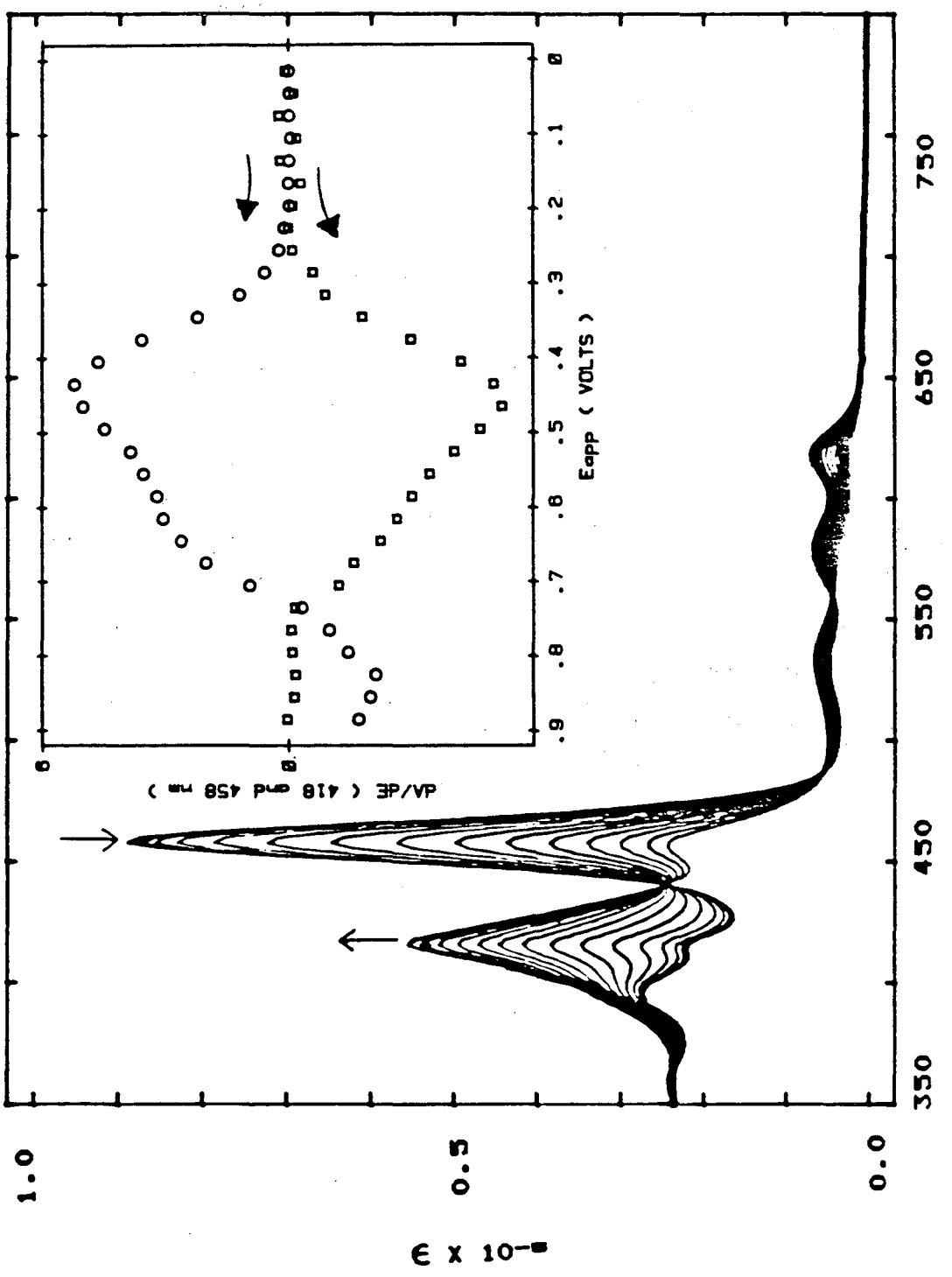

FIGURE 3-21

RESULTANT $[Mn^{+V}TPP]^{2+}$ SPECTRUM

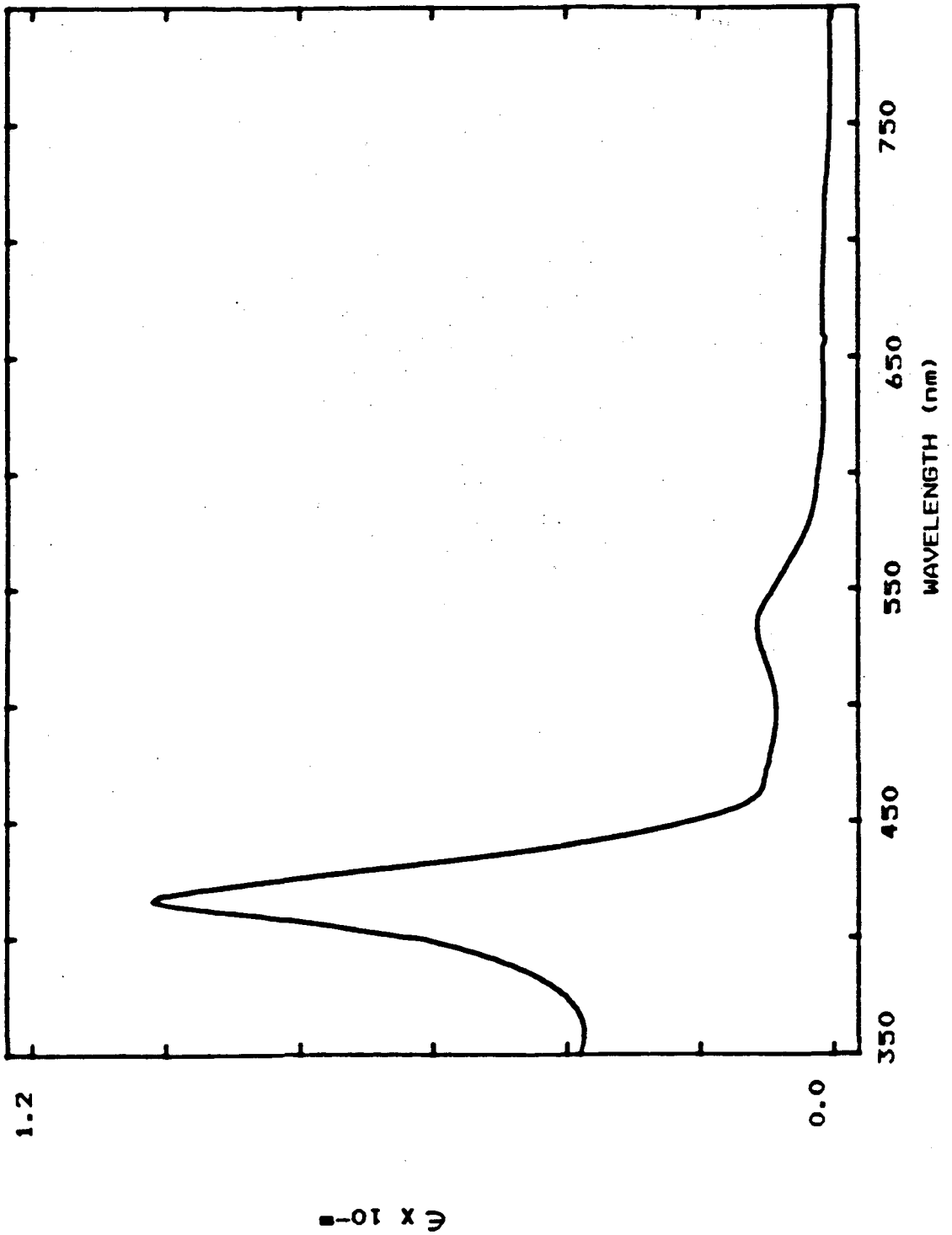

DISCUSSION

I. Spectra of $XMn^{III}TPP$

From the spectral data presented in this chapter and the voltammetric results presented in Chapter 2 a number of previously overlooked properties of manganese(III) porphyrins can now be understood.

Kadish[22] previously reported the equivalent conductance of $XMn^{III}TP$ for $X = ClO_4^-$, I^-, Cl^- and N_3^- in a variety of solvents. From those results it is clear that $(ClO_4)Mn^{III}TPP$ is dissociated, existing in solution primarily as a solvate according to the equation:

$$XMn^{III}TPP + nCH_3CN \rightleftharpoons [(CH_3CN)_nMn^{III}TPP]^+ + X^- \quad (1)$$

where n = 1 or 2. Kadish also showed that the extent of dissociation of $XMn^{III}TPP$ for several X^- decreased in the order:

$$ClO_4^- > I^- >> Cl^- > N_3^-$$

In non-coordinating solvents, such as CH_2CL_2, increasing the ionic strength of the solution by addition of 0.1 M TBAP was shown to enhance the dissociation of the complex.

Based on these results, the spectrum observed for $(ClO_4)Mn^{III}TP$ in CH_3CN alone or with 0.1M TEAP is taken to be that of the solvate and will be used as a reference spectrum for the discussion which follows.

A. BF_4^- and I^-

For each of these anions the similarity of the observed spectra in CH_3CN to that of $(ClO_4)Mn^{III}TPP$ suggests that each of these complexes is highly dissociated. This conclusion for I^- is consistent with the high conductivity reported by Kadish[22]. The dramatic change in each of the respective spectra with the addition of 0.1M TBAX is consistent with a shift in the equilibrium described by equation 1 such that the associated complex becomes the dominant species in solution. The spectra observed in the presence of 0.1M TEAP for each of these $XMn^{III}TPP$ were unexpected since they suggest that the complexes of BF_4^- and I^- are more strongly associated in solutions of high ionic strength than in CH_3CN only. This differs from the finding by Kadish that increasing ionic strength favors dissociation of the complex for the anions Cl^-, Br^- and N_3^-. A possible explanation for this apparent discrepancy may be found in the differences in polarizability of the anions involved. The free anions I^- and BF_4^- are much more polarizable than are the other anions used in this study. Hence, complexes with these two anions are more likely to be associated in polar solvents. Presence of an electrolyte would be likely to enhance this association still further.[26]

B. Cl^- and Br^-

Interpretation of the spectral results for these

$XMn^{III}TPP$ complexes is straightforward. It appears that Br^- fits between I^- and Cl^- in the relative degree of dissociation of $XMn^{III}TPP$. This conclusion is based on the observations that: 1) the spectrum of $BrMn^{III}TPP$ is more profoundly affected by the addition of TBABr than is that of the chloride (See Figures 3-9 and 3-10), and 2) the spectrum of $BrMn^{III}TPP$ in CH_3CN alone or in the presence of 0.1 M TEAP is, nevertheless, different from that of the perchlorate. Both $ClMn^{III}TPP$ and $BrMn^{III}TPP$ appear to be more highly dissociated in acetonitrile in the presence of TEAP, a result which is expected if increasing ionic strength favors dissociation of the porphyrin complex.

C. NO_2^-, OAc^-, N_3^-, NCO^-, and CN^-

These anions proved to be the most interesting since previously unreported spectra were observed. In CH_3CN only or in the presence 0.1 M TEAP the observed spectra exhibited no unusual features. Each exhibited its own unique spectrum which was similar to that observed for the same complex in solvents such as CH_2Cl_2 or toluene. Furthermore, relatively small spectral changes were observed on addition of 0.1M TEAP to ~1mM acetonitrile solutions of each of these complexes. These observations suggest that each of these porphyrins exists in CH_3CN primarily as the associated $XMn^{III}TPP$. This conclusion is the same as that reported for N_3^- by Kadish.[22]

In the presence of varying concentrations of TBAX, however, the new spectra observed suggest the formation of a previously unreported species. A likely candidate for this species is a six-coordinate complex, $[X_2Mn^{III}TPP]^-$, formed in solution according to the following equlibrium:

$$XMn^{III}TPP + X^- \overset{CH_3CN}{\rightleftharpoons} [X_2Mn^{III}TPP]^- \qquad (2)$$

The spectral changes observed in this study can be rationalized qualitatively in terms of just such a conversion. An increase in the energy of the $e_g(d\pi)$ orbitals would be expected to accompany coordination of a sixth axial ligand. If the absorbance of band V is, indeed, primarily due to a LMCT ($a_{1u}(\pi)$, $a_{2u} \rightarrow e_g(d\pi)$) transition, then bands V, VA, and VI would be shifted to higher energy. In the limiting case a simplification of the spectrum would be expected, and a spectrum resembling the "pseudonormal" metalloporphyrin spectrum described by Gouterman[2] might result.

In each of the examples reported in this study shifts to higher energy of bands V, VA, nd VI were observed; concurrently bands VA and VI decreased in intensity relative to band V. Thus, if the above arguments are correct, the species in solution in the presence of varying concentrations of excess axial anion are six-coordinate Mn(III)porphyrins.

Further support for the assignment of the observed

new spectra to those of six-coordinate complexes comes from a comparison of the electronic spectra of the five-coordinate imidazole complex of manganese(III)TPP, [(ImH)-Mn^{III}TPP][ClO_4] with the spectrum of the six-coordinate imidazolate complex, Im_2Mn^{III}TPP.[25] Inspection of the wavelengths of the absorption maxima (See Table 3-2) reveals a shift in band V to higher energy similar to that observed for the complexes reported in this work.

TABLE 3-2

SPECTRA OF MANGANESE(III)PORPHYRINS IN THF

	ABSORPTION BAND				
Porphyrin	VI	VA	V	IV	I
Im_2Mn^{III}TPP	390	410 425	460	588	628
[ImHMn^{III}TPP]$^+$	370	400 424	473	571	608

The electronic spectrum for $(CN)_2Mn^{III}$TPP in a non-coordinating or weakly coordinating solvent has not been reported. The X-ray crystallographic structure of the five coordinate, CNMn^{III}TPP has been reported, and spectral evidence for the existence of the six-coordinate complex in CH_3OH has been reported.[21] If the band at 492 nm in acetonitrile for ratios of

[CN^-]/[(BF_4)MnTPP] $\leq$ 2 is characteristic of five-coordinate (CN)Mn^{III}TPP, then the shift to 456 nm accompanying formation of the six-coordinate species fits the same pattern as reported for the imidazole and imidazolate complexes and observed in this work for the anions Oac^-, N_3^-, NCO^- and NO_2^-.

In the cases reported in the literature conversion to a *l.s* Mn(III) complex accompanies coordination of the sixth axial ligand. Except for acetate, all of the anions which appear to be capable of forming the six-coordinate X_2Mn^{III}TPP in acetonitrile (NCO^-, CN^-, NO_2^-, and N_3^-) appear higher on the spectrochemical series[26] than do those which form only five-coordinate complexes (Cl^-, Br^- and I^-).[26] Since ligands high on the spectrochemical series are more likely to lead to *l.s.* complexes in six-coordinate complexes of first row transition metals, it is reasonable to expect that some of the six-coordinate Mn(III)porphyrin complexes of these ligands would be low spin. However, while the observed spectral changes argue strongly for the formation of the six-coordinate complex, electronic spectra alone are insufficient to assign the spin state. Hence, magnetic susceptibility, NMR or EPR studies of these complexes would be useful.

It is also interesting that of the anions examined in this study, those which are capable of forming six-coordinate complexes are also those which are known to

stabilize transition metal ions in the +3 oxidation state.[29] Indeed, even the stability constants of divalent metal ions of OAc^-, N_3^-, NCO^-, CN^-, and NO_2^- are significantly greater than are those of Cl^-, Br^-, and I^-.[29]

II. SPECTREOLECTROCHEMICAL STUDIES OF $XMn^{III}TPP$

A. Absence of excess axial anions.

1. Prewave Region

In the prewave region the disappearance of the initial $XMn^{III}TPP$ spectrum and the concomitant appearance of the solvate, $[(CH_3CN)_NMn^{III}TPP]^+$, spectrum is clearly a result of axial ligand oxidation. The failure of the initial $XMn^{III}TPP$ spectrum to reappear after cycling to potentials > 0.9 V is consistent with the low degree of reversibility observed for the prewaves described in Chapter 2.

Although it is not possible from these studies to distinguish between oxidations of free and coordinated axial anions, some speculation based on the results is appropriate. In part I of the discussion section of this chapter it was shown that $XMn^{III}TPP$ (X = Cl^- and Br^-) is somewhat dissociated in acetonitrile solution and does not form six-coordinate complexes even in the presence of large excesses of X^-. Conversely, $XMn^{III}TPP$ (X = OAc^-, N_3^-, NCO^-, CN^- and NO_2^-) is strongly associated and forms six-coordinate complexes in the presence of sufficient

concentrations of excess X^-. Certainly then, for the anions Cl^- and Br^- the prewaves are a result of oxidation of free ligand.

On the other hand, oxidation of a coordinated axial ligand remains a possibility for the anions OAc^-, NCO^-, N_3^-, NO_2^- and CN^-. These $XMn^{III}TPP$ have in common the following:

1) A large discrepancy exists between the reduction potentials of TBAX and of the prewaves observed for $XMn^{III}TPP$.

2) Their five-coordinate manganese(III) porphyrin complexes are strongly associated, even with 0.1 M electrolyte in solution.

If these observations are coupled in a causal relationship, then the prewaves observed for OAc^-, N_3^-. NCO^- and NO_2^- may be due to oxidation of a coordinated ligand.

2. Ring Oxidations

Comparison of the spectrum observed near 1.0 V with authentic manganese(III)TPP π radical cation spectra[13-16] confirms assignment of the process reported in Chapter 2 at 0.96 V to that of the first ring oxidation. A curious feature of this spectrum is its striking similarity to that of the solvate, $[(CH_3CN)_NMn^{III}TPP]^+$. (See Figure 12) Indeed, this very similarity rendered the identification

of this process confusing in the initial stages of this project. Although no theoretical studies have appeared addressing this observation, some comments are in order.

FIGURE 3-22

COMPARISON OF SOLVATE AND π RADICAL CATION SPECTRA

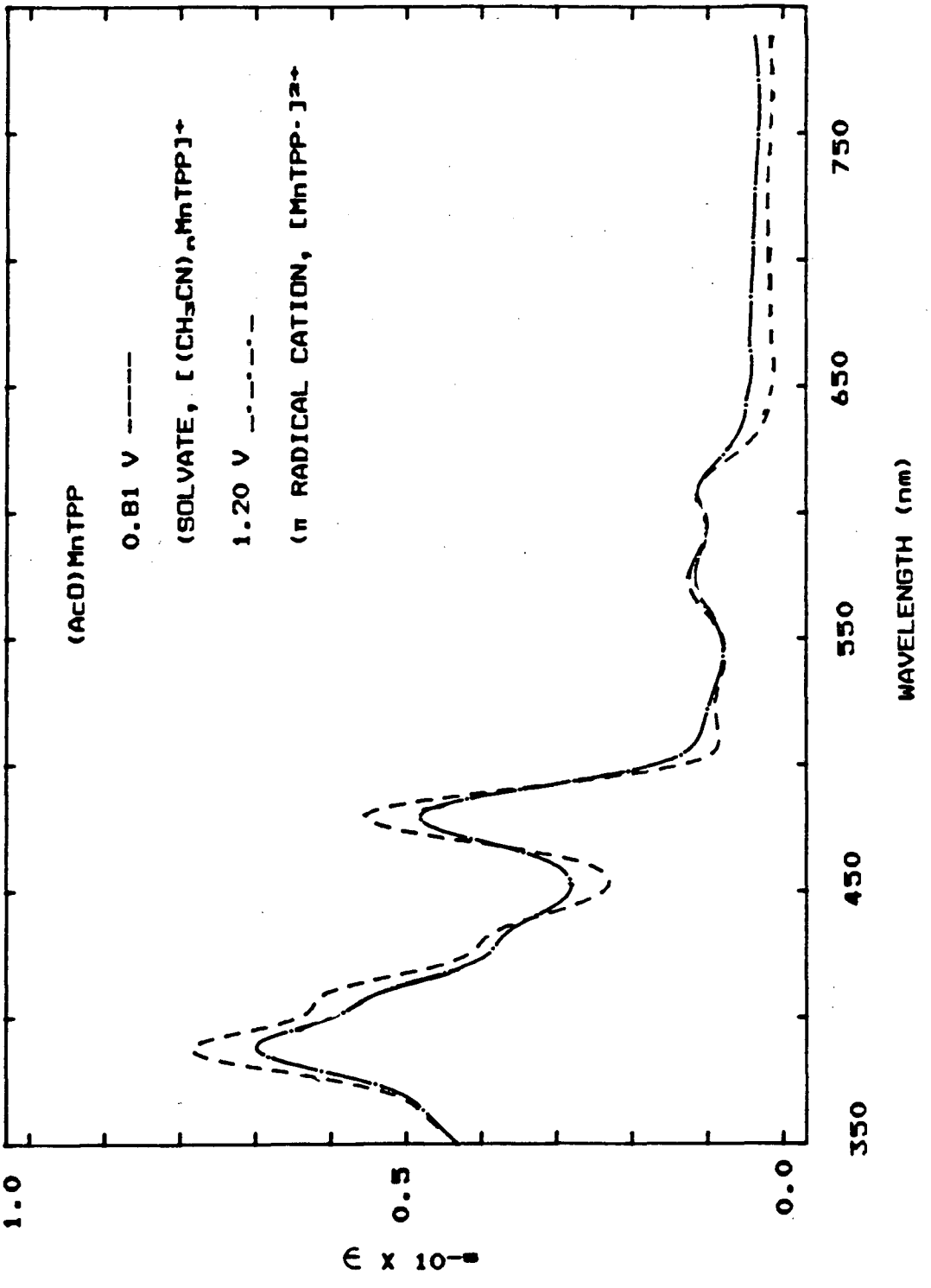

The π radical cation observed in this work and the solvate, $[(CH_3CN)_NMn^{III}TPP]^+$, have in common the absence of coordinating axial ligands. X-ray crystallographic data for a number of metalloporphyrin π radical cations indicate that the ligand geometry is unperturbed by a one-electron oxidation.[27] Furthermore, nmr data show that rapid intermolecular electron transfer occurs between oxidized and unoxidized ligands.[16,28] These observations taken together, suggest a strong similarity in electronic structure between the solvate, $[(CH_3CN)_NMn^{III}TPP]^+$, and the π radical cation, $[Mn^{III}TPP\cdot]^+$. Since the bands observed in the manganese(III)porphyrin spectrum are due to LMCT transition, it is reasonable that the two species having no axial ligands and otherwise similar structures should exhibit similar electronic spectra. The introduction of coordinating axial ligands would be expected to alter this spectrum observably, as is the case.

An argument might be made that previously reported manganese(III) porphyrin π radical cations have been formulated as $[ClMn^{III}TPP\cdot][ClO_4]$.[13,14,16] Since one of these species was generated by controlled potential electrolysis,[13,16] and since each of the complexes were reported as impure and unstable, it is possible that this formulation may be incorrect. From the results reported in this dissertation it is almost certain that Cl^- would have been oxidized during controlled potential electrolysis. If so, the rationale presented above for the simi-

larities between the electronic spectra of the solvate and the π radical cation is valid.

Assignment of the oxidation at 1.26 V reported in Chapter 2 to that of the second ring oxidation is likewise confirmed by the spectroelectrochemical results. Although there are no spectra reported in the literature for the manganese(III)porphyrin dication, the observation of the same spectrum for each complex strongly supports the assignment. It is not surprising that the spectrum of the dication is relatively featureless (See Figure 13) compared to that of the neutral Mn(III)porphyrin or of the solvate. Removal of two electrons from the porphyrin ring would certainly have a more profound effect than removing only one. Since the transitions leading to the observed spectra originate in porphyrin a_{1u} or a_{2u} orbitals, removing two electrons from these orbitals should reduce the number of possible transitions, resulting in a much simplified spectrum.

FIGURE 3-23

SPECTRUM OF PORPHYRIN DICATION $[Mn^{III}TPP\cdot\cdot]^{3+}$

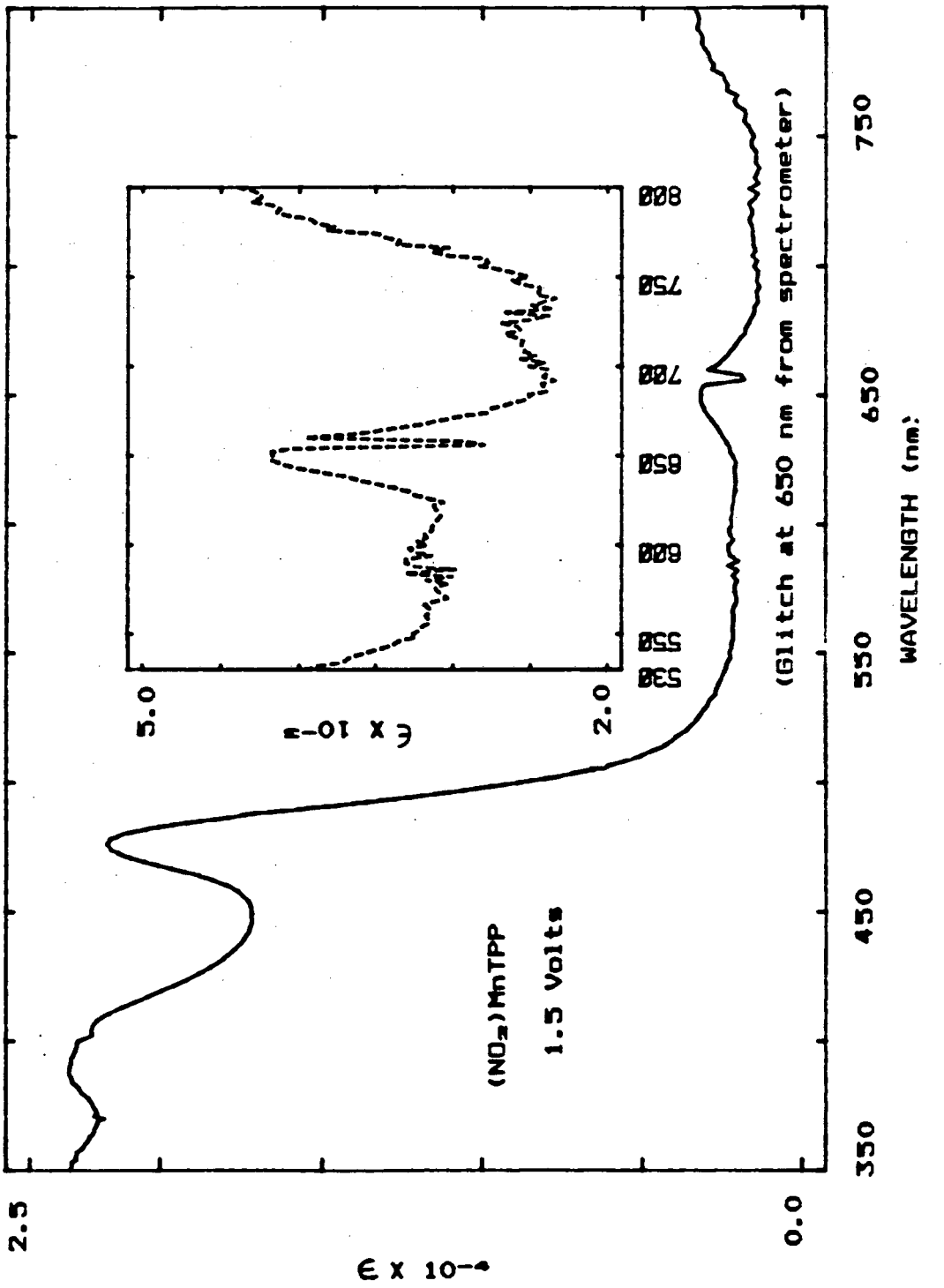

B. Effect of added TBAX

Based on comparisons with known compounds,[6,9,10-12] it is apparent that the new spectra observed in the prewave region for $XMn^{III}TPP$ (X = OAc^-, N_3^-, NCO^- and CN^-) in the presence of excess axial anion are those of $[Mn^{IV}TPP]^{2+}$ species. The observation of the $[Mn^{IV}TPP]^{2+}$ spectra during the spectroelectrochemical experiments confirms the tentative assignments made in Chapter 2 for the new redox processes observed in the prewave region in the presence of excess axial anion. Some of the interesting aspects of this result are: 1) The $Mn^{IV/III}$ couple is observed only in the presence of excess axial anion. 2) It is observed only for some axial anions. 3) It occurs at surprisingly low potentials.

Since all previously reported electrochemical studies (See Chapter 2 and references therein) had yielded only porphyrin- based oxidations, we had expected that any metal-centered oxidation would be more difficult to achieve. It now becomes apparent that a requirement for observation of the $Mn^{IV/III}$ couple is the presence of a strongly coordinating axial anion which can form the *bis*-ligated complex and stabilize the high charge developed on the metal center. This axial anion must be able to stabilize the Mn^{IV} species so that the reduction potential of the $Mn^{IV/III}$ couple is lower than that of the potential required to oxidized the axial ligand itself.

Thus, the $XMn^{III}TPP$ for X = OAc^-, N_3^-, NCO^- and CN^- exhibit stable $Mn^{IV/III}$ couple. It is interesting to note that of the Mn(IV)porphyrin species which have been isolated and well-characterized by chemical oxidations, those with N_3^-, OAC^-, and NCO^- are among the most stable.

Conversely, the anions Cl^-, Br^-, I^-, ClO_4^- and BF_4^- are much too weakly coordinating in acetonitrile to stabilize the Mn(IV) complex. The low reduction potentials for the oxidation of Br^- and I^- further reduce the probability of these ligands' stabilizing a Mn(IV)porphyrin. The anion NO_2^- coordinates strongly enough, but is itself too unstable to oxidation (See Tables 2-6 and 2-7) to form the Mn(IV) complex. $Cl_2Mn^{IV}TPP$ has been synthesized, but it has not been isolated in pure form.[19] Nmr data suggests that it is the least stable of the observed Mn(IV)porphyrins. This is in keeping with the intermediate position of Cl^- in degree of dissociation of the five-coordinate complex and in reduction potential of the free anion.

Estimates of the reduction potentials for the $Mn^{IV/III}$ couples observed in this study made from the data presented in Chapter 2 and in this chapter are shown in Table 3-3. Using these reduction potentials as the criterion, the order of stability of the $X_2Mn^{III}TPP$ is proposed to be:

$$CN^- > N_3^- > OAC^- > OCN^-$$

TABLE 3-3

$Mn^{IV/III}$ REDUCTION POTENTIALS

$XMn^{III}TPP$	[TBAX]/[XMnTPP]	$E_{1/2}$ [a]
OAC^-	2	0.38 [c]
	10	0.13
	100	< 0.2
N_3^-	2	0.11 [b]
	5	0.10
	10	0.08
NCO^-	100	0.45 [c]
CN^-	10	0.05 [b]

a Potentials are reported *vs.* the Ag/Ag^+(0.01 M) reference electrode described in the Experimental section.

b $E_{1/2}$ estimated from semi-derivative LSV studies of Chapter 2.

c $E_{1/2}$ estimated from spectroelectrochemical results in this chapter.

III. SUGGESTIONS FOR FURTHER STUDY

A number of areas for further study are suggested by the results presented in Chapters 2 and 3 of this work.

It would seem reasonable that a correlation ought to exist between the stability of the six-coordinate Mn(III) porphyrins and the ease of oxidation to the Mn(IV) complex. Qualitative observations in this work suggest that there is, but careful measurements of the formation constants should be done. Likewise, isolation and characterization of the magnetic propoerties of the six-coordinate manganese(III)porphyrins reported in this work would be of value. Again, it would be interesting to learn if there is any correlation between the reduction potentials of the $Mn^{IV/III}$ couple and the spin state of the complex.

It is probable that if the $(CH_3O)Mn^{III}TPP$ porphyrin were available for voltammetric or spectroelectrochemical studies, it too, would exhibit a $Mn^{IV/III}$ couple at potentials near those reported in this study. It is also significant that even for the anions CN^-, OAc^-, and N_3^- it is difficult to isolate the Mn^{IV} species by oxidation of the $XMn^{III}TPP$ starting material. Instead, ligand exchange with the $(CH_3O)_2Mn^{IV}TPP$ is the synthetic method of choice. This may be related to the ease of oxidation of each of the axial anions. Without knowledge of the reduction potentials of the $Mn^{IV/III}$ couple of $(OCH_3)Mn^{III}TPP$, of OCH_3^-, and of the oxidant C_6H_5IO this possibility must

remain in the realm of speculation.

Extending these studies to other solvents which enhance the coordination of the axial anions may render observation of the $Mn^{IV/III}$ couple for other ligands possible. The strongest candidate for such a study is $ClMn^{III}TPP$ in CH_2Cl_2. Likewise, it would be helpful to conduct similar studies to those described in these two chapters using some of the isolated Mn(IV) and Mn(V) complexes as the electroactive species.. This was impossible for the Mn(IV) complexes because all of the available complexes decompose quickly in acetonitrile. $(N)Mn^{V}TPP$ is insoluble in most solvents appropriate for electrochemistry. Of more general interest is the application of the results obtained in this work to that of other metalloporphyrins. To date electrochemical studies of other transition metal porphyrin complexes have yielded only ring oxidation potentials. It may be that the use of excess axial anions for porphyrin complexes of metal ions such as Fe^{3+} or Cr^{3+} may lead to the observation of the $M^{IV/III}$ couple for these metalloporphyrins. An obvious experimental difficulty will be the difference in solubility of the TPP complexes of these metals from that of manganese. Use of substituted porphyrin ligands or of other solvents may solve this problem.

SUMMARY

In the electrochemical studies presented in Chapters 2 and 3 a number of important insights into the oxidation chemistry of manganese(III)tetraphenylporphyrins have been obtained. A set of previously unreported redox processes have been shown to be due to axial ligand oxidation. The potentials for the successive one-electron oxidations of $XMn^{III}TPP$ to the porphyrin radical cation and dication have been determined to be 0.96 and 1.26 V *vs.* the Ag/Ag(0.01 M) reference electrode. The spectra of each of these ring-oxidized species has been determined, and some speculation on the electronic origins of each has been presented. Evidence has been presented for the formation of the six-coordinate species, $[X_2Mn^{III}TPP]^-$, in solution in the presence of excess axial anions for X = NCO^-, OAC^-, NO_2^-, and N_3^-. The $Mn^{IV/III}$ couple has been observed, its identity confirmed spectrally, and its stability been shown to be profoundly affected by the nature and concentration of the axial ligand. Some discussion of the insights these observations give to the synthesis of oxidized porphyrins has been presented.

REFERENCES

(1) Zerner, M.; Gouterman, M. *Theoret. Chim. Acta (Berl)*, 1966, 4, 44-63.

(2) M. Gouterman in "The Porphyrins", D.Dolphin, Ed., Vol. III, Academic Press, N.Y., 1979, Chapter 1.

(3) Boucher, L.J., *J. Amer. Chem. Soc.*, 1968, 90, 6640-6645.

(4) Boucher, L.J., *J. Amer. Chem. Soc.*, 1970, 92, 2725-2730

(5) Boucher, L.J. *Coord. Chem. Rev.*, 1972, 7, 289-329.

(6) Loach, P.A.; Calvin, M. *Biochem.*, 1963, 2, 361-371.

(7) Kobayashi, H.; Yanagawa, Y.; Osada, S.; Minami, S.; Shimizui, M.; *Bull. Chem. Soc. JPN*, 1973, 1471-1479.

(8) Boucher, L.J.; Garber, H.K. *Inorg. Chem.* 1970, 9, 2644-2649.

(9) Schardt, B.C.; Hollander, F.J.; Hill, C.L. *J. Amer. Chem. Soc.*, 1982, *104*, 964-971.

(10) Camenzind, M.J.; Hollander, F.J.; Hill, C.L. *Inorg. Chem.*, 1982, *21*, 4301-4308.

(11) Camenzind, M.J.; Hollander, F.J.; Hill, C.L. , *Inorg. Chem.* accepted for publication

(12) Smegal, J.A.; Schardt, B.C.; Hill, C.L. *J. Amer. Chem. Soc.* 1983, *105*, 3510-3515.

(13) Goff, H.M.; Phillippi, M.A.; Boersma, A.D.; Hansen, A.P. *Adv. in Chem. Series.* 1982, *210*, 357-375.

(14) Scholz, W.; Reed, C.A. *unpublished results* personal

communication.

(15) Carnieri, N.; Harriman, A. *Inorg. Chim. Acta*, 1982, *62*, 103-107.

(16) Shimomura, E.T.; Phillippi, M.A.; Goff, H.M.; Schatz, W.F.; Reed, C.A. *J. Amer. Chem. Soc.*, 1981, *103*, 6778-6780.

(17) Buchler, J.W.; Dreher, C.; Kiong, L.L. *Z. Naturforsch.* 1982, *37b*, 1155-1162.

(18) Hill, C.L.; Hollander, F.J. *J. Am. Chem. Soc.*, 1982, *104*, 7318-7319.

(19) Camenzind, M. *This laboratory, unpublished results,*

(20) Shriver, D.F. "The Manipulation of Air-Sensitive Compounds". New York, N.Y., McGraw-Hill, 1969.

(21) Scheidt, W.R.; Lee, Y.J.; Luangdilok, W.; Haller, K.J.; Anzai, K.; Hatano, K. *Inorg. Chem.*, 1983, *22*, 1516-1522.

(22) Kelly, S.L.; Kadish, K.M. *Inorg. Chem.*, 1982, *21*, 3631-3639.

(23) A.P. Hansen, Master's Thesis, University of Iowa, 1982.

(24) Wayland, B.B.; Olson, L.W.; Siddiqui, Z.U. *J. Amer. Chem. Soc.*, 1976, *98*, 94-97.

(25) Landrum, J.T.; Scheidt, W.R.; Reed, C.A. *J. Am. Chem. Soc.*, 1980, *102*, 6729-6735.

(26) F. Basolo and R.G. Pearson. "Mechanisms of Inorganic Reactions,." 2nd Edition, New York, Wiley, 1969, Chapter and references therein.

(27) Scheidt, W.R. in "The Porphyrins", D. Dolphin, Ed., Vol. III, Academic Press, N.Y., 1979, Chapter 10.

(28) Phillippi, M.A.; Goff, H.M.; *J. Amer. Chem. Soc.*, 1982, *104*, 6026-6034.

(29) Bancroft, E.E.; Sidwell, J.S.; Blount, H.N. *Anal. Chem.*, 1981, 53, 1390-1394.

(30) Martell, A.E. and Smith, R.M., "Critical Stability Constants", Plenum Press, N.Y., Vol. 3, Vol 4, and Vol. 5, 1976.

CHAPTER 4

The Chemistry and Electrochemistry of Vanadium Complexes of Rhodotorulic Acid and Related Synthetic Hydroxamates

INTRODUCTION

Hydroxamic acids, RC(O)N(OH)R′ are weak organic acids (pK_a ~ 7 – 11) in which R or R′ may be an organic substituent or H.[1,2] The hydroxamate anion forms a strong chelating group which easily complexes metal ions such as Fe^{3+}, Ti^{4+}, UO^{2+}, and VO^{2+} according to the reaction:[3,4]

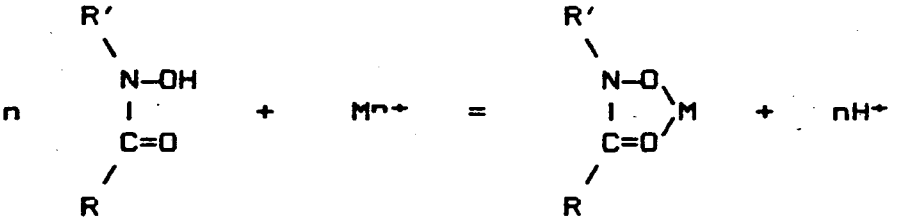

Interest in synthetic hydroxamates has been enhanced by their utility as analytical reagents for a variety of metal ions. The stability and insolubity of neutral complexes in water makes possible their use as gravimetric reagents,[6,7] while the intense color of many of their metal complexes renders them useful as colorimetric reagents in organic solvents such as chloroform.[8,9] Di- and tri- hydroxamates abound in nature and are important in the iron absorption of microorganisms.[2,15]

Electrochemical data on hydroxamic acids are available. Cyclic voltammetry in acetone at a platinum electrode have shown that several hydroxamates and thiohy-

droxamates (R = C_6H_5 or H, R′ = C_6H_5, CH_3, or H) are oxidized between 1.0 and 1.4 V *vs* Ag/AgCl,LiCl(0.1 $M \cdot dm^{-3}$).[10] Some of the thiohydroxamates exhibit quasi-reversible behavior, but the hydroxamates exhibit only irrreversible waves.

Anodic oxidations in acetonitrile at a glassy carbon electrode were investigated by Ozaki and Masui.[11] Using both cyclic voltammetry and exhaustive controlled potential electrolysis the oxidation products for various substituted hydroxamic acids were identified. Some of the important conclusions from this study are: hydroxamic acids are more resistant to oxidation than are the corresponding hydroxylamines; hydroxamic acids with benzoyl groups are more easily oxidized than those with acetyl groups; aceto- and benzo- hydroxamic acids are oxidized to the corresponding corboxylic acids and nitrous oxide; N-substituted hydroxamic acids give the corresponding nitroso compounds and carboxylic acids; O-alkylated hydroxamic acids undergo rearrangement of acyl and O-alkyl groups to give esters and alcohols; when amines were added to the electrolysis solution, the acyl groups were recovered as amides. All of the observed oxidations occurred between 1.2 and 1.6 V *vs* SCE.

A large, and sometimes confusing, body of literature exists on the chemistry of hydroxamate complexes with vanadium.[3-14] It is clear that under aerobic conditions red oxo-alkoxo-(*bis*-hydroxamato)vanadium(V) complexes are

formed regardless of whether oxo-vandadium(IV) or oxo-vanadium(V) is used as the starting material.[12-14] The alcohol solutions of the oxo-vanadium(V) complexes are characterized by intense charge transfer bands (λ_{max} = 410 to 460 nm, ϵ = 1 to 2 x 10^3). The isolation of oxo-vanadium(IV) complexes from water at pH 3-5 has been reported for the ligands benzohydroxamic acid and the closely related *p*-nitro-, *p*-methoxo-, amd *p*-methyl- benzo-hydroxamic acids.[12,13] The rose-violet compounds are reported to be air-stable but to dissolve slowly in alcohol to give initially pale red-violet solutions which deepen to the red solutions characteristic of oxo-alkoxo-(*bis*-hydroxamato)vanadium(V). There appearto have been to be no attempts to prepare hydroxamato-vanadium compounds anaerobically.

Rhodotorulic acid (Figure 4-1), isolated from cultures of the yeast *R.pilimanae*, is one of a class of naturally occurring hydroxamate ligands which have a high affinity for Fe^{3+}.[15] The coordination chemistry of rhodotorulic acid (H_2RA) with trivalent metal ions such as Fe^{3+}, Al^{3+}, and Cr^{3+} has been examined,[16,17] and the iron complex has been characterized in solution as a dimer, Fe_2RA_3.[17] Complexes of H_2RA with the divalent metals Cu^{2+}, Ni^{2+}, Zn^{2+} and VO^{2+} have also been isolated and characterized.[18] When oxo-vanadium(IV) is complexed by the ligand under aerobic conditions, the formation of the oxo-vanadium(V) complex is observed.

FIGURE 4-1

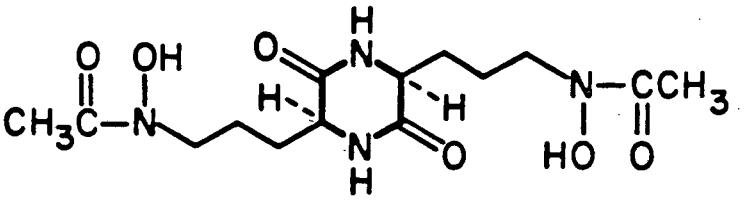

Rhodotorulic Acid (H_2RA)

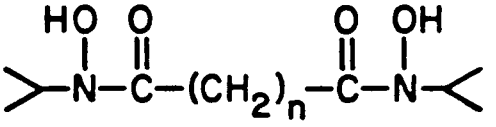

N,N′–dihydroxy–N,N′–diisopropyl(alkane)diamide

Synthetic analogues to Rhodotorulic acid have been prepared[19] (Figure 4-1) for use in biological studies. Since attempts to crystallize either Rhodotorulic acid or any of its metal complexes have been unsuccessful, the synthetic analogues to H_2RA have been useful in structural studies, as well. These dihydroxamate ligands complex Fe^{3+} to yield Fe_2L_3 compounds, Cu^{2+} to form Cu_2L_2 and CuL, and react with VO^{2+} to give oxo-vanadium(V) complexes.

When the oxo-vanadium(V)rhodotorulate complexes were prepared and characterized, a number of interesting questions remained unanswered.[18] A black, glassy solid was isolated from water. The UV/visible spectrum of the "black" solution exhibited a strong absorbance in the UV which tailed into the visible; no other absorptions were observed in the visible. At pH 4.0 this complex exhibited a weak EPR signal equivalent to ~5% of the total complex based on comparison with a standard solution of *bis*(2,4-pentanedionato)vanadium(IV). The black complex was formulated as oxo-hydroxo-vanadium(V)rhodotorulate (VORA(OH)) but was proposed to exist in aqueous solution in equilibrium with the oxovanadium(IV)(rhodotorulate). On the other hand, the red complex isolated from methanol was EPR silent and was formulated as oxo-methoxo-vanadium(V)-rhodotorulate ($VORA(OCH_3)$). Before the oxidation state was assigned, a brief examination of the electrochemistry of these two complexes showed that the solution chemistry of these species was complex, *i.e.* two redox processes

were observed at pH 4.0, and only ligand oxidation was observed at pH 8.0. (See Results) It was also noted that it would be useful to prepare the vanadium complexes using inert atmosphere techniques[20] in order to isolate an oxovanadium(IV) complex.

The present study was undertaken to:

1) explore more fully the electrochemistry of rhodotorulic acid and its vanadium complexes,

2) use anaerobic conditions to isolate vanadium(IV) rhodotorulate complexes,

3) explore the apparent differences in stability toward oxidation of the methanolic and aqueous solutions of vanadium rhodotorulate complexes,

4) examine analogous chemistry with the synthetic dihydroxamate ligands.

Evidence for the existence of both an oxovanadium(IV) rhodotorulate complexe and a vanadium(IV) rhodotorulate complex in which a hydroxamate has displaced the vanadyl oxygen will be presented. Similar chemistry will be shown to exist for the vanadium complexes of the dihydroxamate ligands.

EXPERIMENTAL

MATERIALS

Solvents and chemicals used in syntheses were reagent grade and were used as received. Nonaqueous solvents used for electrochemical studies were purchased from Burdick and Jackson and handled as described in Chapter 2. Water used for electrochemical studies was triply distilled using the apparatus described in Chapter 1 and Appendix 1. The supporting electrolytes, tetraethlammonium perchlorate (TEAP) and teraethylammonium tetrafluoroborate ($TEABF_4$) were prepared by literature methods.[21] Buffers and supporting electrolytes for aqueous electrochemical studies were prepared from reagent grade materials which were used as received.

INSTRUMENTATION

Semiderivative cyclic voltammetric experiments and spectroelectrochemical experiments were performed using the same instrumentation described in Chapter 1. For voltammetric experiments in conentional cells in nonaqueous solvents a planar platinum working electrode was used; for experiments in water the working electrode was modified by adsorbing iodine on the surface immediately before use. Without this procedure it was impossible to observe electron transfer processes for the vanadium rhodotorulate system on platinum in aqueous solution (See

Chapter 1 for a discussion of this method). Cleaning of the electrodes and the adsorption methods are described in detail in Chapter 1.

The working electrode for the optically transparent thin-layer electrochemical cells (OTTLE) was either electroformed gold mesh (200 lines per inch) obtained from Buckbee-Mears or reticulated vitreous carbon (RVC, 100 pores per inch) obtained from ERG, Inc., Oakland, CA. Preparation of the optically transparent electrodes is described in Appendix 1. Each thin-layer gold mesh electrode was used for only one experiment and then discarded; RVC electrodes were rinsed with acid, then water, allowed to dry, and reused unless background scans showed evidence of adsorption of impurities. The OTTLE cells were disassembled after each experiment, rinsed with triply distilled water, and allowed to dry before being reassembled.

A Corning Model 112 Digital pH meter fitted with a combination pH electrode was used to monitor pH.

Infrared spectra were recorded using a Perkin-Elmer Model 597 spectrometer.

EPR spectra were recorded using an X-band Varian Model E-3 spectrophotometer. The field was calibrated with 2,2-diphenyl-1-picrylhydrazyl radical (DPPH).

METHODS

All solutions were degassed by repeated freeze-pump-cycles on a dual manifold Schlenk line[20] before being

transferred to the OTTLE cells. Filling of the cells was as described in Chapter 1 of this dissertation. Reference electrodes appropriate to the solvent were used: in the nonaqueous solvent DMF and DMSO a $Ag/AgNO_3$ (10^{-2} M), solvent electrode was used; in water the Ag/AgCl(s), 0.1 M KCl electrode was the reference of choice. The Ag/AgCl(s) reference electrode was calibrated against the quinhydrone electrode[22] described in Chapter 1; the reference electrodes in nonaqueous solvents were calibrated using the ferrocene/ferrocenium couple.[23]

Spectroelectrochemical data were obtained from linear sweep voltammetric (LSV) experiments similar to those described in Chapter 3. The number of electrons transferred was determined in the OTTLE cells by integration of the current-potential curve under the observed peaks.[24] The volume of the cell was calibrated using the $Fe(CN)_6^{3-}/Fe(CN)_6^{2-}$ couple,[25] while the path length (cell thickness) was calibrated using $ClMn^{III}TPP$ (See Chapter 4). A typical cell volume with gold minigrid electrodes was 40 μ with a path length (cell thickness) of 0.10 to 0.14 mm. When RVC electrodes were used cell thicknesses were typically 0.3 to 0.5 mm. Hence, these cells were not true thin-layer electrochemical cells (See Chapter 1), and only the cells with the gold minigrid electrodes were used for measuring n, the number of electrons transferred.

EPR samples were prepared in ethanol/methanol (4:1, v/v) using inert atmosphere techniques. Once prepared

the samples were immediately frozen in liquid nitrogen. All EPR samples were taken at ~77K.

Elemental analyses were performed by the microanalytical laboratories operated by the Chemistry Department of the University of California, Berkeley.

SYNTHESES

Preparation of oxovanadium(IV)rhodotorulate hydrate, $C_{14}H_{24}N_4O_8V$ (VORA·H_2O):

a) From H_2O: All procedures were carried out in an argon atmosphere using inert atmosphere techniques.[20] In a typical preparation oxo-vanadium(IV)sulfate (60 mg, 0.30 mmoles) was dissolved, degassed by freeze-pump-thaw cycles, and added to a slurry of rhodotorulic acid (105 mg, 0.31 mmole) which had also been degassed. As the rhodotorulic acid slowly dissolved, the solution turned deep red-violet. The solution was concentrated under reduced pressure until a pale violet precipitate appeared and was filtered after ~24 h. The precipitate was washed successively with ethanol and diethyl ether and then dried in vacuo. Yield: 35 mg (~32%) The UV/vis spectrum of the filtrate was characterized by an absorption maximum at 516 nm and a shoulder at ~390 nm.

Anal. Calc. for $C_{14}H_{24}N_4O_8V\cdot H_2O$: C,39.5; H, 5.9; N, 13.11. Found: C, 39.34; H, 5.47; N, 12.81.

b) From methanol: Essentially the same procedure as that in water was followed with the substitution of oxo-vana-

dium(IV)bis-pentandienato as the starting material (80 mg, 0.30 mmole). As the ligand slowly dissolved with mixing of the two solutions, the solution became colorless. This was followed by slow precipitation of a violet powder. Yield: 40 mg (~40%)

The infrared spectrum of the violet powder isolated from either methanol or water exhibited bands characteristic of the ligand and a strong vanadyl oxygen stretch at ~970 nm. In inert atmosphere the violet powder was insoluble in water and alcohols but dissolved slowly when exposed to air to give a red solution (λ_{max} = 436 nm) in methanol and a violet-burgundy solution (λ_{max} = 289, 464 and 556 nm) in water.

Preparation of Vanadium(IV)rhodotorulate, $[V_2RA_3]^{+2}$?: A slurry of oxo-vanadium(IV)sulfate (54 mg, .27 mmole) was degassed and added to a slurry of rhodotorulic acid (188 mg, .55 mmole). A deep burgundy-red color appeared as both the starting materials slowly dissolved. Reducing the volume did not yield a precipitate. The UV/vis spectrum gave absorption maxima at 390 and 516 nm ($\epsilon \sim 2 \times 10^3$). Addition of a solution of sodium tetraphenylborate produced a dark red-violet, powdery precipitate. Elemental analysis was not definitive (C, H, N, V), but gave a ligand to metal ratio, RA:V ≈ 3:2.2 based on the N:V ratio. The infrared spectrum showed no strong band between 800 and 1000 cm^{-1} but was otherwise similar to the spectrum observed for the violet powder, oxo-

vanadium(IV)rhodotorulate, after accounting for bands due to the counterion, $(C_6H_5)_4B^-$.

Preparation of $[(C_{11}H_{22}N_2O_4)_3V_2]^{+2}$:

The ligand, N,N'-dihydroxy-N,N'-diisopropylpentanediamide ($C_{11}H_{22}N_2O_4$), (283 mg, 1.0 mmole) was dissolved in methanol (~10ml), degassed, and transferred under Ar to a slurry of oxo-vanadium(IV)sulfate in methanol (~10 ml). An immediate color change to violet-burgundy was observed; as the $VOSO_4$ slowly dissolved the color deepened in intensity. After filtration the UV/vis spectrum was recorded (λ_{max} = 390 and 516 nm, $\epsilon \geq 2 \times 10^3$ per vanadium). One aliquot of the solution was added to a concentrated methanolic solution of $Na(C_6H_5)_4B$, a second to a $CHCl_3/CH_3OH$ (~3:1) solution of $(C_3H_7)_4NBF_4$. A dark red-violet powder precipitated from the $Na(C_6H_5)_4B$ solution. This solution was filtered, and the precipitate was washed with diethyl ether and dried in vacuo for ~1 h. The infrared spectrum (KBr pellet) showed no V=O stretch in the region 800 to 1000 nm. Elemental analysis was inconclusive, indicating a large quantity of unaccounted for impurity was present (possibly Na_2SO_4). However, based on the V:N ratio, the ligand to metal ratio was estimated to be L:V ~ 1:1.8. The solution with $(C_3H_7)_4NBF_4$ gave no precipitate even when the solution volume was reduced to about half its original volume. This solution was evaporated to dryness, and CH_3CN was added

resulting in a deep burgundy-red solution. Comparison of the electronic spectrum of this solution (λ_{max} = 390 and 516 nm) with that of authentic $VO(C_{11}H_{22}N_2O_4)(OCH_3)$ (λ_{max} = 294, ~460, and 544 nm) in acetonitrile shows that a different product is present in solution in the present case.

RESULTS and DISCUSSION

I. ELECTROCHEMICAL STUDIES

Initial electrochemical experiments were simply attempts to ascertain the oxidation state of the oxo-vanadium rhodotorulate complexes which had been synthesized by Tom Tufano[18] of this research group. The approach used was to record the open circuit potential of cells containing the vanadium complex, then record a cyclic voltammogram. By so doing, it was hoped that the oxidation state of the complex in solution might be deduced. For example, if E_{RXN} = 0.1 V and an oxidation is observed at 0.2 V, the complex in solution can be assigned to that of a vanadium(IV) rather than a vanadium(V) species.

Using this approach voltammograms of the red and black oxo-vanadium rhodotorulate complexes were each recorded in aqueous solution. Data for each compound were recorded at pH 4.0 using 0.1 M acetate buffer and at pH 8.0 using Tris-ClO_4 buffer. At pH 4.0 E_{RXN} for both the red and black compounds ranged from 0.25 to 0.36 V and varied with the concentration of the complex. Some differences were observed between the two compounds (See Figure 4-2). The black compound exhibited two anodic waves (E_{pa} ~ 0.18 and 0.33 V) and a broad cathodic wave (E_{pc} ~0.15 V; the red compound exhibited only one anodic wave (E_{pa} ~ 0.30 V) and two unequal cathodic waves (E_{pc} ~ 0.28 and 0.14 V). For the red compound the wave at high potential was nearly reversible based on peak width, peak

ratios, and the small difference in peak potentials.[26-28] At pH 8.0 only ligand oxidation was observed, as verified by addition of free H_2RA and by comparison with voltammograms for ligand only.

As will be shown the black compound had probably been partially decomposed. The processes near 0.3 V are those of the vanadium rhodotorulate complex, while those near 0.15 V are probably due to an acetate complex (See 4.I.B.)

It became clear from this set of experiments that a more careful investigation was required. This study included a brief examination of ligand electrochemistry, as well as a more detailed study of vanadium and rhodotorulic acid as a function of pH, ligand:metal ratio, and solvent. The chemistry and electrochemistry of other hydroxamate ligands was examined briefly for comparison.

FIGURE 4-2

PRELIMINARY VOLTAMMOGRAMS OF VORA(OCH_3) AND VORA(OH)

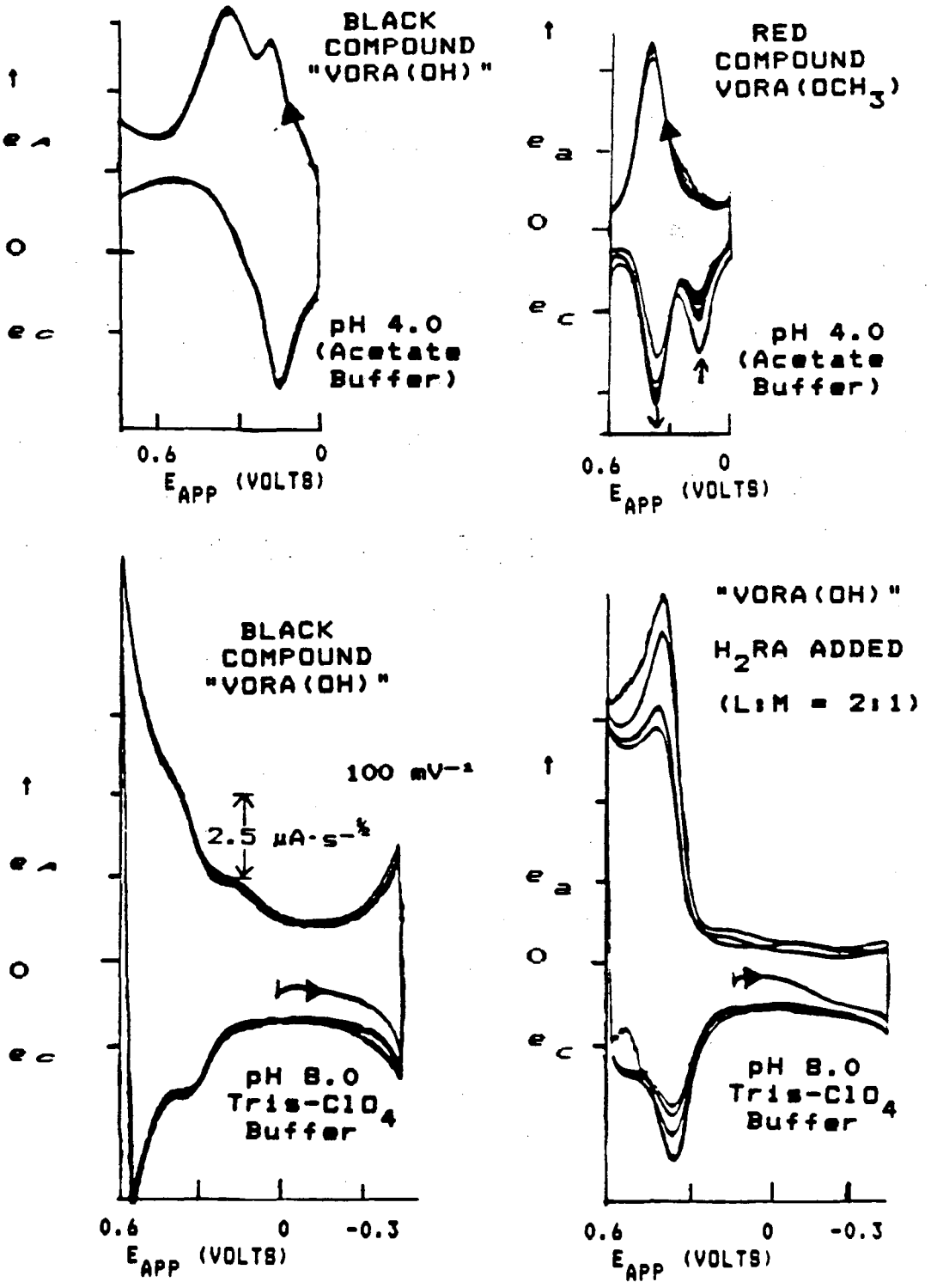

A. LIGAND ELECTROCHEMISTRY

At low pH (pH = 1.3 to 6.8) rhodotorulic acid exhibited an irreversible wave, the potential of which was pH dependent. This process showed quasi-reversible behavior from pH 7.5 to 9.5. At high pH (to ~10) this process once again appeared to be irreversible. The simple hydroxamate, acetohydroxamic acid, $CH_3C(NHOH)CO$, exhibited similar behavior. This observation coupled with the literature reports of hydroxamate oxidations in acetone[10] and acetonitrile[11] confirms that the hydroxamate group was being oxidized rather than the diketopiperazine ring. Typical voltammograms are shown in Figure 4-3.

In DMF or DMSO no activity was observed for the ligand over a wide potential range (1.0 to -2.0 V *vs* a $Ag/AgNO_3$(.01 M), TEAP(0.1 M) reference electrode). Based on the potentials observed for monohydroxamates in acetone and acetonitrile,[10,11] it is not surprising that no oxidations were observed below the potential at which these two solvents are themselves oxidized.

FIGURE 4-3

OXIDATION OF RHODOTORULIC ACID AT VARIOUS pH VALUES

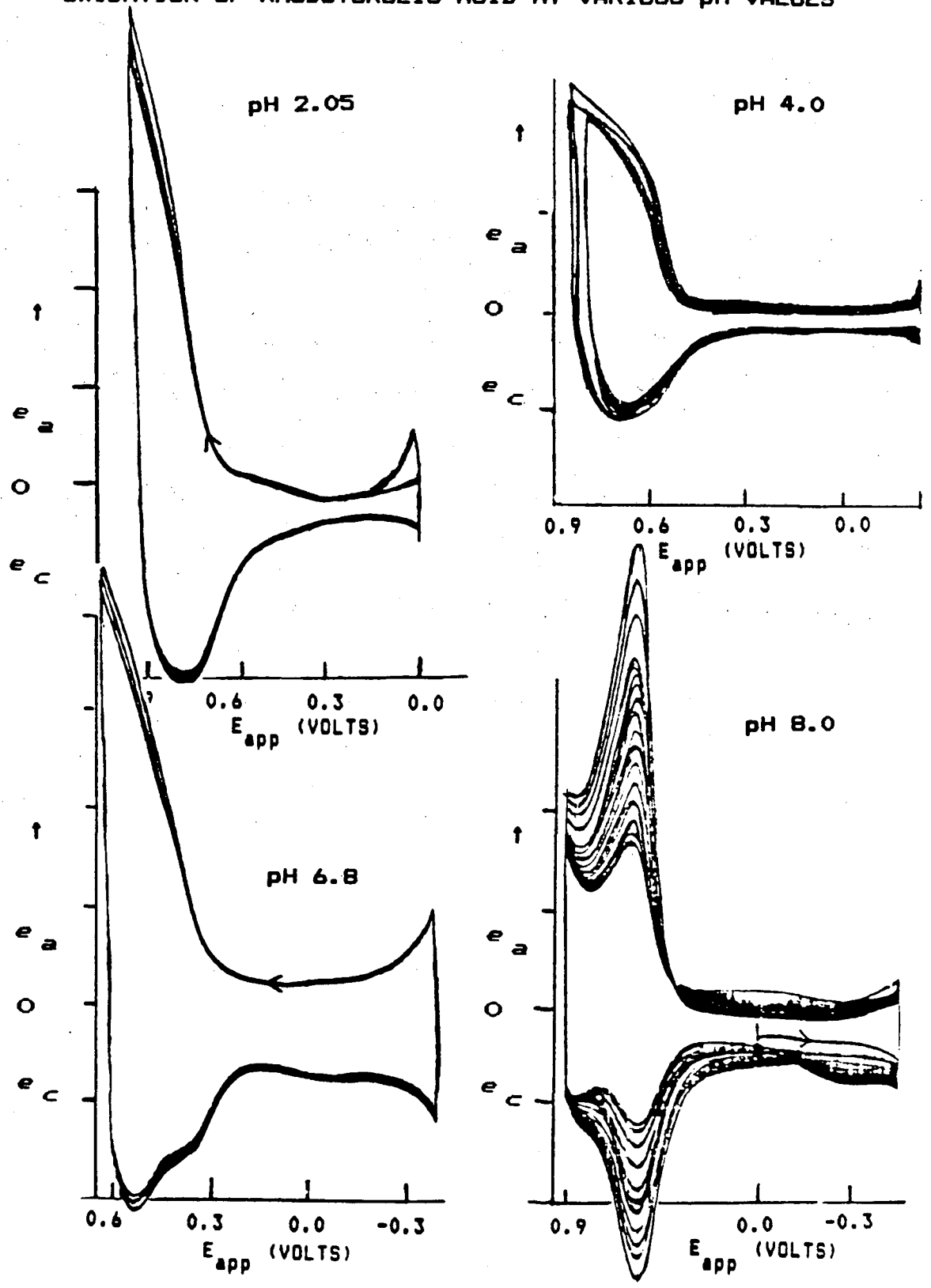

B. Vanadium(IV) and Vanadium(V) Electrochemistry

Cyclic voltammetry of oxovanadium(IV)sulfate ($VOSO_4$) and ammonium metavanadate (NH_4VO_3) in aqueous solution showed no oxidation/reduction behavior within the potential limits of the modified (Pt-I) electrode over a pH range of 1.2 to 8.0 when 0.1 M H_2SO_4 was used as electrolyte (pH was adjusted with KOH(aq)). This result is consistent with the reported potentials of the $V^{V/IV}$ couple in aqueous solution according to the reaction:[29]

$$VO_2^+ + 2H^+ + e^- = VO^{2+} + H_2O \qquad E^\circ = +1.0 \text{ } vs \text{ NHE}$$

However, if acetate buffer (0.1 M) was used as the electrolyte near pH 4.0, both the vanadium(IV) and vanadium(V) compounds showed a quasi-reversible wave for the $V^{V/IV}$ couple. It became apparent at this point that one of the waves observed for the two oxovanadium rhodotorulate complexes was probably that of the acetate complex of the metal. Subsequently, the use of buffers with coordinating anions was avoided.

The observation of these processes confirmed, however, that the comparison of the rest potential with the observed $E_{\frac{1}{2}}$ does yield useful information on the oxidation state of the electroactive species in solution, as shown in Table 4-1. Also shown in Table 4-1 is a summary of potentials observed for (*bis*-pentanedienato)oxovanadium-(IV) ($VO(acac)_2$) in DMSO and DMF. The observed waves are those of the $V^{V/IV}$ couple, and again, the open circuit

potentials, E_{RESET}, relative to the half-wave potentials, $E_{1/2}$, are consistent with the oxidation state of the electroactive species in the bulk solution.

C. Complexes of Vanadium with Rhodotorulic Acid

Voltammetric studies were done on solutions containing H_2RA and vanadium in varying ratios and over a pH range from 2.0 to 9.5. Oxovanadium(IV) sulfate, $VOSO_4$, was used as a source of vanadium(IV) for aqueous studies; (*bis*-pentanedionato)oxovanadium(IV), $VO(acac)_2$, was used in DMSO and DMF. Ammonium metavanadate, NH_4VO_3, was used as a source of vanadium(V) in all three solvents.

TABLE 4-1

POTENTIALS OF VARIOUS VANADIUM COMPOUNDS

COMPOUND	SOLVENT CONDITIONS	POTENTIALS * E_{REST}	E_{pa}	E_{pc}	$E_{1/2}$
$NH_4V^{V}O_3$	H_2O (pH 4.0, Acetate buffer)	0.45	0.18	0.13	0.16
$V^{IV}OSO_4$	H_2O (pH 4.0, Acetate buffer)	0.00	0.16	0.13	0.14
$V^{IV}OSO_4$	DMSO	0.17	0.54	—	0.54
$V^{IV}O(acac)_2$	DMSO	0.20	0.55	0.54	0.54
$V^{IV}O(acac)_2$	DMF	-0.15	0.44	0.43	0.44

* Potentials for aqueous solution are reported *vs* the Ag/-AgCl(s),1.0 M KCl reference electrode which is 0.23 V *vs* NHE at 25°C. For DMF and DMSO the reference was the $Ag/AgNO_3$(0.01 M),TEAP(0.1 M),Solvent. These potentials were recorded to be -0.027 and -0.167 V *vs* the ferrocene/ferrocenium couple at 25°C for DMF and DMSO respectively.

1. EFFECT OF pH:

Voltammograms were recorded of a solution of $VOSO_4$ and H_2RA (1:1) under anaerobic conditions over a pH range of 2.0 to 9.5 (Figure 4-4). The solution was then left at pH 9.5 and exposed to air for ~12 hours. A second set of voltammograms was then recorded from pH 9.5 to 3.0 (Figure 4-5). Plots of $E_{1/2}$ and E_{RECT} *vs* pH (Figure 4-6) showed different behavior for the two solutions. The important features of these results are:

1) $E_{1/2}$ shifted to more negative potentials with increasing pH for both sets of experiments. The solution which had been kept anaerobic showed linear behavior from pH 2.0 to 4.0 (slope = -0.054 V/pH unit, R^2 = 0.99), but showed a break at pH 4.0. From pH 4.0 to 7.3 a second nearly linear region was observed which exhibited a much smaller dependence of $E_{1/2}$ on pH (slope = -0.016 V/pH unit, R^2 = 0.98). For voltammograms recorded after exposure to air the plot of $E_{1/2}$ *vs* pH was nearly linear from pH 7.0 to 3.0, exhibiting no break near pH 4 (slope = -.058 V/pH unit, R^2 = 0.98).

2) For voltammograms recorded before exposure to air the open circuit potential, E_{RECT}, was consistently observed at potentials more negative than $E_{1/2}$ at all pH values. (See Figure 4-6, inset.) After exposure to air only ligand oxidation was observed above pH 8. E_{RECT} for these oxidations was at potentials more negative than the observed peak potentials. From pH 7.0 to 3.0 the vana-

dium(V/IV) couple was observed; for these processes E_{REST} was consistently observed at potentials more positive than $E_{1/2}$ (Figure 4-6).

3) The most nearly reversible behavior (based on peak width, the ratio of e_{pa}/e_{pc}, and the difference in peak potentials[26-28]) was observed between pH 2.5 and 3.5 for both sets of data.

4) Under anaerobic conditions solutions with pH < 5 were pale violet; solutions with pH > 5 were colorless. After exposure to air the solution was pale yellow above pH 6.0; below pH 6.0 it gradually darkened with decreasing pH to a deep purple (λ_{max} = 289, 464, and 556 nm, $\epsilon \sim 10^3$).

5) After exposure to air the observed peak heights for the vanadium (V/IV) couple were reduced by ~50% relative to those of the anaerobic solution. Since the small increase in volume due to addition of acid was insufficient to account for this change, it is probable that some decomposition had taken place. A second, irreversible, reduction was observed at potentials negative of the quasi-reversible couple. With successive scans this peak decreased while the cathodic peak at more positive potential increased (Figure 4-5).

When NH_4VO_3 and H_2RA (1:1) were used under anaerobic conditions, the solution exhibited voltammetric behavior similar to that described above for $VOSO_4$ and H_2RA (1:1) after exposure to air, *i.e.* solutions at pH < 5 were deep

violet, E_{RECT} was more positive than $E_{\frac{1}{2}}$, and two cathodic peaks were observed for solutions below pH 7.0. Furthermore, increasing the ligand to metal ratio had no effect on the half-wave potential or on the degree of reversibility near pH 3.0. H_2RA was also added to aqueous solutions (pH 3.0) of the black and red compounds, formulated as VORA(OH) and VORA(OCH_3). Each of these solutions immediately changed to a deep violet and exhibited voltammetric behavior identical to that of solutions of NH_4VO_3 and H_2RA (1:1).

FIGURE 4-4

pH DEPENDENCE OF VORA UNDER ANAEROBIC CONDITIONS

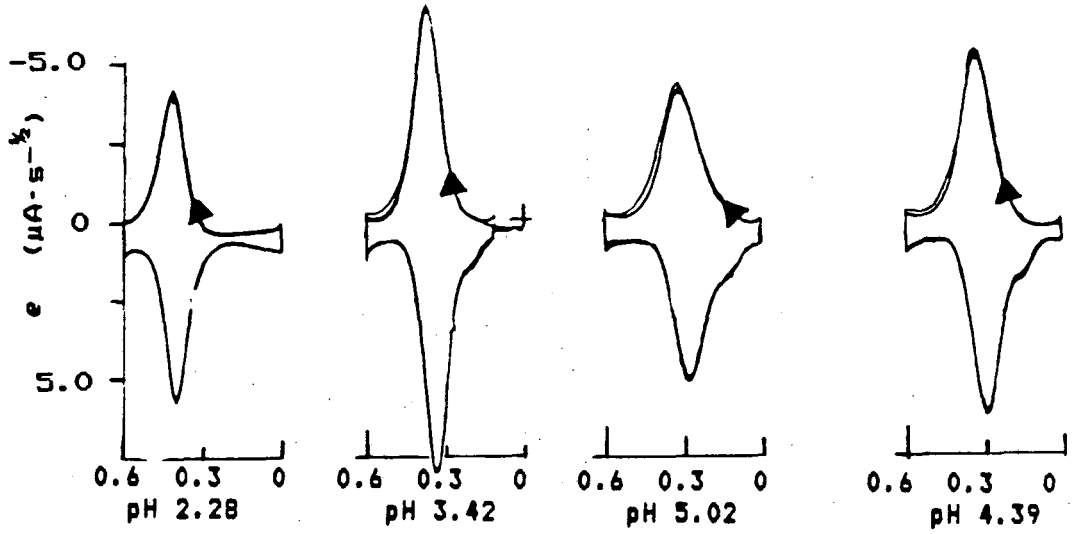

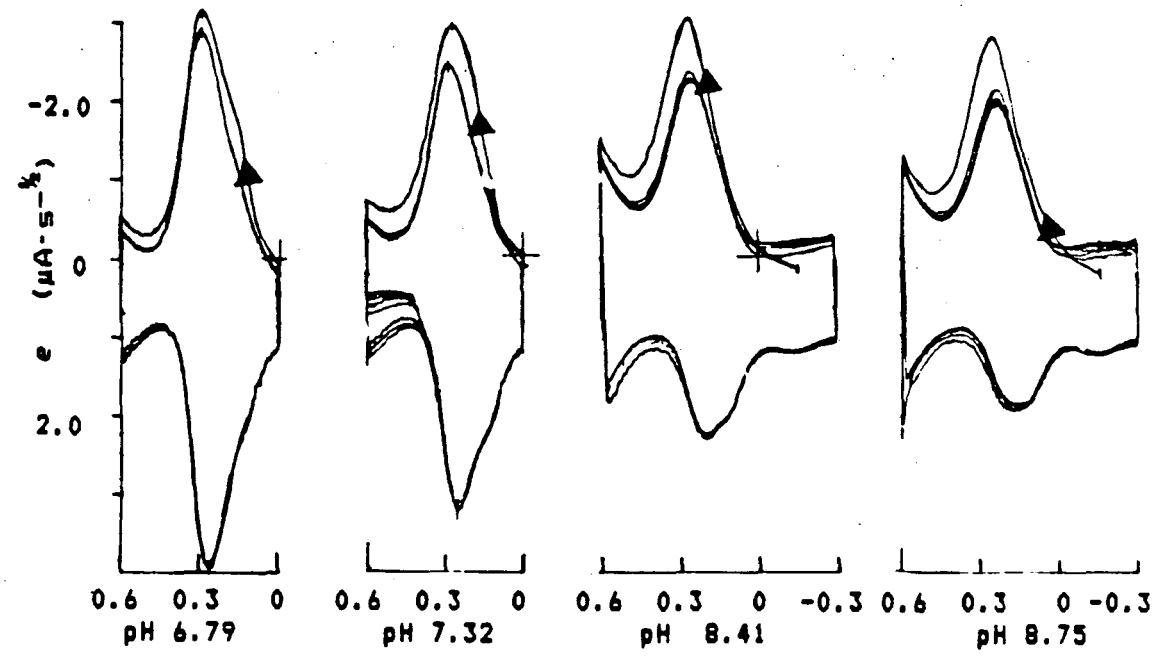

Voltammograms represent repeated cycles. Arrows indicate peaks which increased of decreased after the initial cycle.

FIGURE 4-5

pH DEPENDENCE OF VORA AFTER EXPOSURE TO AIR

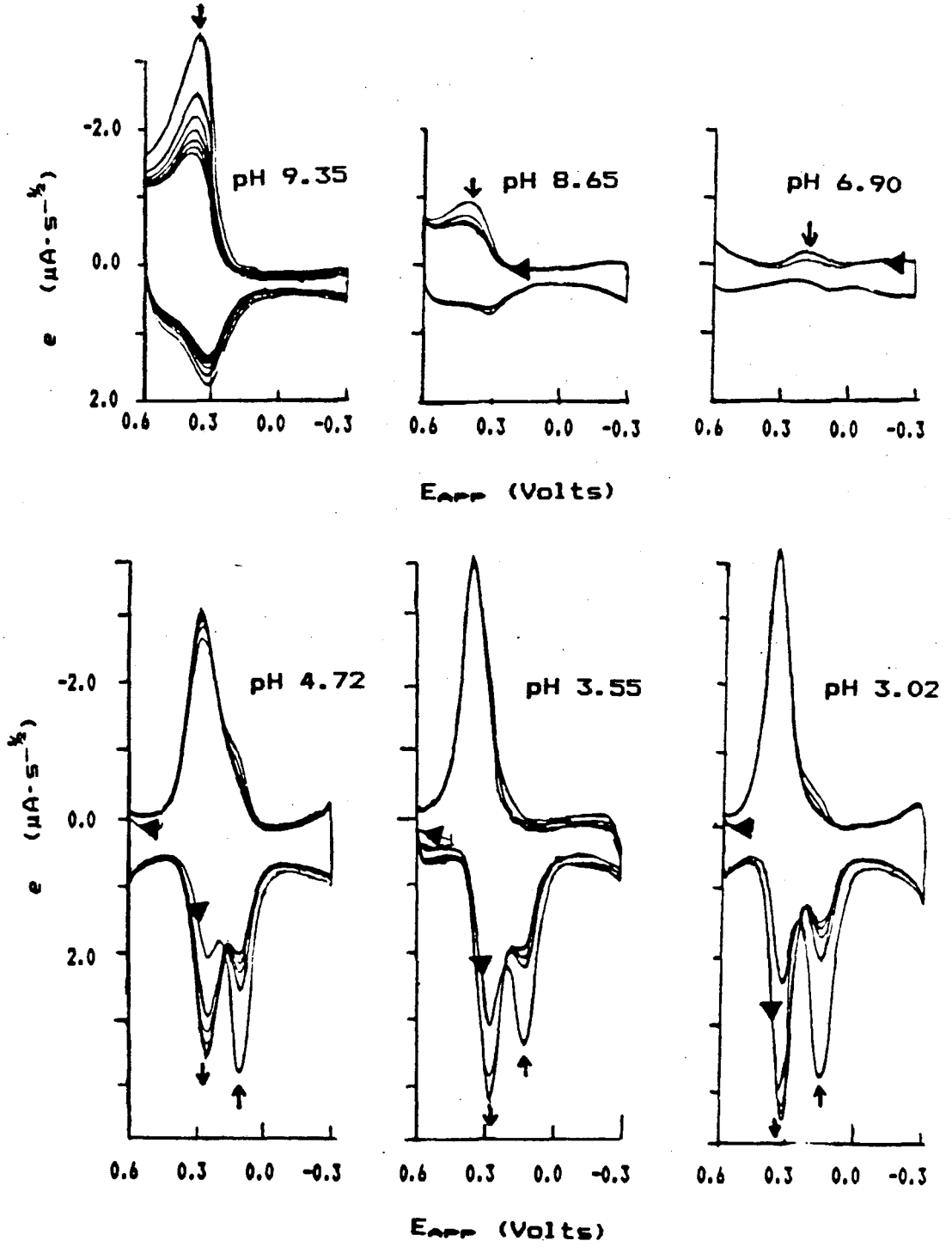

All voltammograms represent repeated cycles. Arrows indicate peaks which increased or decreased after the initial cycle.

FIGURE 4-6

Dependence of $E_{\frac{1}{2}}$ and E_{REST} on pH for VORA

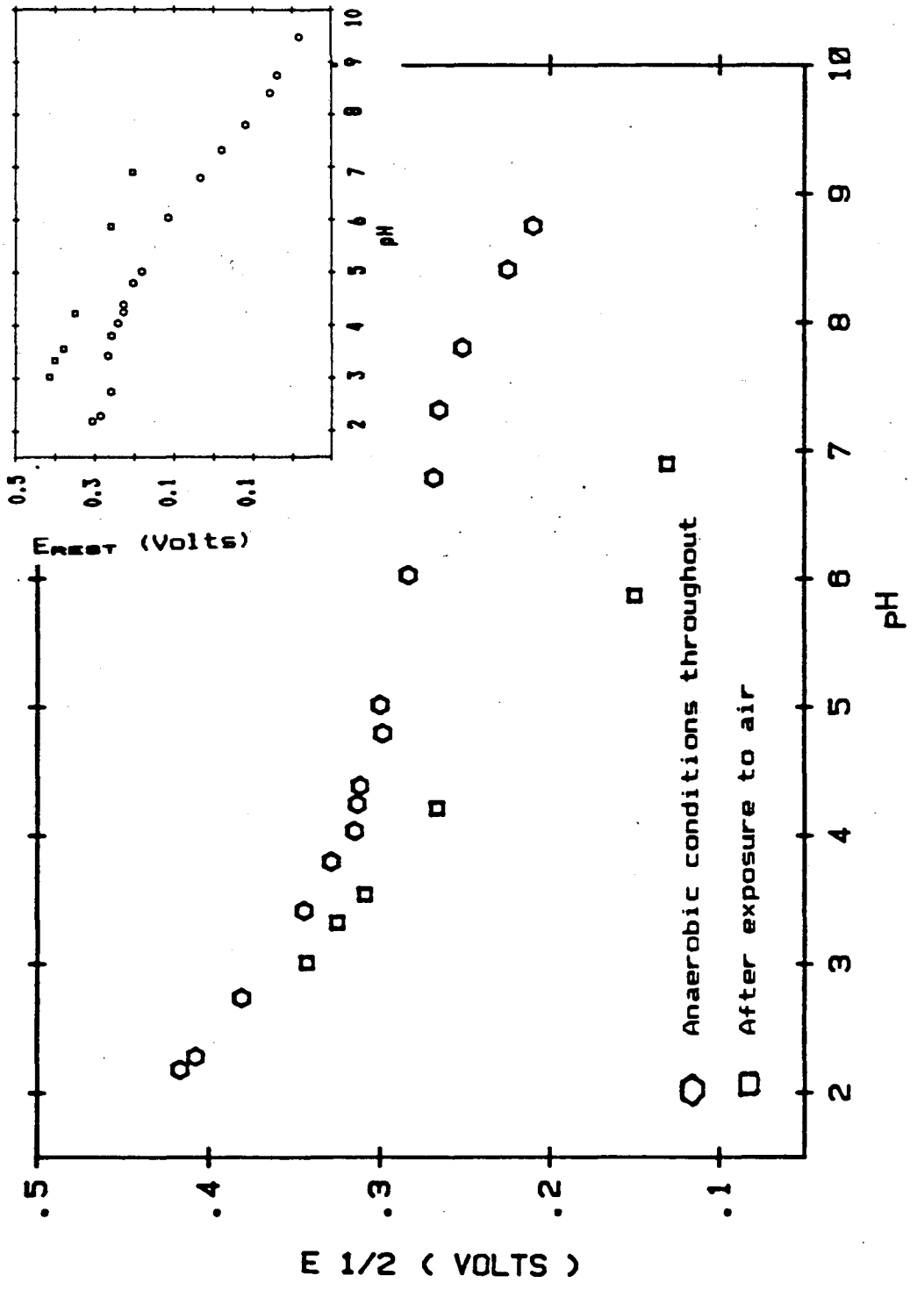

2. SPECTROELECTROCHEMICAL EXPERIMENTS

Spectroelectrochemical experiments were done for three different solutions at pH 3.0, all of which gave the same results (See Figure 4-7). The solutions examined were: 1) H_2RA and $VOSO_4$ (1:1) under anaerobic conditions, 2) H_2Ra and $VOSO_4$ (1:1) in a solution which was first exposed to air, and 3) NH_4VO_3 and H_2RA (1:1) under anaerobic conditions. Repeated cyclic potential sweeps were done between -0.15 and 0.90 V. For each cycle the reduced species was colorless, having no absorption bands in the visible, while the oxidized species was purple, having a spectrum identical to that of the purple solution described previously. Integration of the i-E curve (inset Figure 4-7b) verified that a one-electron transfer was involved. The same pattern of spectral changes was observed for the air oxidation of a solution of $VOSO_4$ and H_2RA (1:1).

FIGURE 4-7

SPECTROELECTROCHEMISTRY OF $VOSO_4$ + H_2RA (1:1)

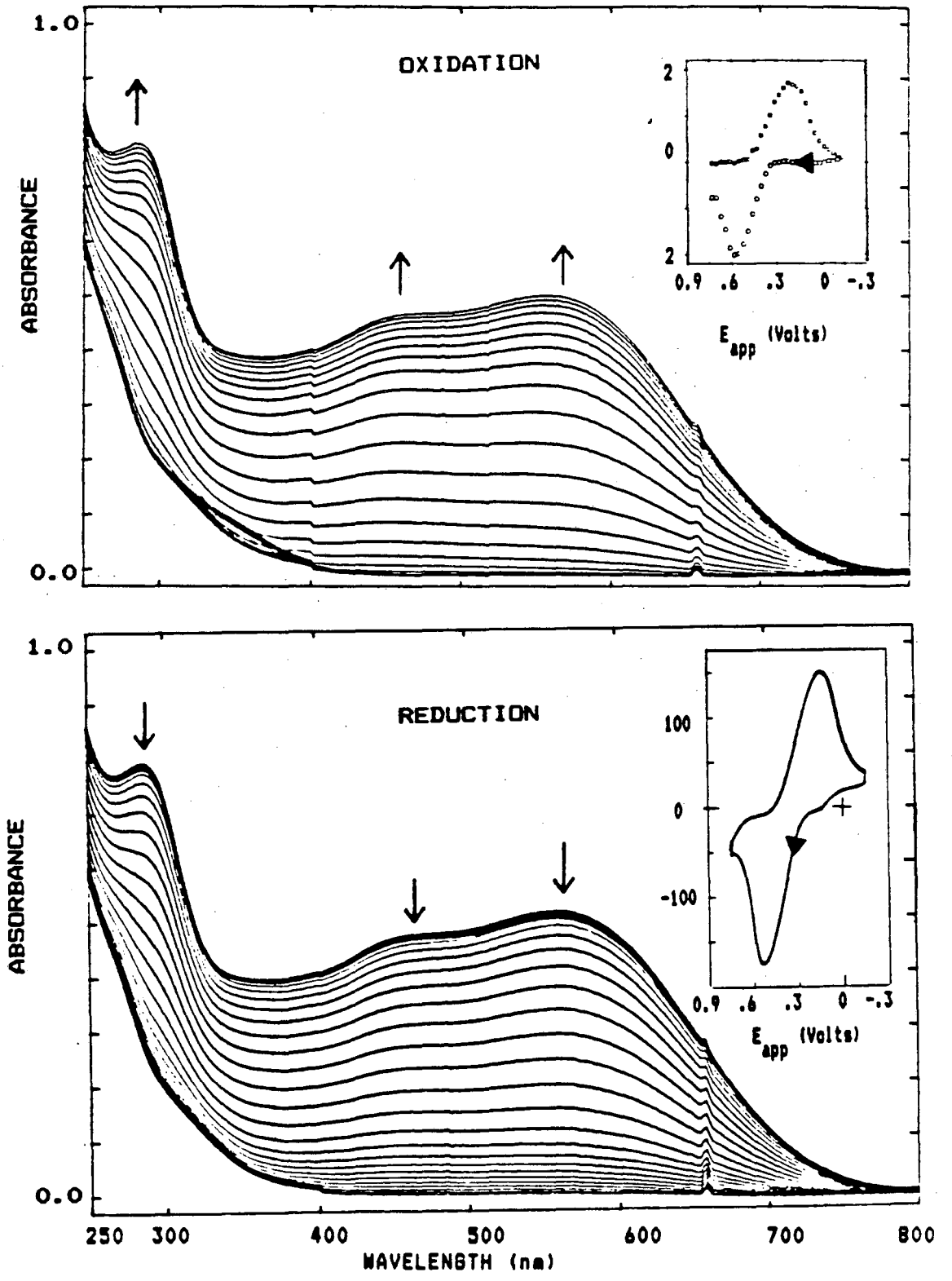

3. VOLTAMMETRY IN APROTIC SOLVENTS

Voltammograms of $VOSO_4$ and H_2RA and of the red $VORA(OCH_3)$ were recorded in the solvents DMF and DMSO. In each case the solvents were degassed with Ar before addition of the electroactive species. In all cases the solutions were pale violet or colorless under anaerobic conditions; after exposure to air the DMF solutions turned deep orange, and the DMSO solutions became dark purple. The observed potentials are listed in Table 4-2. In both solvents the vanadium(V/IV) couple was observed at potentials ~0.4 to 0.5 V more negative than the same couple for $VO(acac)_2$ (Table 4-1). Although the vanadium(V/IV) couple was quasi-reversible in both solvents, more nearly reversible behavior was observed in DMSO as evidenced by the ratios of e_{pa}/e_{pc}, the differences in the peak potentials, E_{pa} and E_{pc}, and the peak width, E_{pw}.[26-28] A second, irreversible wave was observed in DMSO which has been tentatively assigned to the vanadium(III/II) couple. This peak shifted to more positive potential and became quasi-reversible on addition of excess H_2RA.

4. Conclusions from electrochemical studies

The results of the voltammetric and spectroelectrochemical studies are consistent with a one-electron transfer in which a proton transfer is involved below pH 4 according to the equation:

$$VORA + H_2O \rightleftharpoons VORA(OH) + H^+ + e^-$$

The abrupt change in pH dependence of $E_{1/2}$ at pH 4 to onl0.015 V per pH unit suggests that a second species may be in solution. The observation of quasi-reversible behavior for the $V^{IV/III}$ couple with addition of excess ligand to the DMSO solution of H_2RA and $VOSO_4$ (2:1) suggests that this species may be a complex in which the vanadyl oxygen has been replaced by a hydroxamate. Further evidence for the existence of such a species was obtained from EPR and UV/visible spectra.

The differences in the voltammetric behavior for solutions containing oxovanadium(V) rhodotorulate cannot be explained without further experiments. It is highly likely that prolonged exposure to base caused considerable decomposition of the complex. In order to interpret this data, the pH dependence of the half-wave potentials of a freshly prepared solution of NH_4VO_3 and H_2RA (1:1) should be examined.

TABLE 4-2

POTENTIALS OF VANADIUM RHODOTORULIC ACID COMPLEXES IN APROTIC SOLVENTS

SOLVENT	COMPONENTS	POTENTIALS * E_{pa}	E_{pc}	$E_{1/2}$	E_{PC} ($V^{III/II}$)
DMF	$VOSO_4$ + H_2RA (1:1)	-0.030	-0.105	-.068	--
DMF	$VOSO_4$ + H_2RA (1:3)	-0.030	-0.090	-0.060	--
DMF	$VORA(OCH_3)$	-0.030	-0.120	-0.075	--
DMSO	$VOSO_4$ + H_2RA (1:1)	+0.090	+0.069	+0.069	-1.35 [b]
DMSO	$VOSO_4$ + H_2RA	+0.060	+0.027	+0.044	-0.75 [c]
DMSO	$VORA(OCH_3)$	+0.054	+0.027	+0.041	-0.93 [b]

a For DMF and DMSO the reference was the $Ag/AgNO_3$(0.01 M), TEAP(0.1 M), Solvent. These potentials were recorded to be -0.027 and -0.167 V *vs* the ferrocene/ferrocenium couple at 25°C for DMF and DMSO respectively.

b Irreversible.

c Quasi-reversible.

II. EPR and SYNTHESES

For aqueous preparations of oxovanadium(IV) rhodotorulate, $VOSO_4$ was used , and for methanolic preparations, $VO(acac)_2$ was used. In both cases (1:1) solutions of H_2RA and oxo-vanadium(IV) yielded a pale violet powder which has been identified as oxovanadium(IV) rhodotorulate, VORA. In the case of the aqueous preparation a violet color was observed in the filtrate which was initially attributed to contamination by air. However, measurement of the UV/visible spectrum showed that another species was present in solution (λ_{max} = 522 nm, $\epsilon \sim 10^3$). The filtrate of the methanolic solution, on the other hand, was colorless.

In the course of preparing solutions for EPR measurements a solution of $VOSO_4$ and H_2RA(1:1) in methanol was prepared using inert atmosphere techniques. As the ligand and metal each dissolved, a red-burgundy color was observed. The UV/visible spectrum (λ_{max} = 390 and 516 nm, $\epsilon \geq 10^3$) again indicated the presence of a species which was different from either VORA or VO RA(OCH_3). EPR measurements subsequently confirmed that the predominant species in this solution was a vanadium(IV) complex (≥ 70% vanadium(IV) based on comparison with a $VO(acac)_2$ standard).

From these results it was proposed that the hydroxamate chelating group was capable of displacing the vanadyl oxygen to form a (*tris*-rhodotorulate)vanadium(IV) complex. In the only known example of such a reaction in protic

solvents, catecholate ligands have been shown to be able to form both the (bis-catecholato)oxovanadium(IV) and the (tris-catecholato)vanadium(IV). These complexes, which have been isolated and characterized by X-ray crystallography, exhibit some physical propoerties which are quite similar to those reported here for their rhodotorulate analogues. The electronic spectrum of the (bis-catecholato)oxovanadium(IV) complex is characterized by weak d-d transitions ($\epsilon < 100$), but the (tris-catecholato)vanadium(IV) complex exhibits charge transfer transitions ($\epsilon \sim 9 \times 10^3$). Furthermore, cyclic voltammetric results reported in this same study[30] showed that the oxovandium(IV) complex exhibits an irreversible vanadium(IV/III) reduction, while the (tris-catechlato)vanadium(IV) complex exhibited a quasi-reversible vanadium(IV/III) couple.

Thus, comparison of the results reported in the present work with those reported for the vanadium catecholate system lends further support to the proposal that a (*tris*-dihydroxamato)vanadium(IV) complex is formed.

Attempts to isolate the proposed (*tris*-dihydroxamato)vanadium(IV) complex were based on an assumed formulation of $[V_2RA_3]^{2+}$. This formulation seems the most likeley based on its similarity to the known stoichiometry of the Fe^{3+} complex, Fe_2RA_3.[17] Hence, an excess of ligand was used. Since such a species would be cationic, the anion $[(C_6H_5)_4B]^-$ was used to precipitate the crude, dark red-violet product. This approach was used with a similar

result using the dihydroxamate ligand N,N'-dihydroxy-N,N'-diisopropyl(pentane)diamide, which under aerobic conditions had been demonstrated to form the (dihydroxamato)oxo-methoxo-vanadium(V) complex.[19]

Physical characterization of the red powdery products obtained from precipitation by tetraphenylborate was consistent with the displacement of the vanadyl oxygen by ligand. Although the pale violet powder, VORA, exhibits a strong absorbance in its infrared spectrum at ~970 cm^{-1} which is assigned as the V=O stretch, this band is absent in the red products assigned as (*tris*-dihydroxamato)vanadium(IV). The air oxidation of an aliquot of the reaction mixture for the (*tris*-rhodotorulate)vanadium(IV) complex was followed spectrally (Figure 4-8). The observed behavior is clearly quite different from that observed for the spectroelectrochemical studies of the (1:1) oxovanadium(IV): H_2RA system or for the air oxidations of the same system. The absence of isosbestic behavior is indicative of a complex mechanism. This is to be expected, since at least two steps would be required for the overall reaction involved in going from a (*tris*-dihydroxamato)vanadium(IV) complex to an oxovanadium(V) species.

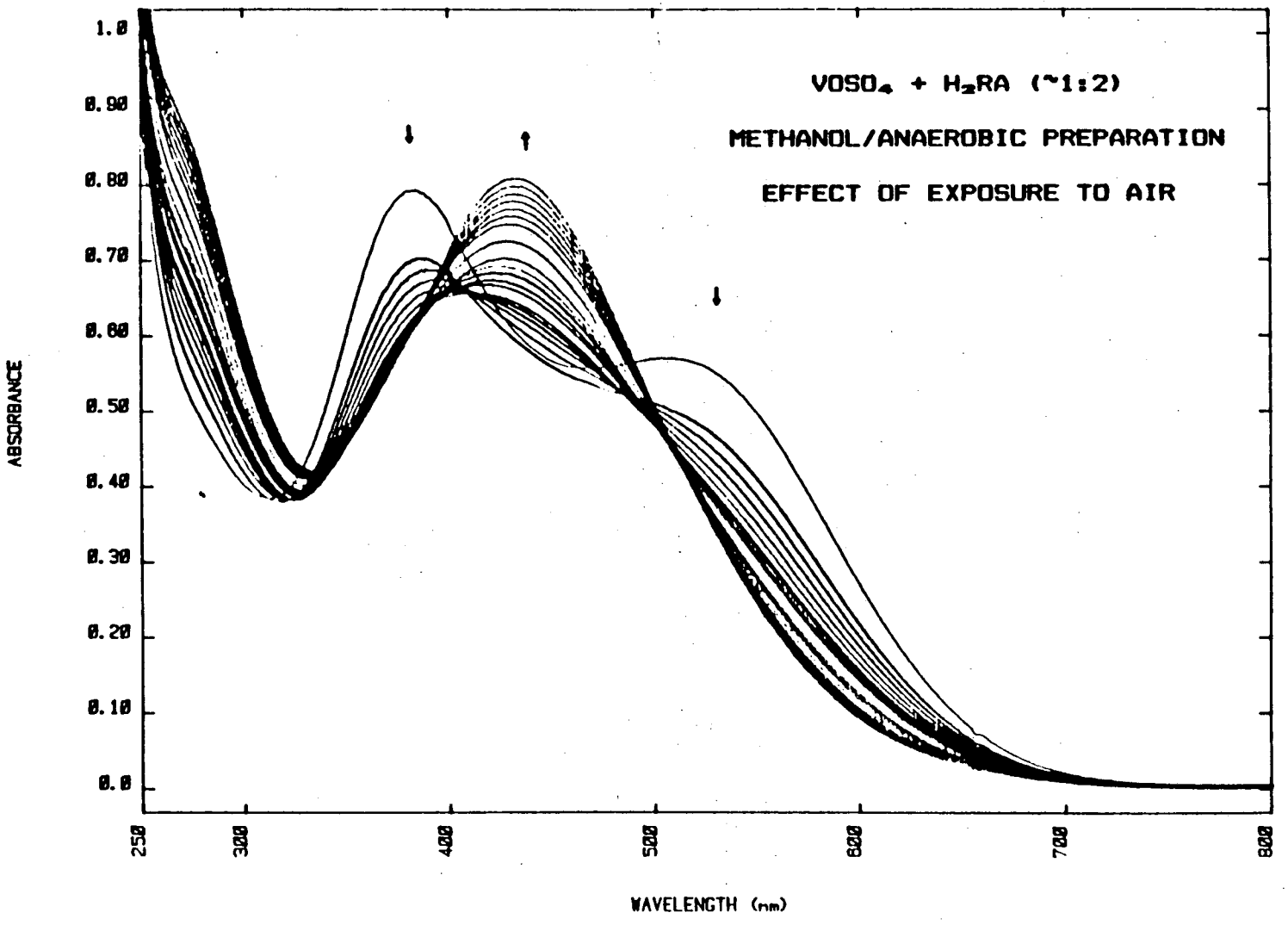
VOSO4 + H2RA (~1:2)
METHANOL/ANAEROBIC PREPARATION
EFFECT OF EXPOSURE TO AIR
ABSORBANCE
1.0
0.90
0.80
0.70
0.60
0.50
0.40
0.30
0.20
0.10
0.0
250
300
400
500
600
700
800
WAVELENGTH (nm)

FIGURE 4-8

TABLE 4-3

ELECTRONIC SPECTRA OF VANADIUM RHODOTORULATE

AND VANADIUM DIHYDROXAMATE COMPLEXES

COMPLEX	SOLVENT	ABSORPTION MAXIMA (nm)(ϵ x 10^{-3})
VORA(OH)	H_2O	289(3.7), 464(2.2), 556(2.3)
VORA(OCH_3)	CH_3OH	432(2.3)
VL(OCH_3) [a]	CH_3OH	272(3.6), 446(3.2)
VL(OCH_3) [a]	CH_3CN	294(?), 440(?), 544(?)
$[V_2RA_3]^{2+}$	H_2O	390sh( ), 516( )
$[V_2RA_3]^{2+}$ [b]	CH_3OH	390($\geq$3.3), 516($\geq$2.4)
$[V_2L_3]^{2+}$ [b]	CH_3OH	385($\geq$3), 516($\geq$3)
$[V_2L_3]^{2+}$ [b]	CH_3CN	381(?), 505(?)

a L = N,N'-dihydroxy-N,N'-didsopropyl(pentane)diamide (See Figure 4-1).

b Proposed stoichiometry, see text.

The Black "VORA(OH)" Compound

EPR results of solutions of $VOSO_4$ + H_2RA (1:1) which had been exposed to air and of the black compound isolated by Tom Tufano[18] indicated that all of the vanadium in each of these solutions was present as vanadium(V). This result was taken as further evidence that the black compound had been decomposed during synthesis and isolation of the complex, probably by heating.[18] The previously reported observation of an EPR signal equivalent to ~5% of the total vanadium was probably a result of the use of acetate ion to buffer the soltuon at pH 4.0.

Proposed studies:

A number of studies could be done to confirm the proposed dimeric structure of the (dihydroxamato)vanadium(IV) complex. Ideally one would like to isolate a single crystal suitable for X-ray diffraction. The use of a variety of counterions for either the RA or the synthetic dihydroxamate complex may be helpful in this endeavor. Since complexes of the synthetic dihydroxamates are soluble in a wider variety of solvents than are the complexes of H_2RA, greater success may be obtained with them. Short of growing single crystals, a sample of high purity is necessary for further study. With such a sample, a "clean" elemental analyses would confirm the stoichiometry, and the molecular weight might be deterined by

mass spectrometry or by gel partition chromatography. Additionally precise measurements of the extinction coefficients of the electronic spectra could be otained. A spectroelectrochemical study of the conversion of the (dihydroxamato)vanadium(IV) complex to the oxovanadium(V) comlex would give useful insight into the mechanism of this reaction. In addition to studies of the complexes reported in this study, it would be interesting to explore analogous chemistry with monohydroxamates.

SUMMARY

Electrochemical studies of vanadium and rhodotorulic acid have been done. It has been shown that in (1:1) solutions of oxovandium(IV) and rhodotrulic acid the oxovanadium(IV) rhodotorulic acid complex is oxidized to the oxo-hydoxo-vanadium(V) complex. While the VORA(OH) complex is formed preferentially in air, the oxovanadium(IV) rhodotorulate complex has been isolated using inert atmosphere techniques. Evidence for the existence of a second vanadium(IV) rhodotorulate complex has been presented. This complex has been shown to be formed in the presence of excess ligand in the absence of air and to be a result of the displacement of the vanadyl oxygen by hydroxamate. This assignment is supported by the absence of a V=O stretch in the infrared spectrum of both the rhodotorulate and the dihydroxamate complexes, and by comparison of the electronic spectra of these complexes with those of anal-

ogous (tris-catecholato)vanadium(IV) complexes. These complexes have been proposed to be the dimers , $[V_2RA_3]^{+2}$ or $[V_2L_3]^{2+}$, analogous to the Fe_2RA_3 and Fe_2L_3 dimers.[17,19] Since the crude product which has been isolated is impure, this formulation has not been confirmed. Suggestions for more definitive identification of this complex and for understanding its solution chemistry have been made.

REFERENCES

(1) Sidgwick, N.V. "The Chemistry of Nitrogen", Clarendon Press: OXford, *1937*, p. 197.

(2) Neilands, J.B. *Struct. Bonding*, 1966, *1*, 59-108.

(3) Mizukami, M.; Nagata, K. *Coord. Chem.*, 1968, 3, 267-267-278 and references therein.

(4) Chatterjee, B. *Coord. Chem. Rev.*, 1978, *26*, 281-303 and references therein.

(5) Selbin, J. *Coord. Chem. Rev.*, 1966, *1*,239-314.

(6) Agrawal, Y.K. *Russ. Chem. Rev.*, 1979, *48*, 948-963 and references therein.

(7) Agrawal, Y.K. *Bull. Soc. Chim. Belg.*, 1980, *89*, 261-265.

(8) Nanewar, R.R.; Tandon, U. *Talanta*, 1978, *25*, 352-354.

(9) Tandon, S.G.; Bhattacharya, S.C. *J. Ind. Chem. Soc.*, 1970, *47*, 583-589.

(10) Brockway, D.J.; Murray, K.S.; Newman, P.J. *J. Chem. Soc. Dalton*, 1980,1112-1117.

(11) Ozaki, S.; Masui, M. *Chem. Pharm. Bull.*, 1977, *25*, 1179-1185.

(12) Dutta, R.L.; Lahiry, S. *J. Ind. Chem. Soc.*, 1962, *39*, 860-870.

(13) Dutta, R.L.; Lahiry, S. *J. Ind. Chem. Soc.*, 1963, *40*, 53-66.

(14) Dutta, R.L.; Ghosh, S.J. *J. Ind. Chem. Soc.*, 44, *1967*, 369-376.

(15) Atkin, C.L.; Neilands, J.B. *Biochem.*, 1968, 7, 3734-3739.

(16) Carrano, C.J.; Raymond, K.N. *J. Am. Chem. Soc.*, 1978, *100*, 5371-5374.

(17) Carrano, C.J.; Cooper, S.R.; Raymond, K.N. *J. Am. Chem. Soc.*, 1979, *101*, 599-604.

(18) Tufano, T.P. Ph.D. Dissertation, University of California, Berkeley.

(19) Barclay, S.J. Ph.D. Dissertation, University of California, Berkeley, 1982.

(20) Shriver, D.F. "The Manipulation of Air-Sensitive Compounds". New York, N.Y., McGraw-Hill, 1969.

(21) House, H.O.; Feng, E.; Peet, N.P. *J. Org. Chem.*, 1971, 36, 2371-2735.

(22) Bates, R.G. "Determination of pH: Theory and Practice". New York, N.Y., Wiley, 1973, Chapter 9.

(23) Diggle, J.W.; Parker, A.J. *Electrochim. Acta*, 1973, *18*, 975-979.

(24) a) Hubbard, A.T.; Anson, F.C. *Electroanal. Chem.*, 1971, 4, 129.

b) Hubbard, A.T. *CRC Critical Rev. Anal. Chem.*, 1973, 3, 201-241.

(25) DeAngelis, T.P.; Heineman, W.R. *J. Chem. Educ.*, 1976, 53, 594-595.

(26) Nicholson, R.S.; Shain,I.; *Anal. Chem.*, 1964, 36, 706-723.

(27) Dalrymple-Alford, P.; Goto, M.; Oldham, K. B. *J. Electroanal. Chem.*, 1977, 85, 1-15.

(28) Toman, J.T. Ph.D. Thesis, University of California, Berkely, Ca, 1982.

(29) Latimer, W.H. "The Oxidation States of the Elements and Their Potentials in Aqueous Solutions," 2nd ed., Prentice-Hall, Englewood Cliffs, N.J., 1938.

(30) Cooper, S.R.; Koh, Y.B.; Raymond, K.N.; *J. Am. Chem. Soc.*, 1982, *104*, 5092-5102.

APPENDIX 1

Synthesis and Characterization of a Malondiamide and Its Copper(II), Nickel(II), and Co(III) Complexes

INTRODUCTION

An ongoing interest in the chemistry and electrochemistry of metal complexes which can serve as biological models has led to the syntheses of the ligand N,N'-di(2-aminomethylpyridyl)-malondiamide, *1*, and its copper(II), *2*, nickel(II), *3*, and cobalt(III), *4*, complexes (Figure A1-1). The ligand is a tetradentate macrochelate, which contains two amides and two pyridines. The amides serve as models for the peptide linkage in proteins, and the pyridines model the imidazole group of a histidine.

It is well documented that deprotonated amide groups coordinate transition metals through an amide-N bond[1-4]. Numerous structural studies of such complexes using amino acids and synthetic peptides as ligands have been reported and reviewed.[25,27] More recently a series of structural studies on bis-amide metal complexes as well as a review of this chemistry has been reported.[5-13]

In this appendix the syntheses and characterization of the ligand and its metal complexes are described. The crystal structure of the copper complex is reported, as well as preliminary results of voltammetric studies of the nickel and copper complexes.

FIGURE A1-1

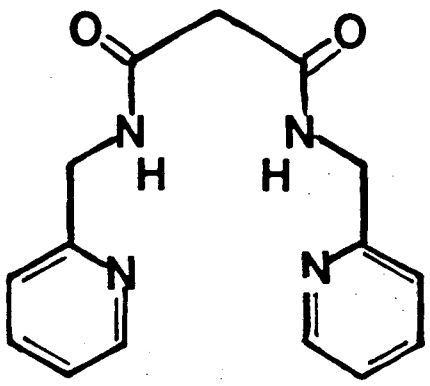

N,N'-di(2-aminomethylpyridyl)-
malondiamide
H_2L

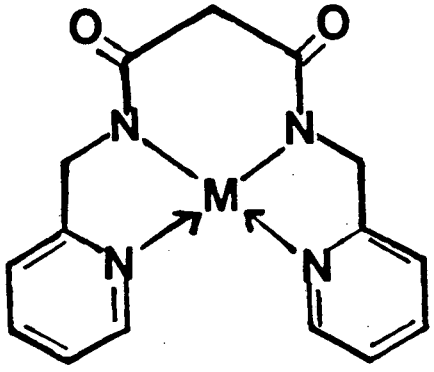

METAL COMPLEX
ML or $[ML]^{+}$
M = Cu^{+}, Ni^{+}, Co^{3+}

EXPERIMENTAL

1. Reagents

Reagent grade triethylamine was distilled under partial vacuum shortly before use. Reagents and solvents used for synthetic procedures were commercially available reagent grade and were used as received. Solvents used for electrochemical studies were treated as described in Chapter 1.

2. Measurements

Elemental analyses were performed by the microanalytical laboratory operated by the Chemistry Department of the University of California, Berkeley. ^{1}H NMR were recorded at 60 MHz on a Varian T-60 Spectrometer. Infrared spectra were recorded on a Perkin Elmer Model 597 spectrometer. Instrumentation and cells used for electrochemical experiments are described in Chapter 1.

3. Syntheses

Chloropentamminecobalt(III)dichloride, $[Co(NH_3)_5Cl]Cl_2$, was prepared by literature methods.[14]

Preparation of N,N'-di(2-aminoethylpyridyl)malondiamide, ($C_{15}H_{14}N_4O_2$). In a typical preparation diethylmalonate (14 ml, 92 mmoles) and 2-aminomethylpyridine (25 ml, 240 mmoles) were added to ca. 60 ml of ethanol in a 250 ml round-bottomed Schlenk flask. The solution was stirred under an atmosphere of N_2 for 5-7 days, after which the

solvent and any unreacted 2-aminoethylpyridine was removed by distillation under reduced pressure. The oily product was dissolved in ethyl acetate and left in the freezer for 1-2 days, during which time a white precipitate appeared. The white powder was separated by suction filtration, washed with diethyl ether and dried in vacuo (16 g, 56% based on diethyl malonate) : mp 76-77°C. ^{1}H NMR (chloroform-d^3) δ3.4 (singlet, 2H), δ4.5 (doublet, 4H), δ8.1 (broad singlet, 2 amide H), δ8.4, 7.5, 7.2 (complex multiplets, 8 pyridine H). The infrared spectrum was characterized by a strong, broad absorbance at ~1670 cm^{-1}. this band, which was attributed to the amide carbonyl stretch, was not present in the spectra of the metal complexes.
Anal.Calc'd for $C_{15}H_{14}N_4O_2$: C, 63.36; H, 5.67; N, 19.71. Found : C, 62.96; H, 5.74; N, 19.37.
Preparation of [N,N'-di(2-methylpyridyl)malondiamido]Copper(II)-Trihydrate, $[(C_{15}H_{14}N_4O_2)Cu(II)]\cdot 3H_2O$. A solution of $CuSO_4.5H_2O$ (0.25 g, 1.0 mmole) and triethylamine (0.28 ml, 2.0 mmole) in 10 ml of methanol was made. To this was added, with stirring, a solution of ligand (0.284 g, 1.0 mmole) in about 5 ml of ethanol. The reaction mixture immediately turned deep purple. The solution was reduced using a rotoevaporator, allowed to stand overnight, and finally filtered to yield shiny, deep purple needles 0.20 g, (58%). Crystals for X-Ray diffraction were grown from $CHCl_3$:CH_3OH (1:1)solution by vapor diffusion from $CHCl_3$. The infrared spectrum was very similar to that of

the free ligand with the absence of the strong absorbance at ~1670 cm^{-1} and the presence of a broad absorbance due to water at ~3400 cm^{-1}. Anal. Calc'd for $CuC_{15}H_{20}N_4O_5$: C, 45.05; H, 5.04; N, 14.01; Cu, 15.89. Found: C, 45.11; H, 4.99; N,14.08; Cu, 16.0.

Preparation of [N,N'-(2-methylpyridyl)malondiamido]Nickel-(II)Dihydrate, $[(C_{15}H_{14}N_4O_2Ni(II))]\cdot 3H_2O$. The preparation of the nickel complex was analogous to that of the copper complex and gave orange-red needles. ^1H NMR (chloroform-d^3) δ2.8 (2H), δ3.2 (4H), δ7.2, 8.0 (Complex multiplet, 8H). The absence of the broad singlet at δ8.1 confirmed that the complexing ligand was the deprotonated amide, and that the nickel was low spin. The infrared spectrum was virtually identical to that of the Cu(II) complex.

Anal. Calc'd for $NiC_{15}H_{18}N_4O_4$: C, 47.78; H, 4.81; N, 14.86.

Found: C, 47.76; H, 4.79; N, 14.94.

Preparation of (N,N'-(2-methylpyridyl)malondiamido)(diammine)Cobalt(III)chloride Trihydrate, $[(C_{15}H_{14}N_4O_2)(NH_3)_2Co(III)]]Cl]\cdot H_2O$. To a hot, aqueous solution (25 ml) of $[Co(NH_3)_5Cl]Cl_2$ (2.5 g, 0.01 moles) and ligand (2.84 g, 0.01 moles) a solution of NaOH (12 ml, 1.0 M) was added slowly, with stirring. A lavender precipitate was observed immediately. The solution was stirred until the precipitation appeared to be complete. The reaction mixture was then filtered, and the burgundy filtrate was reduced in volume to about 20 ml using a rotoevaporator.

After ~12 hours at 0°C copious burgundy crystals formed. The solution was filtered, and the crystals were washed with ethanol and then with diethylelther and dried in vacuo. The infrared spectrum was virtually superimposable on that of the nickel and copper complexes, except for then presence of a broad absorption at ~3250 cm^{-1}, attributed to NH_3. Elemental analysis of the lavender precipitate showed that there was no nitrogen or chlorine present. The infrared spectrum was featureless except for a broad absorbance due to water, and a second broad absorbance at ~cm^{-1}. It is probable that this side product is $Co(OH)_3$.

Anal. calc'd for $CoC_{15}H_{28}N_4O_4Cl$: C, 37.31; H, 5.85; N. 17.41, Co, 12.21.

Found: c, 37.38; H, 5.90; N, 17.44; Cl, 7.50; Co, 11.8.

4. Collection of X-Ray Diffraction Data

The conditions for data collection and the observed crystal parameters are listed in Table I.

TABLE A1-1

Crystal and Data Collection Parameters

Compound: $[Cu(C_{15}H_{14}N_4O_2]\cdot 3H_2O$

A) Crystal Parameters @ 25°C[a,b]

a =	9.932(4) Å	Space Group:	$P2_1/c$ (No. 14)
b =	22.049(9) Å	Formula weight:	399.89
c =	8.076(4) Å	Z =	4
β =	104.54(3)°	d(calc) =	1.552 g/cm³
V =	1711.8 Å³	d(obs) =	1.60 g/cm³

Size: 0.28 x 0.13 x 0.15 mm

B) Data Measurement Parameters

Diffractometer: Enraf-Nonius CAD-4 [18]

Radiation: Mo Kα (λ = 0.71073 Å)

Monochromator: Highly-oriented graphite ($2\theta_m$ = 24°) perpendicular mode, assumed, 50% perfect.

Detector: Crystal Scintillation counter with PHA.

Reflections measured: +H, +K, ±L

2θ Range: 3 to 45°

Scan type: θ - 2θ

Scan speed: Variable, 75s max (θ, deg/m)

Background: Measured over an additional 0.25(Δθ) added to the each end of the scan.

No. of reflections collected: 2462

No. of unique reflections: 1744

Intensity standards: Measured every 2 h. of X-ray exposure time. No decay was observed.

Orientation: 5 reflections were checked every 100 measurements. Crystal orientation as redetermined if any of the reflections was offset by more than 0.25°. Reorientation was not necesaary during data collection.

---

a) Unit cell parameters and their esd's were derived by a least-squares fit to the setting angles of the unresolved Mo Kα components of 24 reflections with 2θ between 27.8° and 30.5°.

b) In this and all subsequent tables the esd's of all parameters are given in parentheses, right-justified to the least significant digits(s) given.

6. Solution and Structure Refinement

The 1744 intensity data were converted to structure factor magnitudes and their esd's by correcting for background, scan speed and Lorentz and polarization factors.[16-18] The copper atom was located from a three-dimensional Patterson map. The non-hydrogen atoms were located and refined anisotropically using standard Fourier and least-squares techniques. All of the hydrogens except for three of the water hydrogens were then located from a at idealized positions with a C-H bond distance of 0.95 Å. Their isotropic thermal parameters were set at $B = 5.0 Å^2$. Anisotropic refinement of the nonhydrogen atoms led to final convergence with R = 0.032, R_w = 0.040 and GOF = 1.62 (266 variables, 1744 observations). Corrections were made for secondary extinctions which resulted in negligible changes in R. A final difference Fourier map showed highest peak to be 0.439 $e/Å^3$ in the region of the water oxygens. The analytical forms from the scattering factor tables were used,[18a] and all nonhydrogen scattering factors were corrected for both real and imaginary compnents of anomalous dispersion.[18b]

The final positional parameters of the nonhydrogen atoms are given in Table A1-2. The thermal parameters of the nonhydrogen atoms, the positions of the hydrogen atoms, and a listing of the values of F_o and F_c are available as supplementary material.

RESULTS AND DISCUSSION

The x-ray diffraction data on the copper complex, *2*, reveal that the coordination environment about the copper(II) ion approximates a square pyramid with the four nitrogens from one ligand forming the base of the pyramid and an oxygen atom from the amide of an adjacent molecule occupying the axial position (Figure A1-2). The Cu-O bond length (Table A1-3) is about 0.1 Å shorter than the van der Waal's radii (2.90 Å)[21] and is within the range observed for intermolecular Cu-O (amide) distances reported for other Cu-amide complexes.[1-13,25] The four nitrogens form a severely compressed tetrahedron about the copper ion with one amide N and one pyridyl N "up" and the other pair "down" with respect to the copper. The pyridyl N's (N1 and N3) are 0.173 Å away from the least-squares plane of nitrogens, while the amide N's (N2 and N4) are 0.194 Å from it. Furthermore,the copper ion itself lies 0.10 Å above the least-squares plane of nitrogens but lies below N1 and N2. The above deviations and distances represent unusual behavior for 5-coordinate copper complexes. Normally deviations from planarity of the four square-planar base atoms are less than 0.03 Å. In addition, the copper in such complexes usually lies about 0.20 Å above the least-squares plane and above all of the ligating atoms. As expected, the Cu-N(amide) bond lengths are shorter than those of the Cu-N(pyridyl) bonds and are in the same range as those reported for metal-

peptide complexes[25] and for other synthetic copper-diamide complexes.[6-12,27]

Several features of the complexed ligand resemble those observed in metal-peptide complexes, while others represent deviations from "normal". The N(amide)-Cu-N(pyridyl) bond angles are in the range reported for typical 5-membered chelate rings to copper,[25] and the well-documented tendency of the peptide region toward strict planarity, even in metal complexes, is observed in 2. In the planar amide region, however, there is a deviation from typical metal-peptide bond angles. The "normal" bond angles corresponding to N2-C7-C8 and N4-C9-C8 would be expected to be about 110-114° in a copper-peptide or copper-amide complex while the angles corresponding to O2-C7-C8 and O1-C9-C8 would be in the range of 120-121°.[7-12,25,27] In the complex, 2, the magnitudes of these two sets of angles are just reversed (Table III). In addition, the bond angle C7-C8-C9 is unusually large (124°) for a methylene group. A similar set of "anomalous" bond angles is observed in the structure of [N,N'-di-(2-aminoethyl)malondiamido)nickel(II)-trihydrate.[5]

The complexes pack as dimeric units which are held together by two intermolecular Cu-O(2) interactions (Figure A1-3). Each half of the dimer is related to the other by an inversion center at the origin. The dimers, in turn, are closely packed such that each is related to another by a translation along c. The shortest distances

between dimeric units involve contacts between pyridine ring carbons of one molecule and peptide and methylene carbons of another molecule. The shortest such distance observed is 3.34 Å between C3 and C9 and is in the range predicted for stacking of aromatic carbons.[21] Even the methylene carbons, C6-C10 exhibit short intermolecular distances, (3.4 to 3.5 Å) to methylene carbons on adjacent dimers, suggesting strong van der Waal's interactions. Finally, there is a hydrogen bonding network formed by the interaction of the three waters of hydration with the amide oxygens (O1) of two neighboring molecules and with each other (Figure A1-4). Curiously, none of the waters is axially bound to the Cu atom.

It is probable that the tight packing imposed by the combined effects of stacking, the hydrogen bonding,and the Cu-O2 interaction creates such a tightly packed crystal that strain is exerted on the the individual molecules. This strain results in the observed deviations from "normal" bond angle patterns in the peptide region and the unusually large methylene bond angle about C8. The methylene is apparently so tightly sandwiched between carbons of adjacent molecules that it is constrained to very small thermal motion. Indeed, unusually small thermal motion is observed for C8 (Figure 1). Similarly such tight packing can account for the unusual positions of the Cu and nitrogens relative to one another in the coordination plane. Lastly, the packing also appears to account

for the failure of one of the water oxygens to bind Cu axially. The aromatic stacking results in a hydrophobic region above and below the copper, thus excluding any water molecules. Hence, the amide(O2) atoms bind the copper axially instead.

Since the nickel complex is diamagnetic, as demonstrated by its ^{1}H NMR signal, color, and electronic spectrum, its structure is postulated to be approximately square planar with the waters forming a hydrogen bond network to the amide oxygen atoms in the crystal lattice, analogous to a similar structure reported by Lewis et al.[5]

The structure of the cobalt complex is clearly six-coordinate. Since the compound is soluble in water and methanol, it is probably ionic. Hence, the two ammines are probably coordinating in a *trans* position, and the chloride is present as a counter ion.

Preliminary voltammetric experiments on the nickel and copper complexes have been done. In aqueous solution (pH 7.0) using a modified Pt-I electrode in a thin-layer electrochemical cell (See Chapter 1), an irreversible oxidation was observed for the copper complex at ~0.81 V *vs* a Ag/AgCl, KCl(1.0 M) reference. Since the ligand itself is not electroactive in this potential region, it is probable that the complex is being irreversibly oxidized to a Cu(III) species.

The nickel complex exhibited no oxidations between

0.0 and 1.0 V in either water or DMF. However, in DMF it exhibited a reversible one-electron reduction at -2.06 V *vs* the $Ag/AgNO_3$ reference electrode. Again since the ligand is not electroactive in this potential region, the nickel is probably being reduced to nickel(I).

Since Ni(I) and Cu(III) complexes are relatively rare, these complexes warrant further investigation. Spectroelectrochemical techniques may be especially helpful in characterizing these processes.

SUMMARY

The ligand N,N'-di(2-aminomethylpyridyl)malondiamide and its copper(II) and nickel(II) complexes have been synthesized and characterized. The copper(II) complex has been characterized by X-ray crystallography. It crystallizes as the trihydrate in the space group $P2_1/c$, with lattice constants $a = 9.932(4)\mathring{A}$, $b = 22.049(9)\mathring{A}$, $c = 22.049(9)\mathring{A}$ and $\beta = 104.54(3)^\circ$ The complex is square pyramidal with a carbonyl oxygen of an adjacent molecule weakly bonding in the axial position. Several unusual features of the complex are described and discussed in terms of the packing in the lattice. The nickel complex, which is diamagnetic has been characterized by ^1H NMR and is proposed to be square planar. The cobalt complex is six-coordinate with two trans ammines ccupying the fifth and sixth coordination sites. Preliminary electrochemical

results suggest that the copper(II) complex may be oxidized to a copper(III) complex, and the nickel(II) complex may be reduced to a nickel(I) complex.

Table A1-2

Positional Parameters and Standard Deviations for

$[Cu(C_{15}H_{14}N_4O_2)]\cdot 3H_2O$.

Atom	x	y	z
CU	-0.01564(5)	0.07305(2)	0.24479(7
O1	-0.4228(3)	0.0942(1)	-0.0226(4)
O2	-0.1531(3)	-0.0810(1)	-0.0163(4)
O3	-0.6027(3)	0.1386(2)	0.1611(4)
O4	-0.4563(4)	0.2062(2)	0.4298(5)
O5	-0.4937(7)	0.1880(2)	-0.2542(5)
N1	0.0231(3)	0.1615(1)	0.2872(4)
N2	-0.0570(3)	-0.0097(1)	0.1786(4)
N3	0.1473(3)	0.0350(1)	0.4165(4)
N4	-0.1983(3)	0.1022(1)	0.1322(4)
C1	0.2439(4)	0.0612(2)	0.5446(5)
C2	0.3591(5)	0.0305(2)	0.6374(5)
C3	0.3754(5)	-0.0291(2)	0.6007(6)
C4	0.2762(4)	-0.0570(2)	0.4771(5)
C5	0.1623(4)	-0.0241(2)	0.3871(5)
C6	0.0514(4)	-0.0531(2)	0.2497(5)
C7	-0.1567(4)	-0.0298(2)	0.0496(5)
C8	-0.2847(4)	0.0076(2)	-0.0183(5)
C9	-0.3027(4)	0.0722(2)	0.0350(5)
C10	-0.2268(4)	0.1643(2)	0.1755(6)
C11	-0.0919(4)	0.1951(2)	0.2583(5)
C12	-0.0879(5)	0.2565(2)	0.2998(6)
C13	0.0396(5)	0.2831(2)	0.3685(7)
C14	0.1582(5)	0.2493(2)	0.3878(6)
C15	0.1467(5)	0.1889(2)	0.3462(6)

Table A1-3

Important Bond Distances and Angles.

ATOM 1	ATOM 2	DISTANCE
CU	N1	2.ØØ2(3)
CU	N2	1.917(2)
CU	N3	2.Ø3Ø(2)
CU	N4	1.924(3)
N1	C15	1.344(4)
N1	C11	1.331(4)
N2	C6	1.448(4)
N2	C7	1.32Ø(4)
N3	C1	1.352(4)
N3	C5	1.34Ø(4)
C1	C2	1.377(5)
C2	C3	1.366(5)
C4	C5	1.385(4)
C5	C6	1.497(4)
C7	C8	1.499(4)
C8	C9	1.512(4)
C1Ø	C11	1.5Ø1(5)
C11	C12	1.393(4)
C12	C13	1.379(5)
C13	C14	1.369(5)
O1	C1Ø	2.678(4)
O1	O3	2.772(3)
O2	C7	1.253(4)
O1	C9	1.263(4)
O4	O3	2.732(4)
O3	H4A	1.696(2)
O4	H4A	1.Ø39(3)
O3	H3A	1.Ø2Ø(2)

ATOM 1	ATOM 2	ATOM 3	ANGLE
N1	CU	N2	173.88(11)
N1	CU	N3	1Ø1.55(11)
N1	CU	N4	82.72(11)
N1	CU	O2	86.ØØ(9)
N2	CU	N3	82.84(1Ø)
N2	CU	N4	94.32(11)
N2	CU	O2	89.9Ø(9)
N3	CU	N4	163.Ø1(11)
N3	CU	O2	88.27(9)
N4	CU	O2	1Ø8.52(9)
N3	C1	C2	122.6(3)
C1	C2	C3	118.9(3)
C2	C3	C4	119.4(3)
C3	C4	C5	119.5(3)
C4	C5	N3	121.9(3)
C5	N3	C1	117.6(3)
CU	N3	C1	129.57(24)
CU	N3	C5	112.72(2Ø)
N1	C11	C12	121.8(3)
C11	C12	C13	118.5(3)
C12	C13	C14	119.4(3)
C13	C14	C15	119.Ø(3)
C14	C15	N1	122.4(3)
C15	N1	C11	118.7(3)
CU	N1	C11	113.1Ø(22)
CU	N1	C15	128.17(23)
N3	C5	C6	116.9(3)
C4	C5	C6	121.1(3)
C5	C6	N2	11Ø.3(3)
CU	N2	C6	115.66(19)
CU	N2	C7	127.23(22)
C6	N2	C7	115.2(3)
N2	C7	O2	122.8(3)
N2	C7	C8	12Ø.2(3)
O2	C7	C8	116.9(3)
C7	C8	C9	124.3(3)
N4	C9	O1	124.Ø(3)
N4	C9	C8	12Ø.9(3)
O1	C9	C8	115.1(3)
CU	N4	C9	128.69(23)
CU	N4	C1Ø	114.64(2Ø)
C9	N4	C1Ø	116.4(3)
N4	C1Ø	C11	1Ø9.1(3)
N1	C11	C1Ø	117.2(3)
C1Ø	C11	C12	121.1(3)

FIGURE A1-2

ORTEP[19] diagram of a monomeric unit showing the numbering of the atoms.

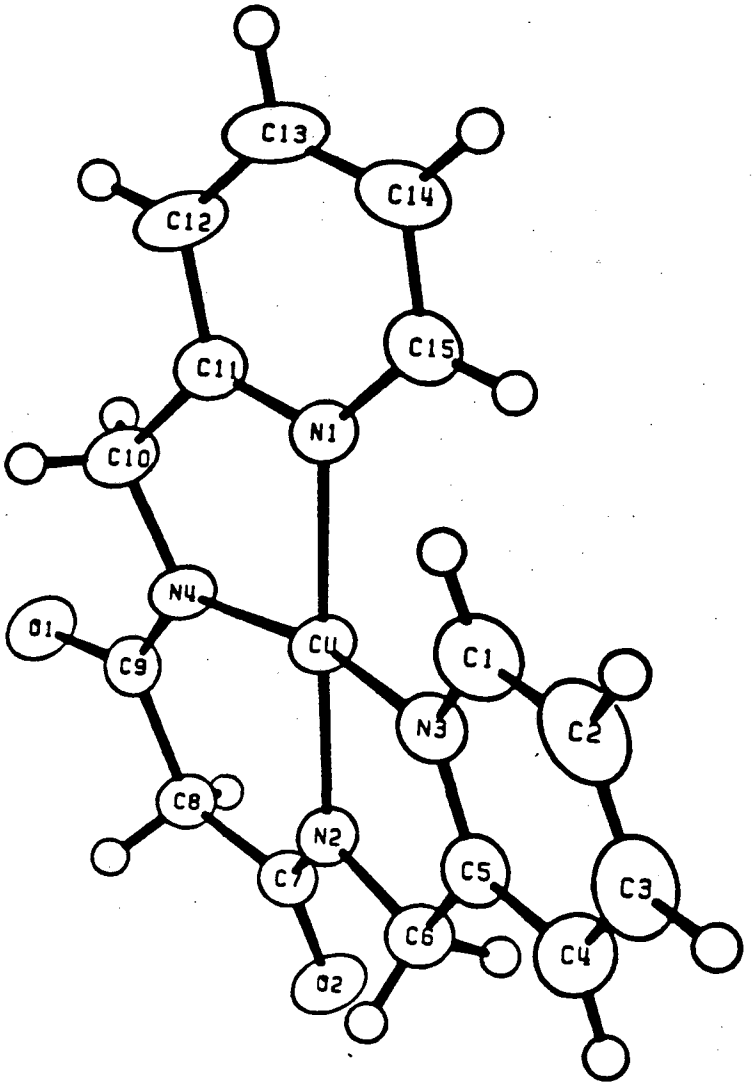

FIGURE A1-3

ORTEP[19] diagram of a dimeric unit showing the Cu-O(2) interactions.

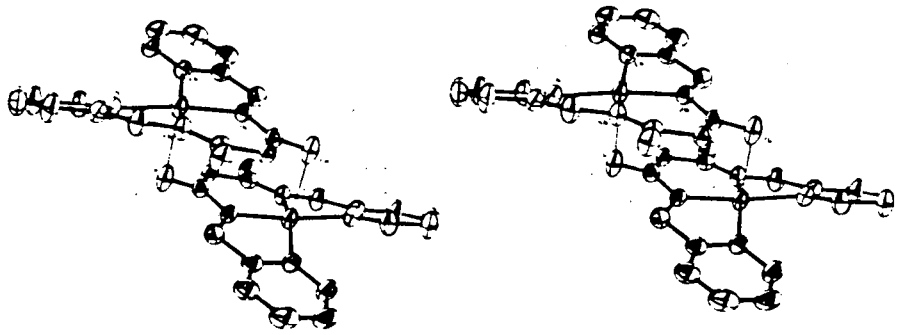

FIGURE A1-4

Stereo view of the packing diagram of the crystallographic unit showing stacking of the aromatic regions.

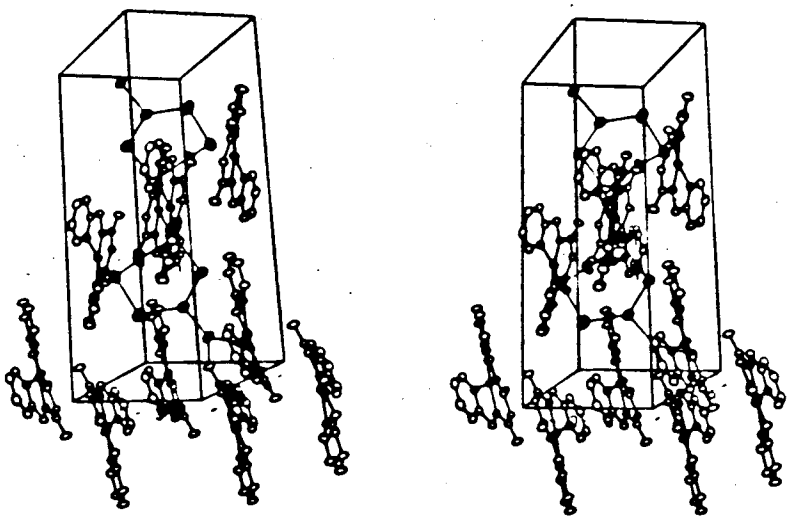

REFERENCES

(1) Nonoyama, M.: Yamasaki, K. *Inorg.Chim. Acta*, 1973, *7*, 373.

(2) Nonoyama, M. *Inorg.Chim. Acta*, 1974, *10*, 59.

(3) Nonoyama, M.G; Tomita, S.; Yamasaki, K. *Inorg. Chim Acta*, 1975, *12*, 33.

(4) Nonoyama, K.; Ojima, H.; Nonoyama, M. *Inorg. Chim. Acta*, 1975, *12*, 139.

(5) Lewis, R.M.; Nancollas, G.H.; Coppens, P. *Inorg. Chem*, 1972, *11*, 1371.

(6) Chapman, R.L.; Vagg, R.S. *Inorg. Chim. Acta* 1979, 33, 227.

(7) Chapman, R.L.; Stephens, F.S.; Vagg, R.S. *Inorg. Chim. Acta*, 1980, 43, 29.

(8) Chapman, R.L.; Stephens, F.S.; Vagg, R.S. *Acta Crystallogr. Sect. B.,* 1981, *B37*, 75.

(9) Stephens, F.S.; Vagg, R.S. *Inorg. Chim. Acta* 1981, *51*, 149.

(10) Mulqi, M.; Stephens, F.S.; Vagg, R.S. *Inorg. Chim. Acta*, 1981, *52*, 169.

(11) Chapman, R.L.; Stephens, F.S.; Vagg, R.S. *Inorg. Chim. Acta*, 1981, *52*, 169.

(12) Mulqi, M.; Stephens, F.S.; Vagg, R.S. *Inorg. Chim. Acta*, 1981, *52*, 177.

(13) Mulqi, M.; Stephens, F.S.; Vagg, R.S. *Inorg. Chim. Acta*, 1981, *52*, 73.

(14) Schlesinger, G.G. *Inorg. Syn.*, 1967, 9, 1960.

(15) The atomic form factors for neutral atoms were taken from 18a. All except those for hydrogen were corrected for the real and imaginary components of anomalous dispersion for Mo radiation.[18b] The quantity minimized by least squares was

$$\sum w(|F_o| - |F_c|)^2$$

where

$$w = \frac{4F_o^2}{\left[\sigma_o^2(F_o^2) + (pF_o^2)^2 \right]}$$

and $\sigma_o(F_o)$ is based solely on counting statistics. The parameter, p, introduced to prevent overweighting of strong reflections was set to 0.03. Agreement indices are defined as:

$$R = \frac{\sum ||F_o| - |F_o||}{\sum |F_o|}$$

and

$$R_w = \left[\frac{\sum w(|F_o| - |F_c|)^2}{\sum w|F_o|^2} \right]^{\frac{1}{2}}$$

The "goodness of fit" (GOF) is defined as

$$GOF = \left[\frac{\sum w(|F_o| - |F_c|)^2}{(N_o - N_v)}\right]^{1/2}$$

where N_o is the number of observations and N_v is the number of variables.

(16) The data reduction formulae are:

$$F_o^2 = \frac{\omega}{Lp}(C \quad 2B) \qquad \sigma_o(F_o^2) = \frac{\omega}{Lp}(C + 4B)^{1/2}$$

$$F = \sqrt{F_o^2} \qquad \sigma_o(F) = \frac{\sigma_o(F^2)}{2F_o}$$

where C is the total count in the scan, B, the sum of the two background counts, ω the scan speed used in deg/min. and

$$\frac{1}{Lp} = \frac{\sin 2\theta(1 + \cos^2 2\theta_m)}{1 + \cos^2 2\theta_m - \sin^2 2\theta}$$

is the correction for the Lorentz and polarization effects for a reflection with scattering angle 2θ and radiation monochromatized with a 50% perfect single-crystal monochromator with scattering angle $2\theta_m$.

(17) a) All calculations were performed on a PDP/11 equipped with 128 kilowords of memory, twin RK07 Mbyte disk drives, Versatec printer/plotter and TU10 tape drive using locally modified Nonius-SDP[3] software operating under RSX-11M.

b) Structure Determination Package User's Guide, April, 1980. Structure Corporation, College Station, Texas

(18) Cromer, D.T.; Waber, J.T. "International Tables for X-Ray Crystallography", Vol. IV, The Kynch Press: Birmingham, England, (1974). Table 2.2B. (b) Table 2.3.1.

(19) Instrumentation at the University of California Chemistry Department X-ray Crystallographic Facility diffractomer, and the other controlled by a DEC PDP 8/e with an RL01 disk. Both use Enraf-Nonius software as described in the CAD-4 Operation Manual, Enraf-Nonius, Delft, Nov. 1977 , updated Jan. 1980.

(20) Johnson, C.K. Report ORNL-3794, Oak Ridge National Laboratory, Oak Ridge, Tenn., 1965.

(21) Bondi, A.J. *J. Phys. Chem.*, 1964, *68*, 441.

(22) Jahn , H.A.; Teller, E.*Proc. R. Soc. A*, 1937, *161*, 220.

(23) Hathaway, B.J.; Billings, D.E. *Coord. Chem. Rev.*, 1970, 5, 143.

(24) Hathaway, B.J.; Hodgson, P.G. *Inorg. Nucl. Chem.*,

1973, 35, 4071.

(25) Freeman, H.C. *Adv. in Protein Chem.*, 1967, *25*, 257.

(26) Klein, C.L.; Majeste, R.J.; Trefana, L.M.; O'Connor, C.J. *Inorg. Chem.*, 1982, *21*, 1891.

(27) H.Sigel and R.B. Martin, *Chem. Rev.*, 1982, *82*, 385-426.

FIGURE A2-1A

DESIGN FOR PYRODISTILLATION STILL

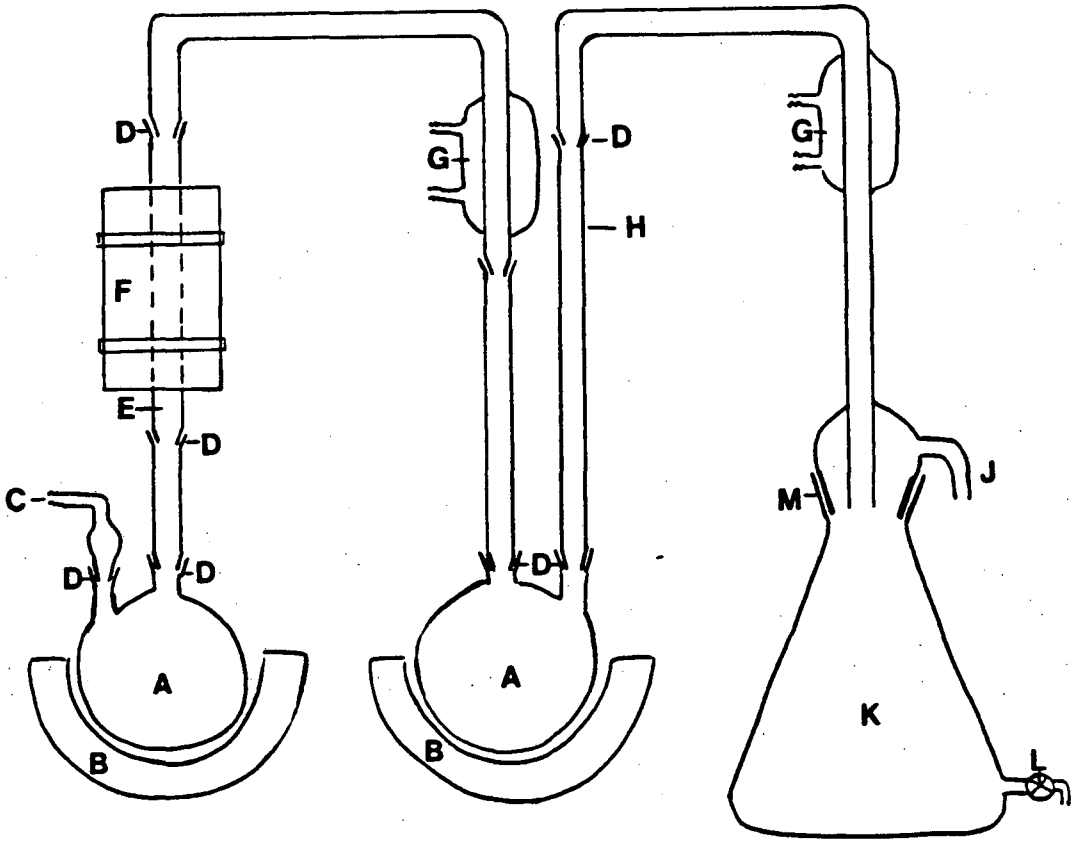

A Round-bottomed flask (3 l)

B Heating mantle

C Oxygen inlet

D 24/40 Ground glass joint

E Quartz tubing

F Tube furnace (See page 239)

G Condenser

H Pyrex tubing

J Outlet to atmosphere (stoppered lightly with glass wool

K 4l Erlenmeyer fitted with "faucet"

L "Faucet" (Corning teflon stopcock.

M 45/50 ground class joint

FIGURE A2-1B

DESIGN FOR TUBE FURNACE FOR STILL

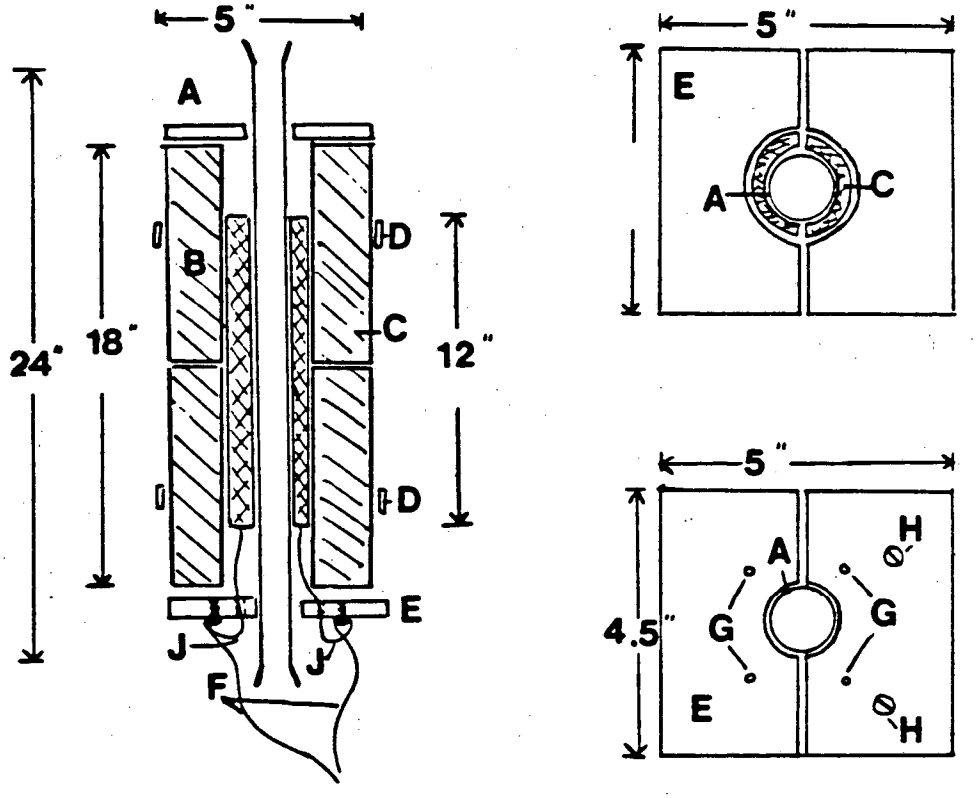

A Quartz tube (1 in. o.d.)

B Firebrick, hollowed out

C Semi-cyclindrical heating unit

D Steel hose clamps

E Transite (½ in. thick)

F Wires from asbestos-wrapped nickel wire. (Must be silver soldered).

G Holes for wire from heating unit

H Screws to connect heating unit to asbestos-wrapped nickel wire.

J High resistance wires from heating unit.

FIGURE A2-1C

CONSTRUCTION OF FURNACE AND CALIBRATION

Machinable firebrick is easily hollowed out and creates enough friction to support the heating units by itself. However, to create some extra support, wrap the heating units in two places - near the top and near the bottom - with several thicknesses of glass cloth electrical tape as in the figure below.

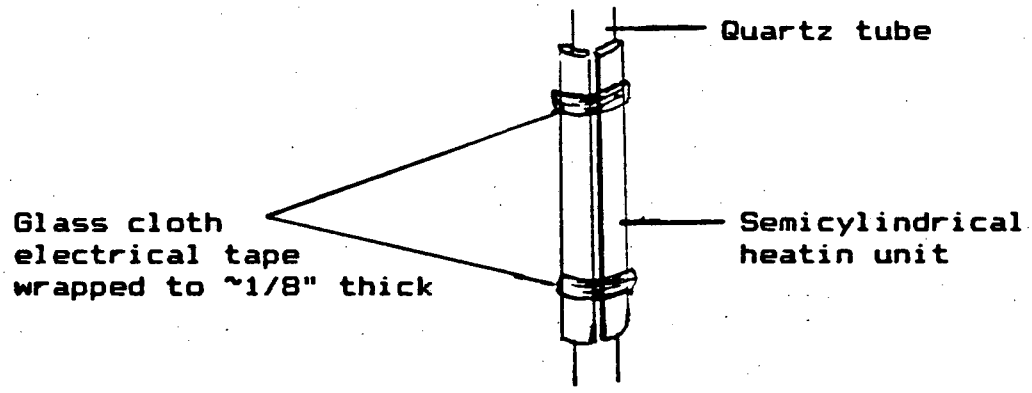

Hold the bricks together with a steel hose clamp, bent to a rectangular shape. After the furnace has been constructed with the quartz tube inside, but *before* it has been attached to the still, heat it gently for ~1 hour (IN A HOOD!). The cloth matrix of the electrical tape will burn off leaving a ridge of melted glass which will serve to hold it securely inside the firebrick. After the furnace has been thus "cured", attach it to the still. Calibrate it with a thermocouple. The goal is to ascertain the correct setting for the inside of the quartz tube to reach 900°C. At this temperature an orange glow can be seen through the cracks between the firebricks.

FIGURE A2-1D

ELECTRICAL CONNECTIONS FROM HEATING UNIT

Use ~1 foot of asbestos-wrapped nickel wire betwen the heating unit and the cord used to plug into the variac unit. *Silver* solder the nickel wire to the electrical cord.

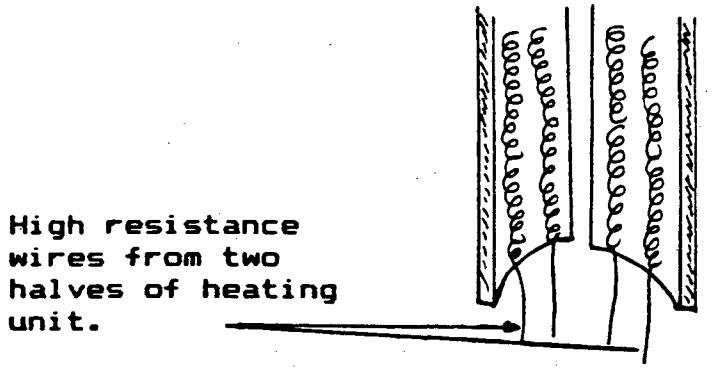

Wire the two halves of the heating unit in prallel to make one unit, 115 volts. Thread wires through holes in bottom of transite block and wrap around screw to make contact with nickel wire which has been similarly wrapped.

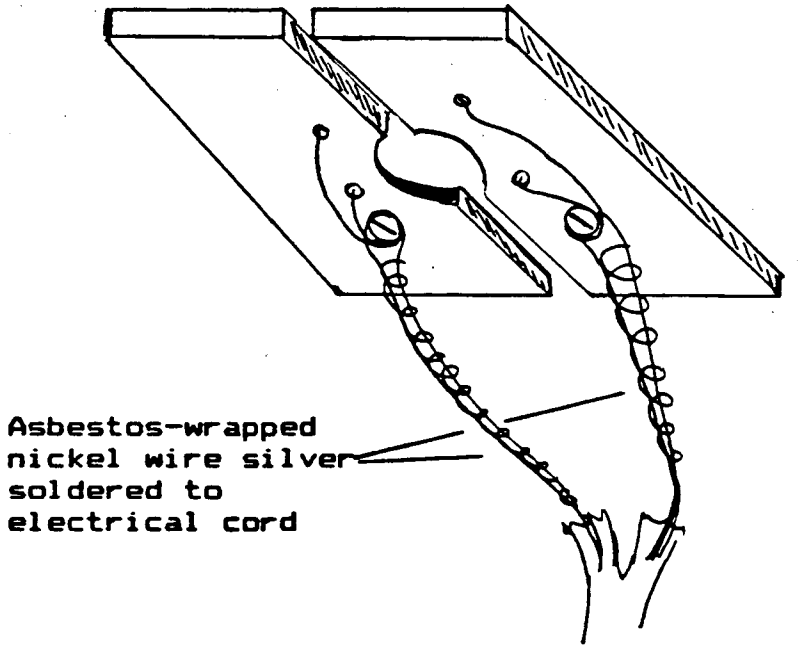

APPENDIX 2-1E

MATERIALS NEEDED FOR CONSTRUCTION OF STILL

1) Machinable firebrick:

   Manufacturer: Babcock and Wilcox

   Insulating Firebrick, K-20

   Supplier: Pyro Minerals

   2510 Wood St.

   Oakland, CA

   (415)839-3900

   Bricks come in boxes of 25 (~$32/box).

2) Semicylindrical heating unit.

   Manufacturer: Lindberg

   304 Hart St

   Watertown, WI. 53094

   (414)262-7000

   Model 50031 (Heats to 1000°C, 375 watts. Length, 12 in.; 115 volts.)

3) Glass cloth electrical tape.

   Scotch brand #27.

4) Kontes Teflon Sleeves

   24/40 for ground glass joints.

5) Teflon plumbing tape for wrapping 45/50 joint to storage flask.

FIGURE A2-2

DESIGN FOR OTTLE CELL HOLDER

MATERIAL: ALUMINUM

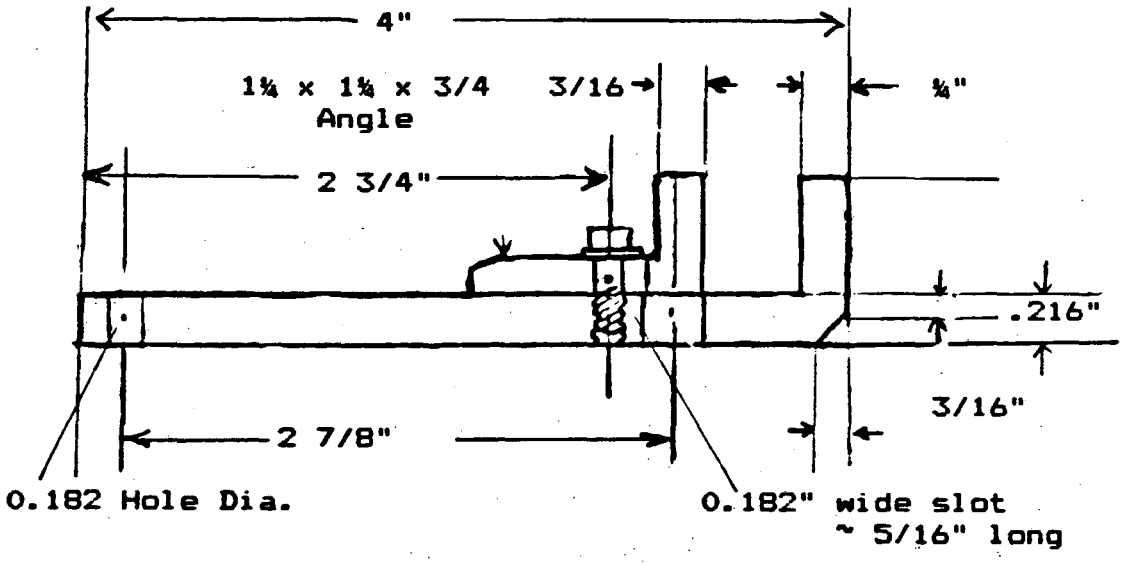

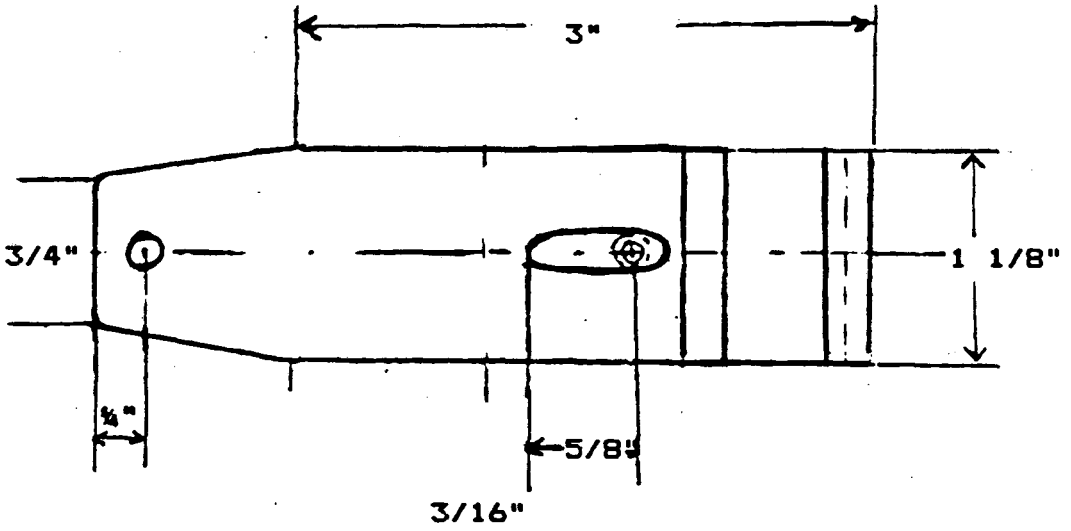

FIGURE A2-3

MOLD FOR GASKETS FOR OTTLE

MATERIAL: Teflon rod

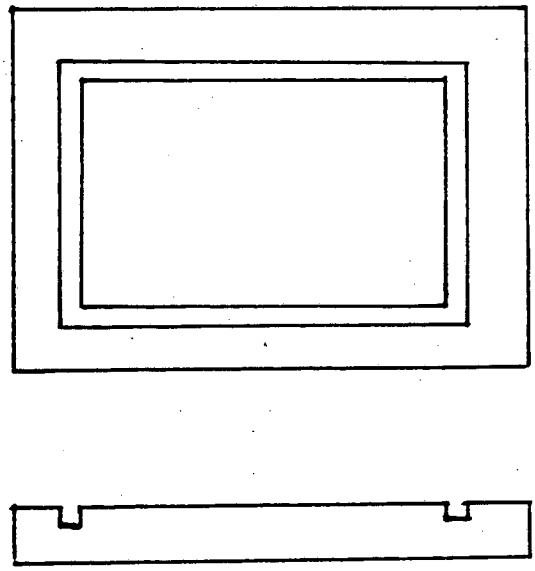

To make mold squeeze a small amount of GE RTV 112 into groove. Use a small pointed stick to remove incipient air bubbles. Leave undisturbed ~12 hours. Peel out of mold and trim using a steel straight edge and a sharp scalpel.

APPENDIX 2-4

METHODS USED ON HP 8450 IN CONJUNCTION WITH SPECTROELECTROCHEMICAL EXPERIMENTS

1. DATA COLLECTION

(METHODS 1 and 2)

```
STOP "KINETIC METHOD" 1<

STOP "FOR STORING" 1<

STOP "SPECTRA IN" 1<

STOP "TAPEFILES" 1<

STOP "USES STANDARD" 1<

STOP "FILES.1" 1<

STOP "INSERT SAMPLES"<

DEV40,0,0,0<

PLOT 0,0<

PLOT 3,0<

PLOT 1,1<

MEAS TO STD0 TAPE-FILE0 ABS L
200 TO 800 Y-SCALE -0.1 TO 1.5
 TIME<

STOP "START ELECTROCHEM"<

METH2,140 TIME 30<


MEAS TO STD* TAPE-FILE* ABS<

PLOT<

DISP DEV40<
```

2. PLOTIING SPECTRA

(METHODS 3 and 4)

```
STOP "METHOD FOR PLOTTING" 1<

STOP "SUCCESSIVE TAPEFILES" 1<

PLOT TAPE-FILE45 L 352 TO 652
 Y-SCALE 0.0 TO 0.14<

METH4,5<


PLOT TAPE-FILE*<
```

3. PRINTING ABSORBANCES

(METHODS 5 and 6)

```
STOP "METHOD FOR PRINTING" 1<

STOP "ABS AT SELECTED WAVELENGTH
S" 1<

PRINT TAPE-FILE1 L 292<

METH6,45<


PRINT TAPE-FILE*<
```

FIGURE A3-1

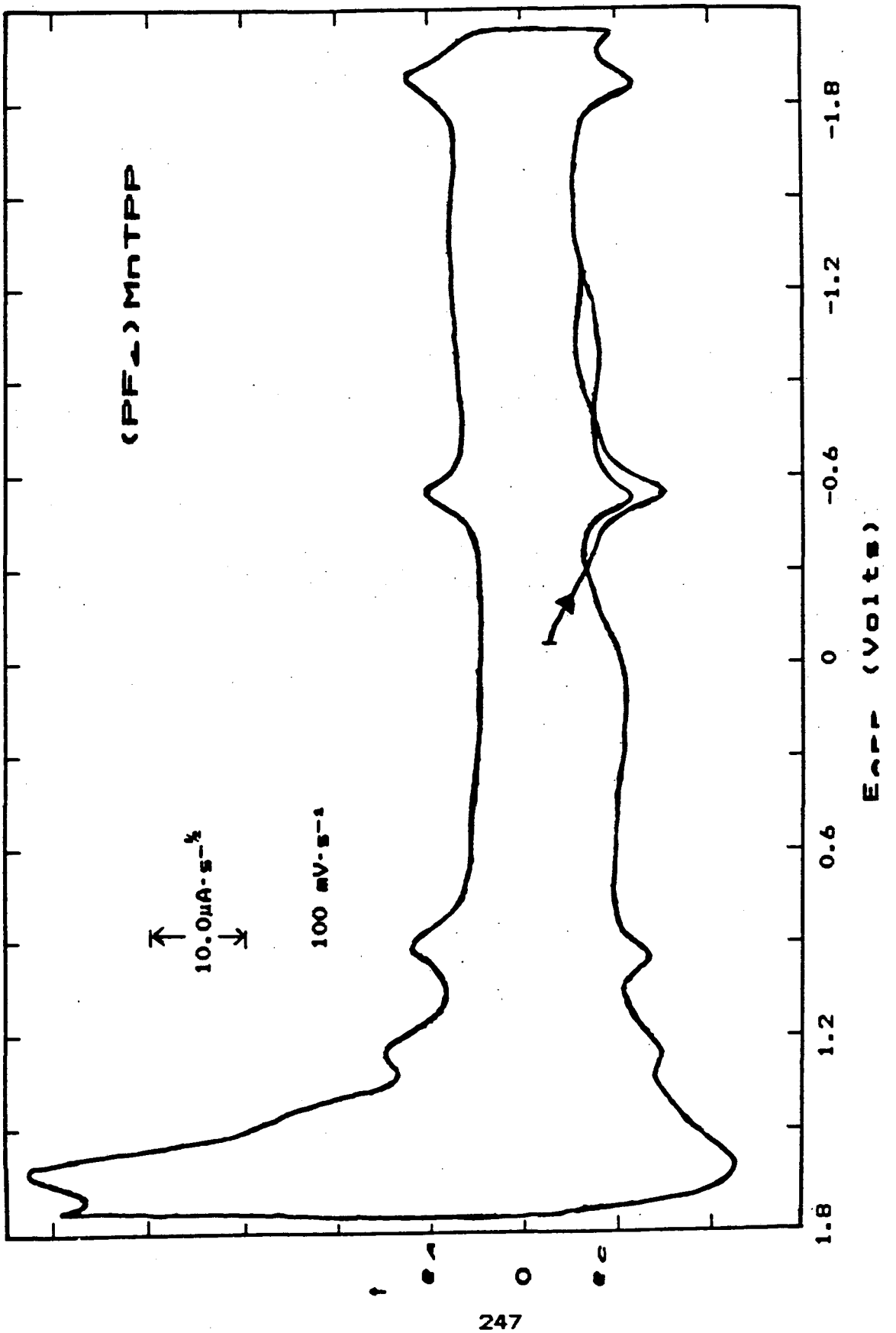

FIGURE A3-2

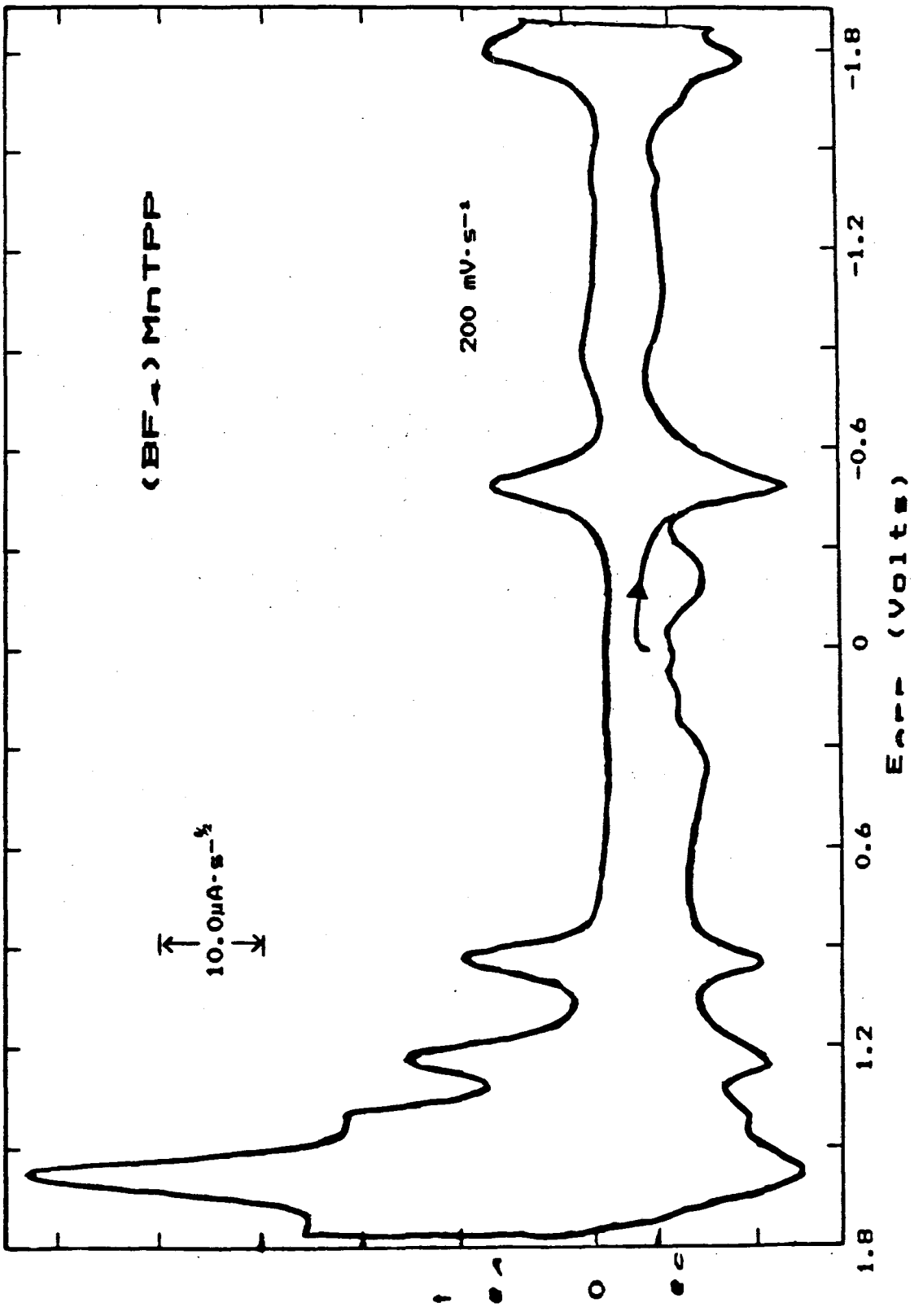

FIGURE A3-3

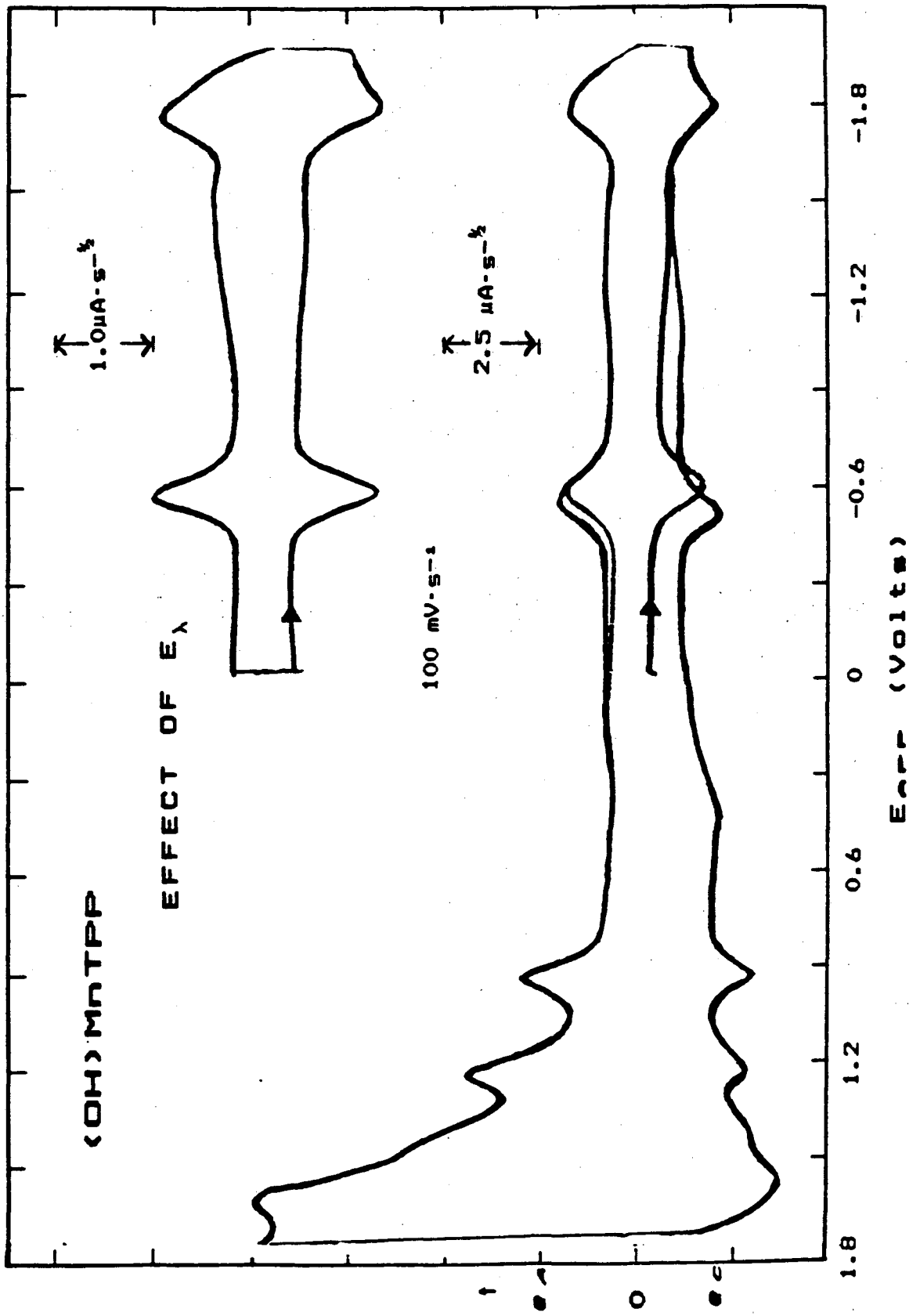
(OH)MnTPP
EFFECT OF E_λ
100 mV·s⁻¹
1.0μA·s^-½
2.5 μA·s^-½
1.8
1.2
0.6
0
-0.6
-1.2
-1.8
E$_{app}$ (Volts)

FIGURE A3-4

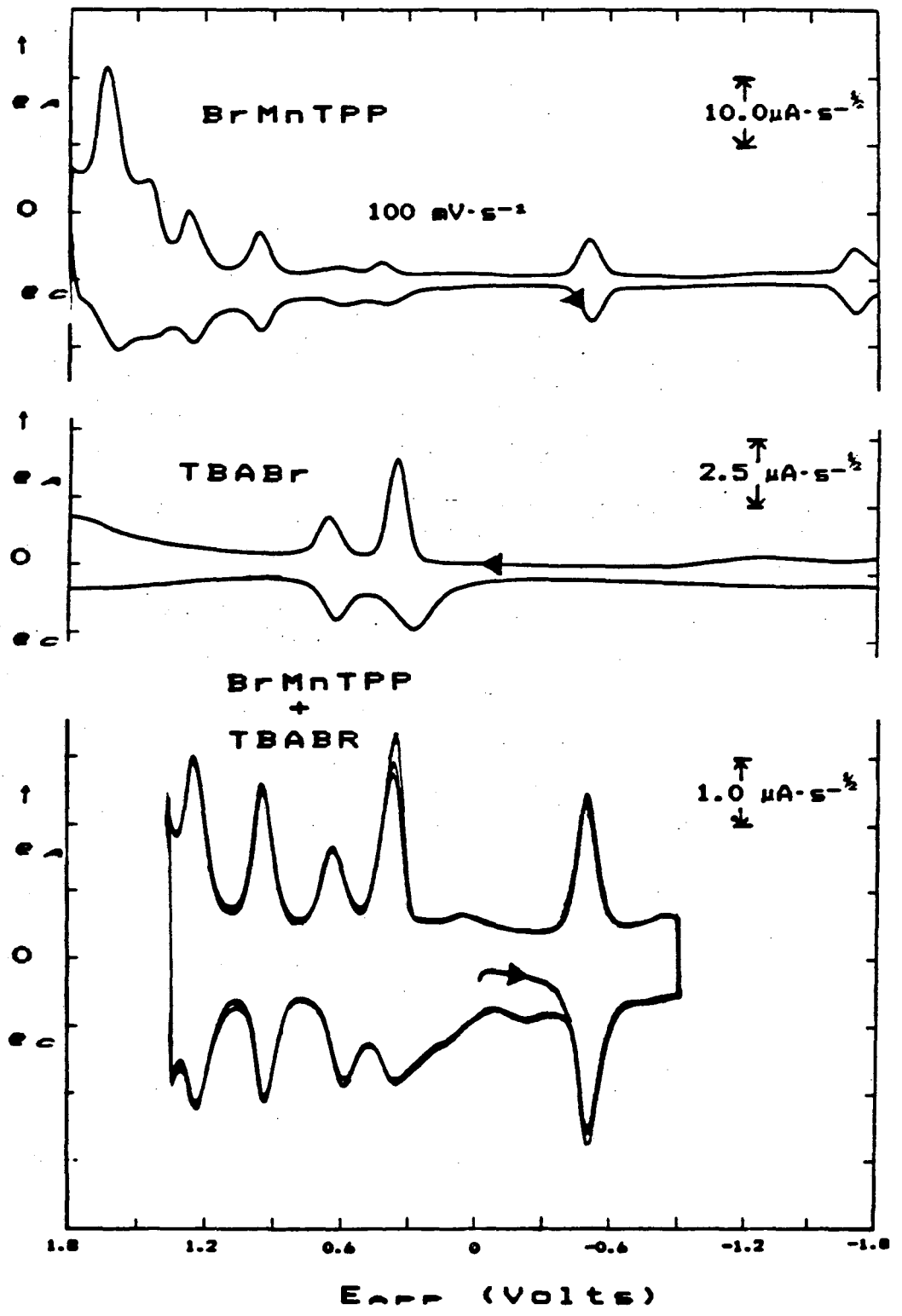
BrMnTPP
10.0μA·s^-½
100 mV·s^-1
TBABr
2.5 μA·s^-½
BrMnTPP
+
TBABR
1.0 μA·s^-½
1.8
1.2
0.6
0
-0.6
-1.2
-1.8
E (Volts)

FIGURE A3-5

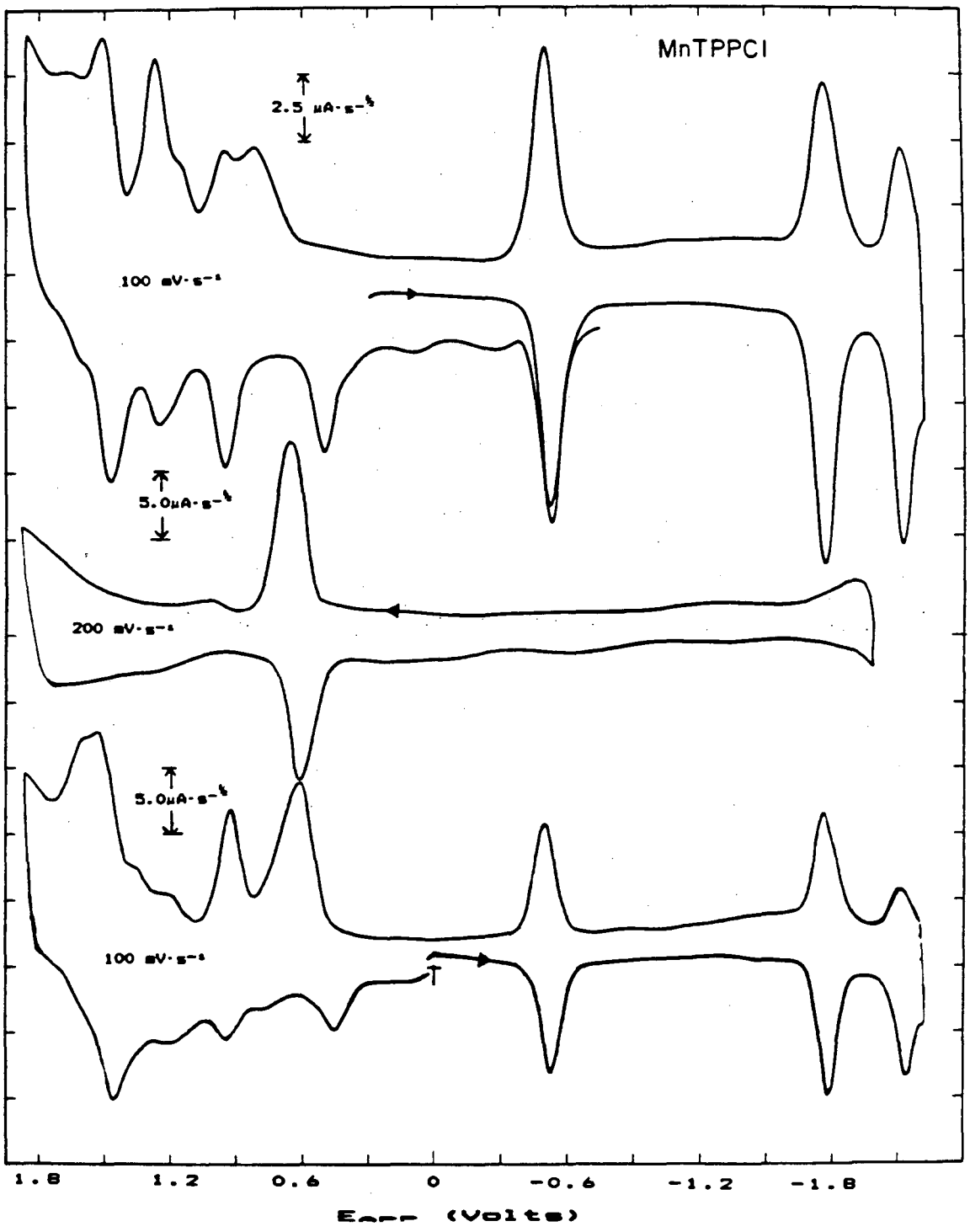
MnTPPCl
2.5 μA·s^-½
100 mV·s^-1
5.0μA·s^-½
200 mV·s^-1
5.0μA·s^-½
100 mV·s^-1
1.8
1.2
0.6
0
-0.6
-1.2
-1.8
E (Volts)

FIGURE A3-6

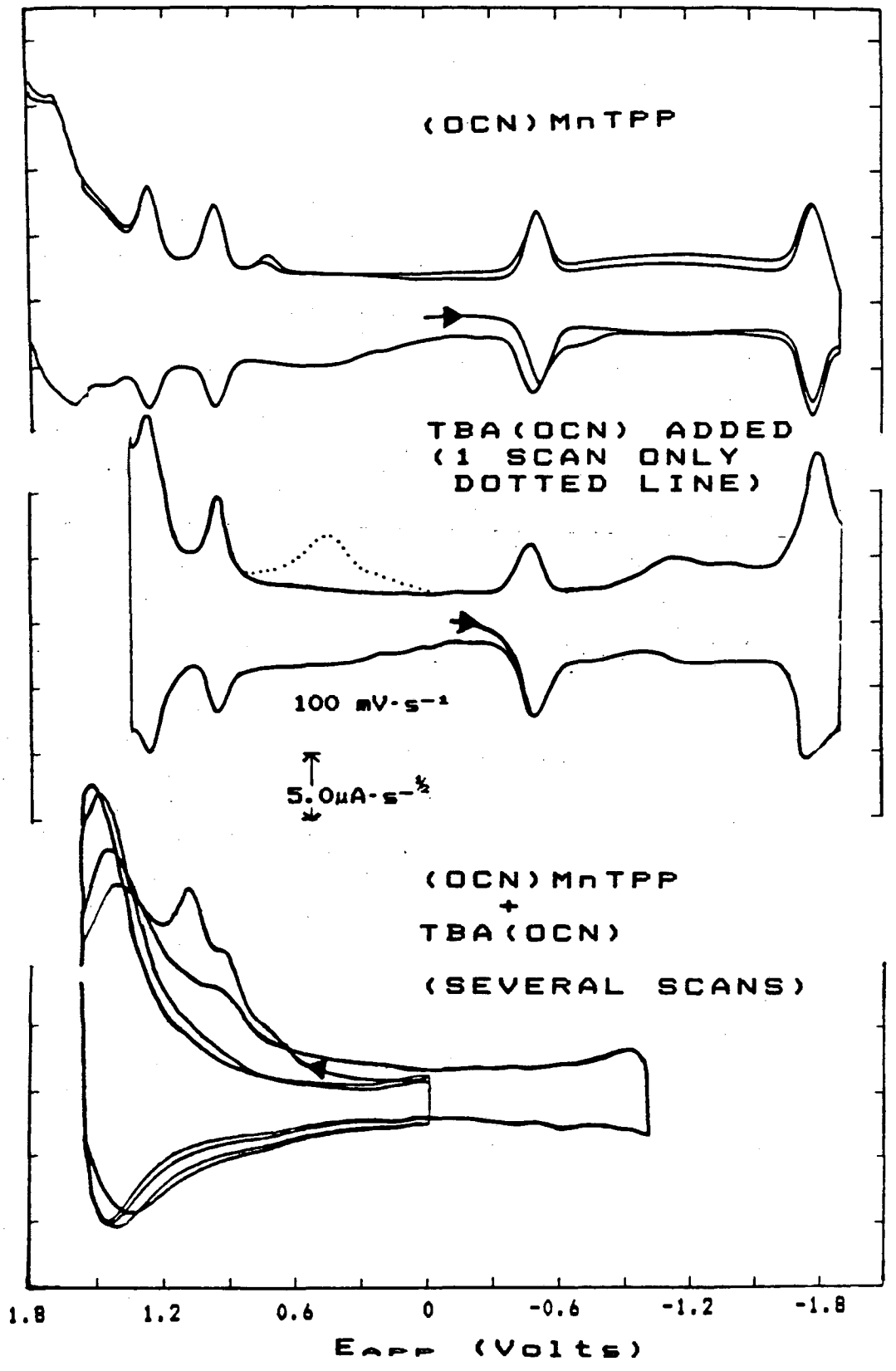
(OCN)MnTPP
TBA(OCN) ADDED
(1 SCAN ONLY
DOTTED LINE)
100 mV·s⁻¹
5.0μA·s^-½
(OCN)MnTPP
+
TBA(OCN)
(SEVERAL SCANS)
1.8
1.2
0.6
0
-0.6
-1.2
-1.8
E app (Volts)

FIGURE A3-7

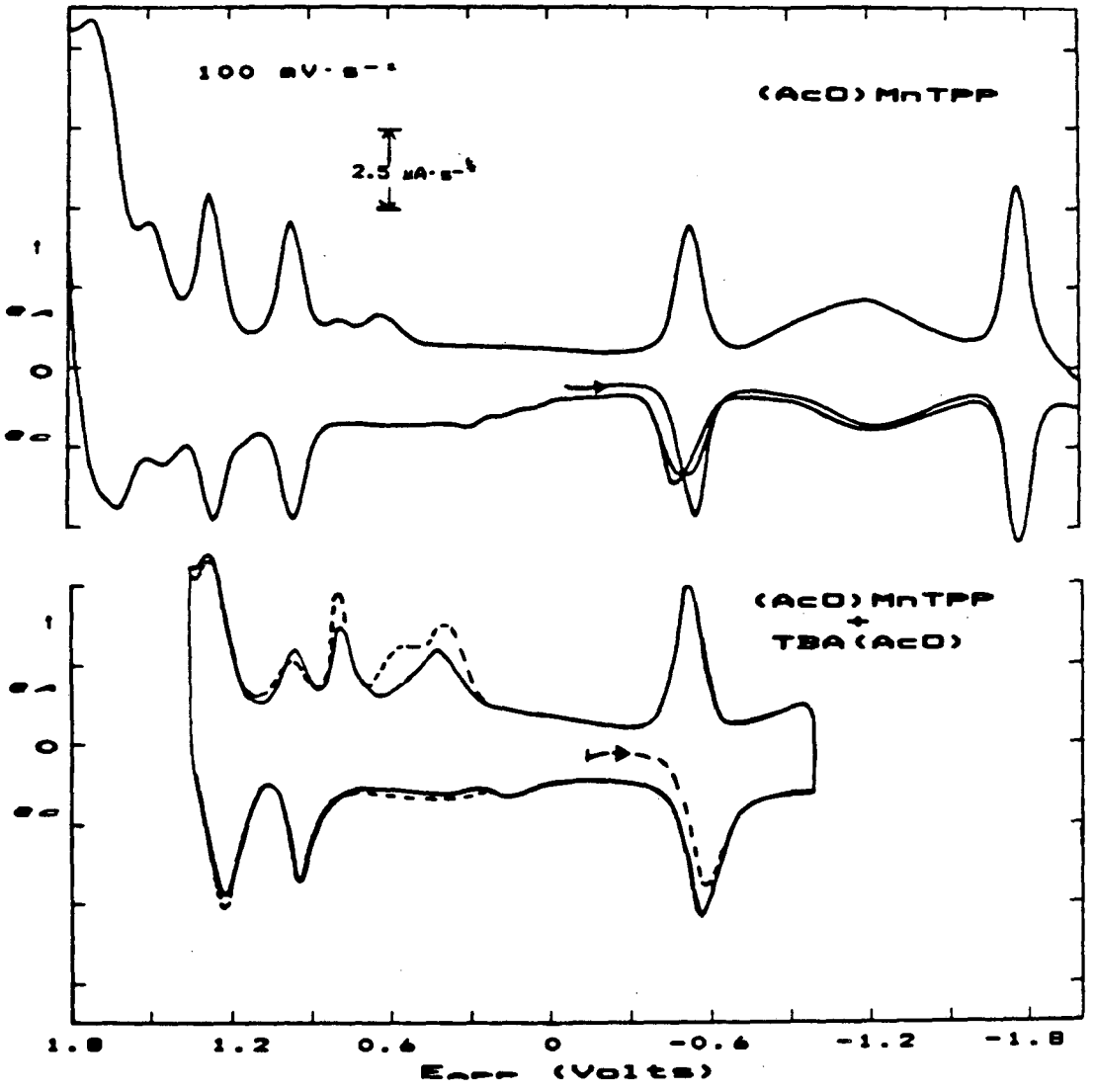
100 mV·s⁻¹
(AcO)MnTPP
2.5 μA·s⁻½
(AcO)MnTPP
+
TBA(AcO)
1.8
1.2
0.6
0
-0.6
-1.2
-1.8
E (Volts)

FIGURE A3-8

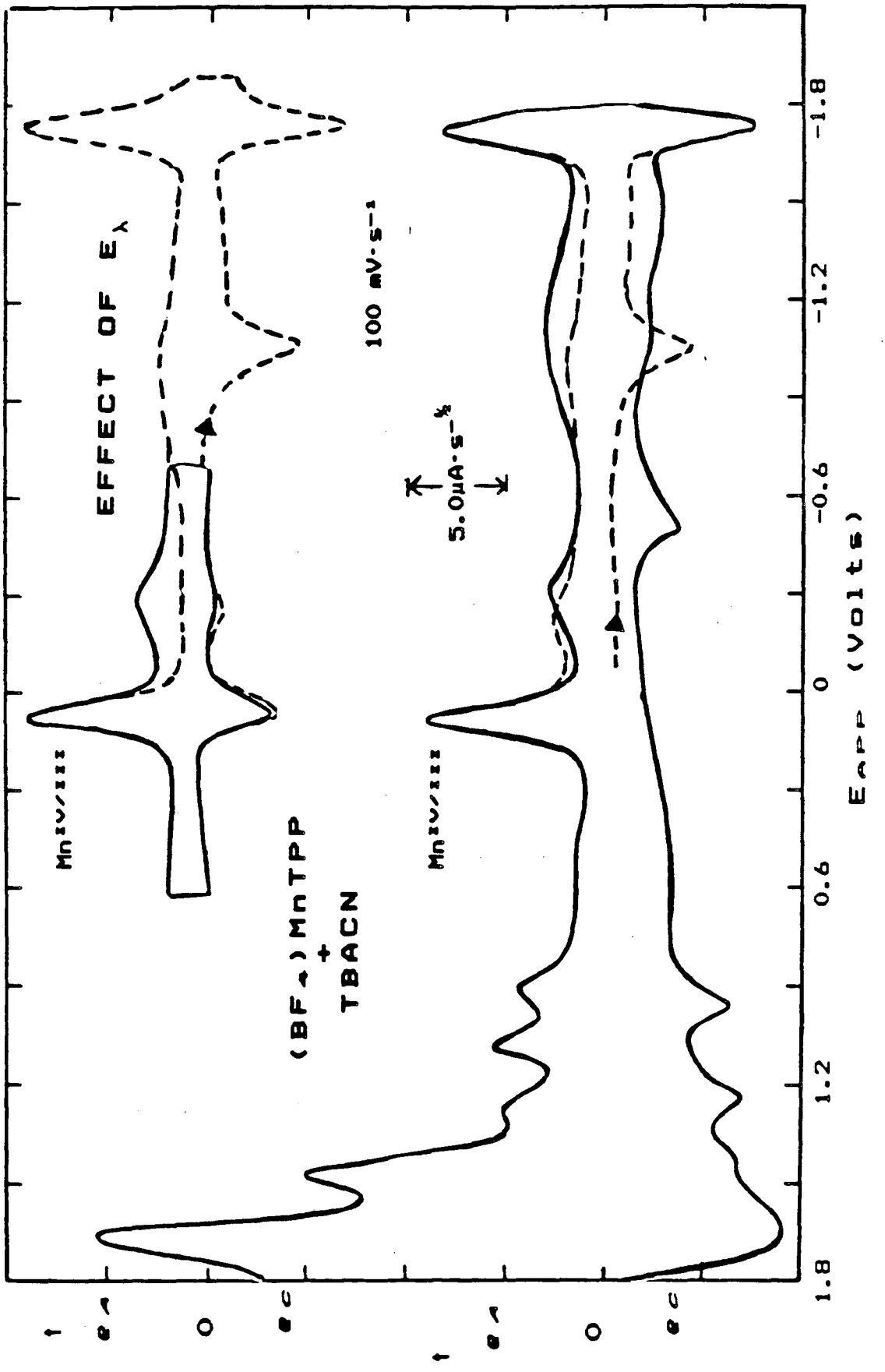
EFFECT OF E_λ
100 mV·s⁻¹
5.0μA·s^-½
(BF₄)MnTPP
+
TBACN
Mn^IV/III
Mn^IV/III
E_APP (Volts)
1.8
1.2
0.6
0
-0.6
-1.2
-1.8

FIGURE A3-9

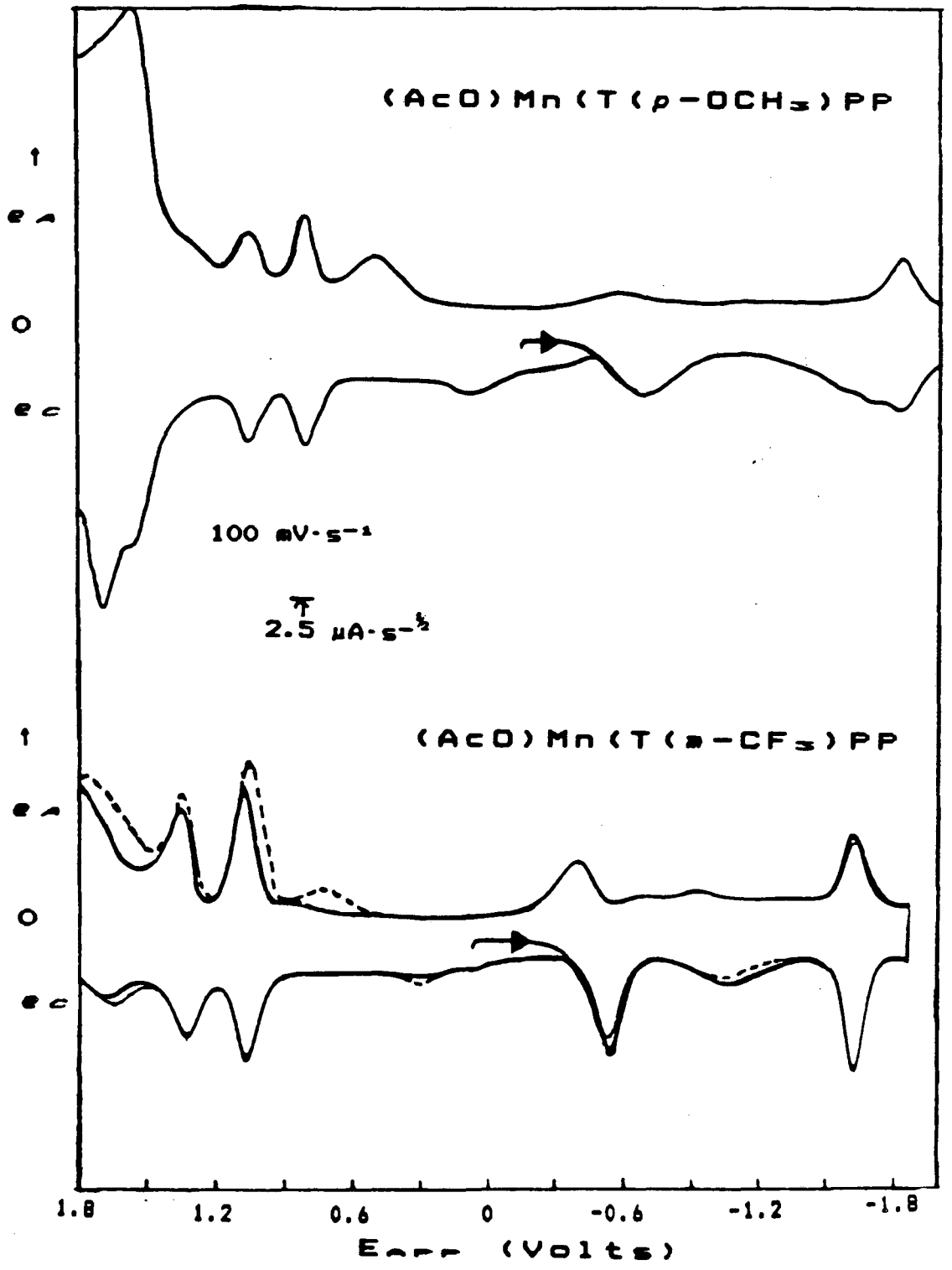
(AcO)Mn(T(p-OCH3)PP
100 mV·s⁻¹
2.5 μA·s^-½
(AcO)Mn(T(m-CF3)PP
1.8
1.2
0.6
0
-0.6
-1.2
-1.8
E corr (Volts)

APPENDIX 4

SPECTRA OF XMnTPP

FIGURE A4-1

Spectra of substituted XMnPorphyrins showing that the electronic spectrum is more perturbed by axial ligand changes than by changes in the porphyrin periphery.

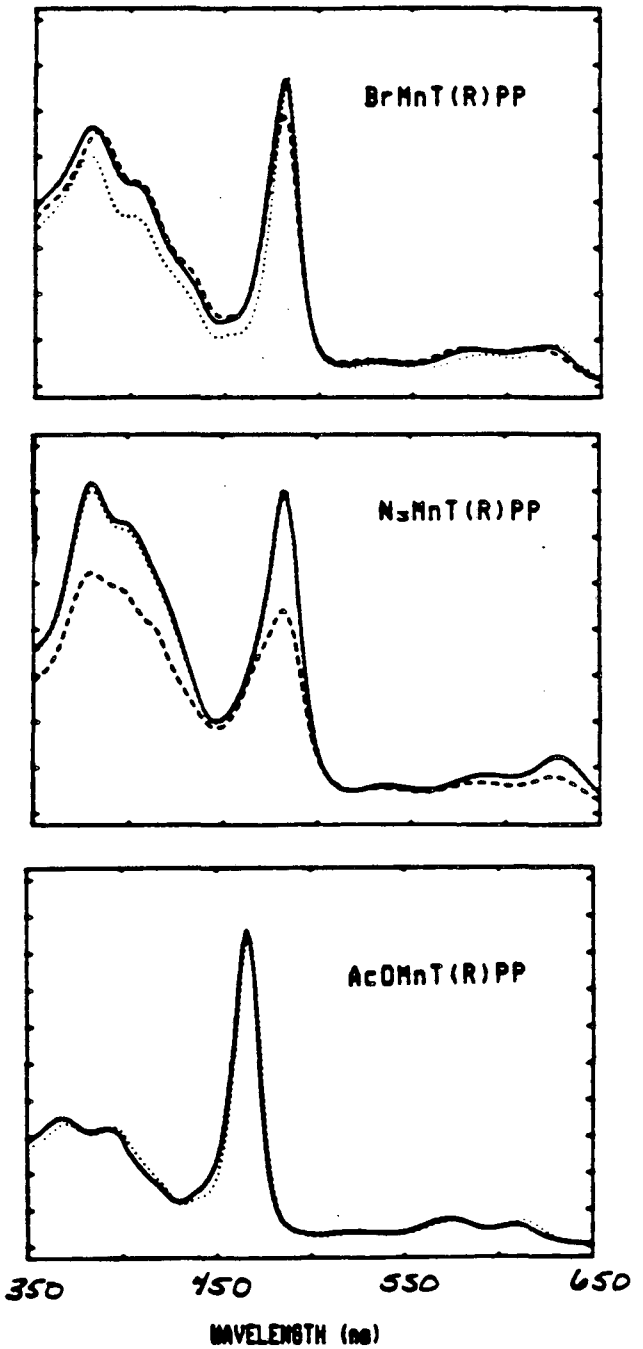

Figure A4-2

ClO_4MnTPP

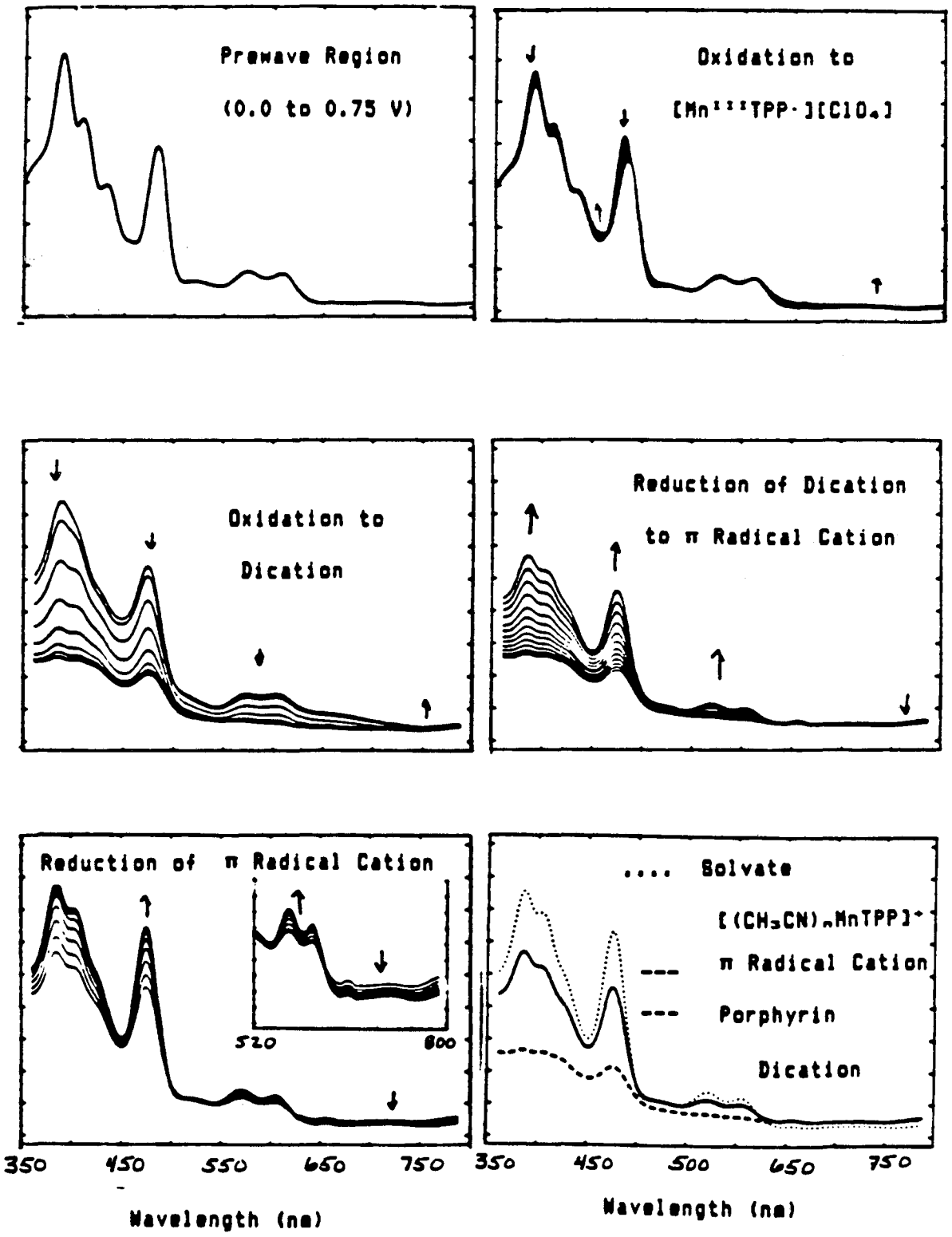

Figure A4-3

ClMnTPP

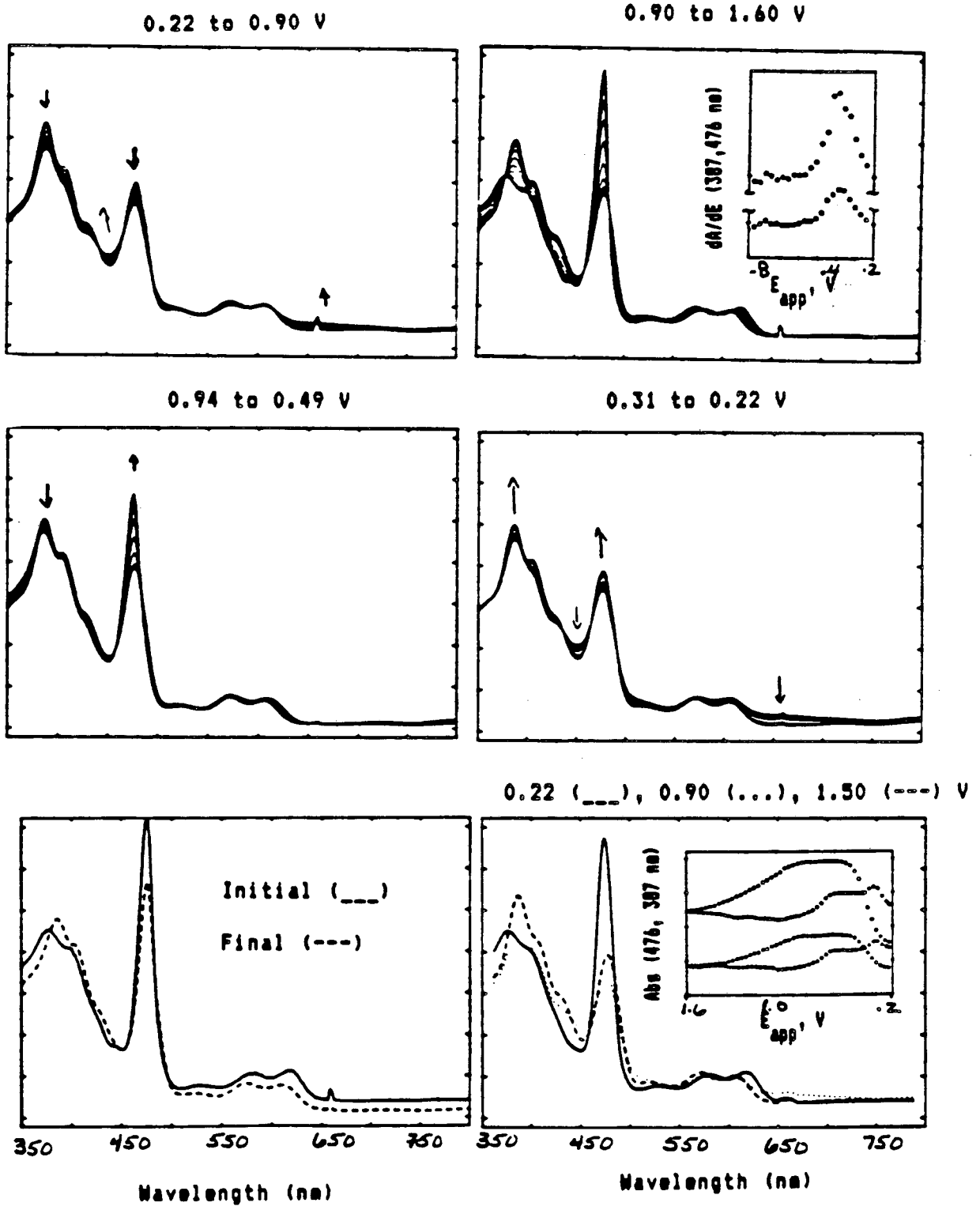

Figure A4-4A

BrMnTPP (Oxidations)

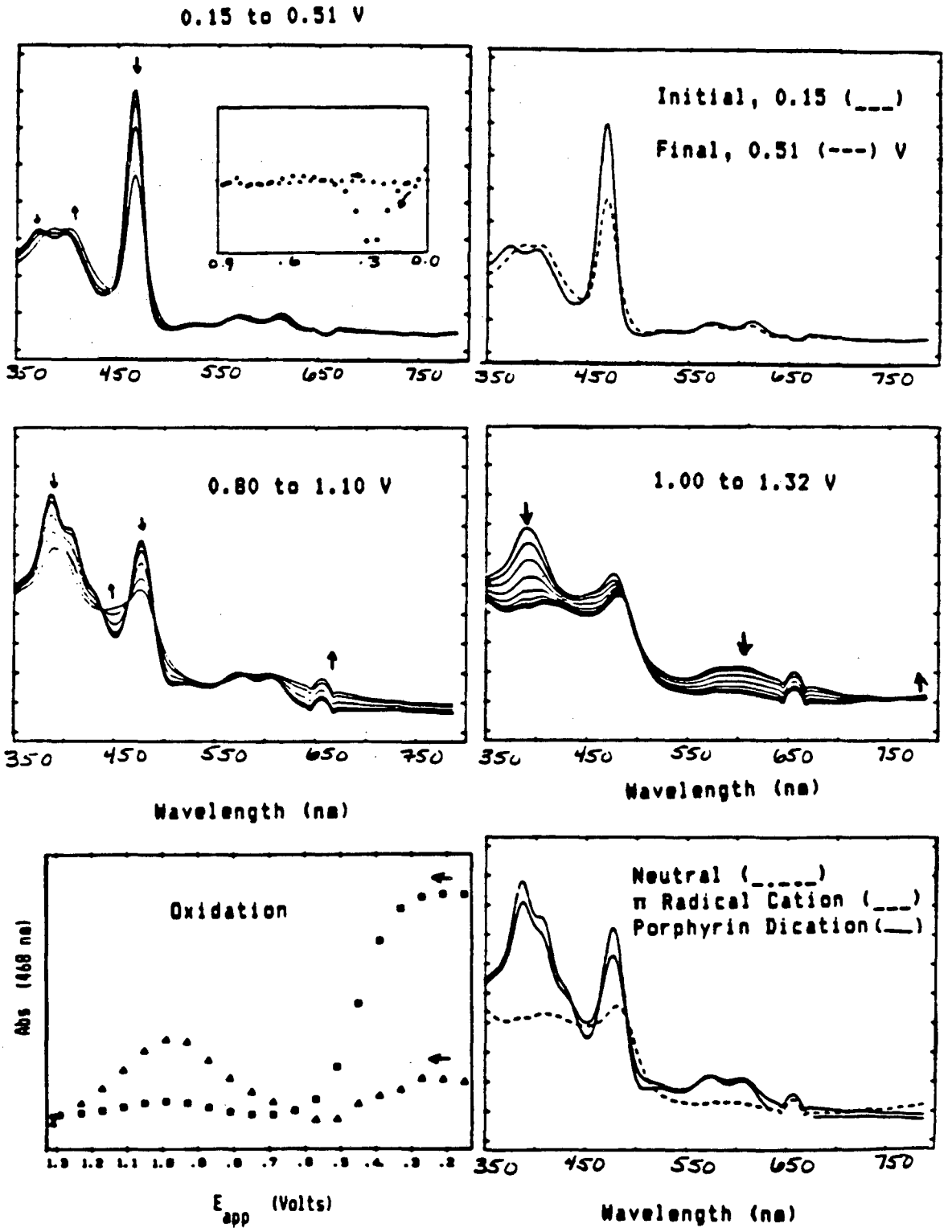

Figure A4-4B

BrMnTPP (Reductions)

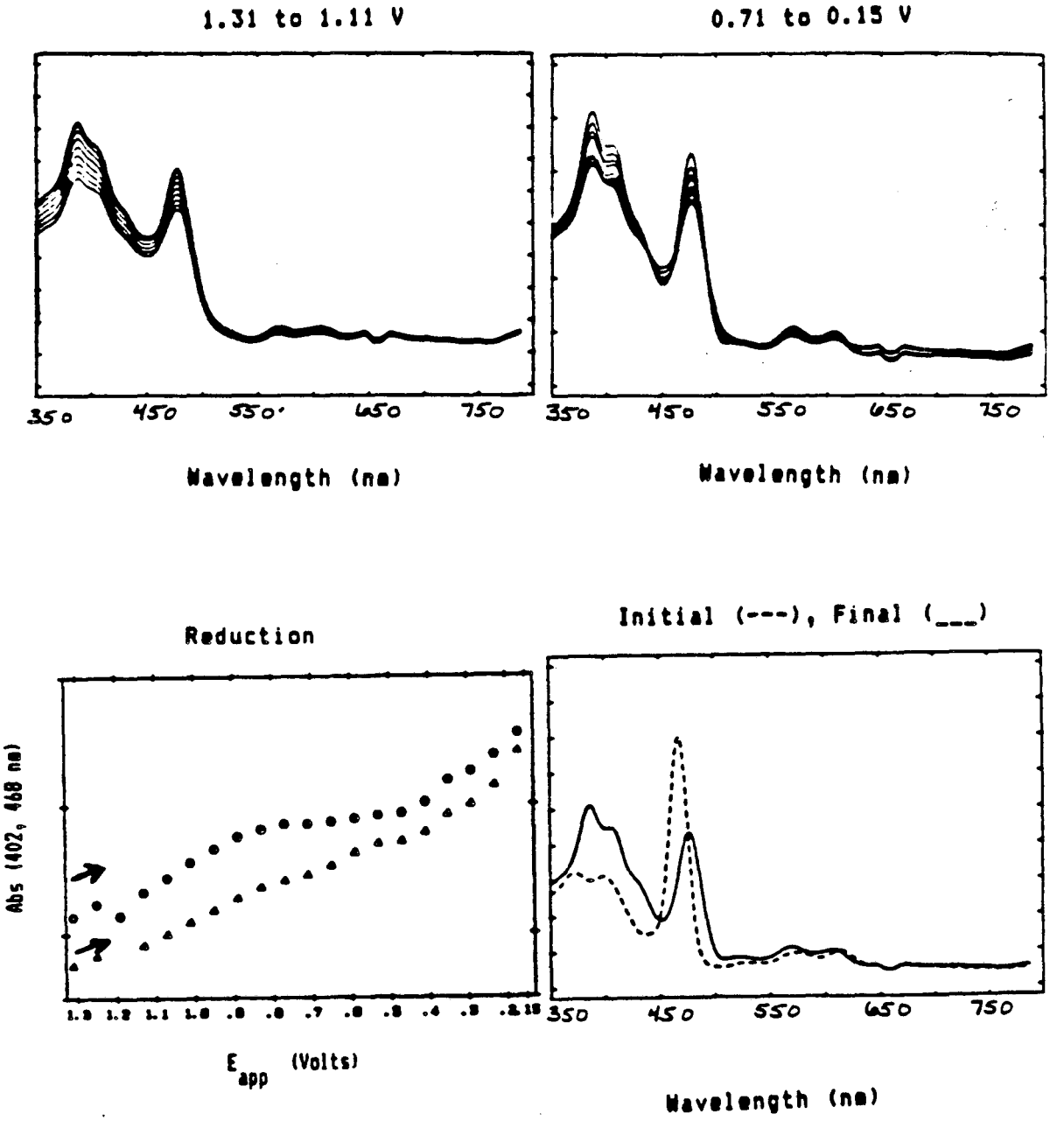

Figure 4-5A

NO_2MnTPP (Prewave Region, TEAP only)

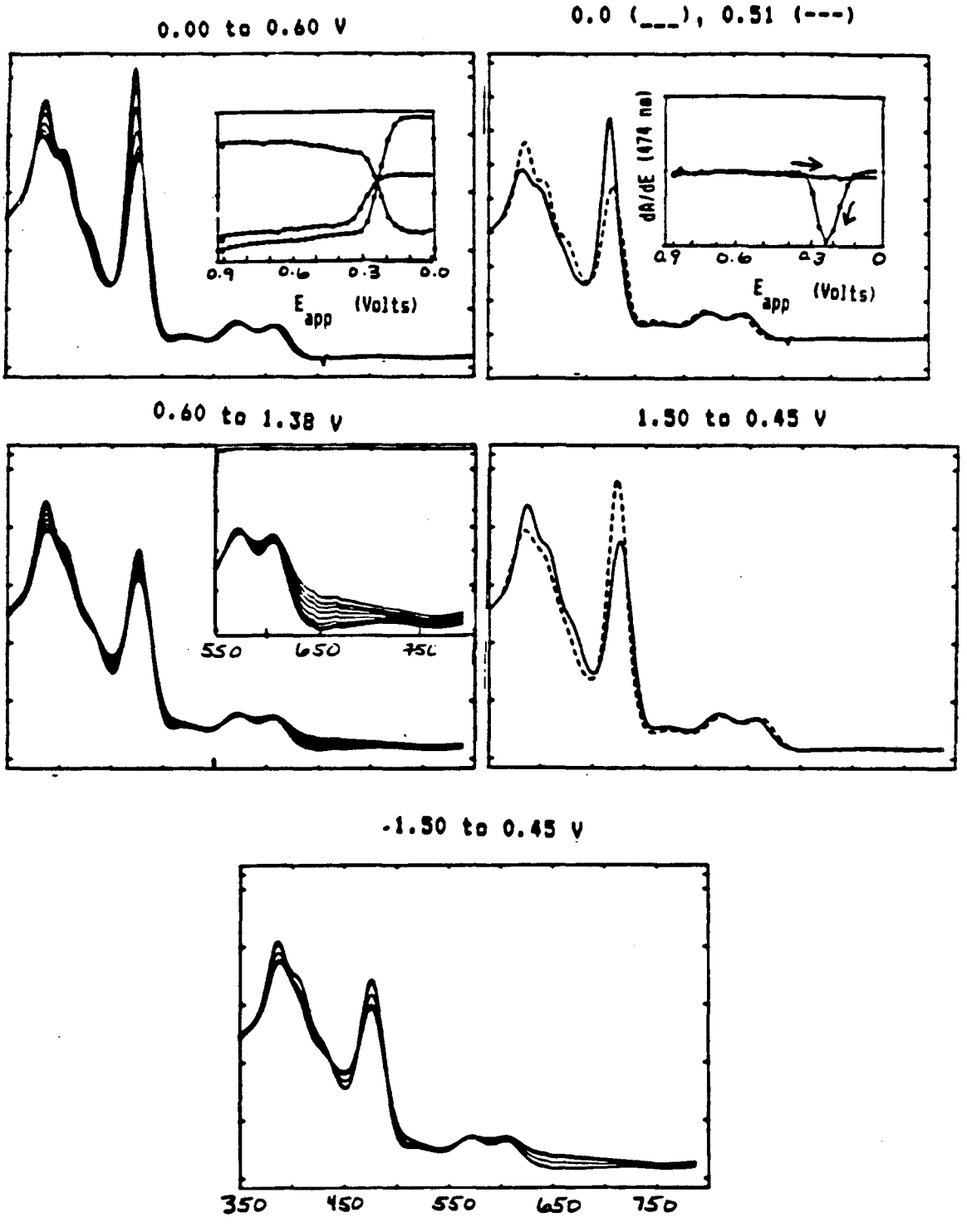

Figure 4-5B

NO_2MnTPP (Prewave Region, $TBANO_2$ Added)

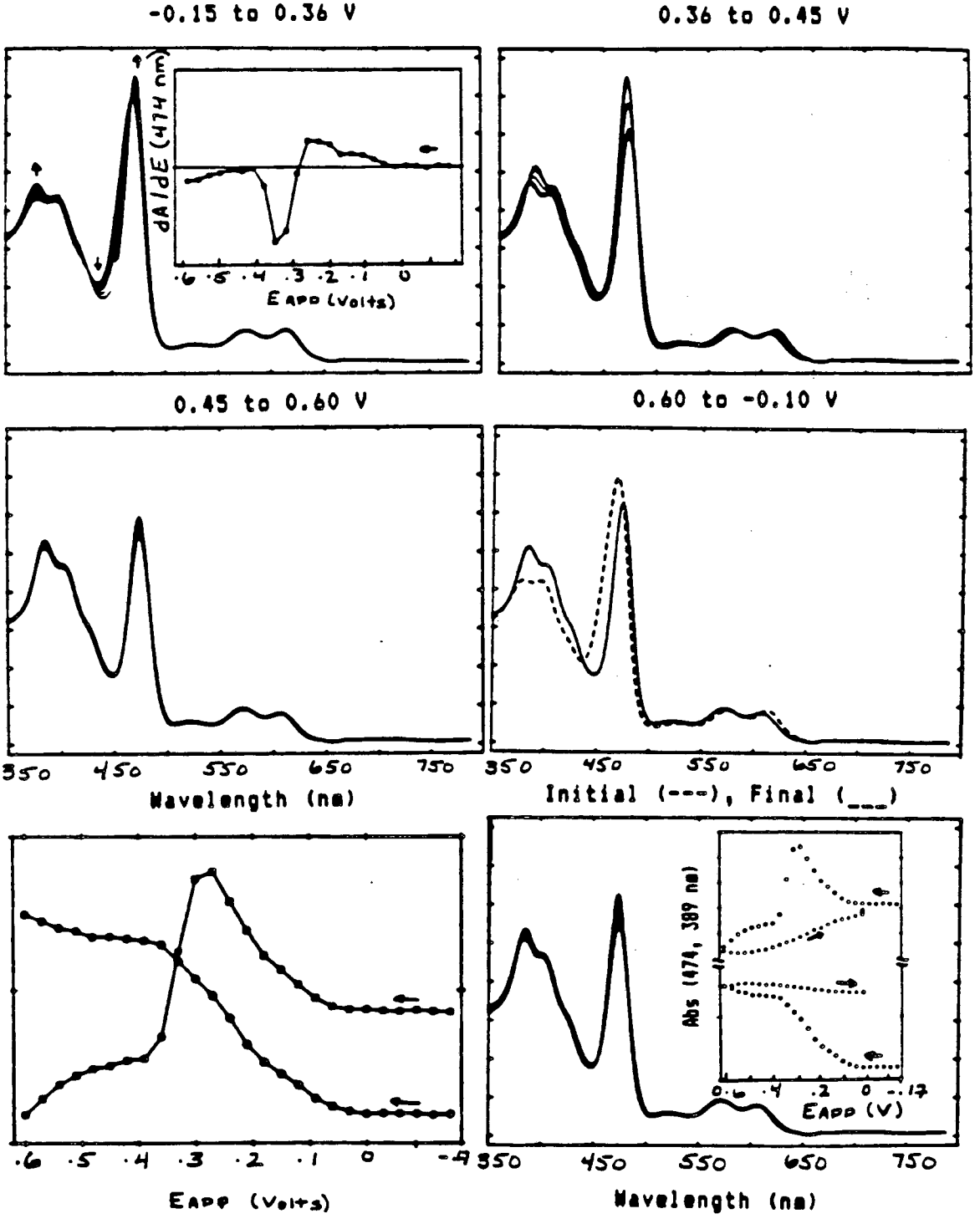

Figure 4-5C

NO_2MnTPP (π Radical Cation Region)

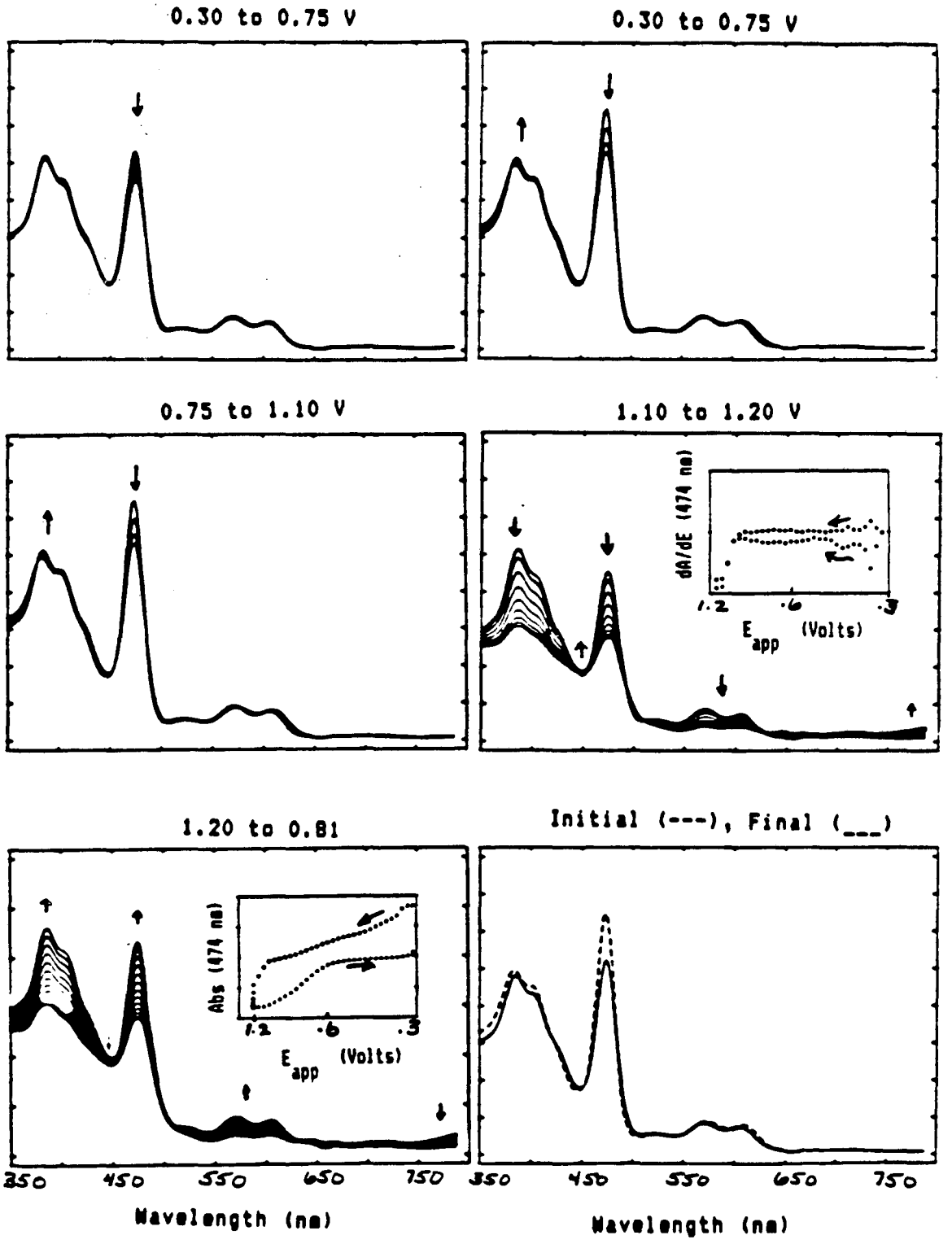

Figure 4-5D

NO_2MnTPP (Dication Formation)

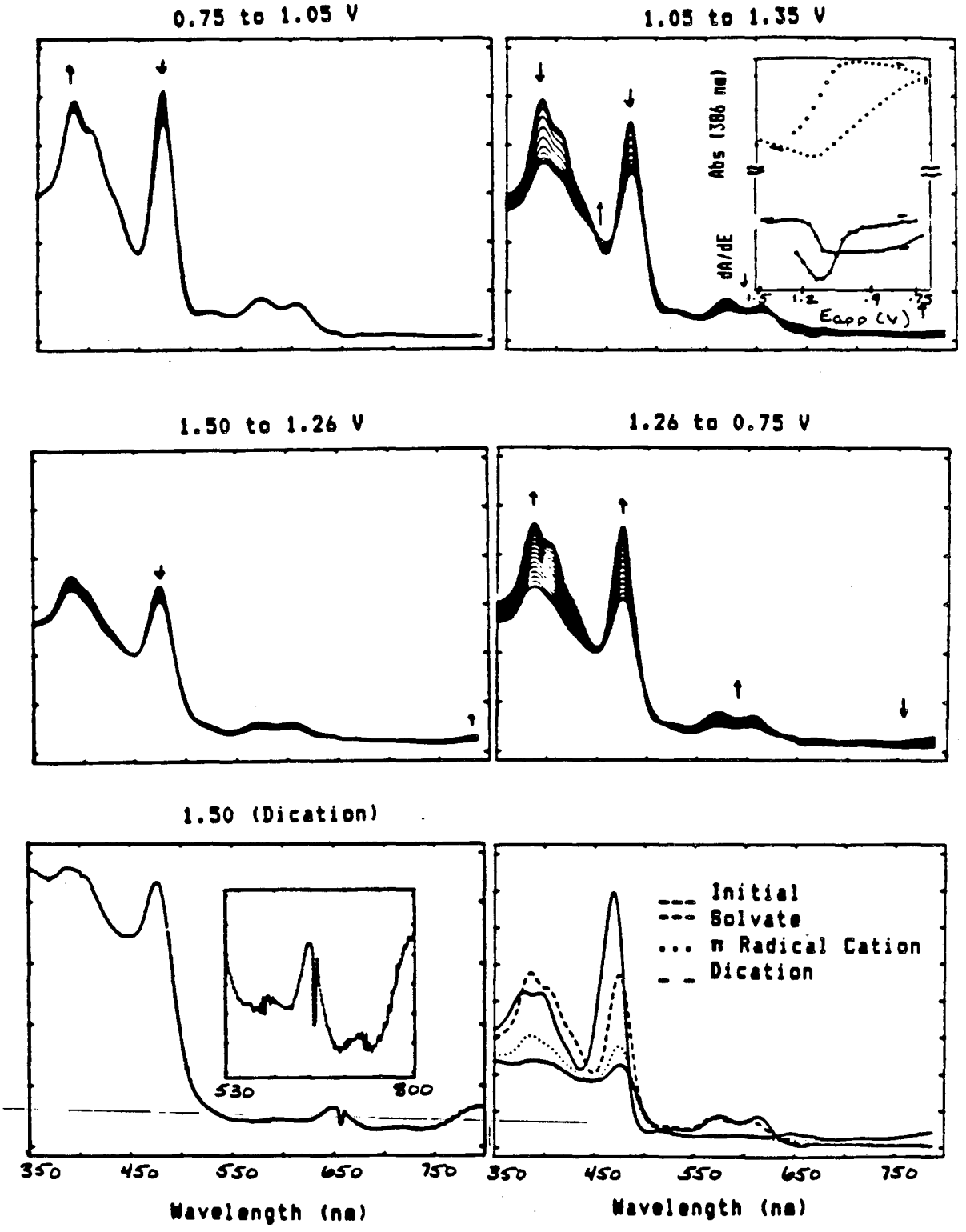

Figure 4-6A

AcOMnTPP (Prewave Region, TEAP only)

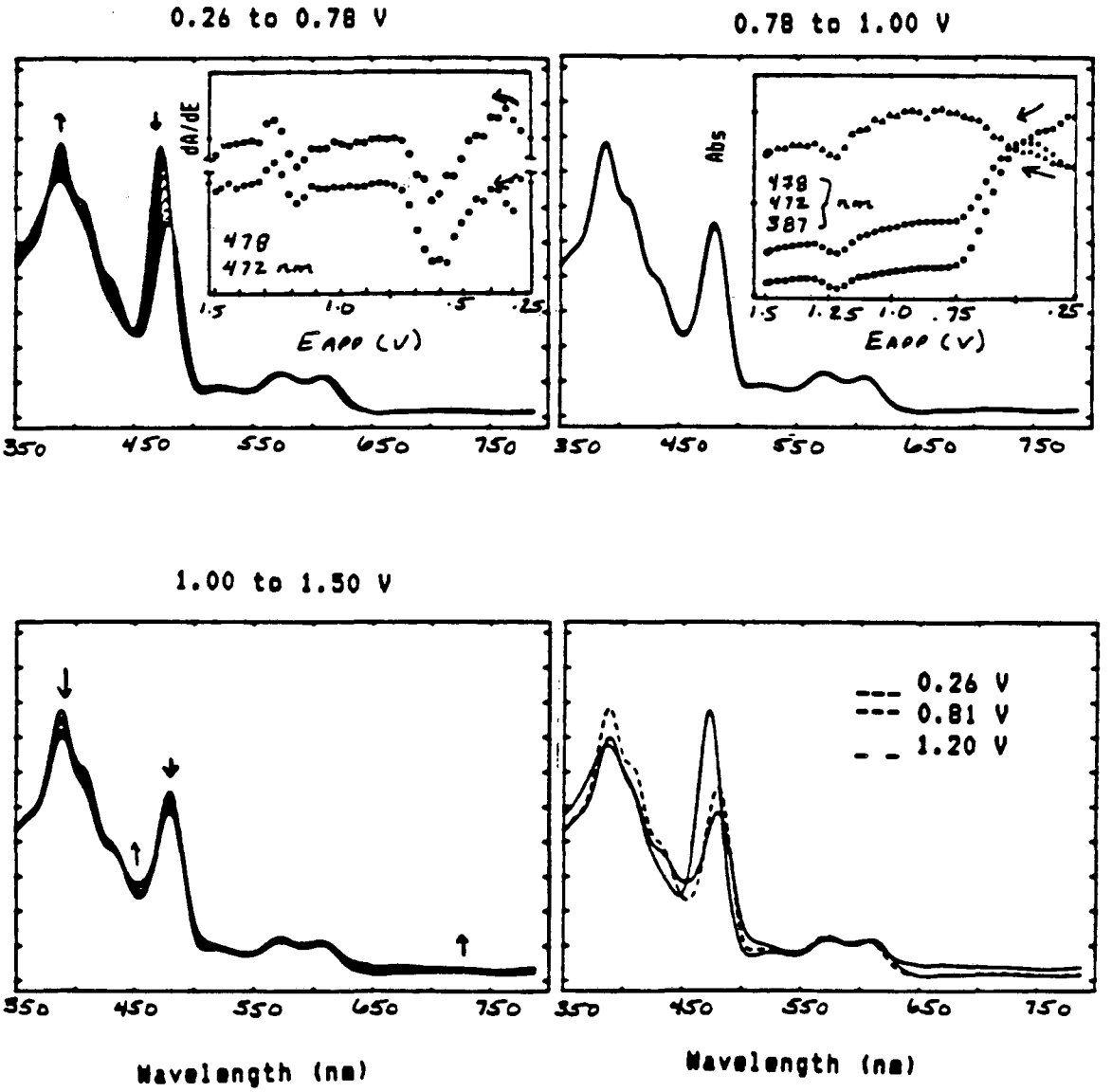

Figure 4-6B

AcOMnTPP (Prewave region, TBA(AcO)Added)

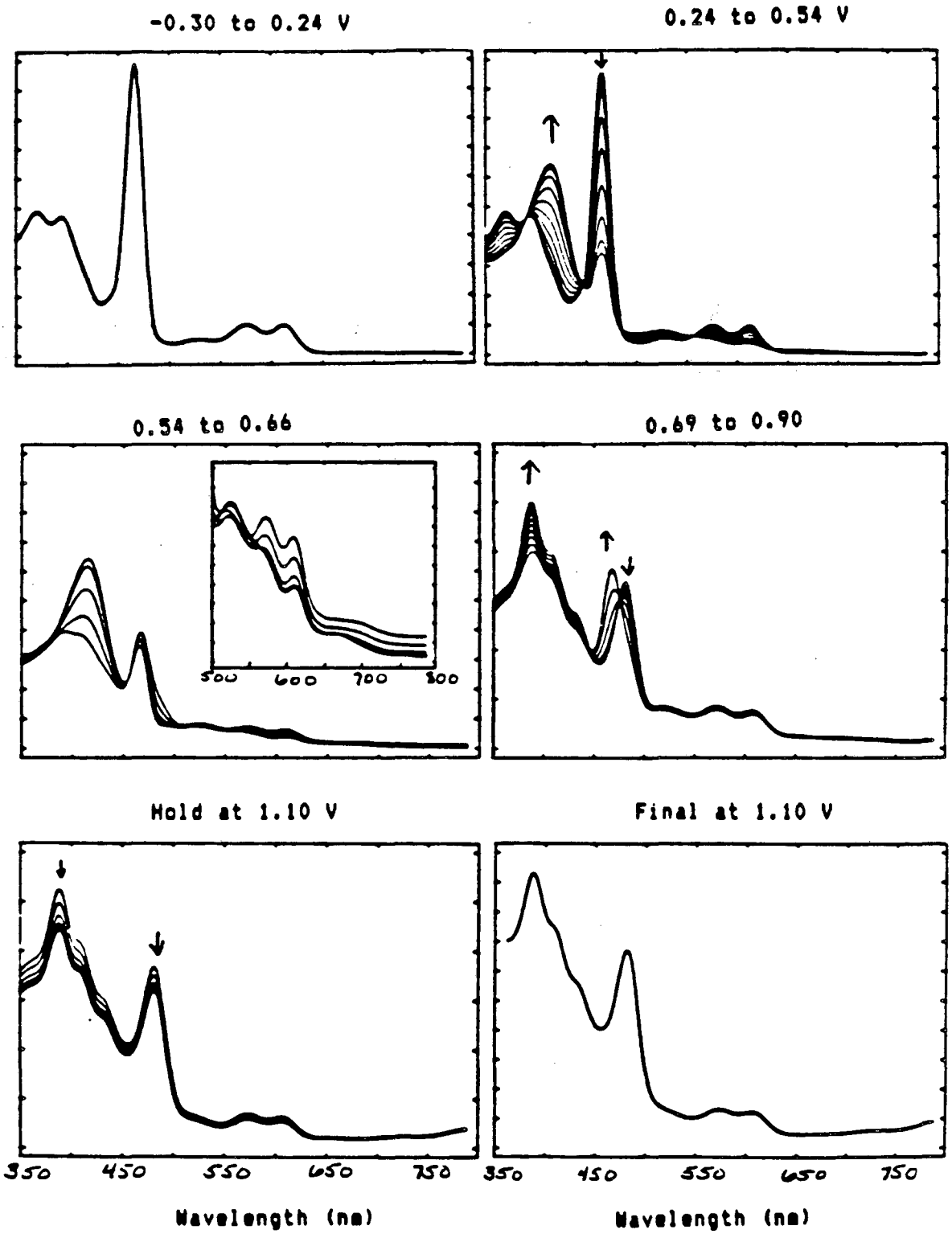

Figure 4-6C

AcOMnTPP (π Radical Cation and Mn(IV) Region, Added TBA(AcO)

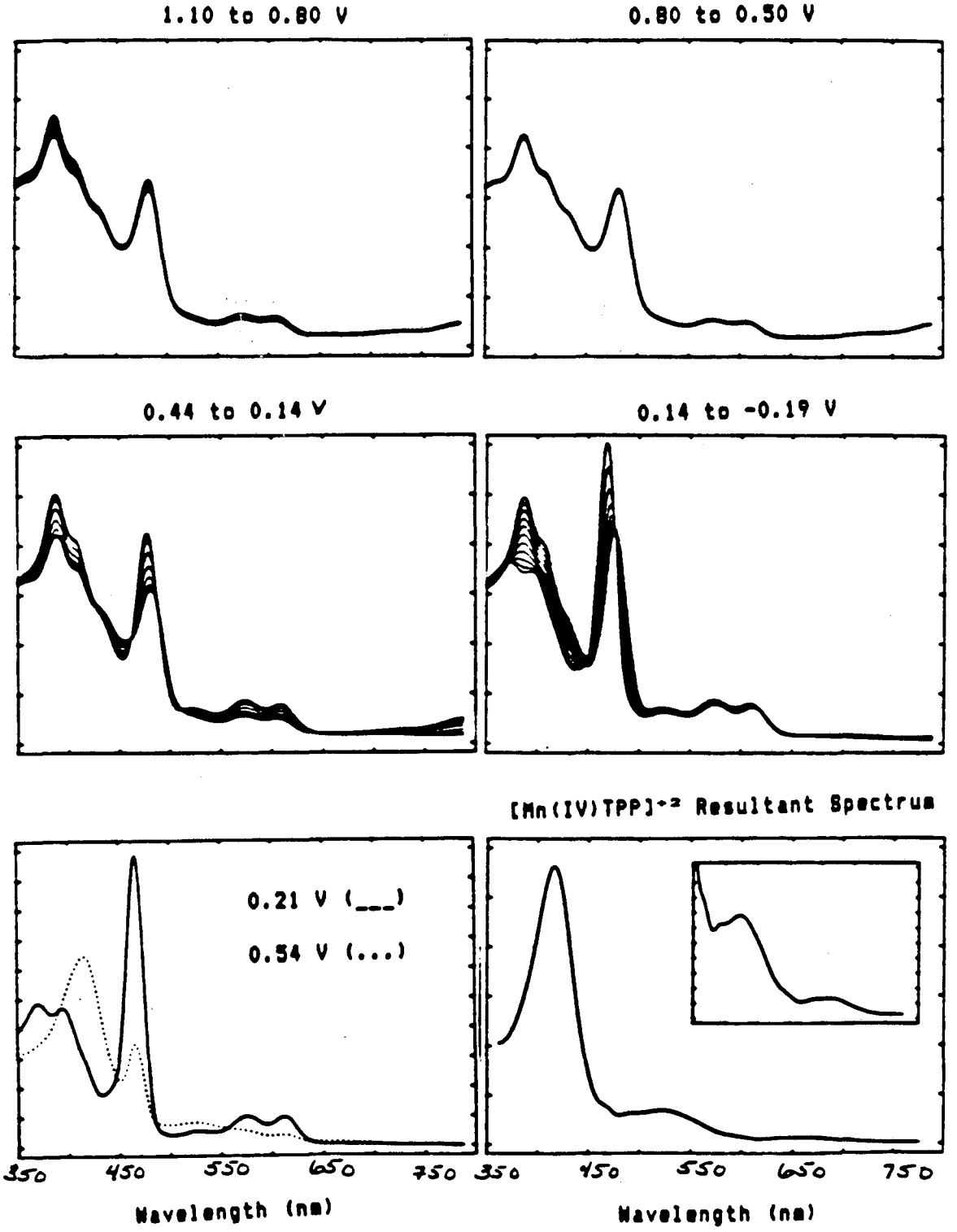

Figure 4-6D

Absorbance *vs* $E_{\frac{1}{2}}$

Oxidation/Reduction

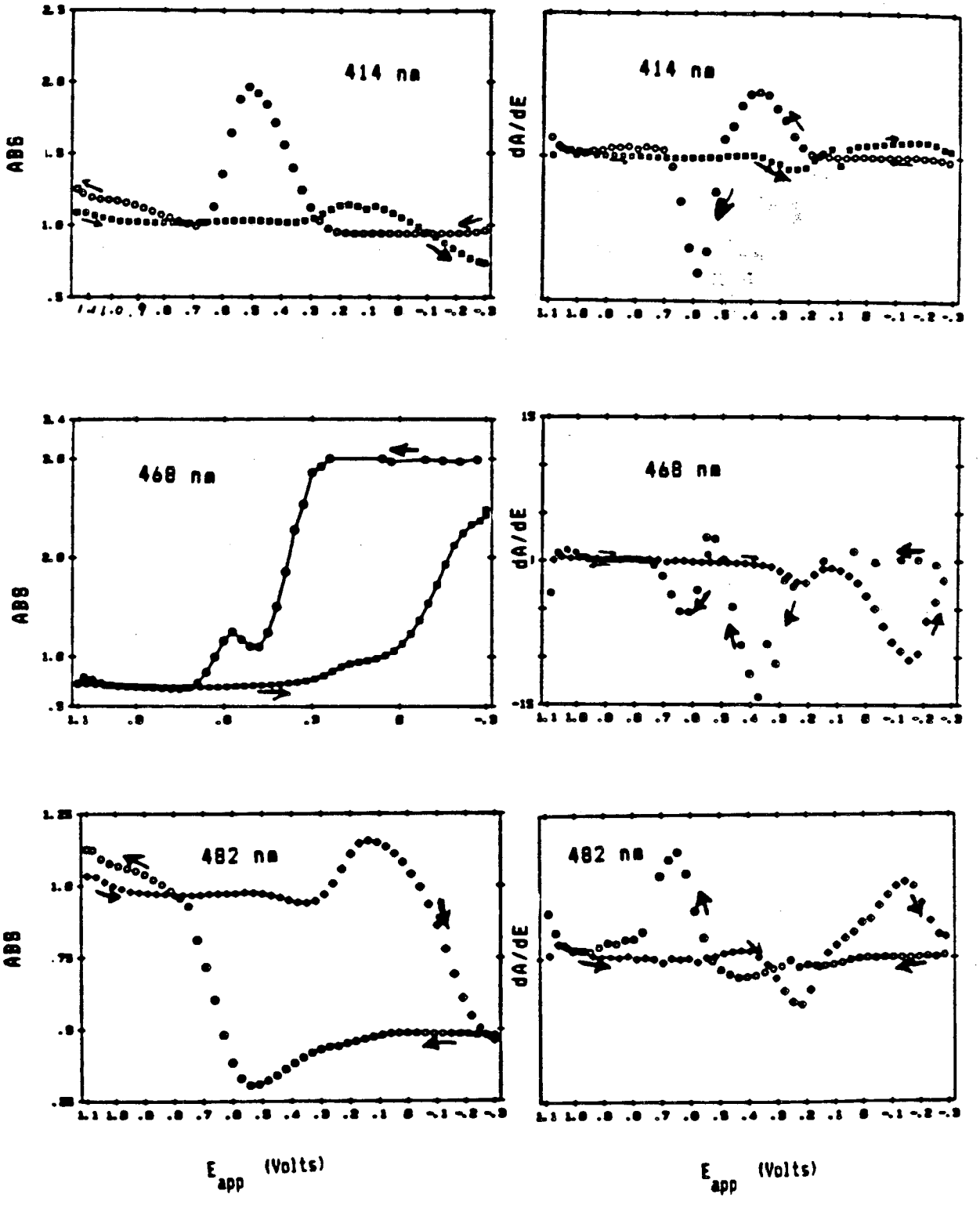

Figure 4-6E

AcOMnTPP (Mn(IV))

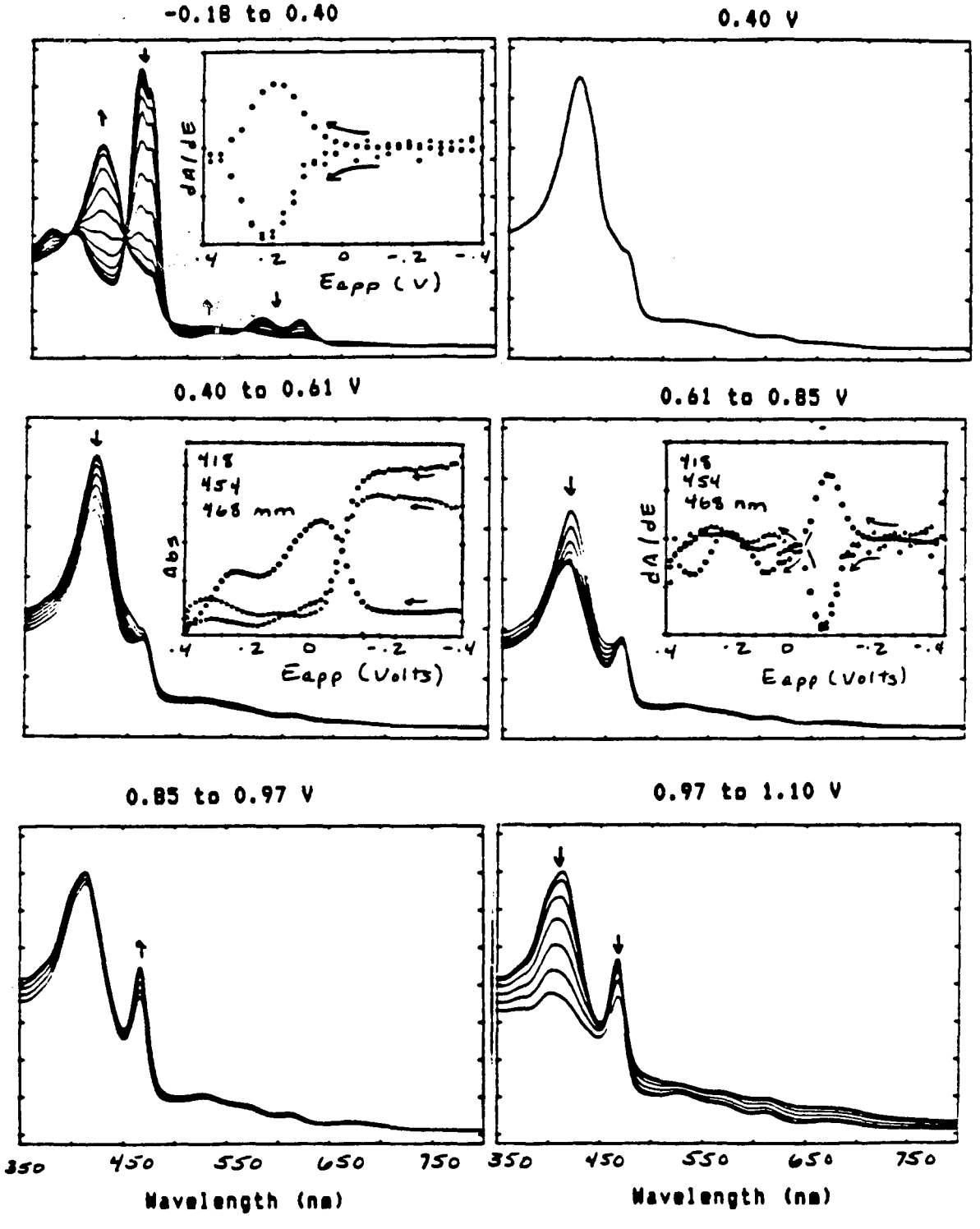

Figure 4-6F

AcOMnTPP ((Mn(IV), Effect of E_λ)

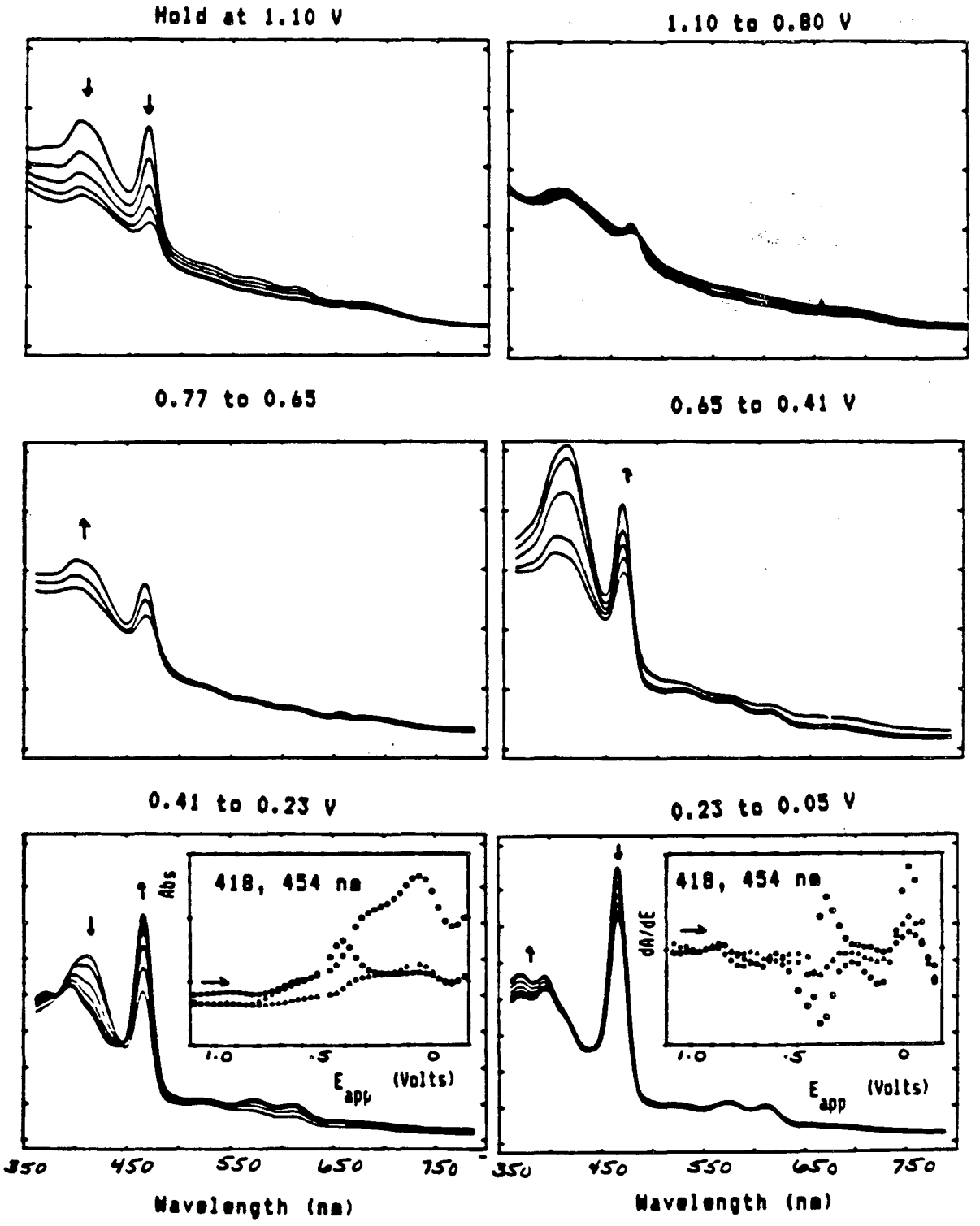

Figure 4-7A

N_3MnTPP (Added $TBAN_3$)

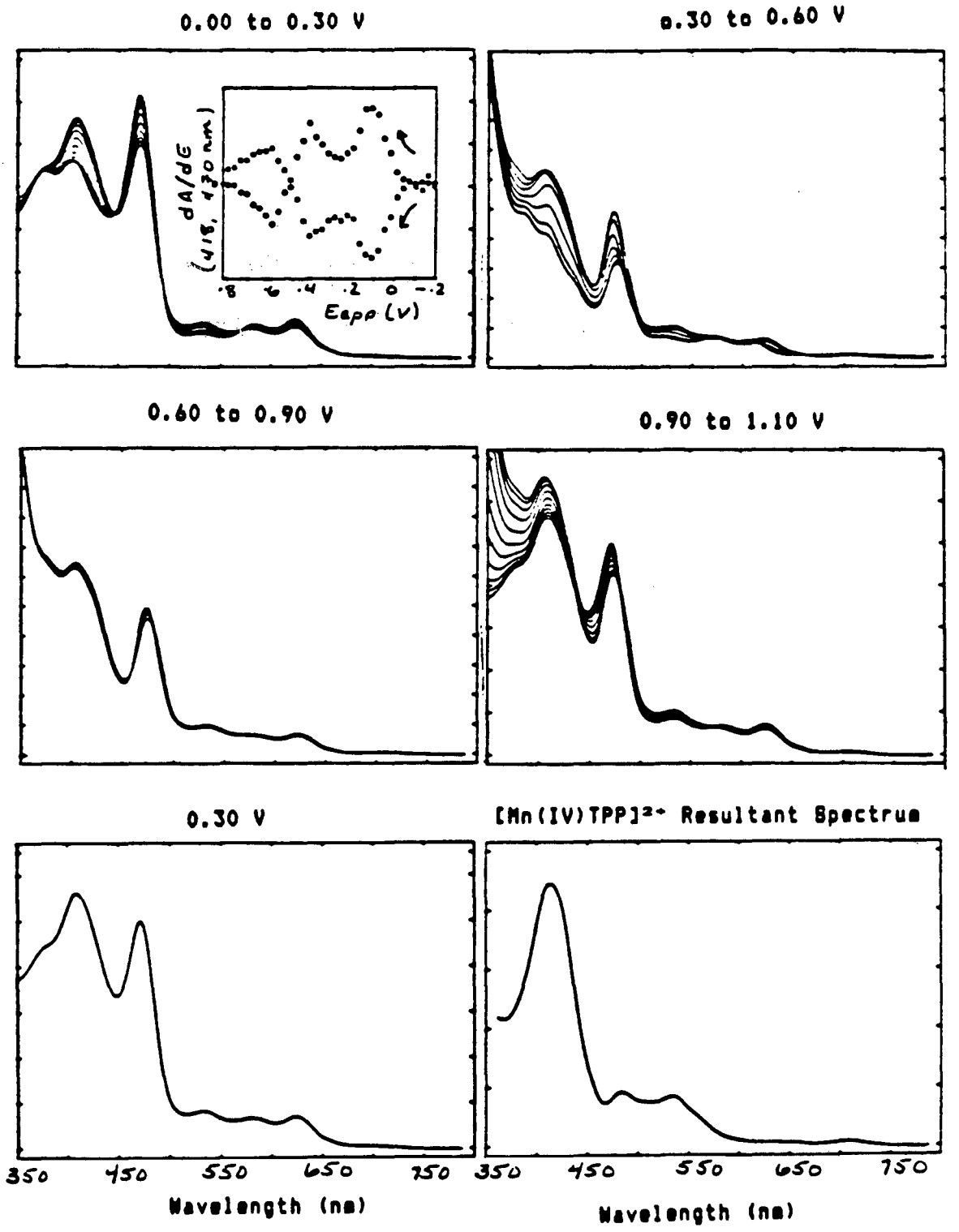

Figure 4-7B

N_3MnTPP (Absorbance *vs* $E_{1/2}$)

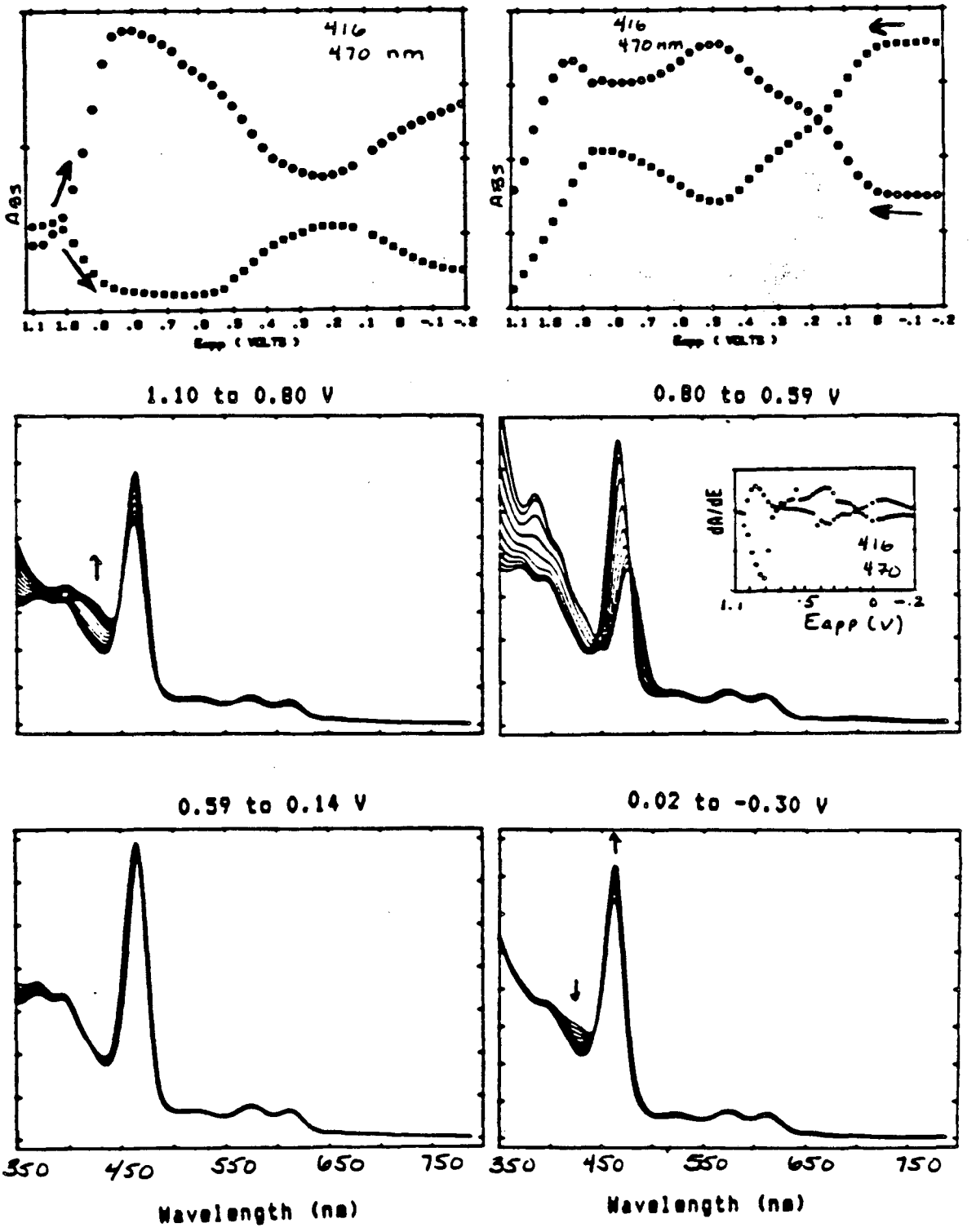

Figure 4-7C

N_3MnTPP (Mn(IV))

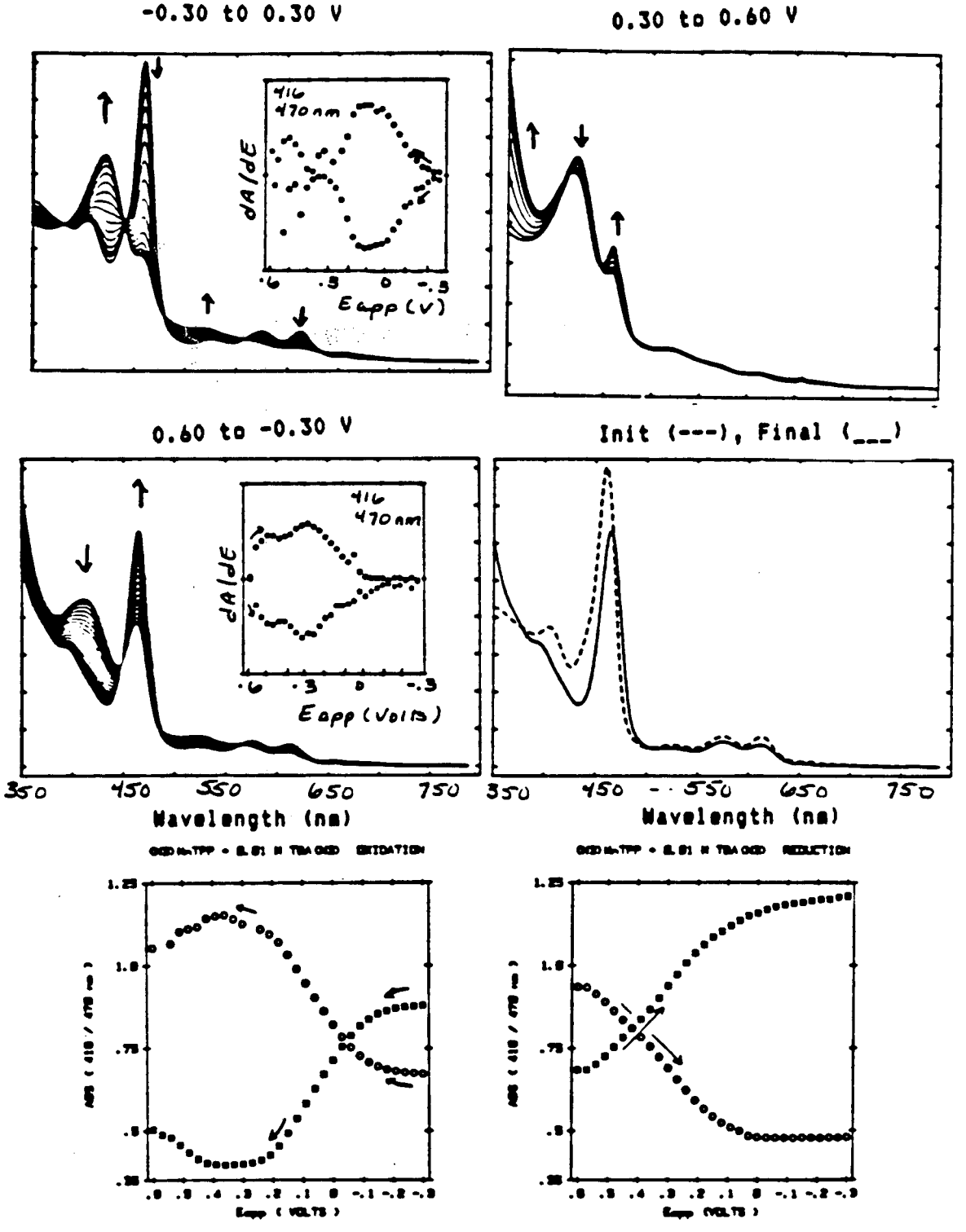

Figure 4-8A

(OCN)MnTPP (0.01 M TBANCO)

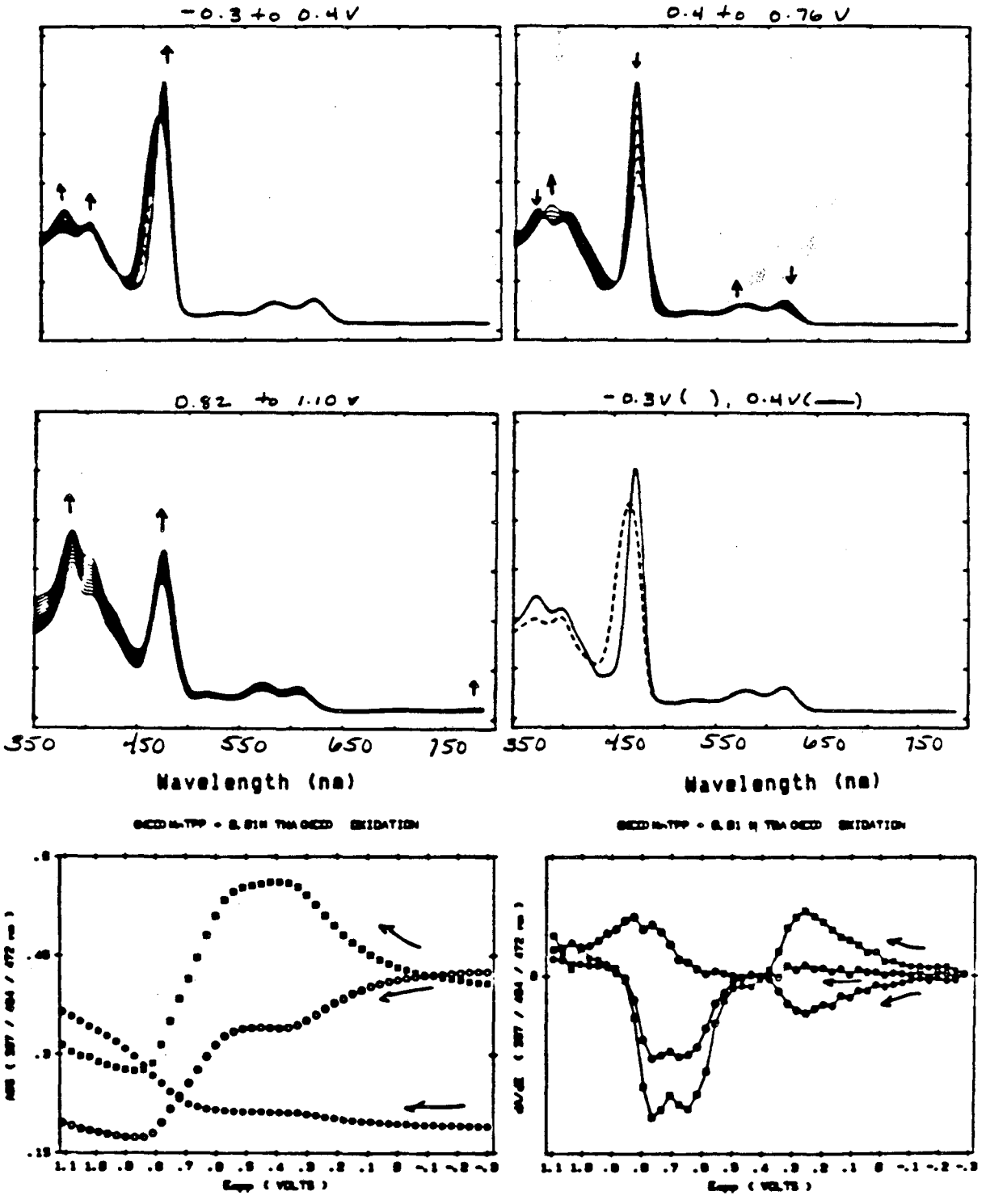

Figure 4-8B

(OCN)MnTPP (0.1 M TBANCO)

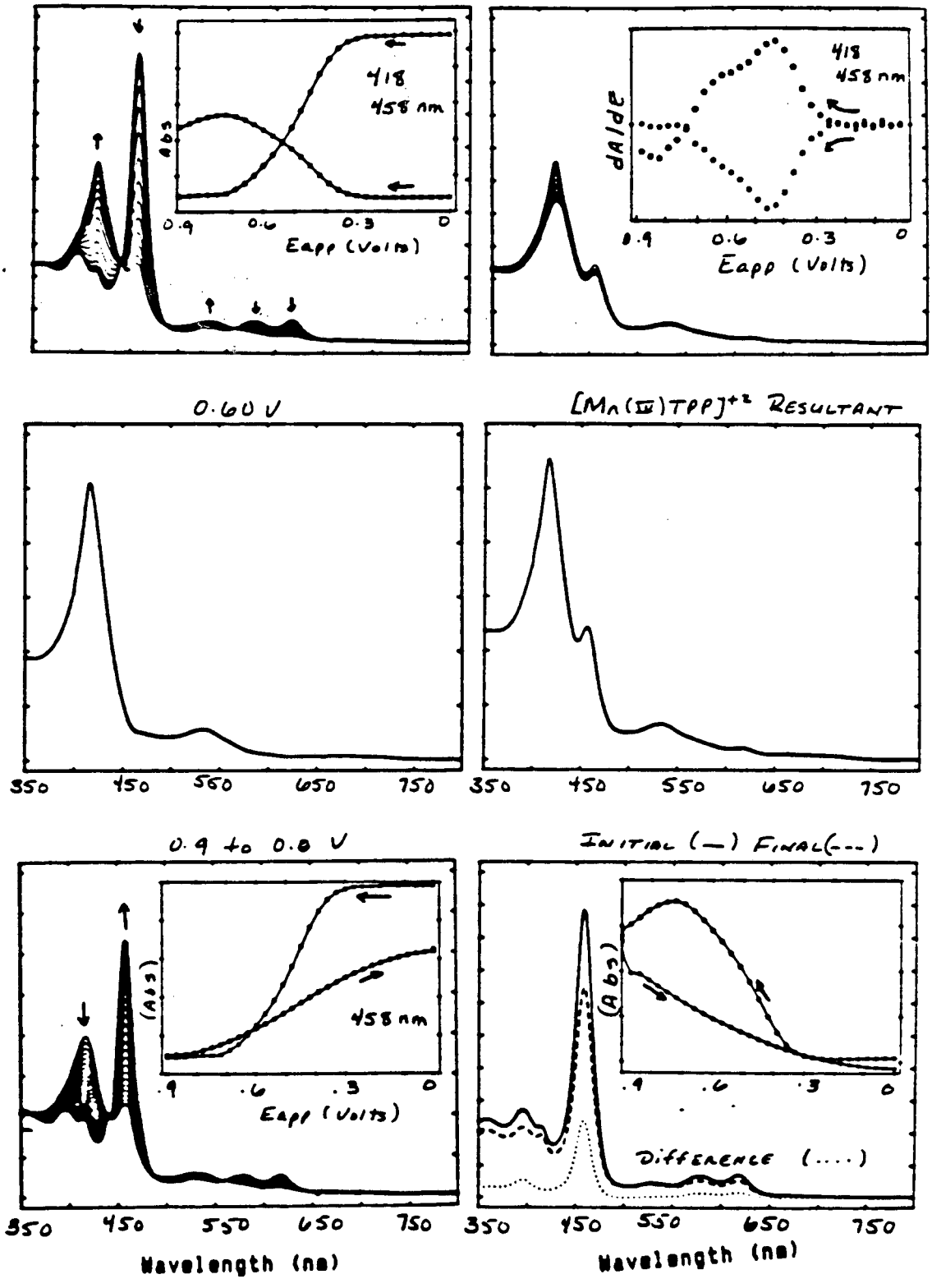

Figure 4-8C

(OCN)MnTPP (π Radical Cation Region)

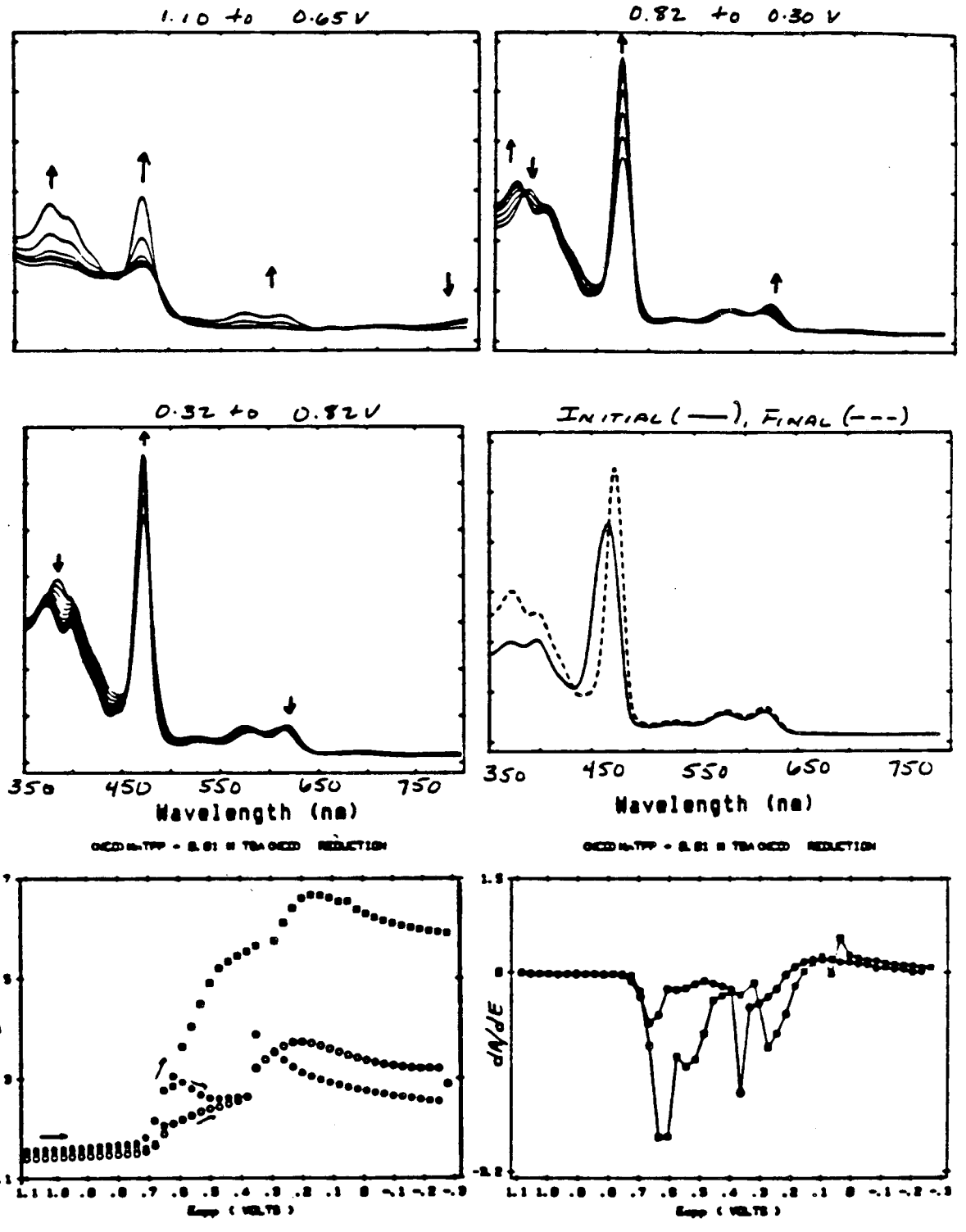

TECHNICAL INFORMATION DEPARTMENT
LAWRENCE BERKELEY LABORATORY
UNIVERSITY OF CALIFORNIA
BERKELEY, CALIFORNIA 94720